THE OXIDATIVE ADDITION OF PALLADIUM(0) TO HYDRO- AND HALO-SILANES: MECHANISMS AND APPLICATIONS

by

MICHAEL R. HURST

A DISSERTATION

Presented to the Department of Chemistry and Biochemistry
and the Division of Graduate Studies of the University of Oregon
in partial fulfillment of the requirements
for the degree of
Doctor of Philosophy

March 2022

DISSERTATION APPROVAL PAGE

Student: Michael R. Hurst

Title: The Oxidative Addition of Palladium(0) to Hydro- and Halo- Silanes: Mechanisms and Applications

This dissertation has been accepted and approved in partial fulfillment of the requirements for the Doctor of Philosophy degree in the Department of Chemistry and Biochemistry by:

Mark Lonergan	Chairperson
Amanda Cook-Sneathen	Advisor
Kenneth Doxsee	Core Member
Gregory Bothun	Institutional Representative

and

Krista Chronister	Vice Provost for Graduate Studies

Original approval signatures are on file with the University of Oregon Division of Graduate Studies.

Degree awarded March 2022

DISSERTATION ABSTRACT

Michael R. Hurst

Doctor of Philosophy

Department of Chemistry and Biochemistry

March 2022

Title: The Oxidative Addition of Palladium(0) to Hydro- and Halo- Silanes: Mechanisms and Applications

The activation of silanes by transition metals is a crucial step in many transformations, including hydrosilylation, cross-coupling, and carbene insertion. Palladium is a common metal in catalysis and its activity is usually ascribed to Pd(0) species. Yet, the fundamental oxidative addition of Pd(0) to silanes has not been studied systematically or mechanistically. Thus, we undertook studies to probe the oxidative addition of Pd(0) to Si–H and Si–X bonds, focusing on elucidating mechanisms and uncovering trends in reactivity that will contribute to catalytic development and optimization.

Chapter 1 motivates the study of oxidative addition to silanes, including a discussion of current challenges and potential benefits.

Chapter 2 describes our work on elucidating the mechanism of oxidative addition of Pd(0) to Si–H. Unique insights into the reaction with tertiary silanes led to our proposal of a concerted mechanism for oxidative addition. Furthermore, energy barriers for each step in the proposed mechanism were experimentally determined to support this hypothesis.

Chapter 3 extends upon work in Chapter 2 to explore the electronic

influence of silane substituents in their reaction with Pd(0). A pronounced electronic effect is observed to favor silanes with electron-poor groups.

Chapter 4 focuses on understanding the steric influence of silane substituents in oxidative addition. A side-by-side comparison of reaction energy barriers with silanes of varied steric hindrance suggests that differences in reactivity arise primarily from thermodynamic, not kinetic, factors.

Chapter 5 utilizes silyl palladium hydrides as catalysts in alkyne hydrosilylation, showing good agreement with trends in oxidative addition. Mechanistic studies suggest a complicated mechanism in which intermediate equilibria impact the reaction.

Chapter 6 reports on the oxidative addition of Pd(0) into Si–X bonds of halosilanes (X = Cl, Br, I). Mechanistic proposals and evidence are presented for the reaction with three distinct Pd(0) complexes to indicate disparate activation pathways for each.

Chapter 7 details our efforts to use fundamental understanding of oxidative addition in synthesizing a new class of heterogeneous catalyst. Experimental methods for the formation of surface silyl palladium hydrides and their role in catalysis is presented.

This dissertation includes previously published and unpublished coauthored material.

CURRICULUM VITAE

NAME OF AUTHOR: Michael R. Hurst

GRADUATE AND UNDERGRADUATE SCHOOLS ATTENDED:

University of Oregon, Eugene
Black Hills State University

DEGREES AWARDED:

Doctor of Philosophy, 2022, University of Oregon
Master of Science, 2019, University of Oregon
Bachelor of Science, 2017, Black Hills State University

PUBLICATIONS:

Hurst, M.R., Davis, A.G., Cook, A.K. “The Influence of Silane Steric Bulk on the Formation and Dynamic Behavior of Silyl Palladium Hydrides.” *Organometallics* **2022** *(accepted).*

Hurst, M.R., Zakharov, L.N., Cook, A.K. “The Mechanism of Oxidative Addition of Pd(0) to Si–H Bonds: Electronic Effects, Reaction Mechanism, and Hydrosilylation.” *Chem. Sci.* **2021**, 12, 13045-13060.

Dette, C., Hurst, M.R., Deng, J., Nellist, M.R., Boettcher, S.W. “Structural Evolution of Metal (Oxy)hydroxide Nanosheets during the Oxygen Evolution Reaction.” *ACS Appl. Mater. Interfaces* **2019**, 11, 6, 5590-5594.

TABLE OF CONTENTS

LIST OF FIGURES

LIST OF SCHEMES

1. INTRODUCTION

Si–H and Si–X Activation by Late Transition Metals

Organosilicon compounds are found nearly everywhere in our world, both inside and outside of the research laboratory. Some common uses for organosilicon materials are in the creation of consumer goods like polymers (plastics) and adhesives,[1–3] in medicines as "sila-drugs,"[4–6] and in chemical processes as valuable reagents.[7–9] An incredible versatility and complexity in organosilicon chemistry is necessary to achieve such impact on the scale required to meet modern demands for these products. Yet, the remarkable molecules that enable these advances in science, technology, and lifestyle begin as all other molecules do: as exceedingly simple precursors. For organosilicon compounds, most are ultimately generated from simple chlorosilanes produced by the Müller-Rochow "Direct" process.[10] This industrial, copper-catalyzed synthesis reacts elemental silicon with methyl or phenyl chlorides to yield a distribution of chlorinated silicon products: $SiCl_4$, $SiCl_3R$, $SiCl_2R$, and $SiClR_3$ which are then separated by distillation. The fate of these chlorosilanes – ranging anywhere from organic functional group protection reagents[11,12] to biological enzyme mimics[13,14] to silicone used as insulation in the International Space Station[15] – is determined by the scope of methods available for further transformation of these bonds.

The conversion of "Direct" process residues to silyl hydrides is carried out by reduction with metal hydrides,[16–18] by Si–Si bond cleavage with HCl,[19,20] or by hydrogenation with H_2 in the presence of a catalyst.[21–24] Silyl hydrides, or silanes, find broad utility in organic synthesis and catalysis. Some of the most prominent applications for their use is in Fleming-Tamao oxidation to synthesize alcohols, in dehydrocoupling to form polysiloxane polymers, and in transition metal catalyzed hydrosilylation and cross coupling reactions.[7,25–28] Notably, the efficacy of these processes is sensitive to the electronic and steric properties of the other groups attached at silicon, which can complicate the design of a desired organosilicon target.[25–27,29,30]

For these reasons, transition metal catalysis is perfectly positioned to overcome these barriers. One trademark of transition metals is their tuneability with selection of ligands, which can vastly alter the outcome of a reaction or even change the mechanism. In many cases, transition metal catalysis outperforms other methods. One example is in hydrosilylation where, despite the high cost of platinum, industrial-scale hydrosilylations are still conducted with Karstedt's catalyst (a Pt(0)-alkene complex) or its derivatives (Scheme 1.1).[31,32] Considering only its use in the silicone industry, this process comprises ~3% of worldwide platinum production every year.[33,34] Why? Because the practicality of efficient platinum catalysis cannot be matched through other means.

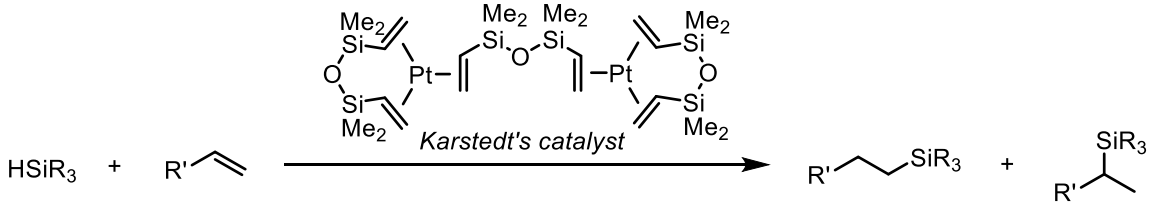

Scheme 1.1. Alkene hydrosilylation with Karstedt's catalyst is a cornerstone reaction in transition metal-catalyzed organosilicon chemistry.

One of the primary factors dictating a metals function in catalysis with silanes is the nature of its interaction with Si–X (Figure 1.1). In general, the structure of a metal-silane complex can span a continuum of bonding character, with the extremes being (a) no interaction of the silane with a metal in *n* oxidation state; to (b) complete oxidative addition to give a complex in *n*+2 oxidation state with no residual Si–X bonding. Between these idealized complexes are σ-complexes of the structure M(η^2-H–SiR_3) with varying degrees of coordination strength.[25–27]

It should be noted that this discussion applies only for oxidative addition proceeding by a concerted pathway, which is well-established with hydrosilanes but less certain with polar halosilanes. If the oxidative addition of halosilanes proceeds instead by an S_N2-like pathway, no intermediates exist and no Si–X bonding should be present in the product – exemplified in the accessibility of products with M–Si and M–X bonded in a *trans*- fashion to one another.

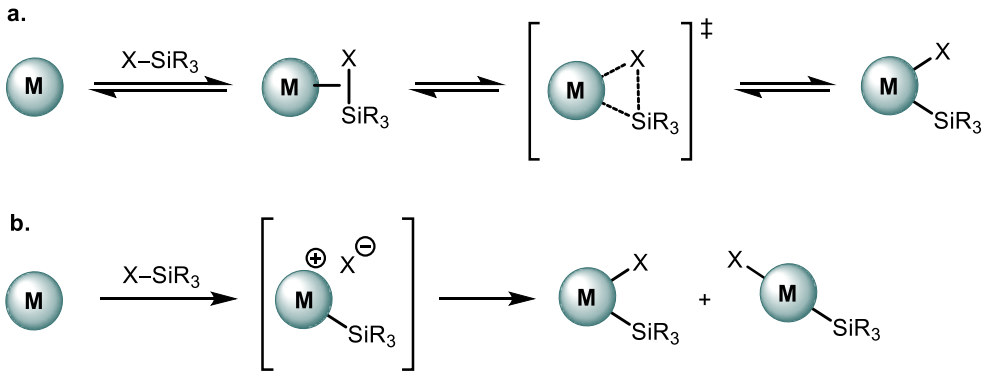

Figure 1.1. (a) concerted and (b) S_N2-like mechanisms of oxidative addition to late transition metals

In any case, the extent of M–Si/H bonding is usually approximated by $J_{Si–H}$ coupling in ^{1}H or ^{29}Si nuclear magnetic resonance (NMR) spectroscopy[35–40] or by determining the distance between Si and X atoms found by single crystal x-ray diffraction (XRD). In situations where these experimental methods are not available, density functional theory (DFT) can be used to calculate an expected transition state geometry or intermediate structure. Because there are not discrete limits in this continuum of bonding character upon which to base the definition of a structure, oftentimes the distinction between a "σ-complex" or an "oxidative addition product" is in relation to arbitrary thresholds that have been accepted by the community.[35,39]

In line with the proclaimed tuneability of late transition metals, the extent of metal-silane bonding is highly dependent on the choice of metal and silyl X identity (e.g. halogen or H), the complex ligand coordination sphere, and the silane substituents.[25–27] With palladium, this interplay has been studied theoretically to explain why the experimental observation of complexes with Pd–Si bonds is so rare despite the prominence of Group 10 congener, platinum, in this area.[41] The difference in reactivity between metals was ascribed to relativistic effects but, more importantly, it was found that the Pd–Si bond strength can be tuned over a range of 60 kJ/mol (14 kcal/mol) by changing the substituents at silicon alone![41] The extent of this de/stabilization by silane substituents has a direct impact on the metal-silane interaction during oxidative addition and plays a significant role in determining the persistence of Si–X bonding character in the product.

While the topic of silane bonding interactions at metal centers is of interest to practicing organometallic chemists, and a major focus in this Dissertation (Chapters 2-4, 6), a more pertinent topic to the average reader is how these interactions contribute to the reactivity of metal complexes during catalysis.

Metal-Silane Interactions in Catalysis

Commonly, in reports that include reactions of silanes with transition metal precursors, the identity and bonding character of complexes formed by Si–X activation are not of explicit primary interest. Rather, much research on the interaction of silanes with metals is framed instead by the development of effective catalysts for transformations in organosilicon chemistry. A main motivation for studying and understanding metal-silane interactions, then, is to leverage that insight towards the discovery and optimization of useful catalytic applications.

The ability to rationalize the behavior of the metal catalyst enables a hypothesis-driven approach to reaction development, and aids in preventing significant time and energy lost to evaluating every variable experimentally. Additionally, perspective into fundamental interactions at the metal center can highlight abnormal or exceptional instances of substrate interactions that suggest an aptitude for a certain outcome, such as a unique intermediate geometry suggesting the potential for enantioselective induction under appropriate conditions. Thus, it is no surprise that many examples exist in the literature where proposed silane-metal interactions have led to powerful retroactive analysis and prediction.

The hydrosilylation of alkenes is by far the most widespread transition metal catalyzed reaction of silanes, and therefore serves as a useful focus for the discussion of metal-silane interactions in catalysis.[31,32] Here, it is necessary to distinguish between the reactivity of early and late transition metals. Although they are less often studied in hydrosilylation than late transition metals, early transition metals find utility as catalysts for this transformation. In most cases, low valent (or d^0) early transition metals are proposed to proceed in hydrosilylation via σ-bond metathesis processes that do not comprise Si–H activation at the metal; rather, the

metal complex intermediates of the reaction have either an M–Si or an M–H bond, and Si–H cleavage occurs with the assistance of R coordinated at the metal (from alkene substrate) interacting with the other atom of the silane (Figure 1.2).[33,42,43] Thus, the metal center undergoes no change in oxidation state throughout the reaction, necessitated by its lack of d electrons.

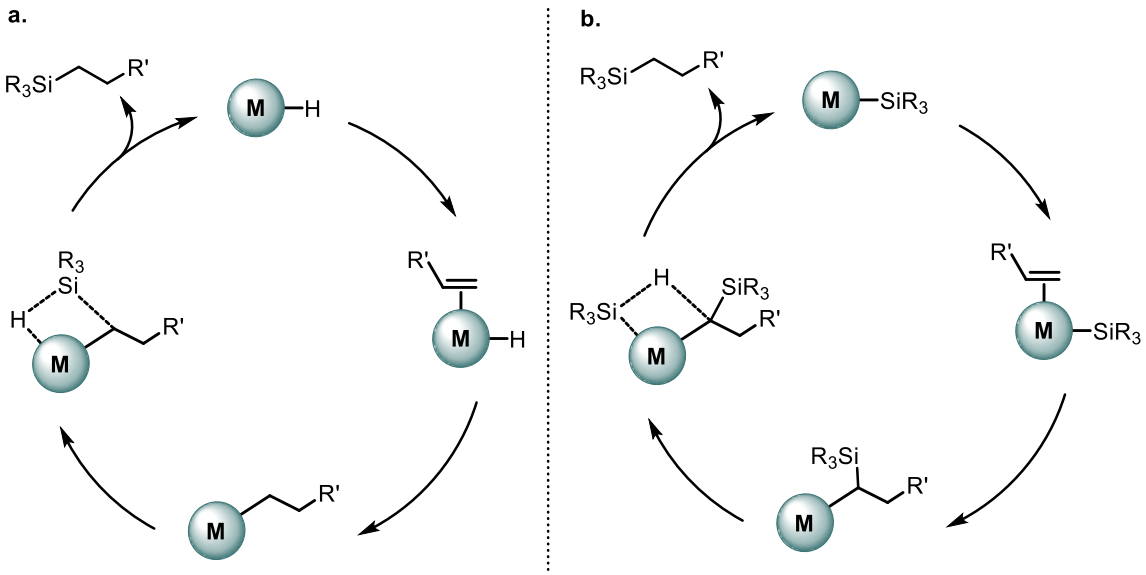

Figure 1.2. Commonly proposed mechanism for alkene hydrosilylation by early transition metals proceeding through (a) metal hydride or (b) metal silyl intermediates.

On the other hand, late transition metals undergo silane activation as described in the previous section. In the context of hydrosilylation, this Si–H activation comprises only the first step of the reaction, followed by migratory insertion of the alkene into the M–H or M–Si bond and reductive elimination to yield the hydrosilylated product (Figure 1.3).[44–46] This mechanistic proposal is referred to as the Chalk-Harrod mechanism of hydrosilylation when insertion occurs to M–H or the modified Chalk-Harrod mechanism of hydrosilylation when insertion occurs to M–Si. Importantly, although oxidative addition of Si–H is overwhelmingly proposed as the first step of the reaction, this is not necessarily the case – many systems exist in which hydrosilylation occurs from M(η^2-H–SiR_3).[25–27]

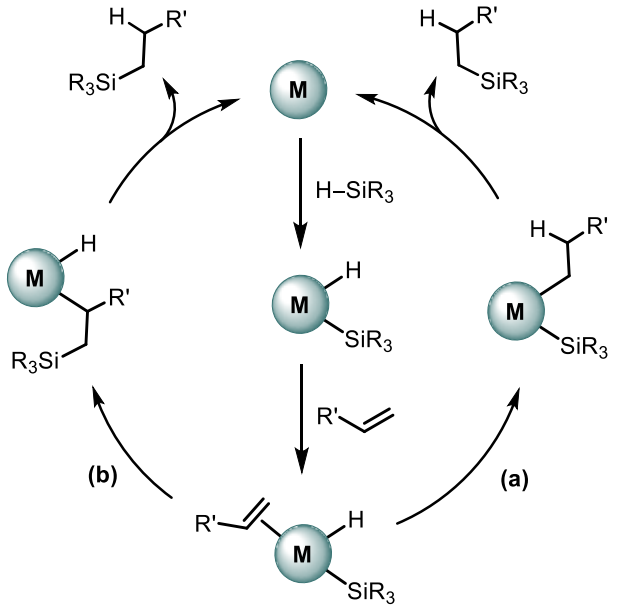

Figure 1.3. (a) Chalk-Harrod and (b) modified Chalk-Harrod mechanisms for alkene hydrosilylation by late transition metals.

An exemplary case of this intermediacy of σ-complexes is in the hydrosilylation of allenes by Pd and Ni complexes stabilized by *N*-heterocyclic carbene (NHC) ligands by Montgomery and co-workers.[47] A main finding in this study was that divergent regioselectivity could be induced by proper selection of the metal and ligand. A computational follow-up to this work by Xiong and co-workers provides insight into the substrate interactions at the metal that contribute to this unique reactivity.[48] Specifically, DFT indicates that the product of Pd oxidative addition to Si–H is unstable due to the large *trans*- effect of a hydride or silyl group *trans*- to NHC. As a result, the oxidative addition/migratory insertion steps of the Chalk-Harrod mechanism occur in a concerted manner to form an intermediate η^3 π-allyl complex that undergoes reductive elimination to release the product. This concerted step is proposed as the rate-determining and regioselectivity-determining step to form either the allylsilane or vinylsilane as the major product.[48] Through these means, the extent and energetics of M–Si and M–H bond formation at the metal center have a profound influence on the outcome of the reaction. In general, the wide variability in intermediate σ-coordination strength amplifies the importance of silane electronic and steric effects, as these contribute significantly to the strength of metal-silane interactions.

Besides informing on catalytic performance, another valuable opportunity provided by studying Si–H activation is in its analogy to C–H activation.[49–51] C–H activation steps such as oxidative addition are observable only in rare circumstances due to their low reactivity with transition metals; on the other hand, due to the increased basicity of silicon-hydrogen bonds compared to carbon-hydrogen bonds, these fundamental reaction steps are more commonly observable in studies of silanes. Taking advantage of this reactivity difference, studying Si–H oxidative addition can offer unique insight into the oxidative addition of C–H bonds, including the possibility to decouple the relative energetics of coordination and oxidative cleavage. Given the ubiquity of C–H bonds in chemistry, and the concentrated effort dedicated to their controlled functionalization, this ability to gain meaningful insight on C–H activation via the study of Si–H activation is certainly cause for attention.

So far, the discussion of Si–X activation at metal centers has focused on the generation of intermediate complexes during catalysis – a concept applied to the hydrosilylation of alkynes detailed in Chapter 5 of this Dissertation. However, in cases where the discrete silyl metal hydrides formed by oxidative addition can be observed or isolated, their utility is not limited to acting as fleeting intermediates.

Surface Organometallic Chemistry

The metal complexes discussed to this point have all been examples of homogeneous catalysts – during a reaction, they are present in the same phase (usually in solution) as the substrates. This allows for their ready observation by accessible spectroscopic methods like solution NMR and, importantly, their tendency to take on well-defined structures before, during, and after catalysis. Together, these factors enable effective control and optimization of their reactivity, but homogeneous catalysts also suffer from drawbacks; namely, they are commonly less stable to harsh reaction conditions than their heterogeneous counterparts and they are poorly recyclable.

Heterogeneous catalysts, on the other hand, offer complementary benefits and disadvantages: they are known to be stable at relatively high temperatures

and pressures and, in an ideal case, they can be efficiently recycled by simple filtration from the reaction mixture. However, heterogeneous catalysis has traditionally not been amenable to in-depth mechanistic study, which has precluded its optimization to the same level as homogeneous catalysis.[52–54] The challenges involved in studying heterogeneous catalysts generally center around their imprecise structure, as common synthetic routes lead to the potential generation of a variety of metal sites on the surface (Figure 1.4a) – any (or none) of which could be catalytically active. To investigate the mechanism of a material such as this, a significant hurdle exists simply in *identifying* the surface species responsible for catalyzing the transformation. Tuning the activity, then, is likewise greatly complicated by potential side reactivity at undesired metal sites.

Yet, heterogeneous catalysts are ubiquitous in industry due to their practicality, with some estimates ascribing their use in 90% of all chemical processes.[53] This seems contrary to their poor definition and potential for imprecise reaction outcomes, but decades of reaction development have negated many of the drawbacks faced by heterogeneous catalysts. The problem is, then, that to diversify the industrial processes that require these materials, researchers must invest massive time, money, and effort to “re-invent the wheel” with scarce structural or mechanistic insight. Therefore, there is great impetus to develop heterogeneous catalysts that meet the benefits of homogeneous catalysis – specifically, allowing for the formation of well-defined and tunable species in a controllable way.

Surface organometallic chemistry (SOMC) is one way to achieve this rigor in catalyst design.[55–57] Using knowledge of organometallic chemistry at a molecular level, SOMC involves the grafting of transition metal complexes onto metal oxide surfaces such as silica, SiO_2. A crucial aspect of SOMC is the precise treatment of support materials prior to grafting. In the case of silica, this usually involves heating to 700 °C under dry air or strong vacuum to dehydroxylate the surface.[58] This removes a large portion of the surface silanols from silica and leaves behind a low concentration of almost exclusively “isolated” silanols. These silanols can then be treated as a standard organometallic ligand, exhibiting

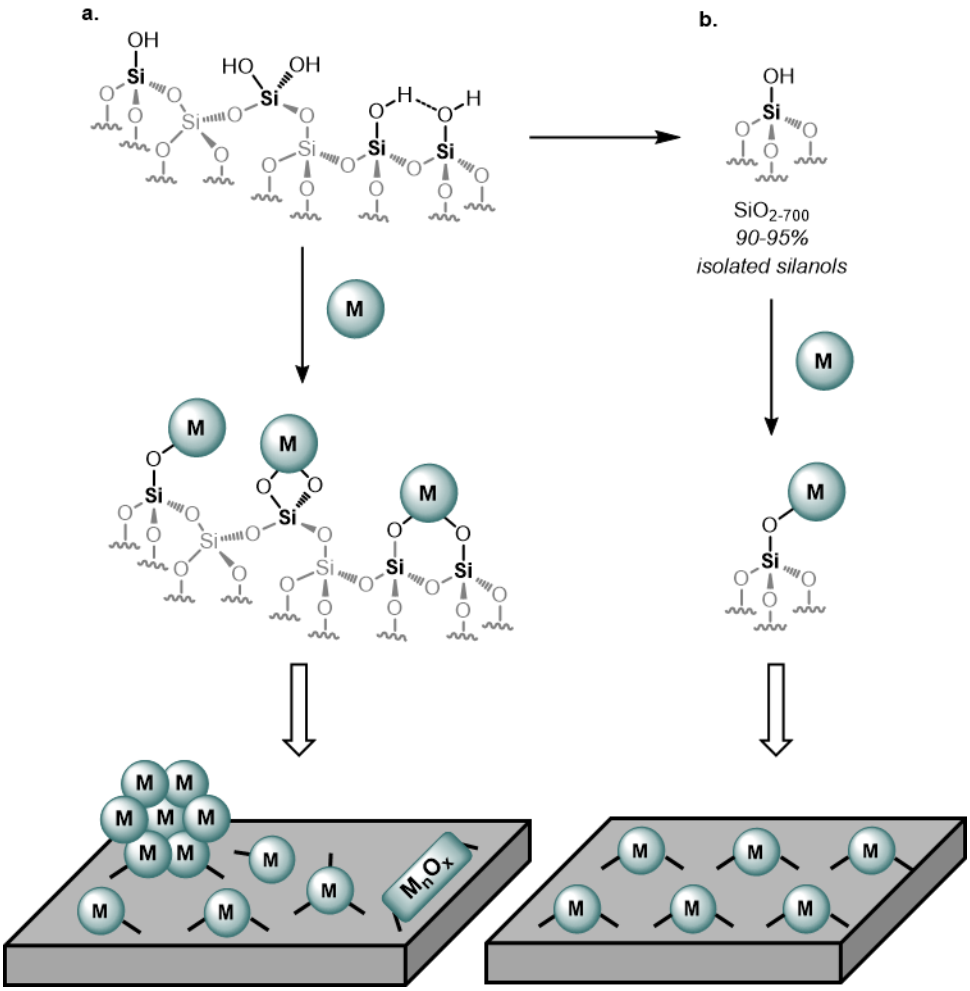

Figure 1.4 (a) grafting of a metal complex to the surface of untreated silica. (b) grafting of a metal complex to the surface of $SiO_{2\text{-}700}$.

predictable reactivity to graft metal precursors to the surface via an Si–O–M linkage (Figure 1.4b).

The use of SOMC to synthesize heterogeneous catalysts from early transition metals (ETMs) has been highly successful due to their oxophilicity.[55–57] However, the application of late transition metals (LTMs) in this method has not been successful because the formed Si–O–LTM bond is weak and easily cleaved.[59] This leads to the degradation of catalysts in situ, forming undesired clusters and terminating catalytic activity. Yet, late transition metals are indispensable for the success of many types of catalytic transformations. Therefore, novel methods are needed to support LTMs to the surface of metal oxides.

Although our investigations to this point have focused heavily on the oxidative addition of Pd(0) to silanes in solution (Figure 1.5a),[60,61] the scope of our interest in this reaction expands beyond molecular studies. Indeed, the basis of our initial interest in this reaction was not in identifying homogeneous catalytic intermediates or uncovering the mechanism of oxidative addition. Rather, we set out study this reaction with the intention to demonstrate proof of concept for the oxidative addition of Pd(0) to Si–H bonds on the surface of silica. Ultimately, the work described in Chapter 7 covers our efforts to synthesize a unique class of heterogeneous catalysts: metal hydrides supported to the surface of silica (or other metal oxides) through an Si–M–H linkage.

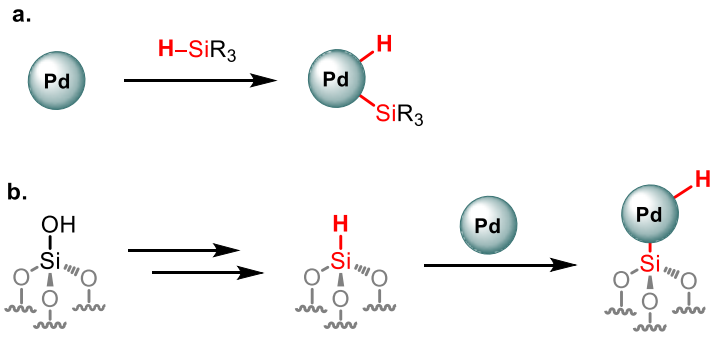

Figure 1.5. (a) generalized example of Pd(0) oxidative addition to a molecular silane. (b) proposed strategy to oxidatively add Pd(0) to silanes on the surface of silica.

In summary, this Dissertation contains our work on understanding the mechanism of Pd(0) oxidative addition to Si–H (Chapter 2) and the role of silane electronics (Chapter 3) and silane steric bulk (Chapter 4) in the reaction. From these findings, we developed a catalytic system for the hydrosilylation of alkynes (Chapter 5). Further, we explored the oxidative addition of Pd(0) to the Si–X bonds of halosilanes (Chapter 6). Finally, the insight gained from this previous work was applied to synthesize silyl palladium hydrides on the surface of silica and to show their preliminary performance in catalysis (Chapter 7). Descriptions of Materials and Methods utilized throughout this Dissertation are provided in the Appendix.

Statement on Previously Published/Co-authored Materials

The research discussed throughout this Dissertation was primarily conducted by me under the supervision of Dr. Amanda Cook. The work described in Chapters 2, 3, and 4 has been published in professional journals with me as the first author (references below). In the projects described therein, Lev N. Zakharov provided characterization of a complex by single crystal x-ray diffraction, and Amanda G. Davis synthesized substrates and conducted oxidative addition experiments under my supervision.

The work described in Chapter 5 was conducted by me and by Lucas Thigpen under my supervision. The work described in Chapter 7 was conducted by me, with characterization data collected by Dr. Shiva Moaven (solid-state nuclear magnetic resonance) and Tawney Knecht (x-ray photoelectron spectroscopy). All of the writing in this Dissertation is mine, with significant assistance from Dr. Amanda Cook to the text of Chapters 2-4 prior to publication in professional journals.

Chapters 2 and 3

Hurst, M.R., Zakharov, L.N., Cook, A.K. “The Mechanism of Oxidative Addition of Pd(0) to Si–H Bonds: Electronic Effects, Reaction Mechanism, and Hydrosilylation.” *Chem. Sci.* **2021**, 12, 13045-13060.

Chapter 4

Hurst, M.R., Davis, A.G., Cook, A.K. “The Influence of Silane Steric Bulk on the Formation and Dynamic Behavior of Silyl Palladium Hydrides.” *Organometallics* **2022** *(accepted).*

2. MECHANISM OF THE OXIDATIVE ADDITION OF PALLADIUM(0) TO HYDROSILANES

From Hurst, M.R., Zakharov, L.N., Cook, A.K. “The Mechanism of Oxidative Addition of Pd(0) to Si–H Bonds: Electronic Effects, Reaction Mechanism, and Hydrosilylation.” *Chem. Sci.* **2021**, 12, 13045-13060.

Introduction

Palladium hydrides are a unique class of organometallic compounds[1,2] which are invoked as key intermediates in a variety of catalytic reactions, including the Mizoroki-Heck reaction,[3–5] alcohol and alkene oxidation,[6–8] nucleocarbonylation reactions, hydrofunctionalization reactions,[9] (co)polymerization reactions,[10,11] and alkene and alkyne (cyclo)isomerization reactions.[12–14] However, despite that these species are often proposed as intermediates, the direct observation or isolation of complexes containing a formal Pd–H bond is uncommon, and fundamental study of their behaviour has largely been precluded.[1,2,13]

Organosilicon compounds are broadly significant, since they are used as monomers to synthesize polysiloxanes (silicones),[15,16] and they have also recently gained attention for their use as biocompatible yet non-natural carbon isosteres[17] in the synthesis of bioactive molecules.[18–20] Transition metal-catalysed hydrosilylation of alkenes and alkynes is the primary method for synthesizing organosilanes,[21–25] with most development and mechanistic work focusing primarily on Pt catalysts.[21,22,26] On the other hand, Pd catalysts show complementary and modular regioselectivity[22,27,28] and are more useful in enantioselective hydrosilylation.[29–32]

A key step in the mechanism of transition metal-catalysed hydrosilylation is the oxidative addition of the metal to the Si–H bond.[21–24,26,33–35] While this fundamental step of organometallic chemistry, to form (silyl)M(H) complexes, has been well-studied for Pt,[36–49] it is much less understood for Pd. In addition to hydrosilylation (Figure 2.1b), the oxidative addition of Pd to Si–H bonds (Figure 2.1a) is also a vital step of carbene insertion reactions (Figure 2.1c),[50–52] C–Si cross-coupling reactions (Figure 2.1d),[53] and hydrodehalogenation reactions

(Figure 2.1e),[54–59] amongst others.[60–65] Because of the importance of this step of many catalytic reactions, we sought to determine the mechanism of Si–H oxidative addition to Pd(0).

Despite being implicated as catalytic intermediates for more than half of a century, it was not until the early 2000's that the Fink group reported the isolation of the first (silyl)Pd(H) complex.[66,67] Since this seminal work, Ishii[68] and Iluc[69,70] have both also published related work. However, while some characteristics of the (silyl)Pd(H) compounds were investigated, the overall reaction mechanism remains unsupported with experimental evidence. The Si–H bond is relatively non-polar, and consequently, the mechanism of the reaction likely proceeds through a concerted pathway.[33–35] Experimental evidence to support this hypothesis is needed, including the identification of the precise rate-limiting step.

Elucidation of the details of the reaction mechanism is also relevant in the context of the oxidative addition of C–H bonds, since Si–H bonds often react analogously; although, Si–H bonds are more basic and therefore more reactive with transition metals. Taking advantage of this

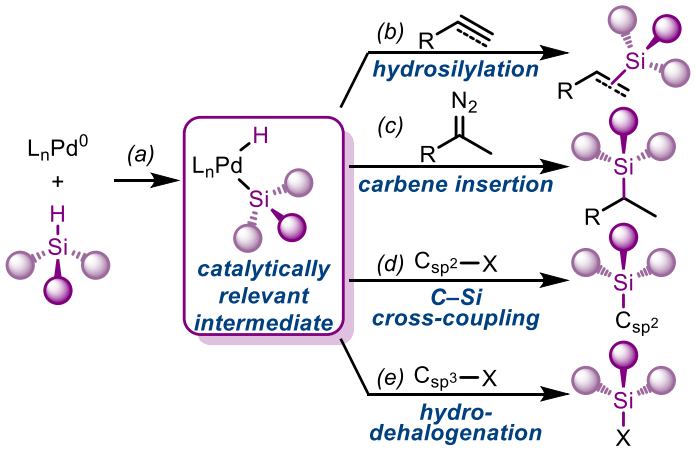

Figure 2.1. a) Oxidative addition to form silyl palladium hydride species implicated in catalysis such as (b) hydrosilylation, (c) carbene insertion, (d) C–Si cross-coupling, and (e) hydrodehalogenation reactions.

reactivity difference, studying Si–H oxidative addition can offer unique insight into the oxidative addition of C–H bonds. *One important challenge in studying the mechanism of oxidative addition of non-polar bonds is decoupling the individual*

steps of the oxidative addition process, which is composed of coordination and oxidative cleavage steps (Figure 2.2). Examining Si–H oxidative addition reactions offers a chance to address that challenge. Ground-breaking work by Jones[71] and

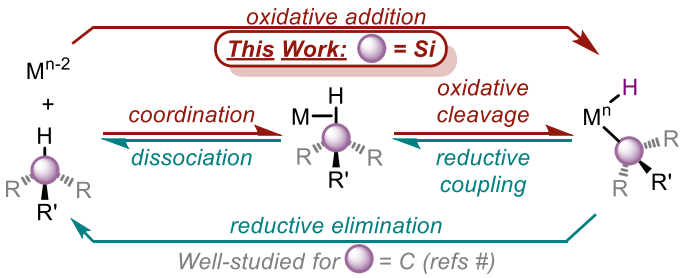

Figure 2.2. Mechanistic relationship between of oxidative addition of Si–H and reductive elimination of C–H bonds.

Parkin[72] has investigated the reverse of oxidative addition: reductive elimination of C–H bonds using KIEs and EIEs as tools to decouple the reductive cleavage and dissociation steps.

Described in this Chapter is our investigation into the mechanism of the oxidative addition of [(μ-dcpe)Pd]$_2$ (**1**) to tertiary silanes. Using a variety of mechanistic tools – ranging from van't Hoff and Eyring analyses to rate and order studies – we discuss the overall reaction mechanism, identity the rate determining step of oxidative addition, and calculate ground state and transition state energies along the pathway. Importantly, this work sets the foundation for detailed investigation of silane electronic and steric effects in oxidative addition, and the application of this fundamental knowledge towards catalysis.

Results and Discussion

Initial reactivity studies of [(μ-dcpe)Pd]$_2$ (1) with silanes

We began by investigating the reactivity of a small library of tertiary silanes **2**-**5** with [(μ-dcpe)Pd]$_2$ (**1**) by ^{1}H and ^{31}P NMR (Figure 2.3). These reactions proceed cleanly and only the reactants and the product are observed by NMR. In the ^{1}H spectrum, the peak corresponding to silane Si–H (4–6 ppm) is consumed during the reaction, along with concomitant appearance of a new resonance below 0 ppm, which corresponds to the newly formed Pd–H in **6-9**. The formation of the

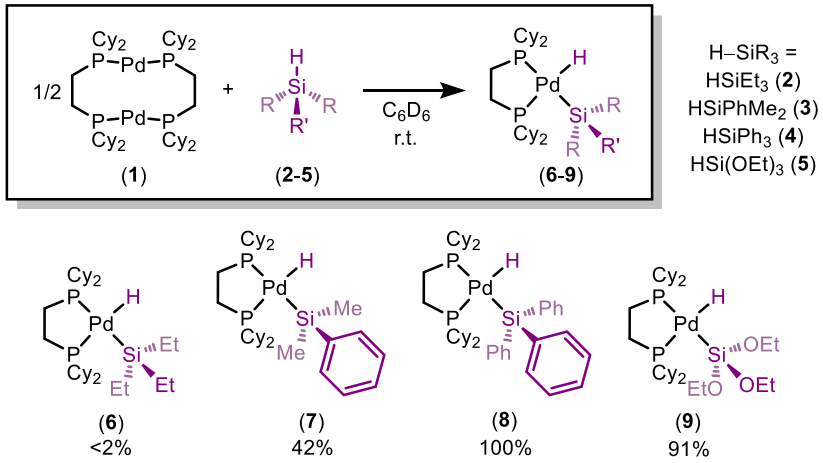

Figure 2.3. Scope of silane reactivity in oxidative addition with [(μ-dcpe)Pd]$_2$ (**1**).

Pd–H moiety is also supported by a new band in the IR spectrum (1838 to 1881 cm^{-1}), which corresponds to the Pd–H stretch. The ^{1}H NMR signal shows an apparent doublet or triplet at room temperature (see Dynamic Exchange Behavior below). The chemical shift and coupling patterns of the hydride and phosphorus signals align well with related Pd and Pt hydrides stabilized by bidentate phosphine ligands.[39,66–68]

To embark upon mechanistic studies, we first sought to determine if this oxidative addition reaction is reversible or irreversible. **1** and **3** were reacted in an NMR tube at 298 K and allowed to reach equilibrium (Figure 2.4). The reaction was then cooled to 253 K, and the conversion of **7** was measured to be to 88%. Warming the reaction to 293 K and then 333 K resulted in concomitant decreases in conversion to **7** (44% and 17%, respectively). Subsequent cooling back to 298 K resulted in a conversion of 41%, which is consistent with the data in Figure 2.3. Because the conversion is consistently ~42% at ambient temperature independent of whether the reaction had previously been heated or cooled, we deemed this reaction to be reversible.

To deconvolute the enthalpic and entropic contributions to the ground state energies of oxidative addition (ΔG^o_{OA}), the equilibrium constants as a function of temperature were measured. van't Hoff analysis was carried out (Figure 2.5) for the reaction of **1** with **3** or **4**. The ΔS^o_{OA} value is large and negative for both silanes,

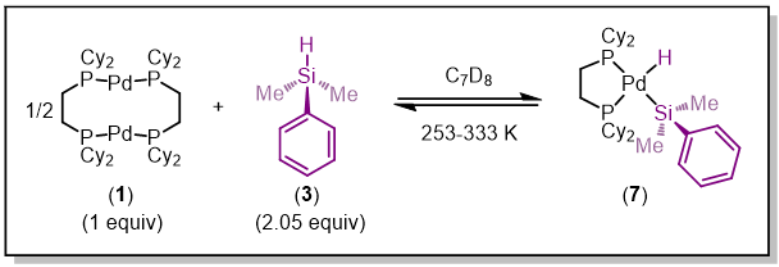

Spectrum order	Temperature (K)	Conversion to **7**
1st	253	88%
2nd	273	72%
3rd	293	44%
4th	313	27%
5th	333	17%
6th	298	41%

Figure 2.4. Conversion values to **7** as a function of temperature and data collection order.

reflecting the loss of entropy in this reaction between three reactants to form two products. ΔH^{o}_{OA} in both reactions is negative, though the reaction with **2** is enthalpically less favorable than that with **3**. Together, these energetic parameters can be used to calculate ΔG^{o}_{OA}; at 233 K, the reaction of **1** with **4** to form complex **8** is nearly 10 kcal/mol more favorable than the reaction with **3**, though both are ultimately exergonic.

Next, we sought to determine the effect of deuterium substitution in the silane. The equilibrium constants for the reactions of protio-silane **3** and deutero-silane **3-d$_1$** were determined independently (Figure 6). The equilibrium isotope effect (EIE) was determined to be 3.7 ± 0.2 at 298 K. The room temperature IR stretching frequencies for the Si–H and Si–D bonds in **3** and **3-d$_1$** are 2116 cm^{-1} and 1539 cm^{-1}, respectively. The EIE measured for this reaction is consistent with the fact that deuterium prefers to form the stronger bond;[72–74] i.e., $K_{eq(D)}$ is lower than $K_{eq(H)}$ because the difference in energy between the Si–D and Pd–D bonds is larger than the difference in energy between the Si–H and Pd–H bonds.

Reaction kinetics

Having examined the ground state, we next turned our attention to understanding the kinetics and reaction mechanism. In probing the mechanism, three possible pathways for oxidative addition were considered: concerted, stepwise, or radical.

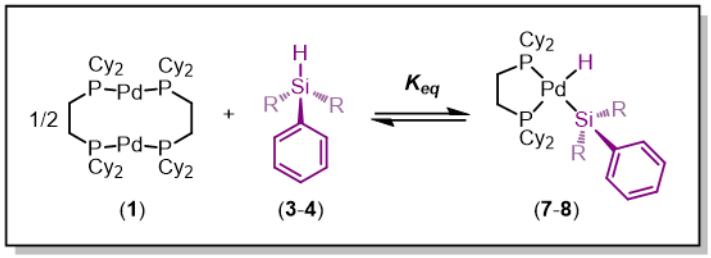

R	Silane	Product	ΔH^{o}_{OA}	ΔS^{o}_{OA}	$\Delta G^{o}_{OA(233K)}$
Me	**3**	**7**	-19 ± 1	-54 ± 5	-6 ± 1
Ph	**4**	**8**	-30.3 ± 0.8	-66 ± 2	-15 ± 1

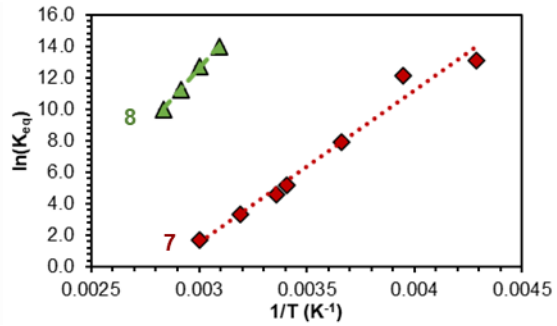

Figure 2.5. van't Hoff analyses of the reaction equilibrium with silanes **3**-**4** and **1**. Conditions: 1.00 equiv of **1**, 2.05 equiv of **3** or **4**, 13.33 mM in C_7D_8, 253-333 K. $\Delta H^{\ddagger}_{OA}$ and $\Delta G^{\ddagger}_{OA}$ are reported in kcal•mol^{-1} and $\Delta S^{\ddagger}_{OA}$ is reported in cal•mol^{-1}•K^{-1}

A concerted pathway was deemed most reasonable as Si–H bonds are non-polar and have been shown to proceed via concerted pathways in related systems. We ruled out the stepwise pathway on the basis of relative acidities of Pd–H ($pK_a \approx 24$)[75] and Si–H ($pK_a \approx 35$)[76] bonds. Additionally, no by-products were observed that would result from a radical pathway (Si–Si bond coupling, H_2, etc.), so we shifted our attention from that pathway as well.

In line with a concerted pathway, the proposed mechanism for oxidative addition is seen in Figure 2.7. *Step i* is dissociation of dimer **1** into monomers **10** in solution.[77] The 14-electron complex **10** can then react with silane in *step ii* to

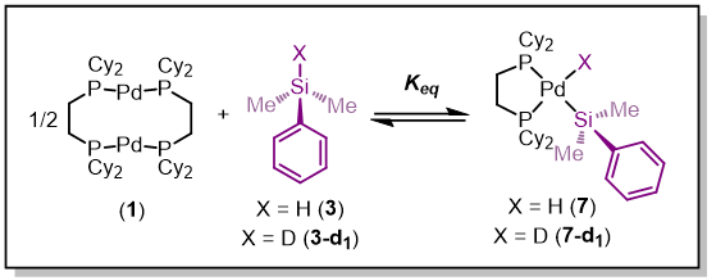

Temperature (K)	Conversion to **7**	Conversion to **7-d_1**	K_H	K_D	EIE
233	95 ± 1%	83 ± 3%	500000 ± 100000	16000 ± 3000	30 ± 10
253	93 ± 1%	81 ± 4%	170000 ± 20000	11000 ± 3000	16 ± 4
273	71 ± 4%	54 ± 3%	2600 ± 600	410 ± 60	6 ± 2
293	46 ± 0%	29 ± 2%	184 ± 0	34 ± 4	5.5 ± 0.6
298	40 ± 0%	28.0 ± 0.7%	102 ± 0	28 ± 1	3.4 ± 0.2
313	27 ± 3%	18.0 ± 0.9%	26 ± 5	7.9 ± 0.7	3.3 ± 0.7
333	16 ± 2%	10 ± 2%	6 ± 1	1.7 ± 0.7	3 ± 1

Figure 2.6. Conversion, K_{eq}, and EIE values for conversion to **7** and **7-d_1** as a function of temperature.

form σ-complex **11**, which then undergoes oxidative cleavage of the Si–H bond to form the product in *step iii*. These steps were taken as the basis for determination of the rate determining step (RDS) of the reaction.

If *step i* is rate-determining, then the rate law will show 0.5th order in **1**, 0th order in silane, and there will be no effect of deuterium substitution in the silane on the rate of the reaction (KIE = 1 (KIE, kinetic isotope effect)). If *step ii* or *step iii* is the RDS, then the reaction will be 0.5th order in **1** and 1st order in silane, and a normal, primary KIE is predicted. We expect that a small KIE would point toward *step ii* being the RDS, since the Si–H bond is only weakened in the transition state (**12** → **13**). A large, primary KIE would point toward *step iii* being the RDS, since it is during that step that the Si–H bond is cleaved.

If *step i* is rate-determining, then the rate law will show 0.5th order in **1**, 0th order in silane, and there will be no effect of deuterium substitution in the silane on the rate of the reaction (KIE = 1 (KIE, kinetic isotope effect)). If *step ii* or *step iii* is the RDS, then the reaction will be 0.5th order in **1** and 1st order in silane, and a normal, primary KIE is predicted. We expect that a small KIE would point toward

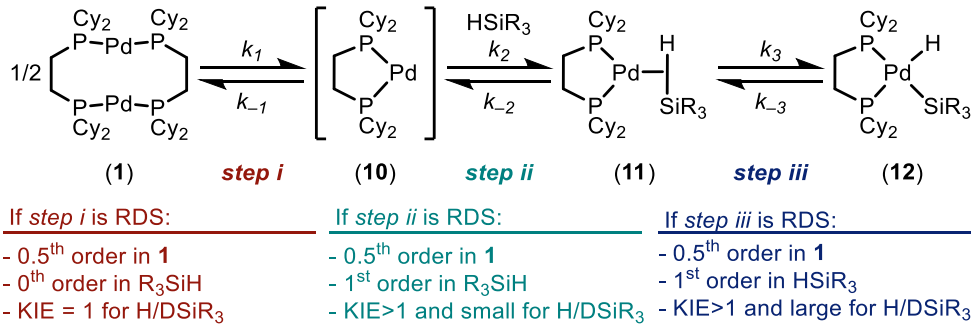

Figure 2.7. Proposed mechanism for the oxidative addition of silanes to **1**.

step ii being the RDS, since the Si–H bond is only weakened in the transition state (**12** → **13**). A large, primary KIE would point toward *step iii* being the RDS, since it is during that step that the Si–H bond is cleaved.

Initial attempts to collect kinetic data by monitoring the reaction of **1** with **3** by NMR proved unsuccessful, since the reaction was complete within a minute at room temperature. We thus set out to determine conditions that are amenable to reaction monitoring by NMR; however, even at low reagent concentrations (1.67 mM **1**, 3.42 mM **3**) and low temperature (233 K), the formation of **8** was too rapid to obtain reliable kinetic data. In line with our findings on reaction equilibria, we reasoned that $HSiPhMe_2$ **2** may also react more slowly in oxidative addition, yet still would have the advantage of being electronically modular. Indeed, the gradual formation of a silyl palladium hydride **7** is observable via $^{31}P\{^1H\}$ and ^1H NMR at 233 K.

As detailed above (Figure 2.7), the rate law distinguishes between *step i* and *steps ii* or *iii* being the RDS; therefore, we first embarked on measuring the orders in the reactants. We utilized the method of initial rates to ensure that the rate of the backward reaction (from **7** to **1** and **2**) is negligible. Data was collected on samples of varied concentrations of **1** (1.67–13.3 mM) or **2** (3.42–27.3 mM) while the concentration of the unexamined reagent was kept constant. The observed rate of each reaction was then plotted against initial reagent concentration to determine the reaction order.

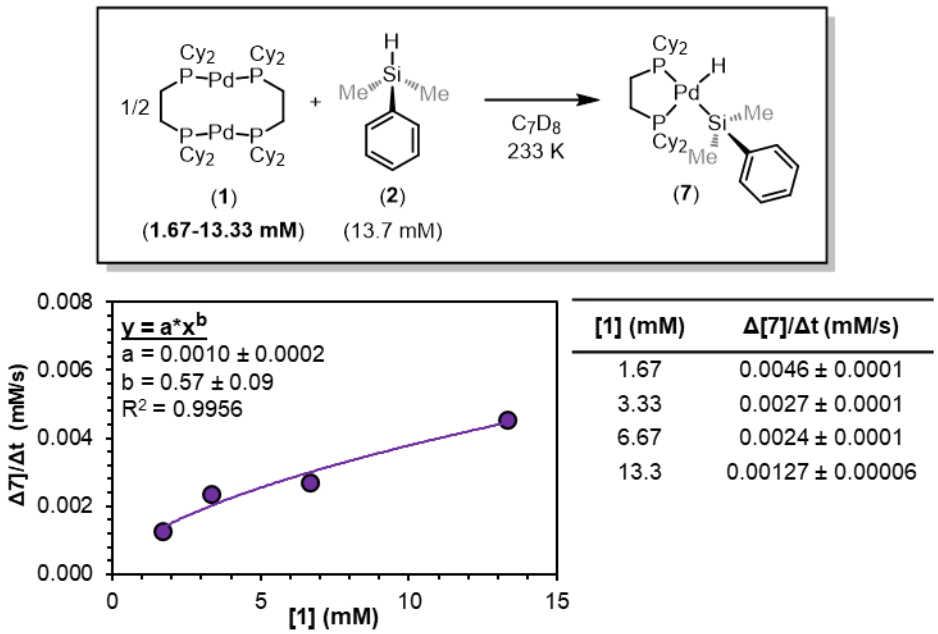

[1] (mM)	Δ[7]/Δt (mM/s)
1.67	0.0046 ± 0.0001
3.33	0.0027 ± 0.0001
6.67	0.0024 ± 0.0001
13.3	0.00127 ± 0.00006

Figure 2.8. Plot of initial rate versus [**1**]. Kinetics data was collected in C_7D_8 as the solvent at 233 K. Product concentration was determined by ^{31}P NMR integration against an internal standard.

As shown in Figure 2.8, the reaction was determined to be 0.5th order (0.57 ± 0.09) in dimer **1**. This result is consistent with any of the three steps in the mechanism of Figure 2.7 being the RDS, and supports the hypothesis that the dimer **1** dissociates into two [(dcpe)Pd] fragments (**10**) prior to or during the RDS. We next determined the order in silane (Figure 2.9). A plot of the initial rate versus the concentration of **2** shows that the reaction is 1st order (0.9 ± 0.1) in silane. This suggests the silane is involved in or before the RDS, and thus dimer dissociation (*step i*) of the mechanism in Figure 2.7 can be ruled out as the RDS.

With these data, the simplified rate law of the reaction can be written (equation 1), showing an overall 1.5th order reaction.

$$Rate = k_{obs}[\mathbf{1}]^{0.5}[\mathbf{2}] \qquad (1)$$

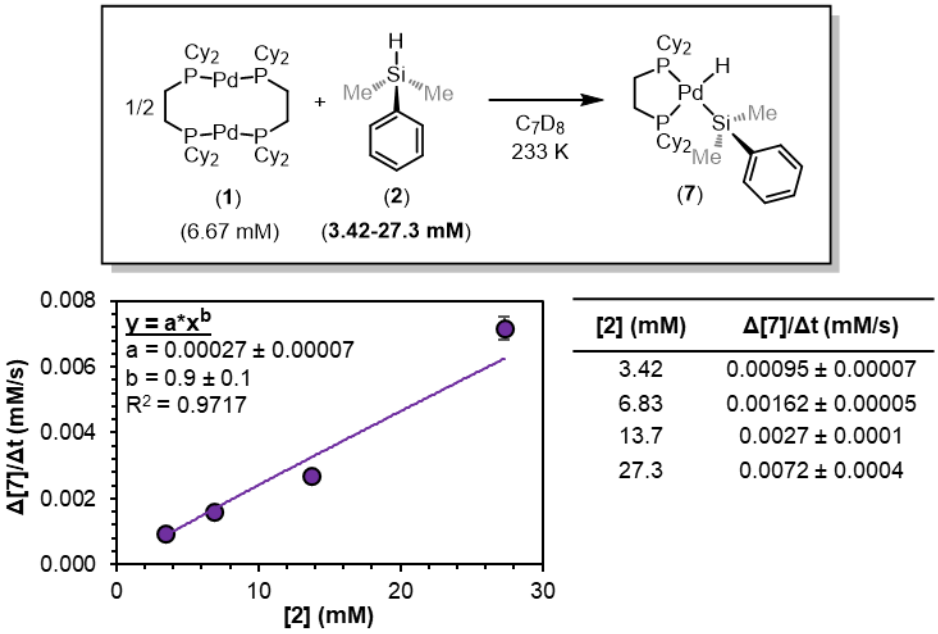

[2] (mM)	Δ[7]/Δt (mM/s)
3.42	0.00095 ± 0.00007
6.83	0.00162 ± 0.00005
13.7	0.0027 ± 0.0001
27.3	0.0072 ± 0.0004

Figure 2.9. Plot of initial rate versus [**2**]. Kinetics data was collected in C_7D_8 at 233 K. Product concentration was determined by $^{31}P\{^1H\}$ NMR integration against an internal standard.

To help differentiate between these two steps being the RDS, the KIE of the reaction was determined. The initial rate of reaction for $DSiPhMe_2$ (**3-d$_1$**) was measured, and it was found to react more slowly than **3**, with a KIE of 1.21 ± 0.04 (Figure 2.10). The maximum primary KIE possible for Si–H/Si–D without invoking tunnelling is ~4. Therefore, a KIE of 1.21 is large enough to be considered a primary isotope effect, but the magnitude is small and challenging to interpret. Either *step ii* is the RDS, in which a smaller magnitude KIE is rationalized by the Si–H bond not being formally broken in the transition state; or *step iii* is the RDS, in which a very early transition state (which is expected due to the high energy of the σ-complex) would lead to a lower magnitude KIE. Notably, the KIE reported here is consistent with those of other oxidative addition studies and catalytic reactions involving Si–H and C–H bond cleavage.[78]

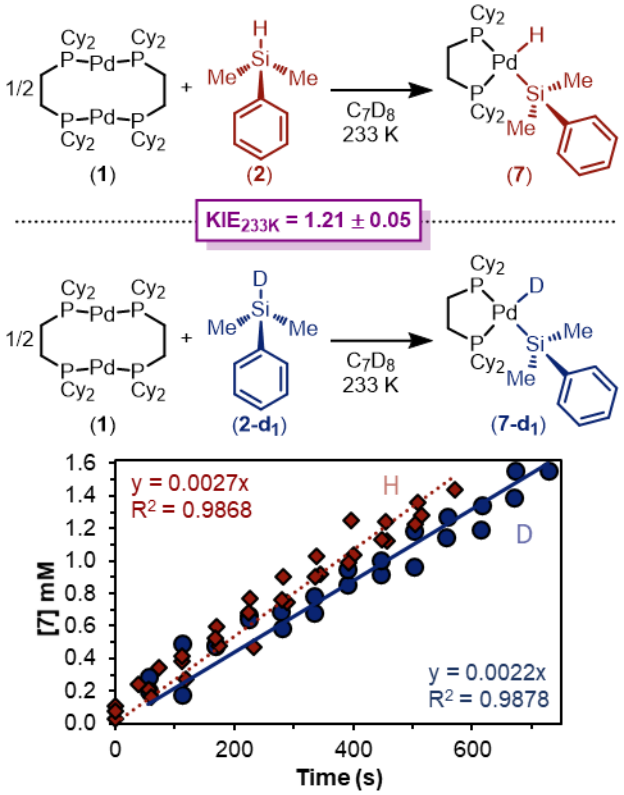

Figure 2.10. Plot of [**7**] or [**7-d$_1$**] versus time. Kinetics data was collected in C_7D_8 (13.33 mM) as the solvent at 233 K after thawing the sample from liquid nitrogen. Product concentration was determined by ^{31}P NMR integration; 1.00 equiv of **1** and 2.05 equiv of **2** or **2-d$_1$** were used.

We next sought to measure the barrier ($\Delta G^{\ddagger}_{OA}$) for the overall reaction by performing an Eyring analysis. The rate of reaction was measured as a function of temperature, and the results are seen in Figure 2.11. $\Delta H^{\ddagger}_{OA}$ and $\Delta S^{\ddagger}_{OA}$ are obtained from the equation of the fit of the data, and as a result, $\Delta G^{\ddagger}_{OA}$ at a given temperature can be calculated. From the data in Figure 2.11, $\Delta H^{\ddagger}_{OA}$ was determined to be 6.0 ± 0.3 kcal•mol^{-1}, $\Delta S^{\ddagger}_{OA}$ was determined to be -40 ± 20 cal•mol^{-1}•K^{-1}, and therefore $\Delta G^{\ddagger}_{OA}$ at 233 K was calculated to be 16.3 ± 0.3 kcal•mol^{-1}. This large, negative value for $\Delta S^{\ddagger}_{OA}$ supports the proposed mechanism in Figure 2.7. The transition state of the RDS is highly ordered relative to the ground state, consistent with *step ii* or *iii* being the RDS.

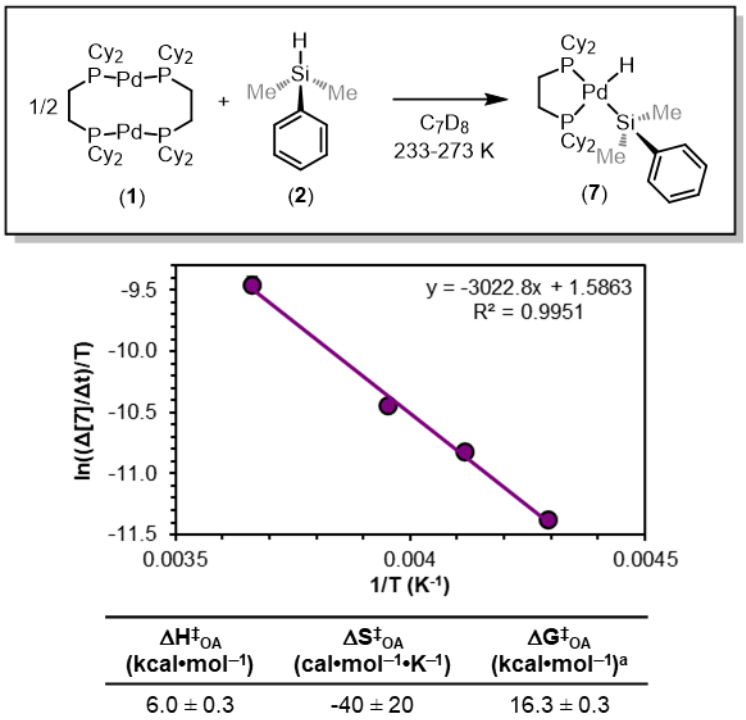

$\Delta H^{\ddagger}_{OA}$ (kcal•mol^{-1})	$\Delta S^{\ddagger}_{OA}$ (cal•mol^{-1}•K^{-1})	$\Delta G^{\ddagger}_{OA}$ (kcal•mol^{-1})[a]
6.0 ± 0.3	-40 ± 20	16.3 ± 0.3

Figure 2.11. Eyring plot constructed from variable temperature kinetics data in C_7D_8 (13.33 mM). Product concentration was determined by ^{31}P NMR integration; 1.00 equiv of **1** and 2.05 equiv of **2** was used. $^{a}\Delta G^{\ddagger}_{DE}$ determined at 233 K.

Dynamic exchange behavior

One interesting feature of these silyl metal hydride complexes is their fluxional behaviour in solution.[33–35,79,80] We recognized that investigating this dynamic exchange (DE) behaviour would provide insight into the overall reaction mechanism of oxidative addition because it offers a unique chance to probe the oxidative cleavage and reductive coupling steps (k_3 and k_{-3}, respectively, in Figure 2.7) independent of the overall oxidative addition process. Accordingly, solution ^{1}H and $^{31}P\{^{1}H\}$ NMR spectra of product **7** were recorded at multiple temperatures (Figure 2.12). At very low temperatures, the $^{31}P\{^{1}H\}$ NMR spectrum shows two singlets (δ 58.4 and 57.4 ppm at 183 K) which undergo coalescence at 213 K, eventually forming a sharp singlet (δ 56.4 ppm at 273 K) (Figure 2.12a). Similar behaviour is seen for the Pd–H peak in the ^{1}H NMR spectra at low temperatures; a doublet of doublets (δ -1.39 ppm, $^{2}J_{P–H(trans)}$ = 192.6 Hz, $^{2}J_{P-H(cis)}$ = 7.9 Hz at 183 K) proceeds through coalescence at 213 K to eventually form an apparent triplet,

centering at -1.71 ppm, $^{2}J_{P-H}$ = 75.4 Hz at 273 K) (Figure 2.12b). Line broadening analysis[81,82] allows for the calculation of the barriers for this dynamic exchange (DE) process. $\Delta H^{\ddagger}_{DE}$, $\Delta S^{\ddagger}_{DE}$, and $\Delta G^{\ddagger}_{DE}$ at 233 K were determined to be 7.7 ± 0.4 kcal•mol^{-1}, -10.7 ± 0.5 cal•mol^{-1}•K, and 10.2 ± 0.4 kcal•mol^{-1}, respectively.

In analogy to reported complexes and their dynamic exchange behavior,[46,66–68] we propose a mechanism in Scheme 1 that accounts for these NMR spectra. **7** and **7'** are proposed to interconvert via the σ-complexes **11** and **11'**, which themselves interconvert by rotation around the Pd–(η^2-H–SiMe$_2$Ph) bond (k_4 and k_{-4}). Conversion of **7** into **11** and **7'** into **11'** are reductive coupling steps (k_{-3}), the microscopic reverse of oxidative cleavage (k_3).

At elevated temperatures, exchange is rapid on the NMR timescale, and the Pd–H signal in the ^{1}H NMR appears as a triplet due to coupling to both P nuclei, and the coupling constant is an average of the trans and the cis $^{2}J_{P-H}$ values. This interpretation is supported by the $^{31}P\{^{1}H\}$ NMR data, which shows a singlet at elevated temperatures. Upon cooling, the Pd–H signal (^{1}H NMR) undergoes coalescence and gradually resolves into a doublet of doublets at sufficiently low temperatures. The splitting pattern is accounted for by the inequivalency of the P nuclei; at low temperature in the $^{31}P\{^{1}H\}$ NMR, two distinct phosphorous environments are observed, as exchange is sufficiently slowed and both P nuclei environments (P and P' in Scheme 1) are discrete. The tuneability of this process from slow-exchange to fast-exchange over an accessible temperature range indicates a relatively small energy barrier for conversion between species, and is consistent with the measured barrier of 10.2 ± 0.4 kcal•mol^{-1} at 233 K.

Important for the overall oxidative addition reaction (formation of **7** from **1** and **2**), the RDS of this dynamic exchange process is either the barrier for reductive coupling/oxidative cleavage (k_{-3}/k_3) or the barrier for rotation (k_4/k_{-4}). Therefore, the oxidative cleavage step (k_3) must be equal to or less than 10.2 ± 0.4 kcal•mol^{-1} at 233 K.

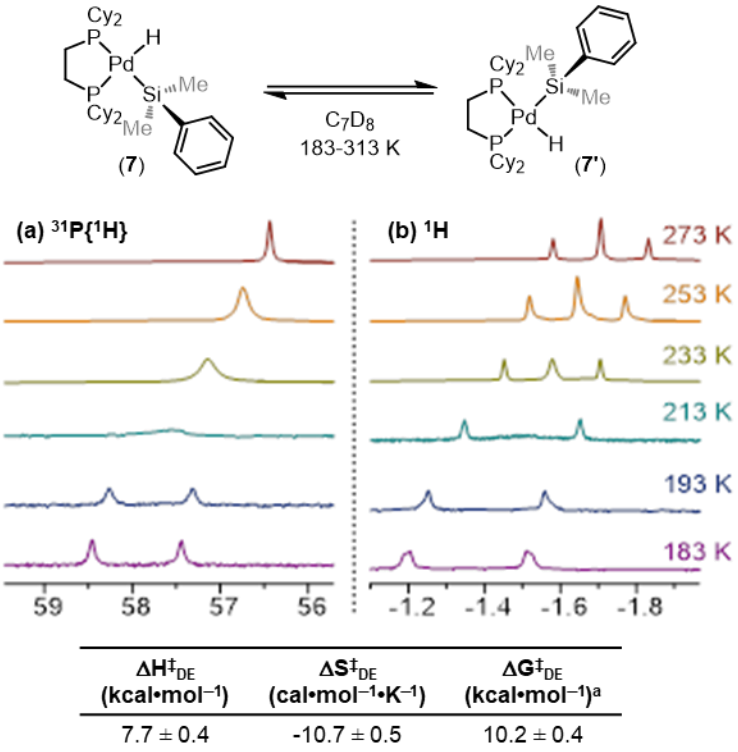

$\Delta H^{\ddagger}_{DE}$ (kcal•mol^{-1})	$\Delta S^{\ddagger}_{DE}$ (cal•mol^{-1}•K^{-1})	$\Delta G^{\ddagger}_{DE}$ (kcal•mol^{-1})[a]
7.7 ± 0.4	-10.7 ± 0.5	10.2 ± 0.4

Figure 2.12. (a) $^{31}P\{^{1}H\}$ NMR and (b) ^{1}H NMR spectra as a function of temperature with the measured barriers for dynamic exchange (DE). Spectra collected in C_7D_8 (13.33 mM). [a]$\Delta G^{\ddagger}_{DE}$ determined at 233 K.

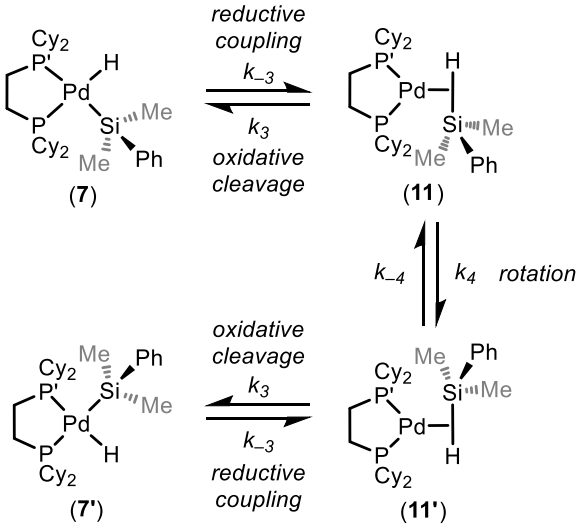

Scheme 2.1 Proposed mechanism for the intramolecular dynamic exchange of –H and –$SiMe_2Ph$ environments

Constructing a reaction coordinate diagram

Taking our findings from equilibrium and kinetic studies, we have constructed a complete mechanistic picture for the oxidative addition of silanes to **1**. With the bulk of the data obtained using dimethylphenyl silane **2**, we focus on those results in the discussion below (Figure 2.13), but we expect the general trends to be analogous for the other silanes studied in this work.

ΔG^{o}_{OA} was determined in the course of studying the reaction equilibrium. K_{eq} for the reaction between **2** and **1** at 233 K was determined to be 125, corresponding to ΔG^{o}_{OA} = -6 ± 1 kcal•mol^{-1} (Figure 2.13). Thus, the silyl palladium hydride **7** is lower in energy by 6 kcal•mol^{-1} than the starting materials **1** and **2**.

The reaction was found to be 1st order in silane **2** (Figure 2.9) and 0.5th order in palladium dimer **1** (Figure 2.8). Because there is a dependence on the silane on the rate of reaction, dimer dissociation (**1** → **10**) is ruled out as the RDS. Therefore, either formation of the σ-complex **11** or oxidative cleavage of the Si–H bond must be the RDS, since both would account for the observed orders in reactants. Based on the small, but primary KIE of 1.21 ± 0.04 (Figure 2.10), we hypothesized that formation of the σ-complex **11** is the RDS, since cleavage of the Si–H bond is expected to result in a larger KIE value. However, this is not definitive evidence.

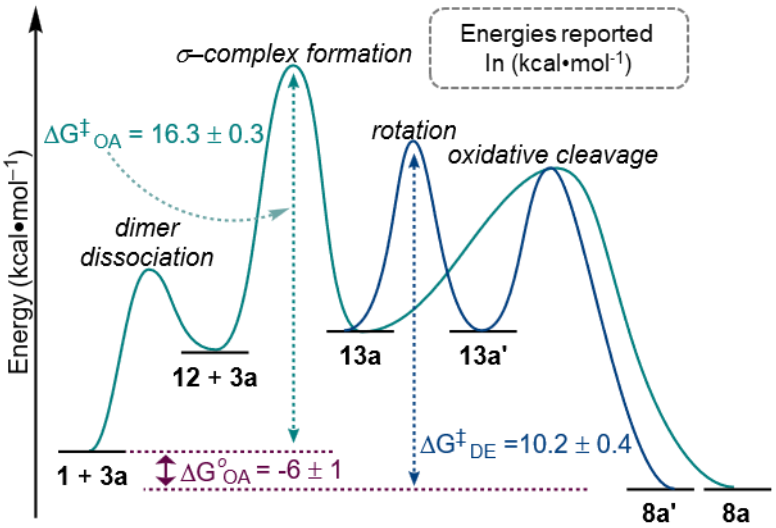

Figure 2.13. Reaction coordinate diagram with experimentally determined free energy values at 233 K. OA, oxidative addition. DE, dynamic exchange..

The reaction barrier for the full oxidative addition process (**1** + **2** → **7**) was determined to be 16.3 ± 0.3 kcal•mol^{-1} by an Eyring analysis (Figure 2.11). By linewidth analysis of the $^{31}P\{^{1}H\}$ NMR spectra of product **7**, we determined that the barrier for the dynamic exchange process between **7** and **7'** via **11**/**11'** is 10.2 ± 0.4 kcal•mol^{-1} (Figure 2.12). Because no significant KIE was observed for the dynamic exchange process, we concluded that the RDS of dynamic exchange is likely rotation. Therefore, the maximum barrier of reductive coupling (the microscopic reverse of oxidative cleavage, or **7** → **11**) is equal to or lower than 10 kcal•mol^{-1}. If oxidative cleavage (**11** → **7**) was the RDS, then the maximum overall reaction barrier for oxidative addition would be the sum of ΔG^{o}_{OA} (-6 ± 1 kcal•mol^{-1}) and $\Delta G^{\ddagger}_{DE}$ (10.2 ± 0.4 kcal•mol^{-1}). This sum (4 kcal•mol^{-1}) is much less than the measured free energy barrier for oxidative addition (16.3 ± 0.3 kcal•mol^{-1}). Therefore, formation of the σ-complex (*step ii* in Figure 2.7) is deduced to be the RDS. Because of the importance in oxidative addition reactions in catalysis, we expect this finding to affect the design of silanes and catalysts for many catalytic reactions.

Conclusion

In this work, we have elucidated the mechanism of oxidative addition of Pd(0) to Si–H bonds. We examined the reaction of **1** with a small library of tertiary silanes **2**-**5** to yield well-defined, mononuclear silyl palladium hydrides **6**-**9**. The formed silyl palladium hydrides exist in a dynamic equilibrium with **1** that is fully reversible with regard to temperature. This reversibility was exploited to conduct a van't Hoff analysis, from which we determined the ground state energy barrier to oxidative addition. Future study will investigate the impact of silane substituents with varied electronic and steric properties.

Further, this system is well-suited to answer long-standing questions in the oxidative addition of palladium to hydrosilanes via mechanism elucidation. The reaction is 0.5th order in starting dimer **1** and 1st order in silane **2**. The reaction barrier was determined to be 16.3 kcal•mol^{-1} using Eyring analysis. This energy far exceeds the barrier of oxidative cleavage of the Si-H bond, (determined to be

equal to or less than 10 kcal•mol^{-1}). In conjunction with a small, primary KIE, we conclude that the RDS of oxidative addition is the formation of the σ-complex, not Si–H bond cleavage. This insight will allow for the rational optimization of new catalysts and reaction partners for hydrosilylation, supporting the importance of in-depth mechanistic studies in catalysis.

Perspective and Outlook

The oxidative addition of Pd to Si–H bonds is a crucial step in a variety of catalytic applications, yet many aspects of this reaction are poorly understood. One important yet underexplored aspect is the mechanism of reaction. In this Chapter we have described a systematic investigation of the formation of silyl palladium hydride complexes through the oxidative addition of **1** to tertiary silanes. Our results give unique insight into the individual steps of oxidative addition and suggest the initial formation of a σ-complex intermediate to be rate-limiting. The insight gained from these mechanistic studies will be applied to studying hydrosilylation reactions catalyzed by **1**, motivating the importance of studying the mechanism of individual reaction steps within multistep catalytic transformations. Importantly, this work lays the foundation for the mechanistically driven development of new catalysts and new transformations in organosilicon chemistry.

3. SILANE ELECTRONIC EFFECTS IN THE OXIDATIVE ADDITION OF PALLADIUM(0) TO HYDROSILANES

From Hurst, M.R., Zakharov, L.N., Cook, A.K. “The Mechanism of Oxidative Addition of Pd(0) to Si–H Bonds: Electronic Effects, Reaction Mechanism, and Hydrosilylation.” *Chem. Sci.* **2021**, 12, 13045-13060.

Introduction

Palladium hydrides are a unique class of organometallic compounds, commonly proposed as intermediates in various Pd-catalyzed transformations.[1,2] One interesting class of molecular palladium hydrides are silyl palladium hydrides, which are formed from the oxidative addition of Pd(0) to the Si–H bond of a silane.[3–5] Silyl palladium hydrides are implicated as active species or important intermediates in reactions such as carbene insertion to triorganosilanes,[6–8] cross-coupling of C(sp3)–Si bonds,[9,10] hydodehalogenation of organic halides;[11–16] yet, direct observation or isolation of these species is uncommon and thus their study in experimental work is limited.[1–5,17]

Perhaps the most prominent reaction that relies on the formation of silyl metal hydrides is alkene and alkyne hydrosilylation.[18–23] Hydrosilylation is the main route to synthesizing important organosilicon compounds that go on to be used in polymers,[24–27] medicines,[28–31] and fine chemicals, among other applications.[32] Given this broad importance, much study has gone into optimizing this reaction with traditional platinum catalysts.[20,33–35] Palladium-catalyzed hydrosilylation offers powerful and complementary reactivity to these systems and is likewise proposed to proceed through silyl metal hydride intermediates.[20,36–41]

A key limitation that unifies late transition metal-catalyzed hydrosilylation and other reactions of silanes is the dependence on silane identity; most reactions are heavily dependent on the number of substituents (primary vs. secondary silanes, etc.) on silicon, and most protocols do not investigate the electronic and/or steric effects of the silane substituents.

Furthermore, in the limited reports on observable silyl palladium hydrides,[42–46] the effect of silane substituent has not been systematically explored.

In these previous studies, the silane substituents were restricted to alkyl and phenyl groups (Figure 3.1), yet trends found computationally suggest that inductive electronic effects of silane substituents dictate reactivity.[47,48] Given the importance of electronic and steric diversity in substrates for catalysis, this dearth of experimental support is detrimental to efforts in developing and optimizing catalytic processes; a more thorough investigation into how silane substituents affect the reaction with Pd(0) complexes is needed.

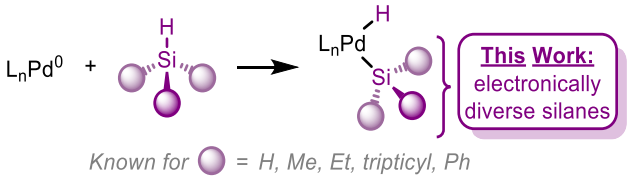

Figure 3.1. Previously examined silanes for oxidative addition with Pd

In this Chapter, we fill in the crucial gaps in knowledge regarding the effect of silane electronics on the thermodynamics and kinetics of the oxidative addition of Pd(0) to tertiary silanes. These results show a pronounced electronic effect to strongly favor silanes with electron-withdrawing groups both kinetically and thermodynamically. Additionally, insight into this electronic influence supports the proposed mechanism that we recently proposed for this reaction (Chapter 2).

Results and Discussion

Initial reactivity studies of [(μ-dcpe)Pd]$_2$ (1) with silanes

We began by investigating the reactivity of a library of tertiary silanes with [(μ-dcpe)Pd]$_2$ (**1**) by ^{1}H and ^{31}P NMR (Figure 3.2). As described in Chapter 2, these reactions proceed cleanly and, by NMR, only the reactants and the product are observed. For silanes with at least one phenyl ring or alkoxide substituent, the reactions proceed in good to excellent conversions (formation of complexes **8**-**11**), but peralkyl-substituted silanes are unreactive (complex **7**). A comparison of the data shown in Figure 3.2 reveals that higher conversions are obtained with increasing number of aryl and alkoxide substituents on the silane. This trend

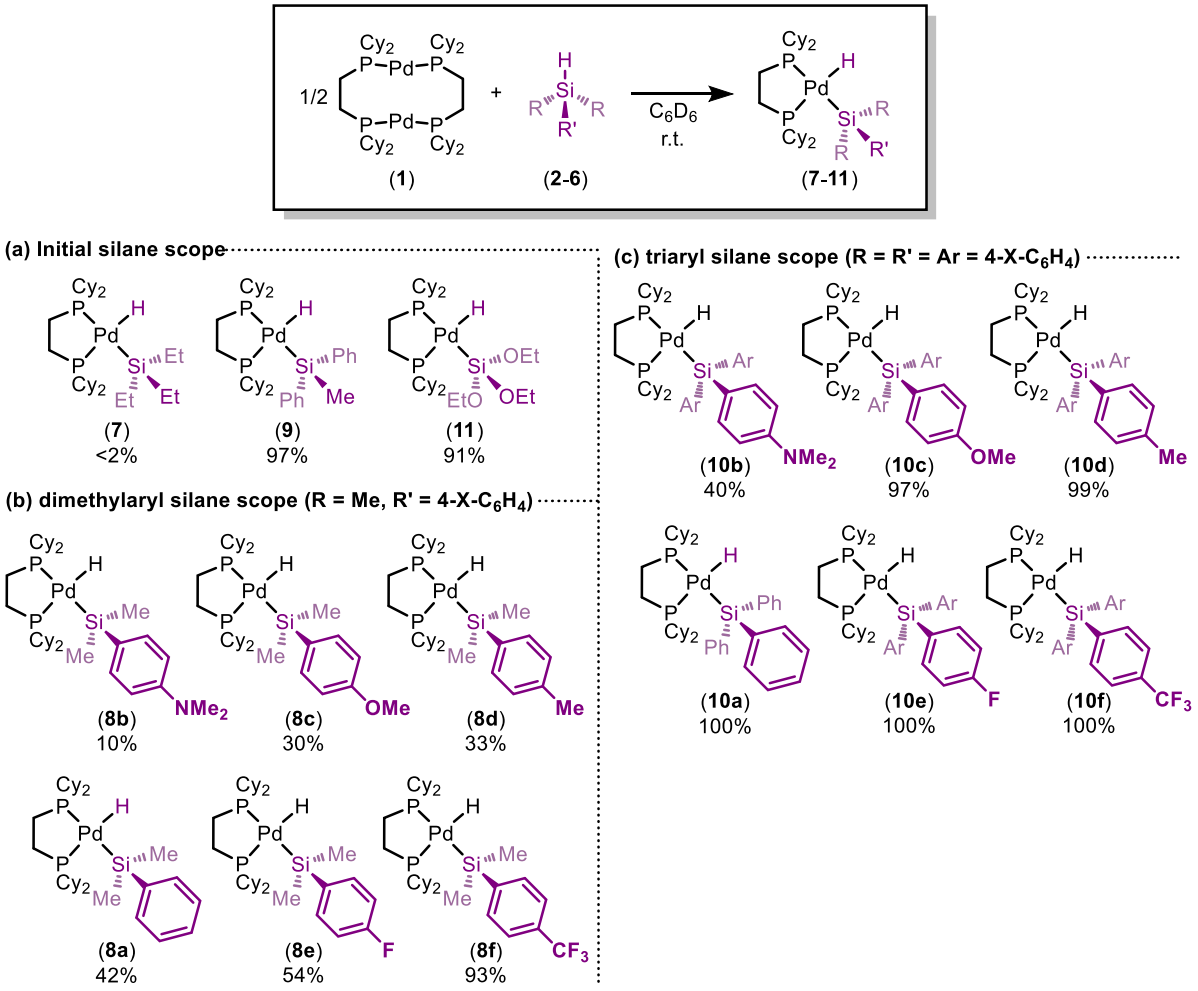

Figure 3.2. Scope of silane reactivity in oxidative addition with [(μ-dcpe)Pd]$_2$ (**1**). Percent conversions were determined by NMR integrations. Reaction conditions: 1.00 equiv of **1**, 2.05 equiv of **2**-**6**, 13.33 mM in C_6D_6, and 4-6 h. (a) Initial silane scope. (b) Scope of electronically diverse dimethylaryl silanes. (c) Scope of electronically diverse triaryl silanes.

correlates well with the electronegativity of the atoms attached to Si (11 > 10a > 9 > 8a > 7).[49] While this trend is revealing, we sought to decouple the kinetic effects from the thermodynamic effects and systematically investigate the electronic influence on each parameter of the reaction.

Electronic effects in oxidative Addition of Pd(0) to silanes

To probe our hypothesis that the oxidative addition of silanes to Pd(0) is more facile with electron-poor silanes, a library of electronically diverse

triarylsilanes were synthesized and evaluated in the reaction. The targeted silanes span a gradient of electronic character, with substituents in the para position ranging from electron-donating (X = NMe_2, OMe, Me) to electron-withdrawing (X = F, CF_3). Reactions of these silanes **5** with **1** cleanly yield the expected (dcpe)Pd($SiAr_3$)(H) complexes **10a**-**f** (Figure 3.2c), all in excellent NMR conversions except for the reaction with the electron-rich 4-dimethylaminophenyl-substituted silane (**5b** → **10b**, mass balance is remaining starting material).

A translucent, off-white crystal of (dcpe)PdH(Si(4-CF_3-Ph)$_3$) (**10f**) suitable for single crystal diffraction was grown from a reaction mixture of **1** and HSi(4-CF_3-Ph)$_3$ (**5f**) in benzene/hexane (Figure 3.3). Product **10f** displays nearly ideal square planar geometry around the palladium atom, with the summed total of bond angles equal to 360°. To get a more precise measure of the structure's geometry, the structural parameter τ_4 was calculated from crystallographic data.[50,51] Analysis of **10f** gives τ_4 = 0.15, where τ_4 = 0 indicates an ideally square planar complex, and τ_4 = 1 represents a tetrahedral complex. The τ_4 value of **10f** can be compared to

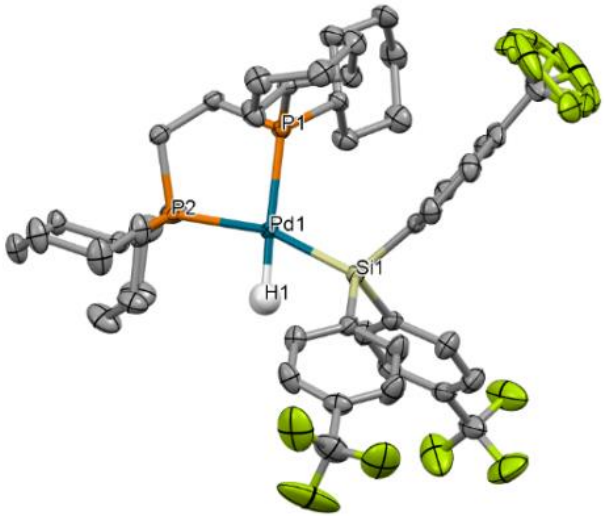

Figure 3.3. Molecular structure of (dcpe)Pd(H)[Si(4-CF_3Ph)$_3$] (**10f**). Thermal ellipsoids are drawn at 50% probability level. Hydrogen atoms except for Pd–H are omitted for clarity. Selected bond lengths (Å) and angles (deg): Pd1–H1 1.59(3), Pd1–Si1 2.3412(7), Pd1–P1 2.3422(7), Pd1–P2 2.3584(7), H1–Pd1–Si1 67(1), H1–Pd1–P2 96(1), P1–Pd1–P2 86.45(2), P1–Pd1–Si1 111.01(2). One CF_3 group is highly disordered and was refined as being located in three positions with an occupation factor of 0.33 each.

similar complexes that include the Pd–H bond (allowing calculation of τ_4): Ishii's (dcpe)PdH(SiH_2Trip) (Trip = 9-triptycyl)[44] complex gives τ_4 = 0.11 and Iluc's (P~P)Pd(H)($SiHPh_2$) complex gives τ_4 = 0.39 (Table S38).[45] **10f** is therefore comparable to known square planar silyl palladium hydride complexes. Deviation from square planarity is likely due to steric repulsion between the cyclohexyl substituents of dcpe and the aryl groups of the silane.

Solid-state geometry also gives information on the strength of each ligand's trans influence. Silyl ligands are known for being among the strongest trans-influencing ligands.[52–54] Therefore, we expect that the Pd–P bond trans to the silyl ligand will be longer than the Pd–P bond trans to the H; indeed, this is the case for complex **10f**, which has Pd–P bond lengths of 2.3584(7) Å and 2.3422(7) Å, respectively.

Comparing the Pd–P bond lengths in related complexes gives insight into the trans-influencing ability of the 4-CF_3-phenyl substituents of the silane. The Pd–P bond length trans to the silyl ligand in complex **10a**[42] and Ishii's complex[44] are 2.350(2) Å and 2.3319(14) Å, respectively. With no change in ancillary ligand (dcpe) across all three cases, these results indicate that the –Si(4-CF_3-Ph)$_3$ group has a stronger trans influence than the –$SiPh_3$ group, which in turn is stronger than –SiH_2Trip**.**

Returning to our hypothesis on the effect of electronic character of the silane on oxidative addition, no useful distinctions could be made using the data in Figure 3.2c, as most triaryl silanes exhibit similar reactivity. We thus turned to less reactive dimethylaryl silanes to further probe the influence of silane electronics on oxidative addition. The reaction of each dimethylaryl silane with **1** yielded the desired products (**8a**-**f**) (Figure 3.2b), though to lower conversion than with triaryl silanes. The formed (silyl)Pd(H) complexes exhibit similar spectroscopic characteristics as described for their triaryl counterparts. The data in Figure 3.2b show a clear trend with respect to the electronic nature of the silane: more electron-poor silanes give higher conversions to the silyl palladium hydrides **8**.

Reaction Equilibrium

We previously observed that the reaction with $HSiPhMe_2$ (**4a**) was fully reversible with changing temperature (Chapter 2). We were interested to take advantage of the differential reactivity of electron-rich and -poor silanes to further probe this phenomenon: if the reaction is indeed reversible, then we expect that a silyl palladium hydride formed from an electron-rich silane should convert to the corresponding product of oxidative addition of an electron-poor silane if one is added. This reaction is expected to occur through reductive elimination of the electron-rich silane, followed by preferential oxidative addition of the electron-poor silane. [(4-tolyl)$_3$Si]Pd(H) (**10d**, formed in situ from **1** and **5d**) was reacted with triphenyl silane (**5a**), and conversion to an equilibrium mixture of 1:3.3 (**10d**/**10a**) was observed (Scheme 3.1). An analogous experiment with tris(4-fluorophenyl)silane (**5e**) added to a solution of pre-formed **10a** shows an equilibrium ratio of 1:2.8 (**10a**/**10e**) (Table S13). The formation of H_2 or *bis*-silyl by-products was not observed, and mass balance is consistently 100% against an internal standard. These data imply that the formation of silyl palladium hydrides is completely reversible with respect to product distribution.

To quantify the thermodynamic trend imparted by silane electronic character, we measured the equilibrium constants (K_{eq}) for the reactions of **1** with

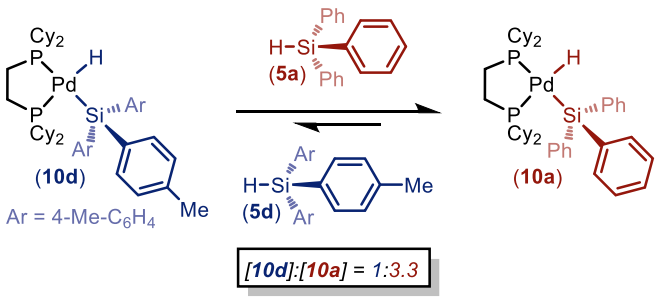

Scheme 3.1. Conversion of **10d** into **10a** via reversible oxidative addition. Experiment was performed in C_7D_8 and relative conversions were determined by ^{31}P NMR integration; Reaction conditions: 1.00 equiv of **1**, 2.05 equiv. each of **5a** and **5d**, 13.33 mM in C_7D_8, and 3 h.

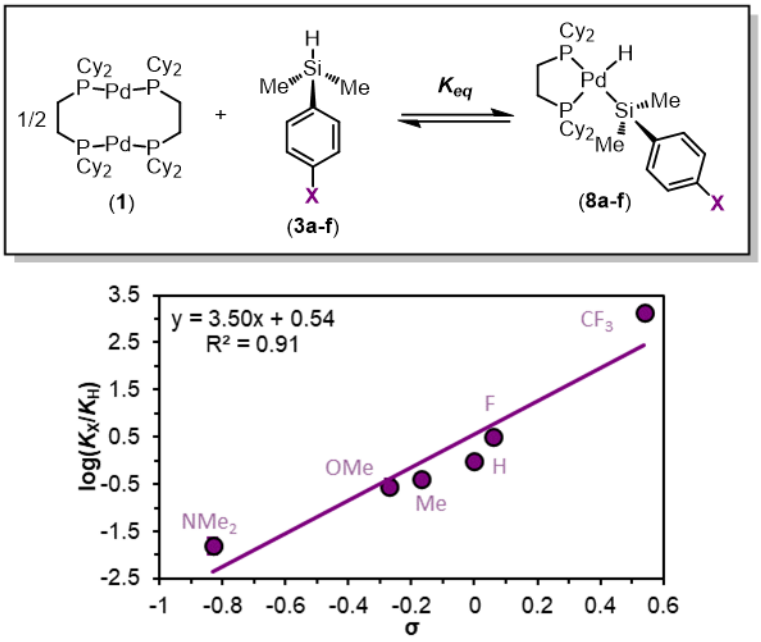

Figure 3.4. Hammett plot of the equilibrium constants for the reaction between dimethylaryl silanes **3** and **1**. K_{eq} values were determined using the NMR integrations of each product. Reaction conditions: 1.00 equiv of **1**, 2.05 equiv of **3a**-**f**, 13.33 mM in C_6D_6 at 298 K.

each silane **3a**-**f** and constructed a Hammett plot. This analysis gave a sensitivity constant, ρ_{eq} (eq indicates that this value is derived from equilibrium constants, as opposed to rates of reaction) of 3.5 ± 0.5 (Figure 3.4), consistent with the data in Figure 3.2b showing that the reaction is more favourable with electron-poor silanes.

We hypothesized that this observed trend in K_{eq}, and thus ΔG^o_{OA} (OA, oxidative addition), of the reaction is dictated by the varying bond strengths of the Pd–Si bonds, where stronger Pd–Si bonds are formed with electron-poor silanes. To deconvolute the enthalpic and entropic aspects to ΔG^o_{OA}, the equilibrium constants as a function of temperature were measured. van't Hoff analysis was carried out (Figure 3.5) for the reactions of **1** with **3a** (X=H), **3c** (X=OMe), and **3f** (X=CF_3). These particular silanes were chosen to represent a breadth of electronic character. The ΔS^o_{OA} values are large and negative, reflecting loss of entropy in this reaction between three reactants to form two products. ΔH^o_{OA} is negative for all three substrates, but more importantly, a clear trend is observed: **8f** < **8a** < **8c**

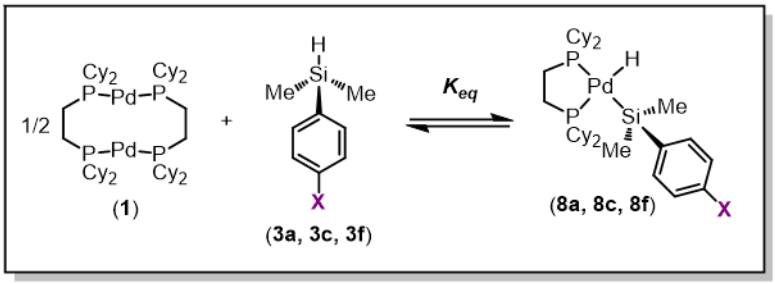

Entry	Product	–X	σ value[a]	ΔH^{o}_{OA} (kcal•mol^{-1})	ΔS^{o}_{OA} (cal•mol^{-1}•K^{-1})
1	8c	–OMe	-0.27	-15.3 ± 0.5	-45 ± 2
2	8a	–H	0	-19 ± 1	-55 ± 5
3	8f	–CF_3	0.54	-30 ± 3	-80 ± 10

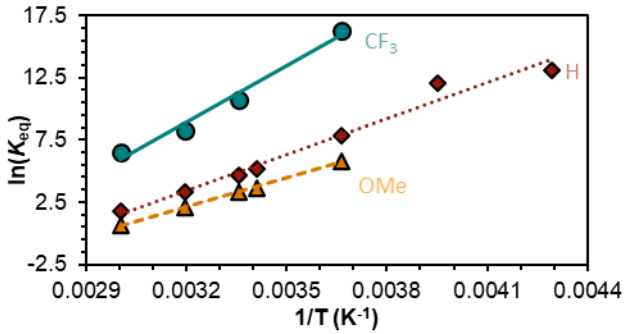

Figure 3.5. van't Hoff analyses of the reaction equilibrium between dimethylaryl silanes **3** and **1**. Reaction conditions: 1.00 equiv of **1**, 2.05 equiv of **3a, 3c or 3f**, 13.33 mM in C_7D_8, 253-333 K. [a]Reference [55].

(CF_3 < H < OMe) in ΔH^{o}_{OA}. These data show that the reaction between **1** and silanes **3** is more favourable with electron-poor silanes, which we interpret to mean that there is an increased strength of the Pd–Si bond in products **8**.[47]

To determine if this trend in the electronic influence of silanes is more general, we returned to triaryl silanes **5**. Because the equilibrium constants are too large to measure at room temperature under our standard conditions, we took advantage of the reaction's full reversibility in product distribution by performing competition experiments. In these experiments, 2.05 equivalents of each $HSiPh_3$ (**5a**) and $HSi(4\text{-X-Ph})_3$ (**5b**-**f**, X = NMe_2, OMe, Me, F, CF_3) were added to one equivalent of **1** (Figure 3.6).

As with the non-competitive oxidative addition reactions of dimethylaryl silanes **3a**-**f** (Figure 3.4), these data show that oxidative addition occurs preferentially with the more electron-poor silane. For example, when **5a** (a

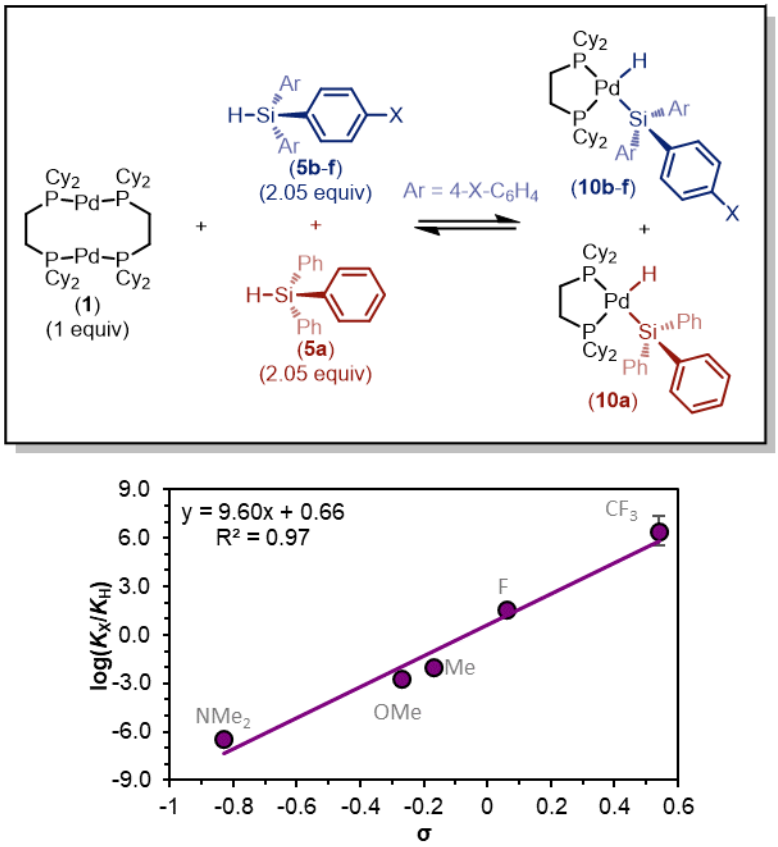

Figure 3.6. Competition experiment between **5a** and electronically diverse silanes **5b**-**f** for oxidative addition with **1**. Reaction conditions: 1.00 equiv of **1**, 2.05 equiv of **5a** plus 2.05 equiv of **5b-f**, 13.33 mM in C_6D_6, 298 K. Hammett plot constructed from K_{eq} values derived from conversions.

comparatively electron-neutral silane) and **5e** (an electron-poor silane) compete over the reaction with **1**, oxidative addition preferentially occurs with **5e** over **5a**, forming **10e** in larger concentrations than **10a**. Because the relative ratios of products are proportional to the ratios of equilibrium constants, a Hammett plot was constructed to quantify the effect of electronic factors on the equilibrium constant of oxidative addition (Figure 3.6). For triaryl silanes, Hammett analysis gives $\rho_{eq(comp)}$ = 9.6 ± 0.9, showing a more dramatic effect on K_{eq} than monoaryl silanes (non-competitive equilibrium data in Figure 3.4, ρ_{eq} = 3.5 ± 0.5). However, to allow for a direct comparison of the two systems, we additionally performed the same competition studies with dimethylaryl silanes **3a**-**f**. $\rho_{eq(comp)}$ was found to be

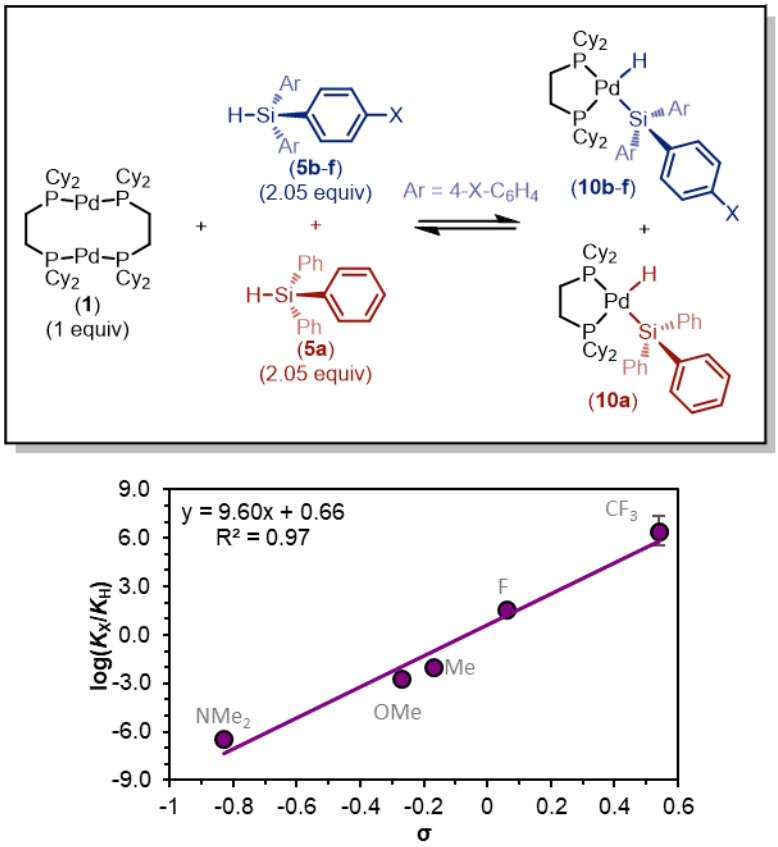

Figure 3.7. Competition experiment between **5a** and electronically diverse silanes **5b**-**f** for oxidative addition with **1**. Reaction conditions: 1.00 equiv of **1**, 2.05 equiv of **5a** plus 2.05 equiv of **5b-f**, 13.33 mM in C_6D_6, 298 K. Hammett plot constructed from K_{eq} values derived from conversions.

3.4 ± 0.3 with these dimethylaryl silanes. Notably, these data trend proportionally to the number of changing substituents at silicon.

Reaction kinetics

We next examined the effect of electronic substitution at silicon on rates of reaction via a Hammett analysis. Rates of reaction were measured using dimethylaryl silanes **3a**, **3c**, and **3f**, and these experiments reveal a marked influence of silane electronics on the initial rates of product formation. Analysis of kinetic trials for each silane gives a trend in k_{obs} of X = CF_3 > H > OMe, which follows the same trend as in equilibrium studies: strongly electron-withdrawing

substituents at silicon favour rapid oxidative addition, while electron-donating substituents hinder the reaction rate.

A Hammett plot was constructed from these data (Figure 3.7), which shows $\rho^{\ddagger}$ = 1.2 ± 0.3 (‡ notation is used to distinguish this sensitivity constant obtained from rates of reaction from the sensitivity constant obtained from reaction equilibrium constants (ρ_{eq})). Comparing the ρ values obtained for the reaction equilibrium (ρ_{eq} = 3.5 ± 0.5) with that obtained for rates ($\rho^{\ddagger}$ = 1.2 ± 0.3) reveals that the observed rate of oxidative addition is approximately three times less sensitive to changes in electronics as the equilibrium constant (K_{eq}).

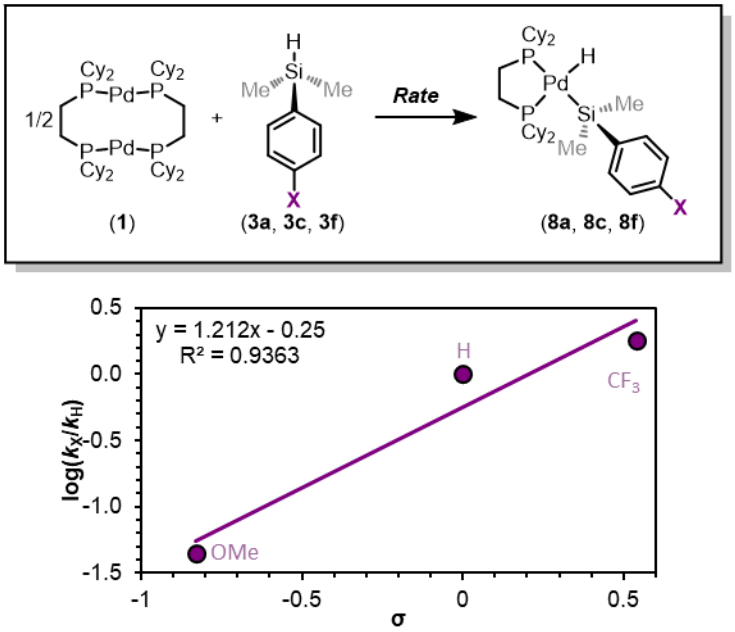

Figure 3.8. Hammett plot constructed from kinetic data. Kinetic data was collected in C_7D_8 (13.33 mM) as the solvent at 233 K. Product concentration was determined by ^{31}P NMR integration; 1.00 equiv of **1** and 2.05 equiv of **3a**, **3c**, or **3f** were used.

Dynamic exchange behavior

As described in Chapter 2, the formed silyl palladium hydride complexes **10** exhibit an intramolecular H/SiR_3 exchange process. In analogy to other examples reported with silyl metal hydrides,[3–5] we propose that this exchange proceeds first by reductive coupling of Si–H to form an intermediate Pd(η^2-H–SiR_3) σ-complex about which the silyl group rotates. Oxidative cleavage results in reformation of product **10'**. Importantly, for the silyl palladium complexes studied here, this

process occurs at rates observable on the NMR timescale. This results in a broadening of peaks in the NMR spectra that is dependent on the rate of exchange.

Taking advantage of line broadening analysis of the NMR spectra,[56,57] we sought to investigate the effect of silane substitution on the barriers for DE. We focused on triaryl silanes **5** because not all products with dimethylaryl silanes **3** reached the slow exchange regime at temperatures accessible in toluene-d_8. The activation parameters (Figure 3.8) show that there is no significant effect of electronic substitution on the rate of dynamic exchange for triaryl silanes since the measured barriers are mostly within error of one another. $\Delta H^{\ddagger}$ varies from 10-14 kcal•mol^{-1}, and $\Delta S^{\ddagger}$ is close to zero.

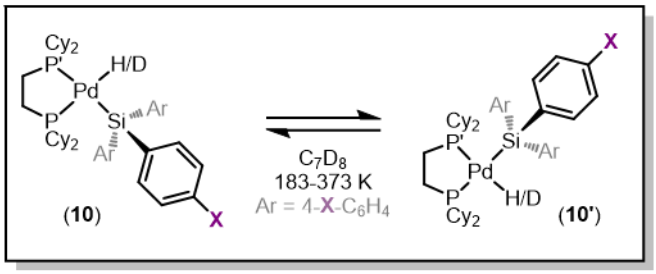

Entry	Pd Complex	H/D	X	$\Delta H^{\ddagger}_{DE}$	$\Delta S^{\ddagger}_{DE}$	$\Delta G^{\ddagger}_{DE}$
1	**10a**	H	H	12 ± 1	3.5 ± 0.3	11 ± 1
2	**10a-d_1**	D	H	10.0 ± 0.4	-2.46 ± 0.09	10.6 ± 0.4
3	**10c**	H	OMe	10.1 ± 0.4	-2.80 ± 0.09	10.7 ± 0.4
4	**10f**	H	CF_3	13.7 ± 0.5	5.5 ± 0.2	12.5 ± 0.5

Figure 3.9. Dynamic exchange (DE) barriers determined by linewidth analysis of ^{31}P NMR spectra at variable temperature. $\Delta H^{\ddagger}_{DE}$ and $\Delta G^{\ddagger}_{DE}$ are reported in kcal•mol^{-1} and $\Delta S^{\ddagger}_{DE}$ is reported in cal•mol^{-1}•K^{-1}. $\Delta G^{\ddagger}_{DE}$ determined at 233 K.

Together with equilibrium, competition, and kinetics experiments described above, these results are in line with the proposed mechanism we determined in Chapter 2. The pronounced electronic effect observed in the formation of silyl palladium hydrides – but not in their dynamic exchange behavior – presents greater insight into the factors dictating oxidative addition and, further, catalytic processes involving oxidative addition. Future work will apply these findings in catalyzing useful transformations of hydrosilanes, such as the hydrosilylation of arylacetylenes (Chapter 5).

Conclusion

In this work, we have studied the oxidative addition of [(μ-dcpe)Pd]2 (1) with tertiary silanes with the goal of determining the influence of silane electronics. To accomplish this, we synthesized a library of electronically varied silanes, and examined their reaction with 1 in equilibrium, competition, and kinetics experiments. Across all of these experiments, and quantified via Hammett analyses of both equilibrium constants and kinetic rates, electron-poor silanes were favored in the reaction.

The energetics of the oxidative addition with respect to silane electronic character was calculated based on van't Hoff and Eyring analyses of variable temperature equilibrium and kinetics experiments. Both kinetic and thermodynamic factors favor the formation of silyl palladium hydrides 10 with electron-poor silanes. On the other hand, the intramolecular H/SiR3 exhibited by these complexes is not significantly affected by silane electronic properties.

Overall, the work described in this Chapter supports our mechanistic proposal for the oxidative addition of **1** to silanes and provides a solid foundation for the development of catalytic applications using Pd(0) complexes. These findings complement our investigation into the role of silane steric bulk (Chapter 4) to provide the first systematic studies on the impact of silane substituents in the oxidative addition of Pd(0), which will have broad implications in late transition metal-catalyzed organosilicon chemistry.

Perspective and Outlook

In this Chapter, we uncovered a pronounced effect of silane electronics in the oxidative addition of Pd(0) to hydrosilanes based on both thermodynamic and kinetic trends. This fundamental reaction step is commonly proposed in Pd-catalyzed processes involving hydrosilanes, and thus understanding the role of silane substituents has the power to greatly optimize the study of these important reactions. We hope the results of this work will be applied to develop and rationalize the catalytic behavior of Pd species in important transformations in organosilicon chemistry.

4. SILANE STERIC EFFECTS IN THE OXIDATIVE ADDITION OF PALLADIUM(0) TO HYDROSILANES

From Hurst, M.R., Davis, A.G., Cook, A.K. “The Influence of Silane Steric Bulk on the Formation and Dynamic Behavior of Silyl Palladium Hydrides.” *Organometallics* **2022** *(accepted)*

Introduction

Organosilicon compounds find broad use in manufacturing and fine chemical synthesis.[1,2] Industrially, organosilicons are utilized as monomers in the production of various commercial products, primarily as polysiloxanes used in plastics, adhesives, and lubricants.[1,2] In synthesis, organosilicon compounds are useful as precursors in Hiyama cross-coupling,[3-5] in Fleming-Tamao oxidation to form alcohols,[6] and as biocompatible carbon isosteres in the synthesis of bioactive molecules or “sila-drugs.”[7,8]

Organosilicon compounds and polymers are typically prepared by the hydrosilylation of alkenes and alkynes, commonly catalyzed by late transition metals.[9-11] The first step in this catalytic cycle with platinum and related metals is usually oxidative addition of the metal center to the Si–H bond of a silane to form a silyl metal hydride intermediate (Figure 4.1a).[12,13] Studies employing palladium catalysts in hydrosilylation suggest a similar pathway;[9,14-16] however, little is known about the oxidative addition of Pd(0) to Si–H,[17-19] particularly with regard to silane substituent effects.[20-24] In addition to hydrosilylation, silyl palladium hydride complexes are implicated as catalysts or important intermediates in transformations ranging from the hydrodehalogenation of organic halides,[25,26] borylation of alkenes,[27-29] hydrocarboxylation of allenes and dienes,[30-33] carbene insertion to triorganosilanes,[34] cross-coupling to form C(sp^3)–Si bonds,[35-41] isomerization of olefins,[42-44] and reduction of alkenes, carbonyls, and allylic compounds,[43,45-48] amongst other reactions.[49-53] This broad applicability emphasizes the need to understand the formation and reactivity of silyl palladium hydrides.

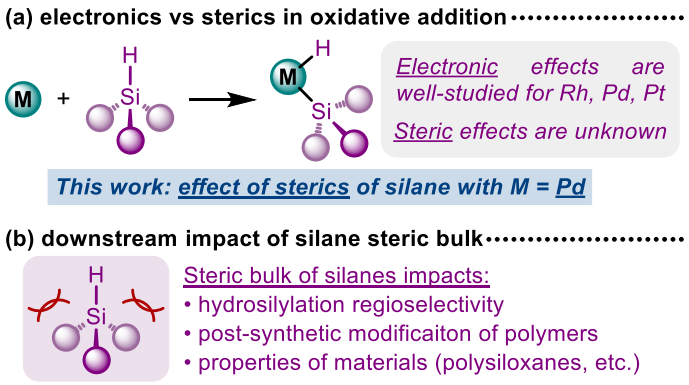

Figure 4.1. (a) Electronic effects in oxidative addition of silanes to metal centers is well-studied for Rh, Pd, and Pt, but steric effects are not well-understood. (b) Steric bulk of silanes impacts downstream properties of reactions (e.g., regioselectivity of hydrosilylation) and materials.

Recently, we investigated the impact of silane electronics on oxidative addition to Pd(0) and on Pd-catalyzed hydrosilylation. Oxidative addition of tertiary silanes to Pd(0), forming silyl palladium hydrides, is kinetically and thermodynamically more favorable with electron-poor silanes.[24] Importantly, we also showed that these trends translated to hydrosilylation activity: reaction rates and yields parallel the trends observed in oxidative addition, demonstrating the relevance of trends in oxidative addition to catalysis.

In addition to electronic factors, the steric profile of silanes plays an important role in their reactivity and properties, from the synthetic reactions to material properties (Figure 4.1b).[54,55] For example, the properties of polysiloxane polymers can be tuned by modification of the steric bulk of the sidechains at silicon,[56-59] and the aggregration behavior of siloxane-based surfactants is heavily affected by steric effects at silicon.[60-64] Late-stage modification of polysiloxanes and polybutadiene by transition metal-catalyzed hydrosilylation is hindered by sterically large substituents at silicon.[65-73]

In hydrosilylation reactions, the steric hindrance of silane substituents is observed to impact the regio- and stereoselectivity of the reaction for a wide range of metal catalysts including Pt,[74-79] Pd,[80-83] Ni,[84] Rh,[85-92] and other late transition metals.[93-98] Nonetheless, despite the proposed role of silane steric hindrance in

transformations involving silyl metal hydride intermediates, focused study on the impact of silane steric bulk in oxidative addition with late transition metals is scarce. In examples of oxidative addition using Ni,[99,100] Pd,[101-103] and Pt complexes,[104-106] tertiary silanes are observed to yield discrete silyl metal hydrides, while reacting the same complexes with secondary or primary silanes gives metal bis(silyl) species; yet, some silyl metal hydride complexes of Pd and Pt have been isolated from very bulky, primary silanes.[22,107,108] In contrast, systematic variation of silane substituents in the oxidative addition of tertiary silanes to Rh complexes reveal pronounced decrease in the rate of oxidative addition (and stability of formed products) with increasing steric bulk at silicon.[109,110] *Deeper understanding of the impact of silane steric bulk on the formation and stability of silyl metal complexes is necessary to more fully understand hydrosilylation reactions.*

Presented here is an investigation of the impact of the silane's steric bulk when undergoing oxidative addition with Pd(0). We focused this study on triaryl silanes, as aryl groups are easily tunable with sterically bulky substituents. Equilibrium studies and van't Hoff analyses reveal a high degree of steric dependence on the reaction, correlating well with Charton-Taft parameters and favoring less-bulky groups at silicon. Variable temperature studies likewise show that reaction rates depend on silane steric hindrance, with faster rates occuring with smaller substituents. On the other hand, bonding character and intramolecular exchange of H/SiR_3 ligand environments in the products (dcpe)PdH(SiR_3) are unaffected by steric bulk. Analysis of the energetics at each step sheds light on the factors that dictate the formation of silyl palladium hydrides, and reveal thermodynamics to be more important than kinetics in oxidative addition.

Results and Discussion

Steric effects in oxidative addition of Pd(0) to silanes

We initiated our study of silane steric effects by first investigating the reaction of [(μ-dcpe)Pd]$_2$ (**1**) with silanes varying numbers of 2-tolyl substituents: $HSiPh_3$ (**2**), $HSiPh_2$(2-Me-Ph) (**3a**), HSiPh(2-Me-Ph)$_2$ (**4**), and HSi(2-Me-Ph)$_3$ (**5**) (Figure 2a). We hypothesized that oxidative addition would be less favorable with

sterically bulky silanes because the silyl palladium hydrides would be more sterically encumbered than the starting materials. Previous work has shown that the stoichiometric reaction of **1** with **2** gives quantitative conversion to (dcpe)PdH($SiPh_3$) (**6**), as monitored by ^{31}P and ^{1}H NMR.[20,24] The silyl palladium hydride product exists in equilibrium with **1** and free silane in solution.

We first sought to determine whether substituents ortho to the silyl group on the silane were tolerated. Reacting 1 with silanes **2**, **3a**, **4**, and **5** at room temperature in benzene-d_6 resulted in product formation with **2**, **3a**, and **4**, but no new species were observed in the reaction with silane **5**. The products (dcpe)PdH($SiPh_3$) **6**, (dcpe)PdH[$SiPh_2$(2-Me-Ph)] **7a**, and (dcpe)PdH[SiPh(2-Me-Ph)$_2$] **8** show triplets in the upfield region of the ^{1}H NMR (~-1.9 ppm, $^{2}J_{H-P} \approx 76$ Hz), consistent with a Pd–H that is coupled to two phosphorus atoms. The $^{31}P\{^{1}H\}$ NMR spectra shows one singlet (~56 ppm), consistent with both phosphorus atoms being in one chemical environment, and the $^{29}Si\{^{1}H\}$ NMR spectra show one triplet (~5 ppm, $^{2}J_{Si-P}$ = 79 Hz), indicating coupling between the Si atom and both phosphorus atoms. All NMR data are consistent with the stucture drawn in Figure 2 and with previously published data.[20,24]

Quantifying the conversion of the oxidative addition reaction between **1** and silanes **2**-**5** reveals that a higher number of 2-Me-Ph substitutents at silicon decreases the reaction conversion (Figure 4.2). Conversion follows these trends for the formation of silyl palladium hydrides from silanes **2**, **3a**, **4**, and **5**, respectively: **6** (100%) > **7a** (85%) > **8** (15%) >> **9** (no reaction). In fact, oxidative addition to the highly sterically encumbered silane HSi(2- Me-Ph)$_3$ (**5**) does not proceed to form **9** under our standard conditions. These results confirm our hypothesis that increased steric bulk decreases the converstion to the silyl palladium hydride. More fine-tuning of the steric bulk was achieved using silanes of the form $HSiPh_2Ar$ (Ar = 2-Et–Ph, **3b**; Ar = 2-*i*-Pr-Ph, **3c**; Ar = mesityl, **3d**) (Figure 2b). Similar trends were observed, with the highest conversions occurring with silanes with the smallest steric profile.

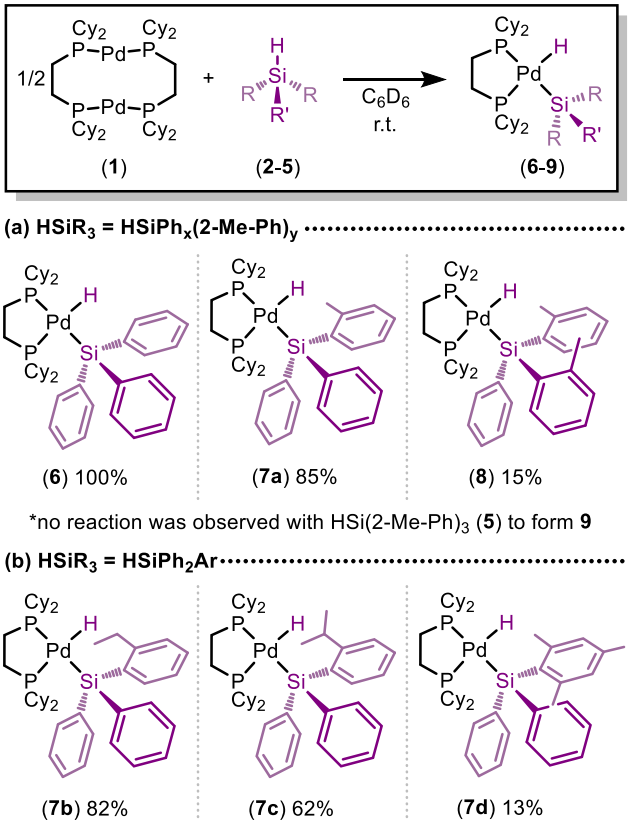

Figure 4.2. Scope of silane reactivity in oxidative addition with [(μ-dcpe)Pd]$_2$ (**1**). Percent conversions were determined by NMR integrations. Reaction conditions: 1.00 equiv of **1**, 2.05 equiv of **2**-**5**, 13.3 mM in C_6D_6, and 4-6 h. (a) Scope of Ph_x(2-Me-Ph)$_y$ substituted silanes **2**-**5**. (b) Scope of Ph_2(2-R-Ph) substituted silanes **3b**-**3d**.

We sought to investigate whether the substituents at silicon affect the strength of bonding between the silyl ligand and the metal center. It is well known that complexes of metals and silanes exist along a continuum spanning from the σ-complex M(η^2-H–SiR_3) to the fully oxidatively added complex, (silyl)M(H), which has no bonding character between the Si and the H. To differentiate (silyl)M(H) complexes from the non-classical σ-complexes, the measurement of $J_{Si–H}$ coupling constants in ^{1}H and/or ^{29}Si NMR is commonly used,[111-114] although it not a perfect measure of this bonding interaction.[115,116] Lower $J_{Si–H}$ values are indicative of a weaker residual Si–H interaction and, consequentially, more “complete” oxidative addition. By ^{1}H NMR, a modest increase of $J_{Si–H}$ is observed for complexes **6**, **7a**,

and **8** with larger silane substituents: **6** (29.2 Hz) < **7a** (30.5 Hz) < **8** (31.7 Hz), but does not constitute a significant change in bonding character.

Having qualitatively observed the importance of silane steric hindrance on oxidative addition, we next sought to probe this trend quantitatively. Electronic effects are commonly quantified by comparison of kinetic rates or equilibrium constants to substituent Hammett parameters.[117-119] Work by Taft,[120,121]I later modified by Charton and validated by Hansch,[122-124] established Taft-Charton steric parameters (*v*) as an empirically derived Linear Free Energy Relationship between rates of reaction and substituent steric bulk. Seeking to take advantage of these steric parameters, we studied the reaction between **1** silanes **3a**-**d** because of their systematic increasingly large alkyl substituents.

As shown in Figure 4.2b, conversion decreases with increasing steric bulk. The equilibrium constants for these reactions were found and are reported in Figure 4.3. The log(K_{eq}) values were plotted as a function of the Charton parameter, and excellent agreement is observed. Bulky $HSiPh_2Mes$ (**3d**; Mes, mesityl) follows well with this trend in K_{eq} when considering the Charton constant as the sum of its *ortho*-substituents. The measured steric sensitivity factor (ψ_{eq}) for oxidative addition with silanes **3a**-**d** is large and negative (-7.3 ± 0.6), confirming that oxidative addition of **1** to silanes with smaller alkyl substituents is thermodynamically more favorable than those with more encumbering substituents.

To shed light on the origin of this dependence on silane steric bulk in oxidative addition, variable temperature studies were conducted next. In these experiments, a stoichiometric mixture of **1** and silane **2**-**4** was monitored by ^{31}P, $^{31}P\{^1H\}$ and ^1H NMR as the solution was gradually warmed in 10-20 degree increments from -90 °C. In all cases, low temperatures favor the formation of silyl palladium hydrides **6**-**8**, while warming the reaction leads to clean regeneration of free silane and **1**. This reversibility is fully dynamic with respect to temperature; upon returning to a cooler temperature, **6**-**8** are reformed to give K_{eq} values within error of the initial measurements.

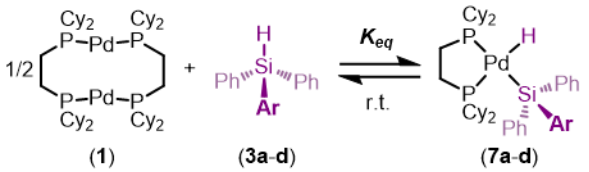

Entry	Silane	Product	Ar	*v* value	Conversion	log(K_{eq})
1	2a	6	Ph	0.00	100%	--
2	3a	7a	2-Me-Ph	0.52	85%	4.3
3	3b	7b	2-Et-Ph	0.56	82%	4.1
4	3c	7c	2-*i*-Pr-Ph	0.76	62%	3.0
5	3d	7d	Mes[a]	1.04[b]	13%	0.7

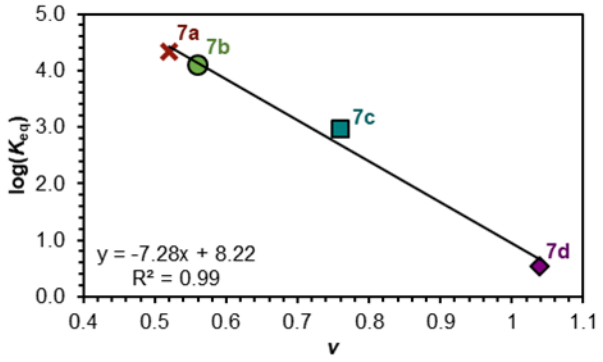

Figure 4.3. Charton plot of the equilibrium constants for the reaction between substituted $HSiPh_2$(2-R-Ph) **3a**-**d** and **1**. K_{eq} values were determined using the NMR integrations of each product. Reaction conditions: 1.00 equiv of **1**, 2.05 equiv of **3a**-**d**, 13.3 mM in C_6D_6 at 298 K. [a]Mes: 2,4,6-Me_3Ph. [b]*v* value for silane **3d** was calculated by summing the *v* values of the two substituents ortho to Si (both methyl groups).

Experiments with silanes **2**-**4** give excellent correlation of temperature-dependent equilibrium constants with increasing steric bulk (Figure 4.4; data for **6**, **7c**, and **7d** shown in plot). van't Hoff analysis of variable temperature experiments across the whole library of silanes allows for the determination of ground state energy parameters for the reaction with respect to silane identity (Figure 4.4). ΔS^o is large and negative for all substrates, which is expected for a reaction that loses entropy (1.5 molecules as reactants converting to 1 molecule as the product). Analysis of ΔG^o calculated at 263 K shows that the reaction is more favorable with decreasing steric bulk, spanning more than 10 kcal•mol^{-1} from **6** to **7d**.

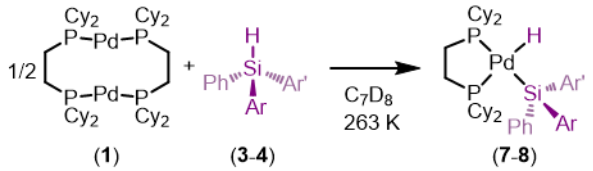

(**1**) (**3**-**4**) (**7**-**8**)

Product	Ar	Ar'	*v*	Δ*H*°	Δ*S*°	Δ*G*°$_{263K}$
6	Ph	Ph	0	-30.3 ± 0.8	-66 ± 2	-13 ± 1
7a	Ph	2-Me-Ph	0.52	-17.1 ± 0.4	-40 ± 1	-6.5 ± 0.6
7b	Ph	2-Et-Ph	0.56	-17.8 ± 0.8	-44 ± 2	-6.2 ± 0.9
7c	Ph	2-*i*-Pr-Ph	0.76	-19.6 ± 0.5	-51 ± 2	-6.2 ± 0.7
7d	Ph	Mes[a]	1.04[b]	-12.6 ± 0.8	-42 ± 3	-2 ± 1
8	2-Me-Ph	2-Me-Ph	1.04[b]	-17.0 ± 0.8	-54 ± 3	-3 ± 1

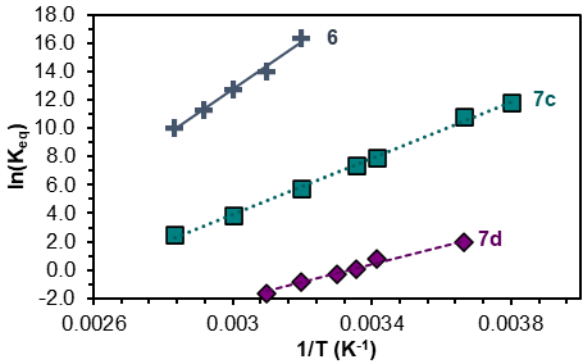

Figure 4.4. van't Hoff analyses of the reaction equilibrium between silanes $HSiPh_x(2\text{-Me-Ph})_y$ **2**-**4** and **1**. Reaction conditions: 1.00 equiv of **1**, 2.05 equiv of **2**, **3c**, or **3d**, 13.3 mM in C_7D_8, 273-353 K. Δ*H*° and Δ*G*° are reported in kcal•mol^{-1}; Δ*S*° is reported in cal•mol^{-1}•K^{-1}. [a]Mes: 2,4,6-Me_3Ph. [b]*v* value for products **7d** and **8** was calculated by summing the *v* values of the two substituents *ortho* to Si.

Kinetics studies

We next investigated the influence of silane steric effects on the rate of oxidative addition. Previous work in our lab has shown the reaction of **1** with triaryl silanes to be facile, with $HSiPh_3$ (**2**) giving full conversion to product **6** within seconds at -40 °C in toluene-*d*$_8$.[24] However, we found that the rate of oxidative addition with sterically hindered silanes **3b**-**d** and **4** is slowed considerably in comparison to silanes **2** and **3a**, enabling the study of the reaction kinetics by NMR. In these experiments, the reaction rate is determined by monitoring the growth of product against internal standard in sequential $^{31}P\{^1H\}$ spectra.

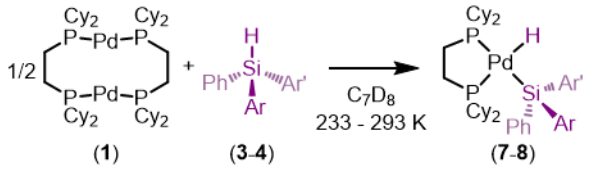

(**1**) (**3-4**) (**7-8**)

Product	Ar	Ar'	*v*	Rate (mM/s)	log(*k*)
7b	Ph	2-Et-Ph	0.56	0.041 ± 0.001	-1.39
7c	Ph	2-*i*-Pr-Ph	0.76	0.0095 ± 0.0003	-2.02
7d	Ph	Mes[a]	1.04[b]	0.00051 ± 0.00003	-3.29
8	2-Me-Ph	2-Me-Ph	1.04[b]	0.00094 ± 0.00004	-3.02

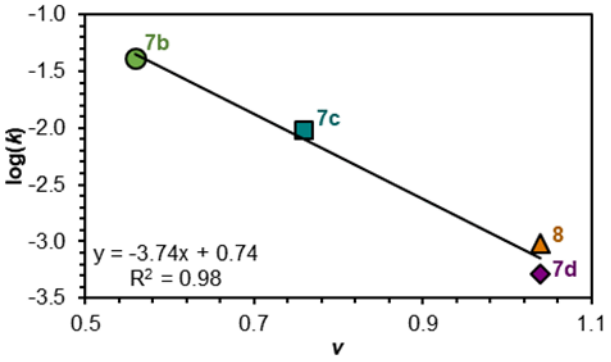

Figure 4.5. Charton plot using initial rates for the reaction between substituted HSi(Ph)(Ar)(Ar') **3b-d/4** and **1**. Rates were determined using the NMR integrations of each product against internal standard. Reaction conditions: 1.00 equiv of **1**, 1.00 equiv int. std., 2.05 equiv of **3b-d/4**, 13.3 mM in C_7D_8 at 263 K. [a]Mes: 2,4,6-Me_3Ph. [b]*v* value for products **7d** and **8** was calculated by summing the *v* values of two substituents *ortho* to Si (both methyl groups).

We conducted a Charton analysis by measuring and plotting the intial rates of reaction measured at -10 °C with each silane against the Charton parameters. The results are summarized in Figure 4.5. The sensitivity constant $\psi^{\ddagger}$ was found to be moderately large and negative (-3.7 ± 0.4), indicating that increasing steric bulk is kinetically disfavorable for oxidative addition, though to a lesser degree than thermodynamic considerations (ψ_{eq} = -7.3 ± 0.6).

We next turned to Eyring analyses to determine the kinetic energy parameters for oxidative addition with silanes **3b-d** and **4**. Produt formation was monitored over time at various temperatures between -40 °C and 20 °C. Results are summarized in Figure 4.6.

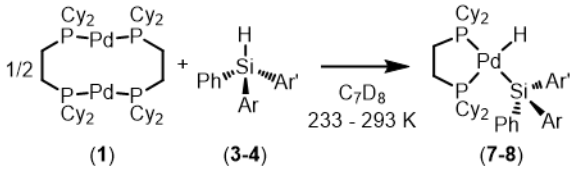

(**1**) (**3-4**) (**7-8**)

Product	Ar	Ar'	Δ*H*‡	Δ*S*‡	Δ*G*‡$_{263K}$
7b	Ph	2-Et-Ph	4.3 ± 0.1	-50 ± 20	17 ± 4
7c	Ph	2-*i*-Pr-Ph	4.2 ± 0.1	-52 ± 4	18 ± 1
7d	Ph	Mes[a]	8.4 ± 0.1	-41 ± 2	19.3 ± 0.6
8	2-Me-Ph	2-Me-Ph	7.4 ± 0.1	-44 ± 6	19 ± 1

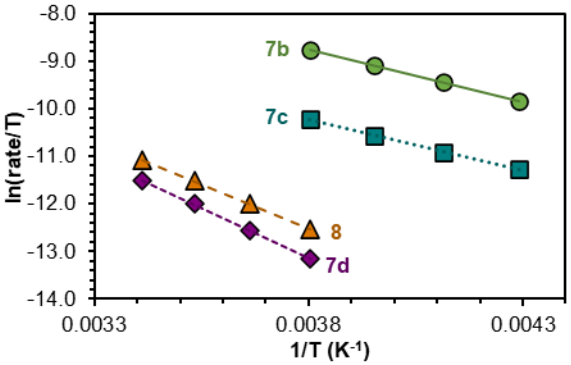

Figure 4.6. Variable temperature kinetics and Eyring analysis of oxidative adddition with silanes **3b**-**d**/**4** and **1**. Δ*H*‡ and Δ*G*‡ are reported in kcal•mol^{-1}; Δ*S*‡ is reported in cal•mol^{-1}•K^{-1}. [a]Mes: 2,4,6-Me$_3$Ph.

Eyring analysis shows that silane steric hindrance has a measurable effect on the energetics of oxidative addition. A clear trend in Δ*H*‡ is observed: with increasing steric bulk, Δ*H*‡ increases; however, Δ*S*‡ is consistent across the series and is large and negative (-40 to -50 cal•mol^{-1}•K^{-1}). These data show that the rate-determining transition state is highly ordered and is consistent with two molecules reacting in one transition state. Δ*G*‡, calculated at 263 K from Δ*H*‡ and Δ*S*‡, increases slightly from 17 kcal•mol^{-1} with the least sterically bulky silane **3b** to 19 kcal•mol^{-1} with the most sterically bulky silanes **3d** and **4**.

To summarize our study into the effect of silane steric hindrance on the kinetics of oxidative addition, we measured a decrease in rates with increasing steric bulk of the silane. The kinetic sensitivity constant ψ‡ at -10 °C was found by Charton analysis to be large and negative (-3.7 ± 0.4), in support of this trend. Eyring analysis of reaction kinetics at variable temperature reveals a preference for less

sterically hindered silanes, giving a difference in $\Delta G^{\ddagger}_{263K}$ of 2 kcal•mol^{-1} across the range of silanes studied, with $\Delta H^{\ddagger}$ being the major contributor to differences due to steric effects.

Dynamic exchange behavior

Through the course of study, we observed dynamic exchange behavior of the silyl palladium hydrides in solution, whereby the H and SiR_3 ligand environments are exchanged. This process is fully reversible and proceeds via reductive coupling to form the H–Si bond, rotation about the Pd–(η^2-H–Si) bond, and oxidative cleavage of the H–Si bond (Figure 4.7a). Prior study of this process shows that it occurs without a measurable kinetic isotope effect or dependence on silane electronics,[24] suggesting that the rate-determining step is rotation rather than oxidative cleavage or reductive coupling. Because rotation is likely hindered by increasing steric bulk at silicon, we hypothesized that silanes with larger substituents would undergo this exchange more slowly.

Importantly, for silyl palladium hydride complexes **6**-**7**, this intramolecular exchange behavior proceeds at rates observable on the NMR timescale at accessible temperatures in toluene-d_8. At different temperatures, the rate of exchange proceeds through “slow” and “fast” regimes (Figure 4.7b; see Supporting Information for analogous spectra with complexes **7a**-**c**). The slow exchange regime is evidenced by the presence of two peaks in the product’s $^{31}P\{^1H\}$ NMR spectrum, arising from two distinct phosphorus environments (e.g., at 203 and 213 K in Figure 4.7b); from non-decoupled ^{31}P NMR, the phosphorus atom *trans* to the hydride ligand can be assigned, since it appears as a doublet, and the P *trans* to the silyl group is a singlet. Upon warming, the slow exchange regime gives way to coalescence, whereby the ^{31}P signals broaden and begin to converge (e.g., at 243 K in Figure 4.7b). Upon further warming, the peak resolves to a sharp singlet, eventually reaching a minimum linewidth at higher temperatures. Analysis of the linewidth and peak separation in $^{31}P\{^1H\}$ NMR spectra gives the rate of rotation at

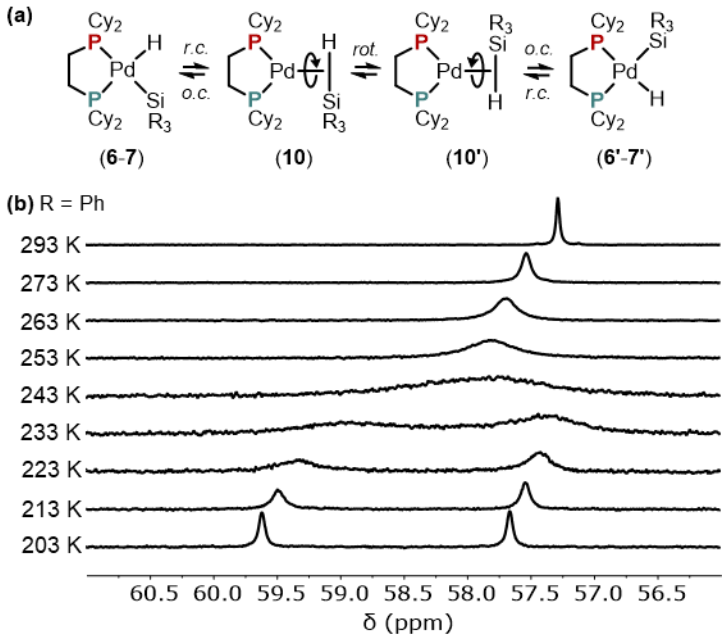

Figure 4.7. (a) Proposed mechanism for the intramolecular dynamic exchange of –H and –SiR_3 environments, proceeding through reductive coupling (r.c.), rotation (rot.) about Pd–(η^2-H–SiR_3) (**10**/**10'**), and oxidative cleavage (o.c.). (b) variable temperature $^{31}P\{^1H\}$ NMR spectra of (dcpe)PdH($SiPh_3$) (**6**/**6'**).

a given temperature, which can be converted using an Eyring analysis to give $\Delta H^{\ddagger}$, $\Delta S^{\ddagger}$, and thus $\Delta G^{\ddagger}$ values (Figure 4.8).[125,126]

Contrary to our hypothesis, linewidth analysis of our library of silyl palladium hydride complexes **6** and **7a-c** reveals a negligible effect of silane substitution on the energetics of dynamic exchange. Modest trends are observed in $\Delta H^{\ddagger}$ and $\Delta S^{\ddagger}$, indicating that of the four complexes investigated, the dynamic exchange process in **6**, the least sterically hindered complex, is most favorable enthalpically (lowest $\Delta H^{\ddagger}$) and least favorable entropically (lowest $\Delta S^{\ddagger}$). Nevertheless, the rate of intramolecular H/SiR_3 ligand exchange in complexes **6** and **7a-c** is not significantly affected by the steric bulk of silane substituents, and all complexes studied give $\Delta G^{\ddagger}_{263K}$ of approximately 10 kcal•mol^{-1} (Figure 4.8). This value is consistent with prior studies of the dynamic exchange with electronically-varied triaryl silanes.[24]

This result with varying steric bulk is perhaps surprising given that we previously found rotation to be the rate determining step of this intramolecular H/SiR_3 exchange. One hypothesis is that the silane coordinated in the sigma

complex is sufficiently far from the (dcpe)Pd center to be unaffected by steric hindrance of the dcpe ligands; yet, “loose” coordination of silane in the sigma complex is at odds with our previous finding that silane coordination is the rate determining step of oxidative addition.[24] Another possibility is that oxidative cleavage plays a larger role in H/SiR_3 exchange when using sterically bulky silanes, offsetting the effects of a possible hindrance in rotation.

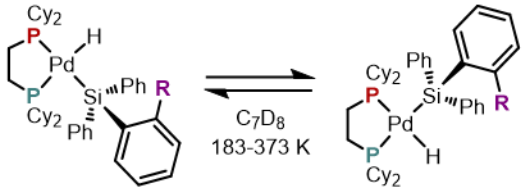

(**6**-**7**) (**6'**-**7'**)

Product	R	*v*	$\Delta H^{\ddagger}_{DE}$	$\Delta S^{\ddagger}_{DE}$	$\Delta G^{\ddagger}_{DE(263K)}$
6	H	0	10.4 ± 0.2	-1.66 ± 0.03	-10.8 ± 0.2
7a	Me	0.52	11.1 ± 0.3	3.6 ± 0.1	-10.2 ± 0.3
7b	Et	0.56	11.5 ± 0.4	4.8 ± 0.1	-10.2 ± 0.4
7c	*i*-Pr	0.76	11.8 ± 0.2	6.1 ± 0.1	-10.2 ± 0.2

Figure 4.8. Dynamic exchange (DE) barriers determined by linewidth analysis of $^{31}P\{^{1}H\}$ NMR spectra at variable temperature. $\Delta H^{\ddagger}_{DE}$ and $\Delta G^{\ddagger}_{DE}$ are reported in kcal•mol^{-1}; $\Delta S^{\ddagger}_{DE}$ is reported in cal•mol^{-1}•K^{-1}.

Comparing reaction coordinate diagrams

To summarize the effect of silane steric hindrance in the oxidative addition of Pd(0) to Si–H bonds, the energetics from all above experiments were used to construct a reaction coordinate diagram for the formation of representative complexes **7b** and **7d**, which represent a relatively smaller (**7b**, teal) and a relatively larger (**7d**, purple) silyl group (Figure 4.9) for which we have nearly complete sets of energetic data. First, **1** dissociates to form two equivalents of the 14-electron (dcpe)Pd fragment (**1’**).[24,102,127] The energetics of this step are not known, but are assumed to play a negligible role in the oxidative addition pathway as dissociation to **1’** is spontaneous and **1’** is never observed in solution.[127]

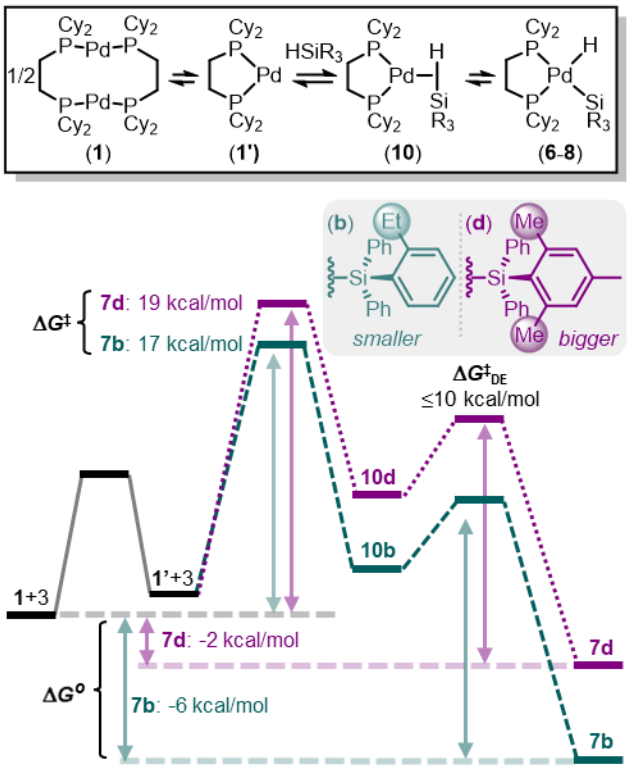

Figure 4.9. Reaction coordinate diagram for the oxidative addition of **1** with silanes **3c** and **3d**.

Previously, we found that the interaction of **1'** with silane to form the σ-complex Pd–(η^2-H–SiR_3) (**10**) is the rate-determining step.[24] For the two silanes under analysis here, **3b** and **3d**, the barrier ($\Delta G^{\ddagger}_{263K}$) was determined by kinetic Eyring analysis to be 17 kcal•mol^{-1} and 19 kcal•mol^{-1}, respectively. Intermediates **10** proceed through oxidative cleavage to give the desired silyl palladium hydride products **7** with ΔG^{o}_{263K} equal to -2 kcal•mol^{-1} and -6 kcal•mol^{-1} for **7b** and **7d**.

As suggested by the observed dynamic exchange behavior, intermediate **10** can also undergo rotation prior to oxidative cleavage. In this process, rotation about the Pd(η^2-H–SiR_3) σ-bond in **10** is rate-limiting with a barrier ($\Delta G^{\ddagger}_{DE}$ at 263 K) of approximately 10 kcal•mol^{-1} independent of silane identity. This value implies the barrier to oxidative cleavage is equal to or less than 10 kcal•mol^{-1}, and is not rate-limiting for oxidative addition.

Comparing the reactivity of **1** with **3b** and **3d**, both thermodynamic and kinetic factors favor the formation of **7b** over **7d**, as evidenced by lower barriers ($\Delta\Delta G^{\ddagger}_{263K} \approx 2$ kcal•mol^{-1}) and more favorable thermodynamics ($\Delta\Delta G^{o}_{263K} \approx 4$

kcal•mol^{-1}) for **7b** compared to **7d**. These results are in agreement with Charton analyses in kinetics ($\psi^{\ddagger}$ = -3.7) and equilibrium (ψ_{eq} = -7.3) studies, which show that rates and thermodynamics are both more favorable with smaller silanes. However, comparing the magnitudes of $\Delta\Delta G^{\ddagger}/\psi^{\ddagger}$ and $\Delta\Delta G^{o}/\psi_{eq}$ for the triaryl silanes studied*, increasing the steric bulk of the silane impacts thermodynamic contributions more significantly than kinetic contributions*.

Conclusion

In this Chapter, we systematically investigated the effect of silane steric profile on the oxidative addition of [(μ-dcpe)Pd]$_2$ (**1**) to Si–H bonds. Equilibrium studies at room temperature show a strong dependence on silane steric hindrance, trending well with the Charton constants of the silane's substituents. A large, negative sensivity factor was found (ψ_{eq} = -7.3 ± 0.6), indicating a significant preference for less sterically bulky silanes. van't Hoff analysis of variable temperature equilibrium studies likewise supports a more favorable reaction of **1** with less-substituted HSiPh$_3$ (**2**) than with HSiPh$_2$(2-R-Ph) (**3**) or HSiPh(2-Me-Ph)$_2$ (**4**), giving reaction ΔG^{o}_{263K} ranging from -13 kcal•mol^{-1} to -2 kcal•mol^{-1} across the series.

Kinetics studies were carried out with silanes **3b-d** and **4** by NMR in toluene-d_8. Charton analysis of initial rates at 263 K gives a moderate, negative sensitivity factor ($\psi^{\ddagger}$ = -3.7 ± 0.4), signifying a kinetic preference for less sterically bulky silanes. Eyring analysis of variable temperature kinetics studies give $\Delta G^{\ddagger}_{263K}$ of the reaction ranging from 17 kcal•mol^{-1} (**7b**) to 19 kcal•mol^{-1} (**7d**). These data show that decreased steric bulk of the silane's substituents increases the rate of reaction.

Comparatively, the steric bulk of the silane impacts thermodynamics more significantly than kinetics. This work provides the first systematic measurement of silane steric effects on the oxidative addition of a group 10 metal to Si–H. Given the widespread relevance of palladium, nickel, and platinum catalysis with hydrosilanes, these results provide a fundamental basis for the optimization of processes to selectively synthesize and modify organosilicon compounds.

Perspective and Outlook

Silanes play a versatile role in catalytic transformations, acting as hydride sources, transmetalation reagents, and starting materials in the synthesis of highly valued organosilicon compounds and polymers. Their use in catalysis with palladium is widespread, commonly proposed to proceed via oxidative addition of Pd(0) to Si–H; however, little is known about this fundamental reaction. In this Chapter, we have shown that the formation of silyl palladium hydride complexes (dcpe)PdH(SiR_3) from **1** and tertiary silanes is dependent on the steric profile of the silanes employed. Lower K_{eq} was observed with increasing steric encumbrance at silicon, correlating well with each substituent's Charton value, and van't Hoff analyses showed the reaction with sterically congested silanes to be less thermodynamically favorable. Variable temperature kinetics studies likewise revealed a preference for unhindered silanes as determined by Charton and Eyring analyses. Together, the energetic parameters derived for each of these steps reveal thermodynamic factors to be primarily responsible for favoring (silyl)Pd(H) formation with less sterically bulky silanes. These results present the first systematic study on the role of silane steric effects in oxidative addition of Pd(0) to Si–H and help to inform catalytic transformations in organosilicon chemistry. These findings can also be used to retroactively rationalize poor activity observed in hydrosilylation with sterically bulky silanes. Ultimately, this insight will provide an avenue to expanding the reach of late transition metal-catalyzed organosilicon chemistry.

5. SILYL PALLADIUM HYDRIDES IN THE HYDROSILYLATION OF ARYLACETYLENES

From Hurst, M.R., Zakharov, L.N., Cook, A.K. “The Mechanism of Oxidative Addition of Pd(0) to Si–H Bonds: Electronic Effects, Reaction Mechanism, and Hydrosilylation.” *Chem. Sci.* **2021**, 12, 13045-13060.

The catalytic reactions described in this Chapter were conducted by me and Lucas Thigpen under my supervision. I was the primary contributor to the development of this project and did all of the writing.

Introduction

Hydrosilylation is a fundamental reaction in organosilicon chemistry, widely applied to synthesize silicon-containing materials and molecules by the addition of silicon and hydrogen across carbon multiple (π) bonds.[1–3] The organosilicon products formed in this reaction find broad use in industry and academia, and commonly go on to be used in the creation of fine chemicals, consumer goods, and medicines, among other applications.[4,5] An important factor in the astounding versatility of organosilicon compounds is their ability to undergo further transformations, but with this promise comes a caveat: to allow for further functionalization, there must be reactive sites remaining on the molecule after hydrosilylation. Thus, the design of efficient and selective methods for hydrosilylation has been crucial to its growth as a cornerstone reaction.[6,7]

Although others have been reported, the most successful method for hydrosilylation in terms of activity and selectivity is late transition metal catalysis, inspired by Speier’s seminal work with H_2PtCl_6 in 1957.[3,6,8] In the decade that followed, platinum complexes were established as highly efficient catalysts for the hydrosilylation of alkenes, with early reports showing as much as a 10^6 increase in reaction rate compared to stoichiometric base-mediated methods at catalyst loadings as low as 10^{-6} molar.[8,9] Yet, despite their extraordinary activity, platinum catalysts still present practical challenges in hydrosilylation more than 60 years later, most of which we now recognize to stem from the structure of the catalysts themselves. H_2PtCl_6 and contemporary Pt(0) complexes stabilized by electron-

deficient alkenes (such as the industry standard Karstedt's catalyst) are prone to decomposition, and Pt atoms agglomerate during the reaction to form nanoparticles and other multinuclear species.[4,10,11] These undesired species exhibit catalytic behavior that can vary significantly from that of the intended catalyst, often leading to poorly controllable regioselectivity and to side reactions like isomerization and dehydrogenative silylation.[4,10] Importantly, the ill-defined homo- or heterogeneous nature of the evolved Pt catalysts contributes to considerable difficulty in studying their mechanism of reaction.[7,10]

Since late transition metal-catalyzed hydrosilylation was introduced, and foundational mechanistic studies were conducted by Chalk and Harrod and others,[8,12,13] much work has been done to develop and optimize new catalytic systems. Generally, these catalysts are designed with the aim to overcome limitations faced in early platinum-catalyzed hydrosilylation, and modern systems are known that can achieve excellent yields and regioselectivities with good tolerance for diverse alkenes and silanes.[3–6] Yet, with an ever-growing demand for organosilicon materials in research labs and elsewhere, the ability to effectively achieve hydrosilylation with a wide array of outcomes – for example, forming a disfavored isomer or installing a sensitive functional group – is paramount. Notably, the versatility of hydrosilylation is not confined to platinum, nor to alkenes, and the use of other metals and substrates is one avenue to realize this goal. In efforts to rationally design new catalytic systems, mechanistic studies provide an indispensable tool for understanding and optimizing the reactivity of metal complexes.

One influential area of research is in expanding the substrate scope of hydrosilylation to enable the reaction with various C–X (X = C, N, O) multiple bonds.[5] Although the first examples of hydrosilylation were conducted with alkenes, reports of the reaction with alkynes followed shortly after.[14] Alkyne hydrosilylation is a particularly intriguing reaction because the generated products are alkenylsilanes, which find use in Pd-catalyzed cross couplings,[15,16] electrophilic substitutions,[17] and Tamao-Fleming oxidations.[18–20] Yet, alkyne hydrosilylation also presents several unique challenges, the most prevalent of

which is the accessibility of numerous product isomers. In contrast to alkene hydrosilylation, which gives stable alkanes as a distribution of two isomers (α and β), the alkenylsilanes obtained by alkyne hydrosilylation can exist in up to four isomeric forms – two (*E*) and two (*Z*) (Scheme 5.1) – which must resist further reduction under the reaction conditions. Therefore, the development of practical synthetic methods for selective and efficient alkyne hydrosilylation exemplifies the central importance of catalyst control and tuneability.[5,6,14]

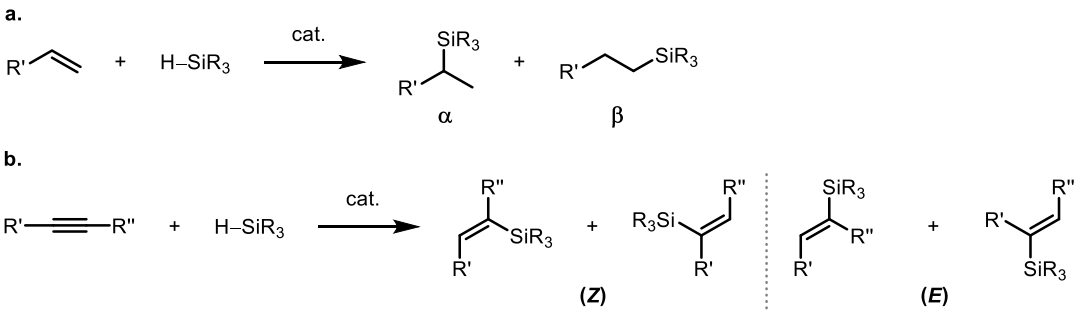

Scheme 5.1. Possible product distributions from the hydrosilylation of alkenes (a) or internal alkynes (b).

Moving up the periodic table from platinum, the other Group 10 metals (nickel and palladium) have also been developed as highly effective catalysts for alkene hydrosilylation.[2,4,14] Surprisingly though, given palladium's ubiquity in catalysis, little is known about the individual reaction steps leading to hydrosilylation in palladium-catalyzed transformations.[21–23] Accordingly, not many Pd complexes have been developed as alkyne hydrosilylation catalysts based on thorough mechanistic understanding. Recently, we described the first systematic studies of silane steric (Chapter 4) and electronic effects (Chapter 3) in the oxidative addition of Pd(0) to Si–H, a key reaction in the catalytic cycle of hydrosilylation.[24,25] We were interested to explore how relationships observed in this fundamental reaction step would affect the overall characteristics of alkyne hydrosilylation. This unique insight, along with classical methods of mechanism determination and reaction development, has promise to provide a comprehensive understanding and optimization of the Pd(0)-catalyzed hydrosilylation of alkynes.

This Chapter details our work on the hydrosilylation of phenylacetylene (**5a**) with triaryl silanes (**2**-**4**) using palladium complex [(μ-dcpe)Pd]$_2$ (**1)** (dcpe = di(cyclohexyl)phosphinoethane). We have studied the effect of silane steric and electronic properties on the reaction and conducted a thorough mechanistic investigation to elucidate key steps in the catalytic cycle, including determination of the rate law, kinetic isotope effects, and catalyst activation. Overall, we provide a detailed report on this powerful but under-explored catalytic system.

Results and Discussion

Effect of silane electronics and steric bulk

We began our study into the hydrosilylation of phenylacetylene by investigating the effect of electronic and steric variation of the silane. Modification of the aryl groups at silicon with electron-donating or electron-withdrawing substituents allows for comparison against the parent substrate (X = H) with regard to electronics. Similarly, modification of the aryl groups with bulky alkyl substituents allows for comparison with regard to steric hindrance. The extent to which these substituents affect the reaction is determined by comparing the observed rates to standardized electronic or steric parameters; when plotted, these correlations give values indicative of the magnitude and "direction" of reaction favorability. When measuring electronic effects, this analysis is referred to as Hammett analysis, and gives an electronic sensitivity constant ρ.[26,27] When measuring steric effects, this is referred to as Taft-Charton analysis, and gives a steric sensitivity constant ψ.[28]

With the parent silane HSiPh$_3$ (**2a**) and phenylacetylene (**5a**), hydrosilylation proceeds under mild conditions and low catalyst loading to give approximately 65% product **6a** at t = 6 hours (Figure 5.1). Looking first at electronic variation, we found that the reaction is both faster and higher-yielding when using electron-deficient silane HSi(4-CF$_3$-Ph)$_3$ (**2b**; 90% yield at t = 30 minutes) and, conversely, it is slower and gives lower yields with electron-rich silane HSi(4-Me-Ph)$_3$ (**2c**; 30% yield at t = 6 hours). Inclusion of more strongly electron-donating substituents in HSi(4-OMe-Ph) (**2d**) led to even lower yields, giving only approximately 20% of **6d** after 18 hours; consequentially, rates were not determined for this substrate. Overall,

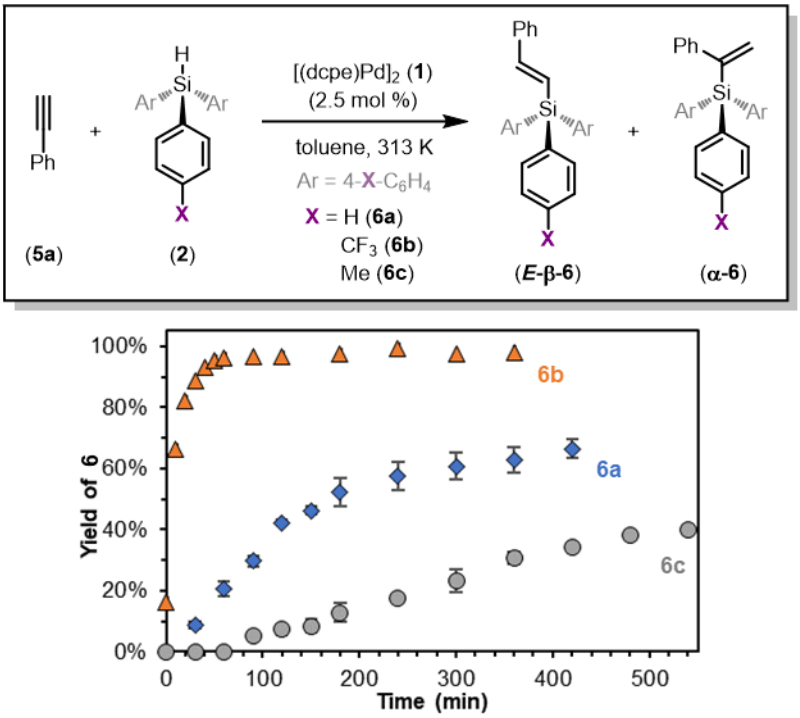

Figure 5.1. Product formation in the hydrosilylation of **5a** with electronically varied silanes **2**. Reaction conditions: 1.0 equiv of **2**, 1.0 equiv of **5a**, 0.025 equiv of **1**, 40.0 mM in toluene. Concentrations were determined by GC against an internal standard. Data was averaged over two trials.

these results align very well with our fundamental study into the oxidative addition of **1** to H–Si, where electron-rich silanes led to a lower K_{eq} and k_{obs} in the formation of (silyl)Pd(H) complexes while electron-poor silanes were favored.[24]

We next evaluated the effect of silane steric bulk on the hydrosilylation of phenylacetylene. In analogy to oxidative addition studies, we anticipated the reaction to be strongly impeded with the introduction of sterically bulky substituents;[25] thus, we conducted initial screening experiments with increased catalyst loading, at higher temperatures, and for longer reaction times than in trials with electronically varied silanes. Nonetheless, for diphenyl aryl substrates with *ortho*-alkyl groups larger than ethyl (**3a**; R = CH_2CH_3), negligible formation of products **7** was observed (Figure 5.2). Further, a profound silane steric effect is maintained even when using a catalyst system previously shown to be highly active for this transformation: Pd_2dba_3 and PCy_3 (presumably forming $Pd(PCy_3)_2$

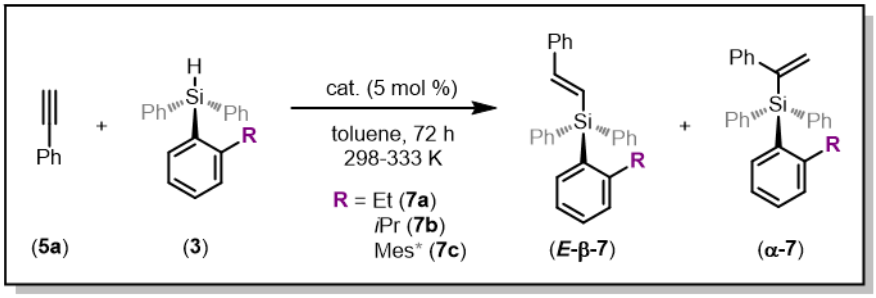

Silane	R	Catalyst	Temp (K)	Yield of **6**
3a	Et	**1**	313 K	17%
		1	333 K	19%
3b	*i*Pr	**1**	298 K	n.r.
		1	313 K	n.r.
		1	333 K	trace
		Pd_2dba_3/PCy_3 **	298 K	trace
3c	Mes	**1**	298 K	n.r.
		1	313 K	n.r.
		1	333 K	n.r.
		Pd_2dba_3/PCy_3 **	298 K	n.r.

Figure 5.2. Results in the hydrosilylation of **5** with sterically bulky silanes **3**. Reaction conditions: 1.0 equiv of **3**, 1.0 equiv of **5a**, 0.05 equiv of **1**, 40.0 mM in toluene. Concentrations were determined by GC against an internal standard. *Mesityl = 2,4,6-Me-Ph. **0.05 equiv Pd_2dba_3, 0.10 equiv PCy_3.

in situ).[24,29,30] Similar to these results with diphenyl aryl silanes, the reaction with phenyl diaryl silane $HSiPh(2\text{-Me-Ph})_2$ was likewise unsuccessful.

We next sought to reduce the total steric bulk of the silane while still allowing for the purposeful introduction of sterically hindering substituents, and so we turned to dihydrosilanes of the structure H_2SiAr_2 (**4**). For initial screenings, only the least and most sterically encumbered silanes (with structures analogous to triaryl silanes used above) were tested: H_2SiPh_2 (**4a**) and $H_2Si(2\text{-Me-Ph})_2$ (**4b**), respectively. These reactions proceed quickly and to full conversion, with product formation occurring at a slightly slower rate with sterically hindered **4b** (Figure 5.3). Despite the promise of these dihydrosilanes in catalysis, and unlike triaryl silanes **2** and **3**, the interactions of **4** with **1** are not easily resolved by spectroscopic methods and thus it is difficult to relate their reactivity with trends in oxidative addition. Therefore,

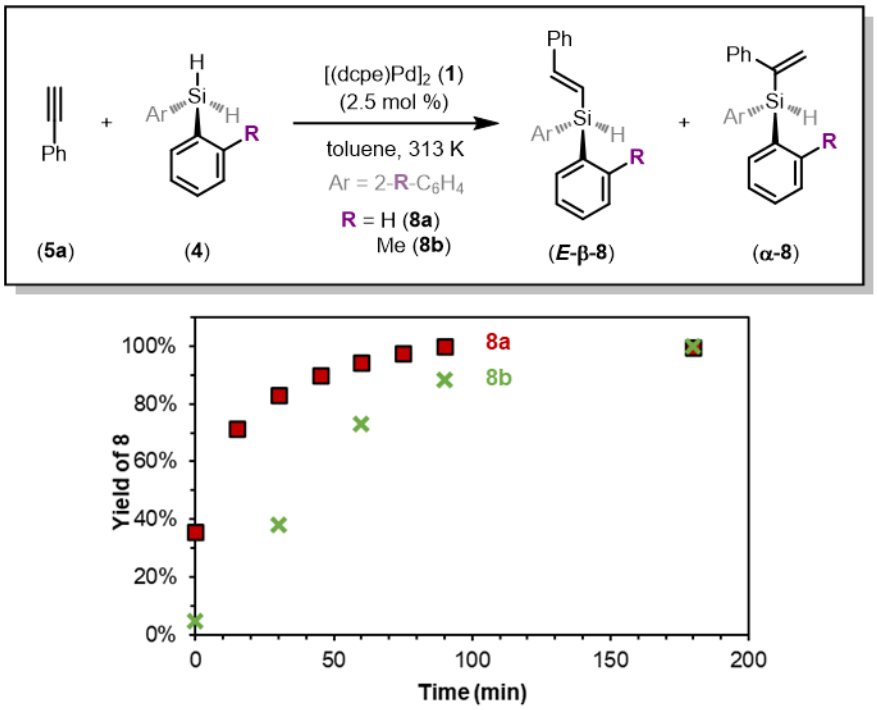

Figure 5.3. Product formation in the hydrosilylation of **5a** with electronically varied silanes **4**. Reaction conditions: 1.0 equiv of **4**, 1.0 equiv of **5a**, 0.025 equiv of **1**, 40.0 mM in toluene. Concentrations were determined by GC against an internal standard.

we did not further explore the use of silanes with sterically bulky substituents in phenylacetylene hydrosilylation.

Returning to electronically varied silanes **2**, we sought to better understand the relationship between their electronic nature and their performance in catalysis. To gain insight into this dynamic, we next conducted kinetics experiments to observe the initial rates of reaction. In these experiments, product formation was monitored by analyzing reaction aliquots by gas chromatography (GC) and integrating the product peak against an internal standard. The resulting concentrations were plotted against time, and the slope of the linear portion of this reaction profile was taken as the rate. These rates were then plotted against Hammett electronic parameter (σ) of the silane substituent to derive the electronic sensitivity constant (ρ) of the reaction.

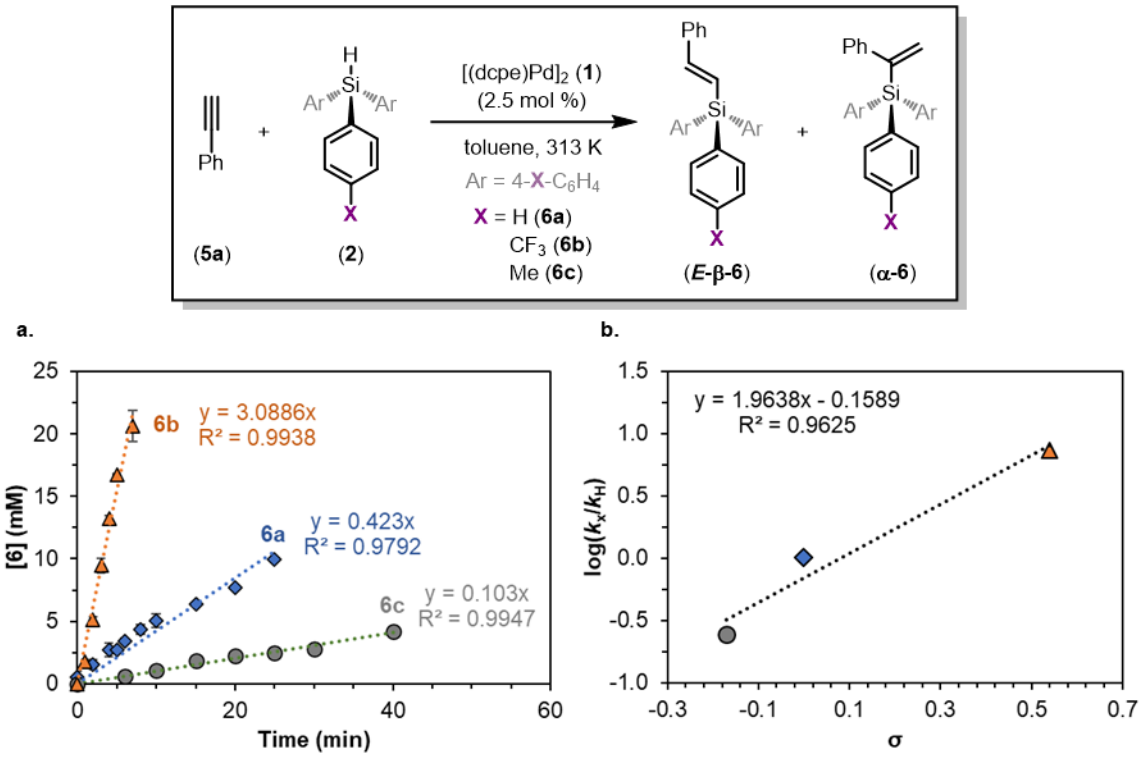

Figure 5.4. (a) rates of product formation in the hydrosilylation of **5a** with electronically varied silanes **2**. (b) Hammett plot constructed from rate data. Reaction conditions: 1.0 equiv of **2**, 1.0 equiv of **5a**, 0.025 equiv of **1**, 40.0 mM in toluene. Concentrations were determined by GC against an internal standard.

As observed in the full reaction profile with electronically varied silanes, there is a pronounced influence of silane substitution on the rate of hydrosilylation, favoring silanes with electron-withdrawing groups. The reaction was studied with a set of representative triarylsilanes to give a positive ρ value of 2.0 ± 0.4 (Figure 5.4), indicating that the electronic effect to prefer electron-poor substrates is approximately twice as strong as in the reference for Hammett analysis (ionization of benzoic acid derivatives).[26] Although based on empirical relationships, the measurement of a ρ value allows for standardized comparison of electronic influence in this work against others.[26] Notably, the ρ observed in this study is larger than we have previously observed for the kinetics of oxidative addition of **1** to aryldimethyl silanes (ρ = 1.2 ± 0.3),[24] though this may simply arise from the degree of aryl substitution at silicon.

With this understanding of silane steric and electronic impact in the hydrosilylation of phenylacetylene, we were interested to learn more about the role of each substrate in the reaction. We thus turned to mechanistic studies to further investigate the interactions of Si–H and **5a** with **1** to efficiently give products **6a**.

Mechanistic studies – in situ reaction monitoring

There are two commonly proposed mechanisms for the late transition metal-catalyzed hydrosilylation.[1,14,19] One of them is analogous to the classical Chalk-Harrod mechanism developed for the hydrosilylation of alkenes.[12] This catalytic cycle proceeds first by oxidative addition of the metal to Si–H, followed by migratory insertion into M–H and reductive elimination of the product (Figure 5.5). As with alkenes, a modified Chalk-Harrod pathway is possible, involving migratory insertion into M–SiR_3 rather than M–H (not shown in Figure 5.5). Notably, both the Chalk-Harrod or the modified Chalk-Harrod pathways afford primarily the (*E*)-β-alkene product.[14] An additional α-alkene product is formed in minor amounts by the insertion of the terminal carbon into the M–H bond or the more substituted carbon into the M–SiR_3 bond.

A second catalytic cycle, termed the Crabtree-Ojima mechanism, has been proposed to account for the formation of (*Z*) isomer products in some systems (Figure 5.6).[1,31,32] This pathway too begins with oxidative addition of the metal to Si–H. After this step, in contrast to Chalk-Harrod, migratory insertion proceeds specifically into M–SiR_3. This is followed by either reductive elimination to afford the (*E*)-alkene product or, importantly, an isomerization at the metal center that ultimately leads to reductive elimination of the (*Z*)-alkene product. As in the Chalk-Harrod-like pathway, the formation of the α-alkene product is possible by migratory insertion of the more substituted carbon on the alkyne into M–SiR_3 (not shown in Figure 5.6).

In the Crabtree-Ojima proposal, the distribution of products is dependent on the relative rate of reductive elimination (to yield (*E*) products) to isomerization (to yield (*Z*) products) at the metal complex intermediate(s), as reductive elimination is the rate determining step. Isomerization is driven forward by steric strain

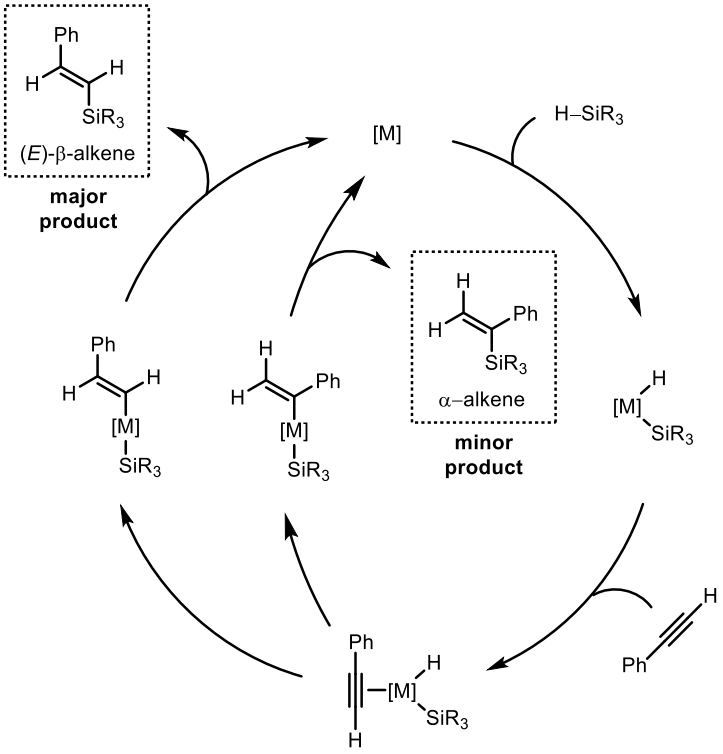

Figure 5.5. Chalk-Harrod-like catalytic cycle for the hydrosilylation of alkynes with late transition metal complexes.

between the silyl moiety and other groups at [M], while reductive elimination is influenced by both steric and electronic effects. Accordingly, reactions proceeding by this mechanism are highly sensitive to steric and electronic effects of alkyne and silane substituents.[1,14]

On the basis of product distributions in our studies, it seems likely that the hydrosilylation of phenylacetylene with **1** proceeds by a Chalk-Harrod-like mechanism. We do not observe significant formation of (*Z*) isomer products regardless of the electronic and steric character of the silane used in the reaction. Additionally, the Crabtree-Ojima mechanistic proposal is not commonly invoked for hydrosilylation with Pd or Pt, and is more common with Group 9 metals Rh and Ir.[14] With these insights guiding our initial mechanistic hypothesis, we sought to further probe the mechanism.

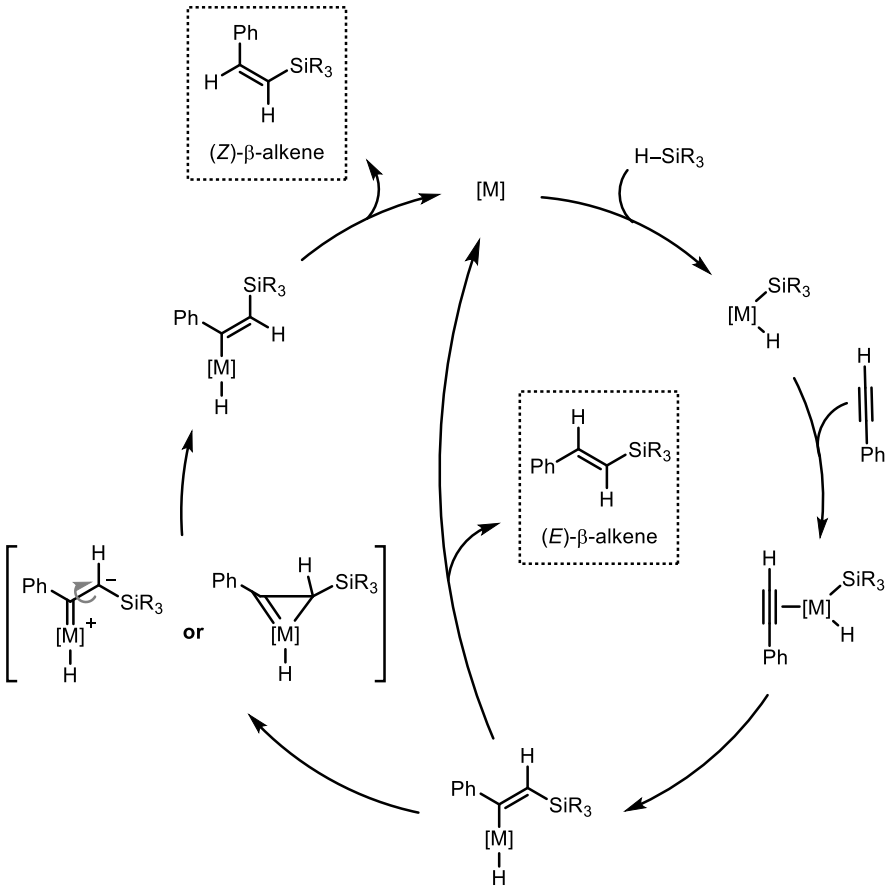

Figure 5.6. Crabtree-Ojima mechanistic proposal for the hydrosilylation of alkynes with late transition metal complexes.

We first monitored the reaction by NMR to observe how speciation of the Pd complex changes over the course of the experiment. Reaction mixtures of **1**, **2a**, and **5a** were prepared similarly to in catalytic trials under standard conditions; however, in these experiments, the use of deuterated toluene, C_7D_8, and slightly higher concentrations were necessary to allow for the observation of non-abundant species in solution NMR. These samples were placed in air-free J Young tubes and allowed to stand at room temperature while ^{31}P and ^{1}H NMR spectra were collected periodically.

First, experiments were performed to examine if the order in which the reagents were added to **1** would affect the formation of metal complexes during the reaction. Samples were prepared by first mixing **1** + **2a** (to form silyl palladium

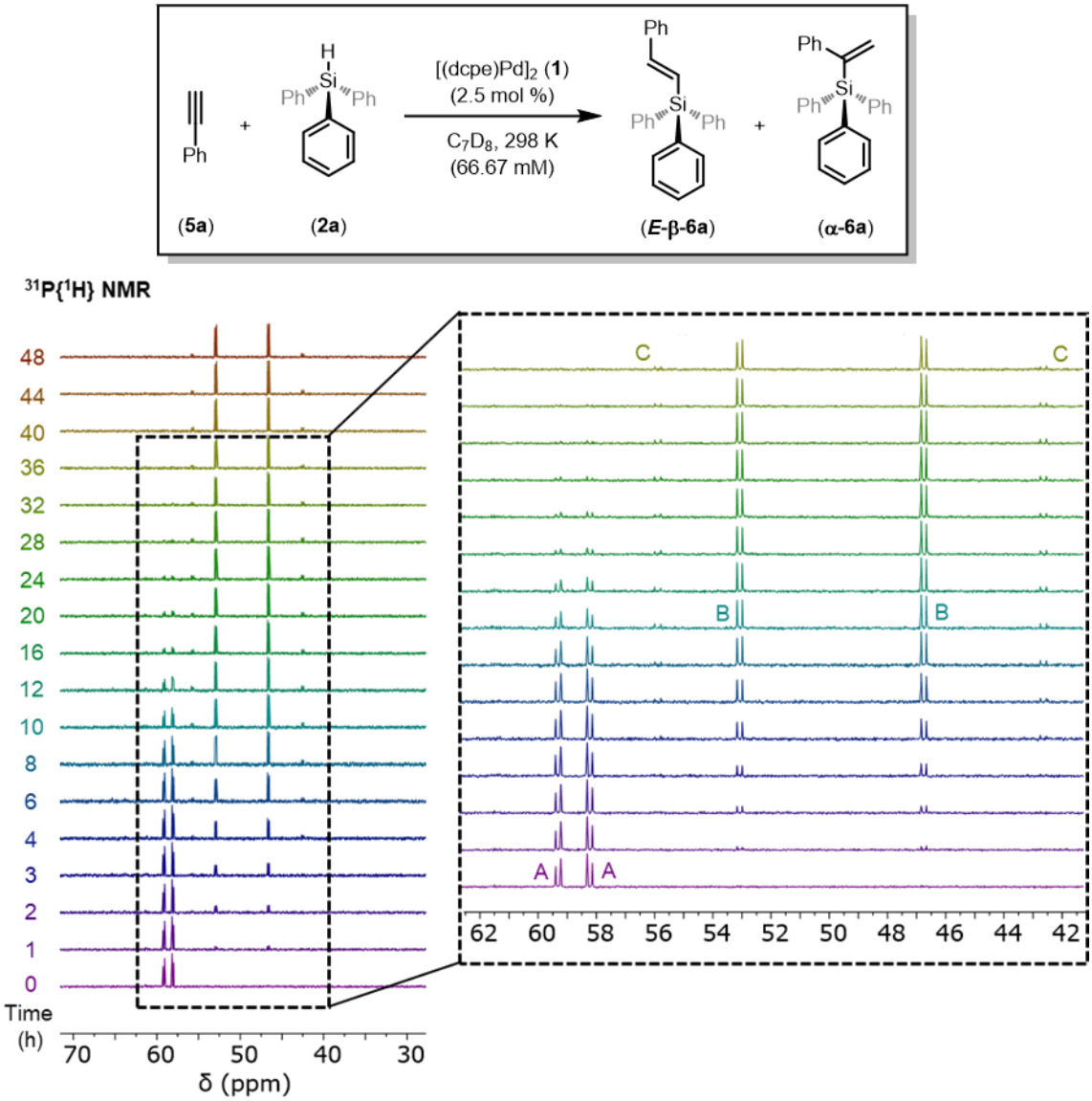

Figure 5.7. $^{31}P\{^{1}H\}$ NMR spectra of the reaction mixture during hydrosilylation of **5a** with **2a**. Reaction conditions: 1.0 equiv of **2a**, 1.0 equiv of **5a**, 0.025 equiv of **1**, 66.7 mM in C_7D_8.

hydride complex **9**) or **1** + **5a**, and NMR spectra were collected before adding the other reagent. Regardless of which reagent was added first, the same species is observed at t = 0 of catalysis (i.e. with all reagents in solution) by $^{31}P\{^{1}H\}$ NMR, and the reaction proceeds comparably thereafter. To determine the fate of the Pd complex(es) in this reaction, then, we can analyze the results from either analogous sample.

The $^{31}P\{^{1}H\}$ NMR spectrum of the reaction at t = 0 shows exclusively one product with two sets of doublets (*J* = 37 Hz) at 58 and 59 ppm (Figure 5.7, Product "A"). This peak pattern is typical for a four-coordinate square planar complex with a bidentate phosphine ligand and two other dissimilar groups at the metal center. Each phosphorous atom is in a different environment due to the distinct *trans*-influence of its partner at Pd, giving rise to the two "sets" of peaks at 58 and 59 ppm. The doublet splitting within each set of peaks is a result of phosphorus-phosphorus *cis*- coupling. Over time, the concentration of this product decreases until it is all consumed at approximately t = 32 hours.

While this complex gradually disappears during the course of the reaction, a new product is observed to form (Figure 5.7, Product "B"). The $^{31}P\{^{1}H\}$ NMR spectrum of this new product shows the same splitting pattern as the initial complex, though the sets of peaks are set further apart at 53 and 47 ppm (*J* = 37 Hz). Further, another minor product grows in, showing peaks at 56 and 53 ppm (J = 43 Hz) (Figure 5.7, Product "C").

Importantly, concurrent monitoring of ^{1}H NMR spectra shows the expected formation of product **6a**, and the relative concentrations of these metal complexes correlate well to the relative rate of the hydrosilylation reaction. At the beginning of the reaction, when there is a greater concentration of Product "A" in solution, formation of **6a** occurs at a faster rate (Figure 5.8). At later timepoints, the rate is significantly slowed until reaching a baseline level after disappearance of all Product "A" and complete formation of Products "B + C." Given the apparent relationship between metal complex speciation and catalytic performance, we set out to distinguish the identity of Pd species formed during catalysis.

Fascinatingly, each product observed in the $^{31}P\{^{1}H\}$ NMR spectra can be independently synthesized from **1** (Figure 5.9). As we and others have established previously, the reactivity of **1** implies its dissociation to two equivalents of 14-electron (dcpe)Pd fragment (**1'**) prior to interaction with substrates.[24,25,33–36] Seeking to identify products in this study, then, we conducted stoichiometric reactions with **1** and two equivalents of relevant species in catalysis, such as substrates **2a**/**5a** and products **6a**.

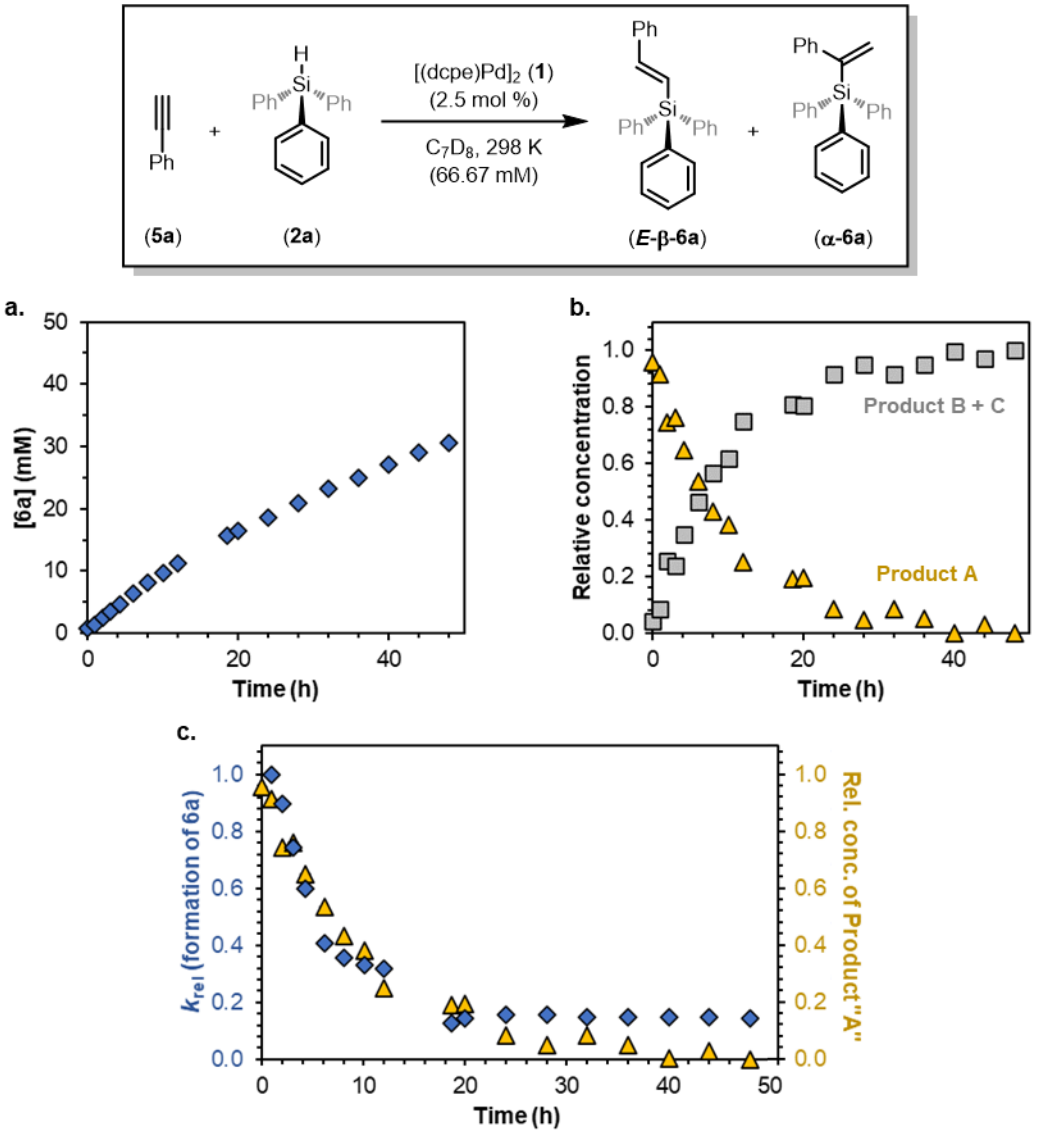

Figure 5.8. (a) **6a** formation monitored by ^{1}H NMR. (b) relative concentrations of Product A and Products B + C over the course of the reaction monitored by ^{31}P{^{1}H} NMR. (c) relative rate of hydrosilylation compared to the relative concentration of Product A.

Looking first at Product "A," this complex can be obtained by simply mixing solutions of **1** and **5a**. We have tentatively assigned this complex as the 1:1 Pd(0):phenylacetylene π-complex **10** based on the square planar character of ^{31}P{^{1}H} NMR spectra and on previously reported reactions of **1** with diphenylacetylene.[34] The formation of this complex predominates at early time points in catalysis and, in the experiment where **1** and **2a** were mixed first to form silyl palladium hydride **9**, the addition of **5a** led to complete elimination of $HSiPh_3$

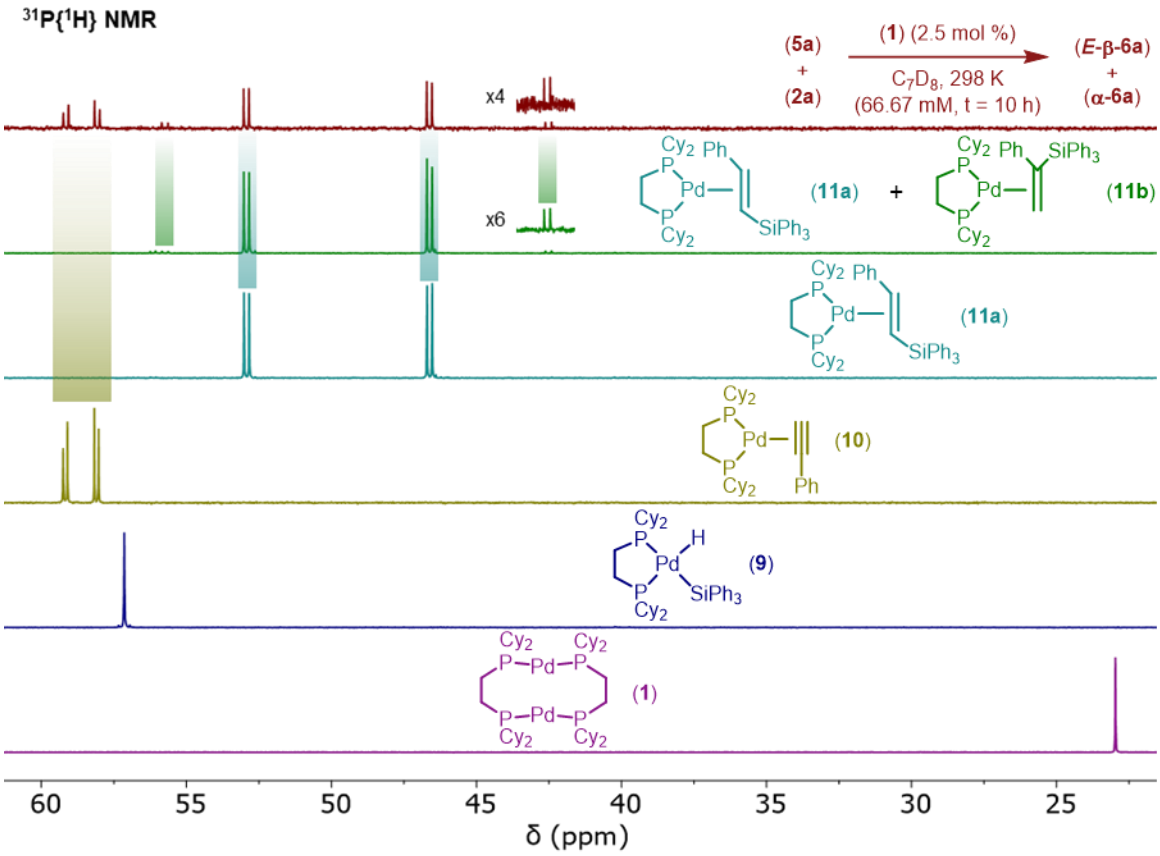

Figure 5.9. $^{31}P\{^{1}H\}$ NMR spectra of potential Pd complexes present during the hydrosilylation reaction. (top) $^{31}P\{^{1}H\}$ spectrum of a reaction mixture during hydrosilylation (t = 10 h).

from the Pd center to form exclusively **10**. Indeed, **9** is never observed during the catalytic reaction. Further NMR study of **10** has not been insightful to determining its true structure, and attempts at growing a single crystal suitable for x-ray diffraction are underway.

On the other hand, Products “B” and “C” do not arise from reactions of any of the starting materials with **1**. Rather, these complexes are generated by the coordination of alkene products **6** to Pd, giving structures postulated as the 1:1 Pd(0):alkene π-complexes **11**. Product “B,” the major phosphorus-containing product at later timepoints in the reaction, forms from **(*E*)-β-6a** to give **11a**. Product “C,” which is only observed in trace amounts, forms from **α-6a** to give **11b**. At intermediate times in the reaction, all of these species are present simultaneously (e.g. t = 10 h, Figure 5.9).

These results provide valuable insight into the mechanism of hydrosilylation. The predominance of complex **10** in the early stages of the reaction points to it being the resting state of the catalyst; over time, as the concentration of product **6a** grows and the concentration of **5a** diminishes, **10** becomes less favored to the products of alkene coordination **11**. Although catalytic activity is not entirely shut down after the disappearance of **10**, significantly slower rates result in the presence of only **11** – this suggests that the formation of **11** is contributing to catalyst inhibition, likely due to the strong coordination of the alkene precluding the entrance of **1'** back into the catalytic cycle. A similar dynamic is observed in the hydrosilylation of alkenes by Karstedt's catalyst.[7]

To examine the thermodynamic drive for this "sequestering" of active catalyst by alkene coordination, experiments were set up to test the reversibility of **5a** coordination to **1**. First, catalytically relevant concentrations of **1** and an excess of **5a** (20 equivalents) were mixed in C_7D_8 to form exclusively **10**. Then, an equimolar amount of product **6a** (20 equivalents) was added to the reaction mixture, and the conversion from **10** to **11** was monitored over time at room temperature and 313 K. After 6 hours at room temperature, the product ratio of **10** : **11** was 1.0 : 0.2. Upon heating the sample for 28 hours at 313 K, the relative concentration of **11** increased to give a ratio of 1.0 : 0.6. This experiment suggests that the coordination of **5a** is reversible under our catalytic conditions, allowing access to **1'** from **10** (Scheme 5.2). This helps to explain the apparent equilibrium existing between **10** and **11** in catalytic studies, where the relative concentration

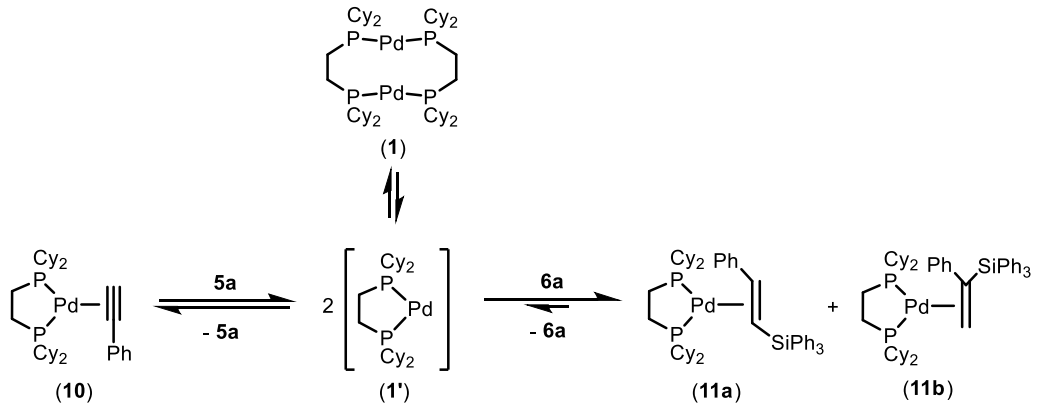

Scheme 5.2. Proposed equilibrium between complexes **10**, **1/1'**, and **11**.

of **5a** to **6a** seems to determine the predominant Pd complex in solution.

Together, these results inform our proposed catalytic cycle for the hydrosilylation of phenylacetylene with **1** (Figure 5.10), which generally follows with a Chalk-Harrod-like mechanism.[14] The first step is dissociation of complex **1** to two equivalents of active catalyst **1'**. The next step is likely reversible coordination of phenylacetylene to form intermediate complex **10**, which is the resting state of the catalyst; however, we cannot rule out that **10** is an off-cycle catalyst resting state in equilibrium with **1'**, and catalysis proceeds instead by reversible oxidative addition of **1'** to Si–H. Nevertheless, migratory insertion follows, then finally reductive elimination occurs to release product **6a** and regenerate **1'**. As **6a** accumulates in solution, **1'** is gradually consumed to irreversibly form off-cycle

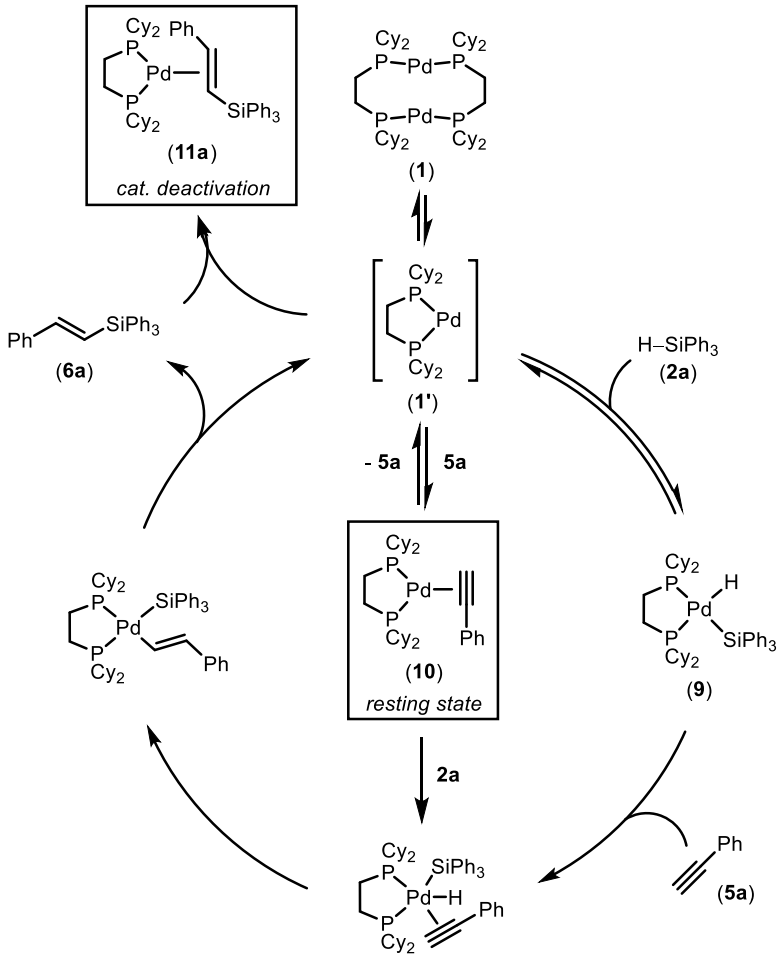

Figure 5.10. Proposed catalytic cycle for the hydrosilylation of **5a** with **2a** catalyzed by **1**.

intermediates **11**.

Unfortunately, the other species in this catalytic cycle were not observable by NMR spectroscopy, even when reaction mixtures were mixed at and/or cooled to 193-233 K. Therefore, greater insight into the mechanism was gained by investigating the rate law and kinetic isotope effect in catalysis.

Mechanistic studies – rate law determination

To determine the rate law of the reaction, variable concentration kinetics experiments were conducted in which the initial concentration of one reagent was altered while the others were kept constant. The formation of product was monitored by GC against an internal standard, and the rate of the reaction under these conditions was taken as the linear portion of the dataset plotted in product concentration against time. The reaction rate for each sample was then correlated to the initial concentration of the reagent of interest, and this relationship was used to determine the order in the reagent.

Varying the concentration of the silane, we found the reaction to be 1^{st} (1.09 ± 0.06) order in **2a** (Figure 5.11). Interpretation of this result is straight-forward, as as the hydrosilylation reaction is expected to consume one equivalent of **2a** in order to yield one equivalent of product **6a**. We thus moved on to finding the dependence on **5a**.

Varying the concentration of phenylacetylene, we found the reaction to be -0.5^{th} (-0.58 ± 0.04) order in **5a** (Figure 5.12). In contrast to the observed order in silane, this relationship is more difficult to explain in the context of the catalytic cycle. As with the silane, we would expect a 1^{st} order dependence on **5a**, as one equivalent of **5a** should be consumed in the formation of one equivalent of product **6a**. Yet, a negative half order suggests that **5a** is involved in other processes during each turnover of the catalyst, such that increasing the initial concentration of **5a** leads to slower reaction rates.

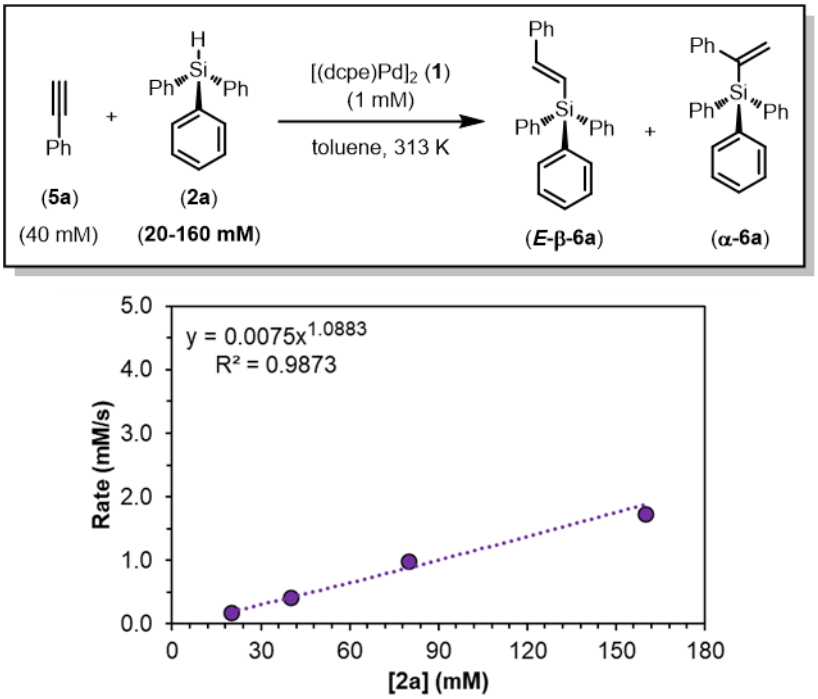

Figure 5.11. Plot of reaction rate versus [**2a**]. Data was collected at 313 K in toluene. Product concentration was determined by GC against an internal standard.

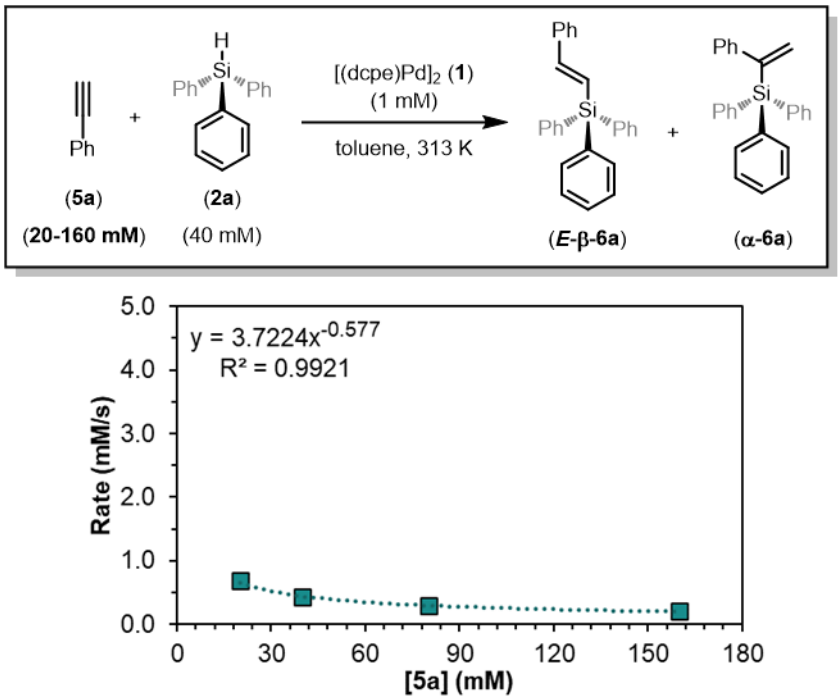

Figure 5.12. Plot of reaction rate versus [**5a**]. Data was collected at 313 K in toluene. Product concentration was determined by GC against an internal standard.

Knowing that one equivalent of **5a** must be incorporated into product **6a** – which would give a 1st order dependence on **5a** in an ideal case – we must consider that other, unobserved interactions contribute to cause a negative reaction order in our system. Given that these interactions are likely to occur at the Pd center, the order in **1** may prove useful in rationalizing this result.

Indeed, kinetics experiments with variable concentration of **1** lead to an unexpected 1.5th (1.4 ± 0.1) order (Figure 5.13). This is inconsistent with the proposed dissociation of **1** to two equivalents of **1'** that then behave as active catalysts, as that scenario would invoke a 0.5th order dependence on **1**. Taken together with the rate dependence on **5a**, these results are interesting – but we must also consider limitations in this analysis. For example, by design of kinetics experiments, we have only observed this dependence to be true in early time points of the reaction during which the rate of product formation trends linearly.

Nonetheless, these results – in addition to those of the NMR monitoring studies (*vide supra*) – suggest a dynamic interaction of the substrates and products

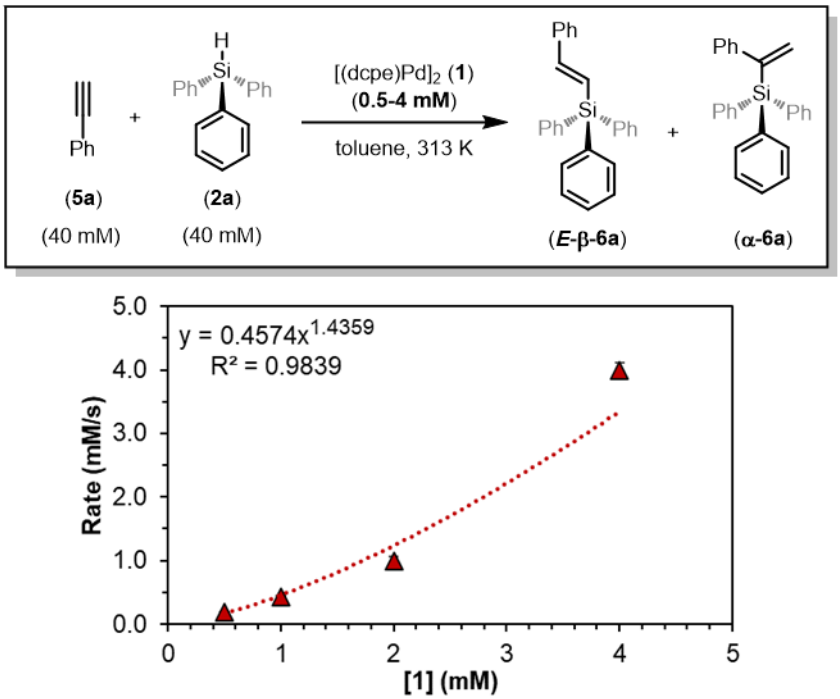

Figure 5.13. Plot of reaction rate versus [**1**]. Kinetics data was collected at 313 K in toluene. Product concentration was determined by GC against an internal standard.

of hydrosilylation during the reaction. Similar reasoning was applied to comprehensively describe the mechanism of hydrosilylation of alkenes with Karstedt's catalyst, including a negative rate dependence on alkene substrate.[7]

A negative order in **5a** and 1.5th order in **1** support the proposed equilibrium process between Pd:phenylacetylene π-complex **10** and active catalyst **1'** that favors **10** in the presence of excess **5a**. This tracks well with the predominance of **10** during early time points of the reaction, after which its concentration decreases as **5a** is gradually consumed in hydrosilylation. At the same time, the increasing concentration of alkenylsilane products **6a** favors the formation of Pd:alkene π-complex **11**. Coordination of **1'** to this alkene is stronger than to the alkyne **5a**, and so access to active catalyst **1'** is suppressed in the presence of excess **6a** at late stages of the reaction. Yet, catalysis continues even after complete disappearance of **10**, albeit at a much slower rate. Then, **11** must also be in equilibrium with active catalyst **1'** but is strongly favored under these reaction conditions. As was found with Karstedt's catalyst, the coordinating strength of species in solution affects the rate of reaction.[7]

To conclude these rate order studies on the hydrosilylation of alkynes with **1**, we can write the rate law of the reaction (equation 1):

$$\text{Rate} = k_{obs}\frac{[\mathbf{2a}][\mathbf{1}]^{1.5}}{[\mathbf{5a}]^{0.5}} \qquad (1)$$

Although this equation provides a crucial metric in studying the overall reaction, we were interested to further understand how the individual steps of catalysis contribute to this odd reaction order. One set of experiments that can assist with the determination of reversible equilibrium steps during the mechanism are kinetic isotope effect experiments.

Mechanistic studies – kinetic isotope effect and deuterium incorporation

We thus moved on to determine the kinetic isotope effect introduced by deuterium substitution on the silane **2a** (**2a-*d*$_1$**) or phenylacetylene **5a** (**5a-*d*$_1$**). In these experiments, one of the deuterated substrates was reacted with the other, protio- substrate, and the reaction rate was recorded. A comparison of these rates

to that of the reaction under standard conditions gives the H/D kinetic isotope effect (KIE) for the hydrosilylation of phenylacetylene with **1**. The interpretation of these KIEs grants insight into the dynamics of Si–H/D and C–H/D bond breakage or hybridization during (or before) the rate determining step of the catalytic cycle.[37] Additionally, the incorporation of deuterium into the products **6a-*d*$_1$** can be tracked by ^{2}H NMR to identify the fate of Si–H/D and C–H/D in the final products; alternatively, scrambling of H/D to give deuterium incorporation at multiple positions would indicate the reversibility of a step (or steps) in the pathway of hydrosilylation.[7]

Looking first at the reaction of **2a-*d*$_1$** with **5a**, we found a KIE of 1.89 ± 0.07 (Figure 5.14a). This value is in line with a normal, primary KIE, indicative that the breaking of the Si–H/D bond occurs at or before the rate-determining step of the reaction.[37] This results in a faster rate with the protio- substrate because the Si–H bond is easier to break than Si–D.[38,39] Seminal mechanistic study of the hydrosilylation of alkenes with Karstedt's catalyst by Stein, Lewis, and co-workers found a similar KIE with deuterated silanes (KIE = 1.8).[10]

On the other hand, the reaction of **2a** with **5a-*d*$_1$** exhibits a large inverse KIE of 0.20 ± 0.05 (Figure 5.14b). This preference for the deuterated substrate **5a-*d*$_1$** likely arises from the change in hybridization at carbon during the reaction, which is known to lead to inverse KIEs. While these are commonly of the magnitude of 0.7-1.0 for carbon-centered hybridization changes of sp^2 to sp^3,[37] we suspect that the extraordinary inverse effect observed here is due to the transformation of an sp-hybridized carbon to sp^2. Importantly, the extent of the kinetic isotope effect is strongly suggestive of phenylacetylene rehybridization – i.e. the breaking or forming of a new carbon-element bond – occurring at or before the slowest step of the catalytic cycle.

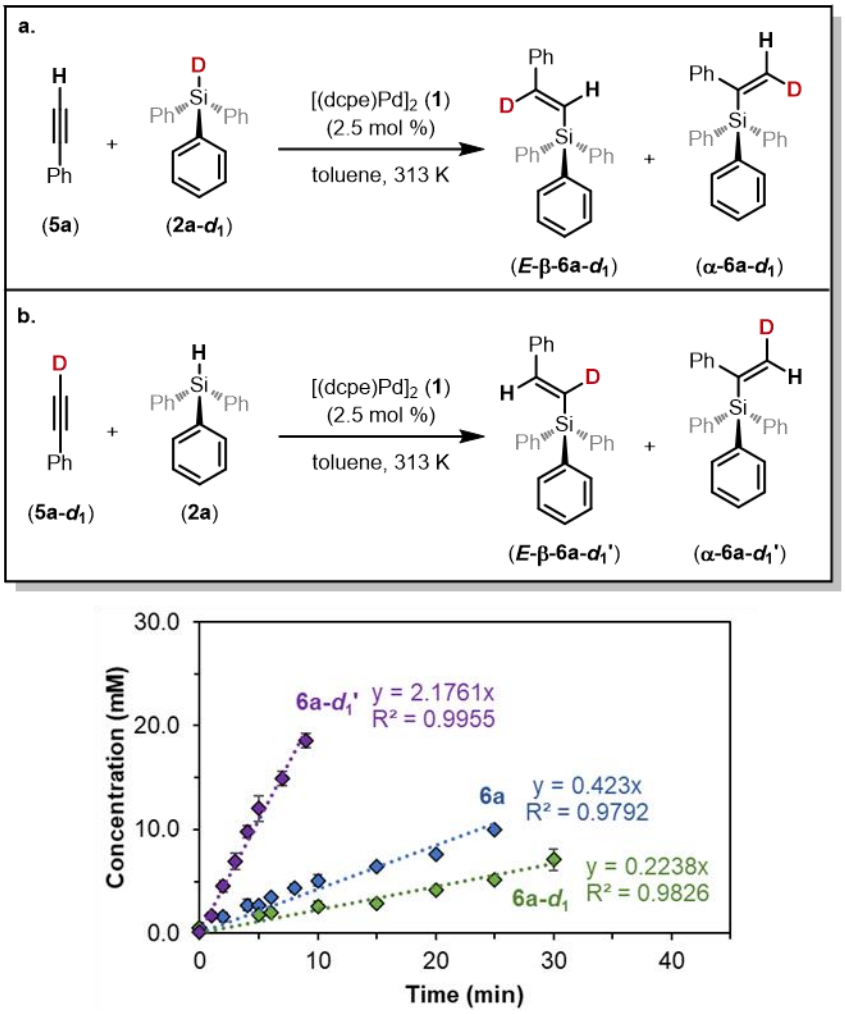

Figure 5.14. (a) kinetic isotope experiment with **2a-*d*1**. (b) kinetic isotope experiment with **5a-*d*1**. (c) plot of **6a**, **6a-*d*1**, and **6a-*d*1'** formation. Reaction conditions: 1.0 equiv of **2 or 2a-*d*1**, 1.0 equiv of **5a** or **5a-*d*1**, 0.025 equiv of **1**, 40.0 mM in toluene. Concentrations were determined by GC against an internal standard.

The results of these studies can be paired with ^{2}H NMR data to rationalize the incorporation of deuterium in the products. A comparison of the collected products from kinetic isotope experiments against a sample of protio-**6a** – showing both the β-*E* and α isomers – allows for the assignment of deuterium incorporation in **6a-*d*1** and **6a-*d*1'** (Figure 15). To our satisfaction, the alkenylsilanes synthesized

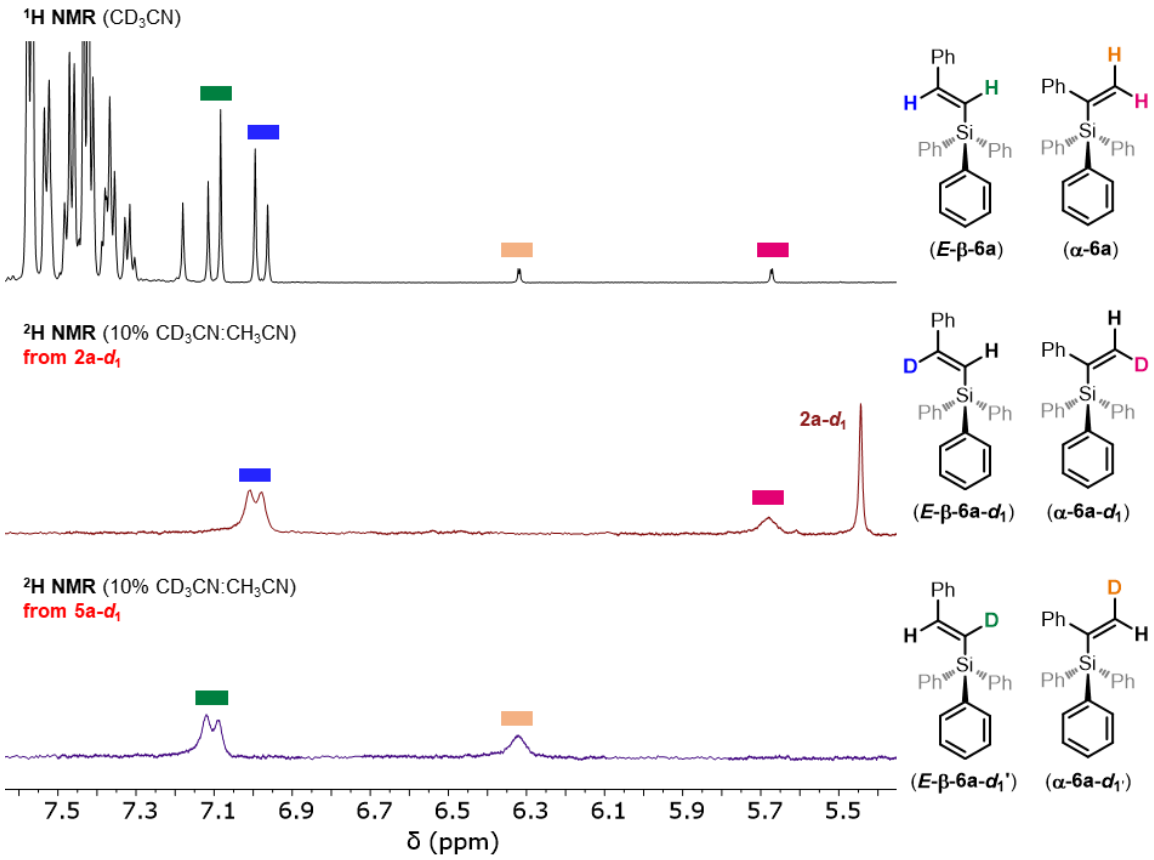

Figure 5.15. ^{1}H and ^{2}H NMR spectra of the dried reaction mixtures from hydrosilylation experiments in the kinetic isotope effect studies.

in reactions of **2a-*d*$_1$** or **5a-*d*$_1$** have exclusive deuterium incorporation at complementary positions, and none of the "protonated" substrate is generated.

This lack of H/D scrambling is consistent with a catalytic cycle in which none of the steps after the introduction of deuterium are reversible. If these steps were reversible, a distribution of deuterated products would be observed by the dynamic and non-specific breaking and forming of Si/C–H and Si/C–D bonds. Returning to our focus on understanding the mechanism of alkyne hydrosilylation with **1**, these isotopic experiments provide valuable insight in determining the order of steps, and the rate-limiting step, in the catalytic cycle.

We propose two possible routes by which the (dcpe)Pd fragment (**1'**) – generated by dissociation from **1** – can react with substrates in the reaction: either by oxidative addition to Si–H or π-coorindation of **5a**. Our previous study into the oxidative addition of **1** to Si–H showed that the reaction to form silyl palladium

hydrides is facile but highly reversible via reductive elimination to reform starting materials.[24] Thus, if coordination of **5a-*d*$_1$** preceded the oxidative addition of Si–H, and reductive elimination was favorable from the silyl palladium hydride intermediate, we might expect to see formation of the corresponding Si–D and **5a**. This is true for proceeding steps in the catalytic cycle as well. Yet, deuterium incorporation occurs exclusively at one position to give products **6a-*d*$_1$**.

From this observation, we propose that the oxidative addition of **1'** to **2a** is the first step of the catalytic cycle, in line with commonly proposed Chalk-Harrod-type mechanisms. In this case, the reversibility of oxidative addition of **1'** to Si–D leads only back to **1'** and **2a-*d*$_1$**, giving no extraneous deuterated products as no other substrates have yet been coordinated at the metal center. This oxidative addition is followed by π-coordination of **5a**, migratory insertion, and reductive elimination of **6a-*d*$_1$**. To generate **6a-*d*$_1$'** from **5a-*d*$_1$**, deuterium is installed instead during migratory insertion from intermediate protio- **9**.

This hypothesis must be reconciled with the sole observation of the proposed π-coordination complex **10** during early stages of catalysis, and only the formation of **11** thereafter. We suspect that **10** is an off-cycle intermediate from which **5a** dissociates to yield active catalyst **1'**. The presence of an off-cycle species in dynamic equilibrium with **5a** during the reaction also helps to explain the unexpected -0.5th order rate dependence on **5a** and 1.5th order rate dependence on **1**. Following this hypothesis, it seems that equilibrium favors **10** at early stages in the reaction (in the presence of excess **5a**) which contributes to a negative reaction order in **5a** – i.e. more **5a** and **1** are being used to form **10** than to generate products **6a**. As the concentration of **5a** decreases due to its consumption in catalysis, and the concentration of **6a** increases, equilibrium begins to favor **1'** and **11**. Accordingly, **5a** is gradually released from **10** to be converted to **6a**. The reversibility of coordination of **6a** from **11** appears to be low but not insignificant: even in the presence of only **11** after full consumption of **10**, catalysis continues, albeit at a much slower rate. Assuming **1'** to be the only active catalyst in this system, this lower rate is attributable to its less favorable release from **11**.

On the basis of KIEs, we can rule out the oxidative addition of Si–H and the coordination of **5a** as rate-limiting, as they come before a rehybridization of carbon in **5a** which is also involved at or before the slowest step. This leaves two options for the rate-determining step in our system: migratory insertion or reductive elimination. In the Ojima-Crabtree mechanistic proposal of alkyne hydrosilylation, reductive elimination is necessarily posited as the rate-determining step, as the relative rate of reductive elimination to isomerization controls the product distribution to sometimes give unusual (*Z*) products.[1] On the other hand, the Chalk-Harrod mechanism of platinum-catalyzed hydrosilylation is commonly postulated to be rate limited by migratory insertion.[7]

Unfortunately, we have no direct evidence of migratory insertion or reductive elimination processes, and at this time cannot unambiguously state which step is rate-determining in the hydrosilylation of alkynes with **1**. The unusually strong, inverse KIE for H/D substitution of **5a** may be suggestive of migratory insertion being rate-limiting, which would fall in line with the behavior observed in this system to typify a Chalk-Harrod-type mechanism. In the mechanistic study of alkene hydrosilylation with Karstedt's catalyst, a lack of deuterium scrambling was used to support the assignment of the rate-determining step as migratory insertion.[7] This leads to our tentative conclusion of migratory insertion as the rate-determining step; yet, more investigation is needed to confirm this proposal. Nonetheless, taken together, our results in mechanistic studies allow for a refinement of the initially proposed catalytic cycle (Figure 5.16).

Conclusion

In this chapter, we have described our work on the hydrosilylation of phenylacetylene with Pd(0) complex **1**. Our interest in this subject stems from our study on the fundamental oxidative addition of **1** to hydrosilanes, which comprises a crucial step in hydrosilylation. Our initial investigation into the hydrosilylation of alkynes showed good agreement with trends in silane electronic and steric properties observed in oxidative addition; more electron-poor and less sterically encumbering silanes give faster and more complete reaction, while electron-rich,

sterically bulky silanes only sluggishly undergo hydrosilylation under relatively forcing conditions. The trend in silane electronic effects on the reaction rate was quantified by Hammett analysis to give $\rho = 2.0 \pm 0.4$.

NMR monitoring of the reaction identified key intermediates in the catalytic cycle; specifically, the observation of complexes **10** and **11** allowed for the determination of the resting state and catalyst deactivation products, respectively. A dynamic equilibrium process between these two species through active catalyst **1'** appears to be at play, giving rise to an unexpected rate law with 1st order dependence in **2a**, -0.5th order dependence in **5a**, and 1.5th order dependence in **1**.

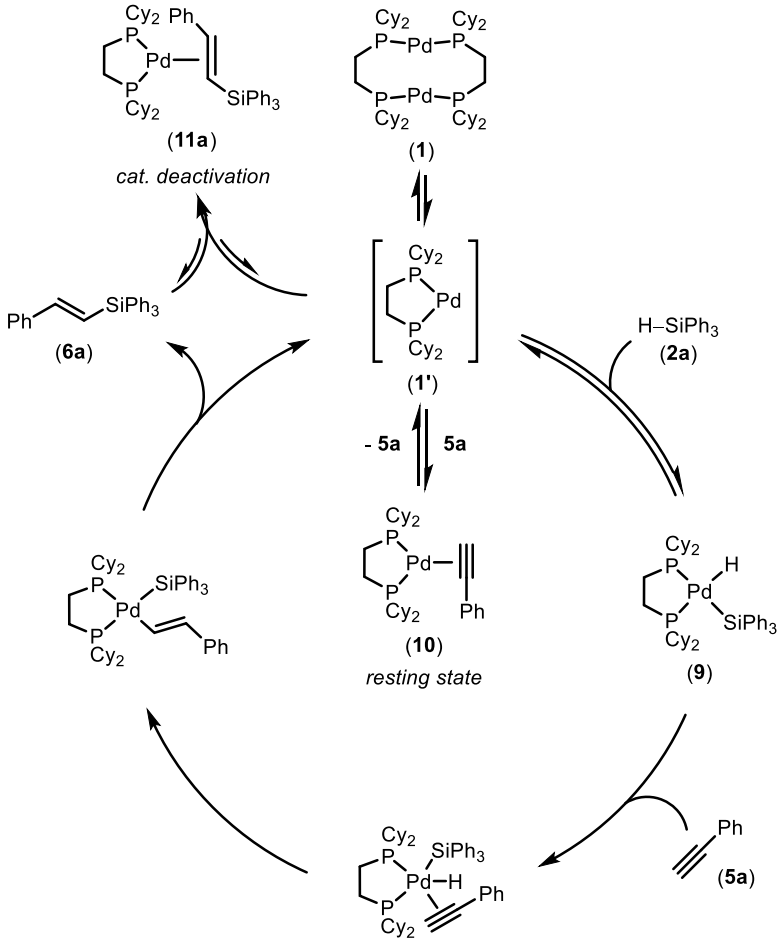

Figure 5.16. Proposed catalytic cycle for the hydrosilylation of **5a** with **2a** catalyzed by **1,** taking into account the results of this study.

Looking towards the mechanism, deuterium incorporation experiments with deuterated substrates **2a-*d*$_1$** and **5a-*d*$_1$** provide evidence for a lack of reversibility in the steps proceeding oxidative addition of **2a** to initiate the catalytic cycle. Additionally, large kinetic isotope effects were observed for each deuterated substrate. Reactions with **2a-*d*$_1$** gave a normal, primary KIE of 1.89 ± 0.07, while those with **5a-*d*$_1$** gave an extraordinary inverse, primary KIE of 0.2 ± 0.05. We suspect that this notable KIE is due to a rehybridization at carbon during migratory insertion but could also be a consequence of the equilibrium processes with **5a** (or **5a-*d*$_1$**).

More work will be done with this system to explore its practicality in hydrosilylation with diverse silane and alkyne substrates, including those necessary to study the effect of arylacetylene steric and electronic effects. More detailed mechanistic studies will help to shed light on some of the unanswered questions brought about in this Chapter, including investigations on the role of products **6** in catalyst deactivation and on the interactions of **1'** with **5a**. These key insights into mechanism and reaction development have the potential to optimize the use of **1** in catalysis for greater levels of efficiency and selectivity.

Perspective and Outlook

This Chapter presents a thorough investigation into the hydrosilylation of phenylacetylene with Pd(0) complex **1**. Trends in the electronic and steric influence of silane substrates were recorded, and the mechanism was elucidated with a variety of experimental tools. Although this work is far from a report on the most efficient state-of-the-art catalyst for alkyne hydrosilylation, we have sought to provide a fundamental basis for understanding this reaction. We hope this will set the stage for further development of **1** in catalytic applications and, more broadly, that the principles uncovered in our studies will hold true in the discovery and optimization of other examples of Pd-catalyzed hydrosilylation – a vitally important reaction in organosilicon chemistry. Thus, we anticipate the work described here will find value in furthering this area of research.

6. OXIDATIVE ADDITION OF PALLADIUM(0) COMPLEXES TO HALOSILANES

Introduction

Halosilanes are commonplace in organic synthesis due to their utility as functional group protection reagents and substrates in halogenation and insertion reactions, among other applications.[1–7] Of the halosilanes, chlorosilanes are most widely available because they are products of the Müller–Rochow "Direct" Process, by which elemental silicon is reacted with alkyl and phenyl chlorides to form chlorosilanes on industrial scale.[8] These chlorosilanes are utilized as precursors for further functionalized organosilicon reagents and polymers, which find broad use across commerce and industry.[9] Although bromo- and iodosilanes are not manufactured at scale and are highly moisture-sensitive, they too are viable substrates for functionalization and organic reactions.[2–4,10] Their reactivity in comparison to Si–Cl reagents can be attributed to the relatively low strength of Si–Br and Si–I bonds; for instance, bond dissociation energies (BDEs) increase 77 < 96 < 113 kcal/mol across the series of $Me_3Si–X$ where X = I < Br < Cl.[11,12] Silyl fluoride bonds are among the strongest bonds known in chemistry, exemplified by a BDE of nearly 160 kcal/mol predicted for $Me_3Si–F$,[11] and thus activation of the Si–F bond is not synthetically viable.

Metal-mediated reactions of halosilanes are known, with examples representing silylation, halogen exchange with aryl and alkyl halides, and ring opening/expansion.[2–4] A more recent and lesser explored application of halosilanes is in late transition metal catalysis to achieve transformations such as Negishi, Kumada, and Heck type cross-couplings.[13]

A prevalent challenge in expanding these catalytic methodologies to abundant chlorosilanes is in overcoming the thermodynamic stability of the Si–Cl bond. In most reported catalytic reactions employing halosilanes, silyl bromides or iodides must be used;[14–21] alternatively, an exogeneous iodide additive may be added to form $R_3Si–I$ *in situ* from silyl chlorides or triflates.[2,10,22–24] Furthermore, while it is generally understood that the reactivities of $R_3Si–X$ (X = H, halogen, C, Si, etc.) bonds increase as electronegative atoms are substituted at silicon,[25–27]

literature remains scarce on systematic studies of silyl halide or substituent identity effects in organometallic chemistry with halosilanes. Understanding of these fundamental factors dictating halosilane reactivity will offer access to underexplored chemical space in their use for catalytic transformations.

In examples of late transition metal catalysis with halosilanes, a near-universally proposed step is the oxidative addition of the metal across the Si–X bond.[13] While oxidative addition to C–X bonds (carbon being the lighter congener of silicon) is ubiquitous in organometallic chemistry and has been studied exhaustively, far less is known about the reaction with halosilanes.[13,25,26] Instances of discrete silyl metal halides formed by oxidative addition of late transition metals to halosilanes exist primarily with Pt,[28–36] Ir,[22,37–41] and Rh,[39,42,43] and the vast majority were reported more than three decades ago. Despite the prevalence of Pt complexes of this type, very few examples are known with the other group 10 metals Pd and Ni.[44–46] In fact, the literature contains only one report of a discrete mononuclear (silyl)Pd(X) complex formed by oxidative addition,[18] and two additional examples formed through multistep mechanisms.[47,48]

Recently, we reported on silane electronic and steric effects in the oxidative addition of palladium complex $[(\mu\text{-dcpe})Pd]_2$ to triorgano- hydrosilanes.[49] These experimental studies revealed a thermodynamic and kinetic preference for silanes with more electronegative and less sterically bulky substituents. However, the (silyl)Pd(H) complexes generated in this reaction are in equilibrium with the starting materials,[49–51] and therefore their potential applications are limited by their propensity to undergo reductive elimination of Si–H. Further, use of $[(\mu\text{-dcpe})Pd]_2$ (dcpe = dicyclohexyl(phosphino)ethane) – which dissociates to transient (dcpe)Pd(0) species in solution – was critical, and no other Pd(0) complex introduced or formed *in situ* was observed to achieve oxidative addition with hydrosilanes.

We wondered, then, if we could leverage the inherent reactivity of Si–X bonds and the stability of Pd–X bonds to investigate the uncommon oxidative addition of halosilanes and form stable, (silyl)Pd(X) complexes from diverse Pd precursors. Following with our studies into the oxidative addition of hydrosilanes,

we were also interested in understanding the thermodynamic and kinetic effects on this reaction with changes in silane substituents and halide identity. Ultimately, we hoped to unravel the mechanism for the oxidative addition of Pd(0) complexes to halosilanes.

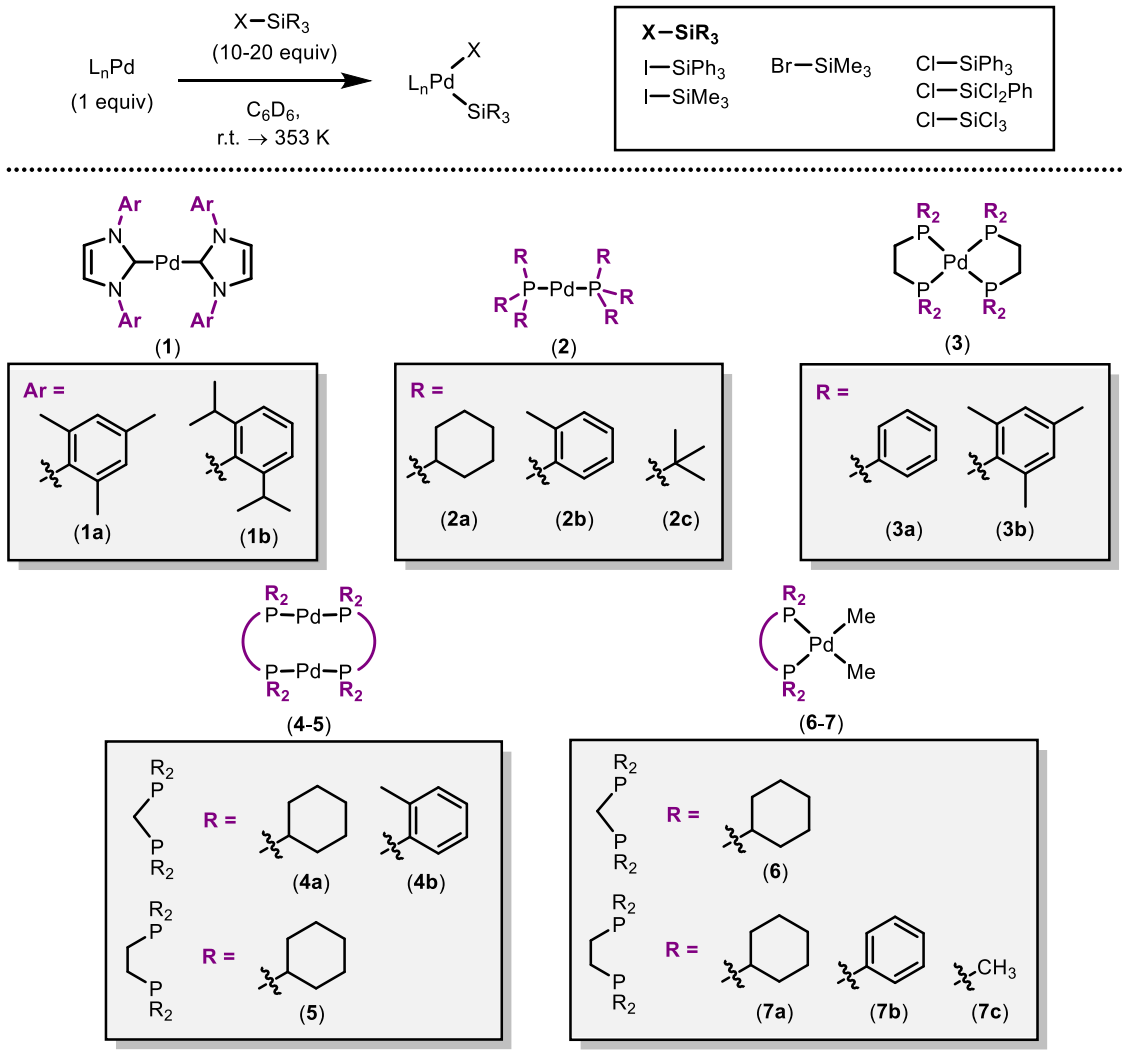

Figure 6.1. Scope of palladium complexes and halosilanes evaluated in preliminary oxidative addition studies.

Results and Discussion

Initial reactivity studies with Pd complexes

To begin our study into the oxidative addition of halosilanes, we first sought to explore a library of Pd(0) complexes or Pd(0) precursors equipped with *N*-heterocyclic carbene (NHC) and monodentate and bidentate phosphine ligands

(Figure 6.1). Experiments were performed to screen a variety of halosilanes with these complexes in solution, and the reactions were monitored by ^{31}P and ^{1}H NMR. An excess of halosilane was used (10-20 equivalents) to push the reaction forward in case oxidative addition was equilibrium-controlled, as observed with hydrosilanes.

From these experiments, trends in the reactivity of halosilanes with Pd complexes were deduced. Bis-NHC Pd(0) complexes **1** were inactive towards oxidative addition with halosilanes, as were bis-monodentate phosphine complexes **2b** and **2c**. In contrast, complex **2a** underwent oxidative addition with $Cl–SiCl_3$ but no other substrate. A crystal of $(PCy_3)_2Pd(Cl)(SiCl_3)$ (**8**) suitable for single crystal x-ray diffraction (Figure 6.2) was grown from a reaction mixture of **2a** + $Cl–SiCl_3$, and reveals a *trans*- ligand environment about the Pd center. This is consistent with fine triplet splitting ($^{2}J_{P\text{-}Si}$ = 5 Hz) in the ^{29}Si NMR spectrum of the complex with no evidence of the *cis*- isomer. This compound is only the third monomeric (silyl)Pd(X) to be crystallographically characterized following Hayashi in 1999 and Watson in 2014.[18,47] One dimeric (silyl)Pd(X) has been reported by Cloke and co-workers.[48]

To better evaluate the geometry about the metal center, the τ_4 structural parameter was calculated from crystal coordinates.[52,53] A τ_4 value of 0.20 was found, where τ_4 = 0 indicates a perfectly square planar complex while τ_4 = 1 indicates ideal tetrahedral geometry. Thus, **8** is well-described as a square planar complex with minor deviation, which is likely due to significant steric hindrance from bulky cyclohexyl groups on PCy_3. A similar distortion was apparent in the crystal structure of related complex *trans*-$(PCy_3)_2PtCl(SiPhCl_2)$ formed by oxidative addition of $(PCy_3)_2Pt$ to $Cl–SiPhCl_2$; accordingly, this product shows the same geometry as **8** (P–Pt–P = 167.8°; Cl–Pt–Si = 164.5°).[30]

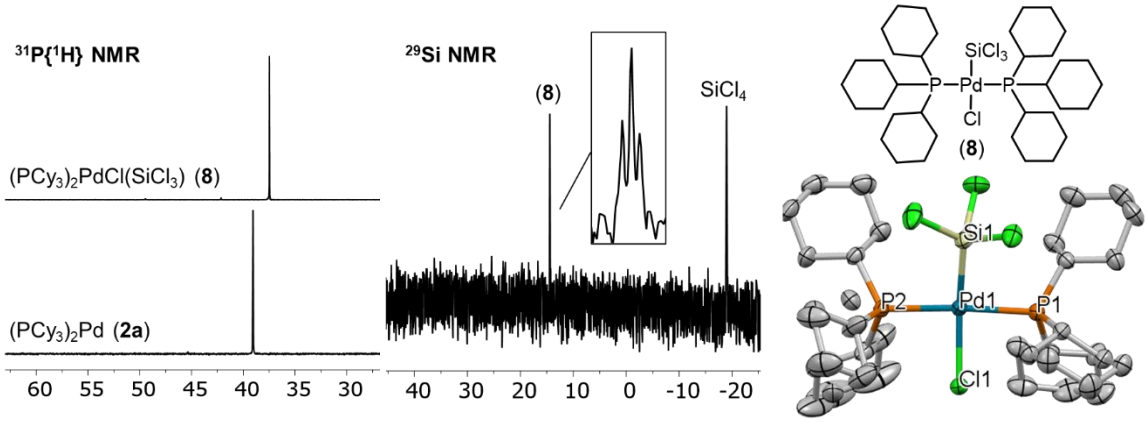

Figure 6.2. Left: $^{31}P\{^{1}H\}$ and ^{29}Si NMR ($^{2}J_{P-Si}$ = 4.4 Hz) spectra of $(PCy_3)_2PdCl(SiCl_3)$ (**8**). Right: molecular structure of (**8**). Thermal ellipsoids are drawn at 50% probability level. Hydrogen atoms are omitted for clarity. Selected bond lengths (Å) and angles (deg): Pd1–Cl1 2.4166(9), Pd1–Si1 2.2834(9), Pd1–P1 2.3893(9), Pd1–P2 2.3845(9), Cl1–Pd1–Si1 162.25(3), Cl1–Pd1–P1 86.10(3), P1–Pd1–P2 168.82(3), P1–Pd1–Si1 92.22(3).

Mononuclear bidentate phosphine complex **3a** did not react with any halosilanes, while **3b** (*vide infra*) successfully underwent oxidative addition with $Cl–SiCl_3$ to form $(dmespe)PdCl(SiCl_3)$ (**9b**) (dmespe = dimesityl(phosphino)ethane); however, like **2a**, **3b** was not active towards oxidative addition with other substrates.

Palladium dimers **4** with methylene-bridged bidentate phosphines – which we envisaged could dissociate (P–P)Pd(0) species **4'**-**5'** in solution in a manner similar to $[(\mu\text{-dcpe})Pd]_2$ (**5**) which would then be trapped by oxidative addition to $X–SiR_3$ (Scheme 6.1a) – did not give the expected products $(P–P)Pd(X)(SiR_3)$ **9**-**10**. Rather, $^{31}P\{^{1}H\}$ NMR spectra after the reaction are characteristic of a symmetrical product in which all phosphorus atoms are equivalent, and the same product is generated regardless of other groups at silicon. There is precedent for simple halosilanes $X–SiMe_3$ to react with dimeric Pd(I) and Pd(II) halide complexes containing similar bidentate phosphine ligands; in these reactions, the halosilanes induce halide exchange via $(P–P)_2Pd_2X'_2{\bullet}Me_3SiX$ adducts to give products $(P–P)_2PdX_4$ and $X'–SiMe_3$ without oxidative addition.[54] The $^{31}P\{^{1}H\}$ NMR spectra collected in our reactions match well with the formation of $(P–P)_2PdX_4$ (δ 0 to -10

ppm)[55] (Scheme 6.1b) but the fate of the silyl groups is unclear. Moving forward, given the lack of oxidative addition observed in these studies, complexes **4** were not studied further.

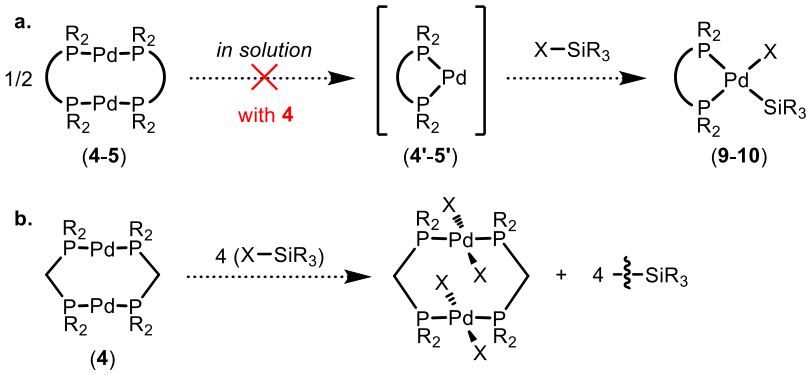

Scheme 6.1. (a) Proposed pathway for dimeric complexes **4**-**5** oxidative addition to halosilanes via dissociation of monomeric **4'**-**5'**. (b) Undesired reaction observed in studies with **4**.

Unlike methylene-bridged dimers **4**, ethylene-bridged [(μ-dcpe)Pd]$_2$ (**5**) readily undergoes oxidative addition with halosilanes to form (dcpe)Pd(X)(SiR$_3$) (**10**) with all of the substrates tested except monochlorosilane Cl–SiPh$_3$. These products are easily identified in $^{31}P\{^1H\}$ NMR spectra as two sets of doublets arising from the inequivalency of phosphorus environments *trans*- to either Pd–X or Pd–SiR$_3$ (Figure 6.3). In these reactions, (dcpe)PdX$_2$ was generated in small amounts as a byproduct alongside the desired product of oxidative addition.

Finally, Pd(II) complexes **6**-**7**, which are known to reductively eliminate ethane to generate transient (P–P)Pd(0) **4'**-**5'** species upon heating,[56] reacted with halosilanes to form products with NMR spectra characteristic of square planar, non-symmetrical Pd(II) complexes as expected for complexes **9**-**10**. However, the identity of the product formed was independent of silane substituents, i.e., all halosilanes with the same halide gave the same product. This spectroscopic data was paired with observation that a precipitate was deposited from the reaction mixture over time, until finally no phosphorus-containing species remained in solution.

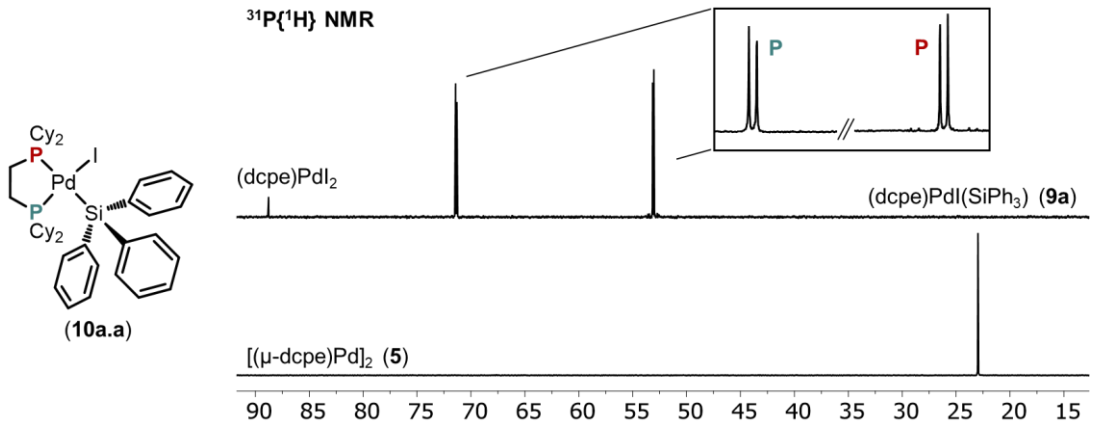

Figure 6.3. $^{31}P\{^{1}H\}$ NMR spectrum showing characteristic peaks of (dcpe)PdI($SiPh_3$) (**10a.a**). Inset: enlarged spectrum of product peak regions.

Taken together, these data imply that oxidative addition to X–SiR_3 does not occur with **4'**-**5'** (Scheme 6.2a). Indeed, the new signals observed by $^{31}P\{^{1}H\}$ NMR can be identified instead as the respective (P–P)PdMeX complexes **11**-**12**, suggesting a direct interaction of halosilanes with **4**-**5**. Although this reactivity precludes oxidative addition of halosilanes to (P–P)Pd(0), it does not absolutely rule out a pathway involving oxidative addition: one explanation for the observed behavior is that oxidative addition of **4**-**5** to X–SiR_3 gives a six-coordinate Pd(IV) intermediate, followed by reductive elimination of Me–SiR_3 and concomitant formation of **11**-**12** (Scheme 6.2b). Formation of an analogous Pd(IV) intermediate resulting from activation of (dmpe)$PdMe_2$ (dmpe = dimethyl(phosphino)ethane) by a disilane has been experimentally supported.[57] Further, this mechanism has been implicated by Schubert and co-workers in similar reactions with (P–N)$PtMe_2$ and I–$SiMe_3$ or Cl–$SiPhMe_2$ to give related products (P–N)PtMeX.[58–60]

Supporting this hypothesis in our experiments, ^{1}H NMR spectra of the reaction mixture show the growth of new peak(s) corresponding to the formation of an organic product postulated as Me–SiR_3. Reactions with I–$SiMe_3$ provide strong evidence for this transformation, as generated $SiMe_4$ is observed in the reaction by both ^{1}H and ^{13}C NMR. Over time, excess halosilane reacts further with **10**-**11** to give (P–P)PdX_2, which precipitates out of solution; this final product is moderately soluble when using the ligand dcpe (complex **7a**) and the

corresponding ^{31}P NMR spectra are characteristic of (dcpe)PdX$_2$ (δ 90 to 100 ppm).[61]

However, an alternate pathway for the reaction of complexes **6**-**7** with halosilanes could proceed by σ-bond metathesis (Scheme 6.2c). Though this mechanism is less commonly proposed with late transition metals than sequential oxidative addition- reductive elimination,[62] examples of σ-bond metathesis have been observed at Pd and Pt, including with silyl substrates.[63–66] Furthermore, the two mechanisms are particularly challenging to distinguish. Given that these reactions did not result in observation of the desired silyl palladium halide species **9**–**10**, we did not explore these Pd(II) complexes further.

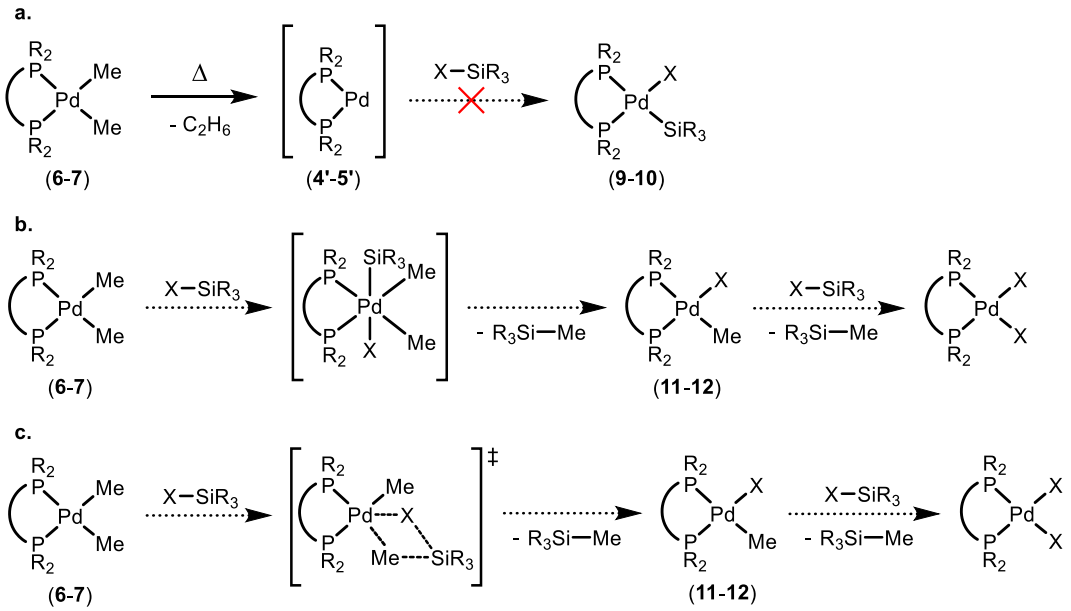

Scheme 6.2. (a) proposed pathway for complexes **6**-**7** oxidative addition to halosilanes via reductive elimination of ethane to form **4'**-**5'**. (b) proposed explanation for the products formed by reaction of **6**-**7** with halosilanes involving sequential oxidative addition-reductive elimination or (c) σ-bond metathesis.

Returning to our goal of evaluating the scope of Pd(0) complexes competent in oxidative addition with halosilanes, we determined only complex **5** to show the desired reaction to form novel products **10** with diverse silane substituents and halide identity. Thus, we focused primarily on this complex for further investigation.

Oxidative addition of 5 with halosilanes – equilibrium studies

We next performed stoichiometric reaction studies to better understand the oxidative addition of complex **5** with representative halosilanes. In these experiments, 2 equivalents of halosilanes X–$SiPh_3$ or X–$SiMe_3$ were added to **5**, and after 5-8 hours NMR spectra of the reaction mixture were collected. Relative concentrations of **5** and **10** were determined by peak integration in $^{31}P\{^{1}H\}$ NMR to approximate product conversion. Results are given in Figure 6.4.

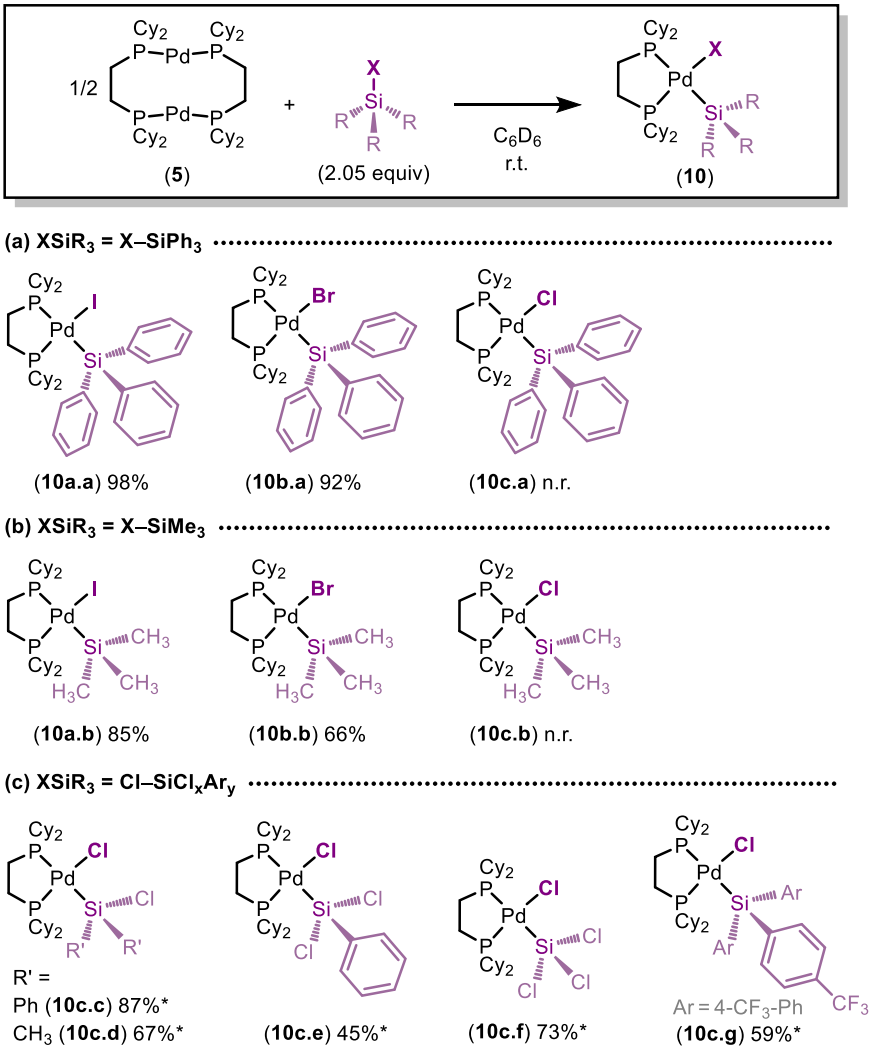

Figure 6.4. Scope of halosilane reactivity with **5**. Percent conversions were determined by NMR integrations (*against an internal standard). Reaction conditions: 1.0 equiv. of **5**, 2.05 equiv of halosilane, 13.33 mM in C_6D_6, 5-8 hours. (a) Triphenyl halosilanes tested (X = I, Br, Cl). (b) Trimethyl halosilanes tested (X = I, Br, Cl). (c) Chlorosilanes tested.

Oxidative addition with I–$SiPh_3$ and Br–$SiPh_3$ to form **10a.a** and **10b.a** proceeded to excellent conversions. On the other hand, as observed in screening studies, there was no reaction with Cl–$SiPh_3$. Similar results with regard to halide identity were obtained using X–$SiMe_3$ substrates, though to lower overall conversion. These findings are fully in line with previously observed trends in oxidative addition of Pt and Rh complexes to halosilanes:[31,33–35,42] as the bond strength of X–Si is decreased and a heavier halogen is used, oxidative addition is increasing facile. Similarly, the substituents at silicon appear to affect the reaction, where more electronegative phenyl substituents are favored to electron-donating methyl groups.

We sought to take advantage of this substituent electronic effect to promote the oxidative addition of chlorosilanes. By using highly electronegative chloro-substituted chlorosilanes, the reaction was achieved in fair to good yields (Figure 6.4c). Further, modification of the aryl substituents on silicon with electron-withdrawing groups enabled oxidative addition with triorgano- chlorosilane Cl–Si(4-CF_3-Ph)$_3$ to form **10c.g**. We are aware of only two reports of monochlorosilane activation at Pd.[67,68] In contrast to our work, the mechanism was not investigated or indirect evidence of Cl–Si activation was used to rationalize results in catalytic reactions, but no discrete silyl metal chlorides were observed in either case.

We next probed the thermodynamics of this reaction by performing competition studies of **5** with halosilanes and triphenylsilane H–$SiPh_3$. In previous work (Chapters 2-4), we showed the oxidative addition of **5** with H–$SiPh_3$ to be favorable but reversible and the product (dcpe)PdH($SiPh_3$) (**13**) in equilibrium with the starting materials. Upon addition of a halosilane to this reaction mixture, an equilibrium will be established between the products of oxidative addition to H–Si and X–Si. The concentrations of these species in solution gives insight into the favorability of the formation of complex **10** against previously studied **13** and allows us to benchmark the oxidative addition of X–Si (Figure 6.5).

The results from these competition studies are in line with equilibrium studies: silyl iodide I–$SiPh_3$ outperforms Br–$SiPh_3$, while silyl chlorides are slightly less active but trend favorably with inclusion of highly electronegative chloride

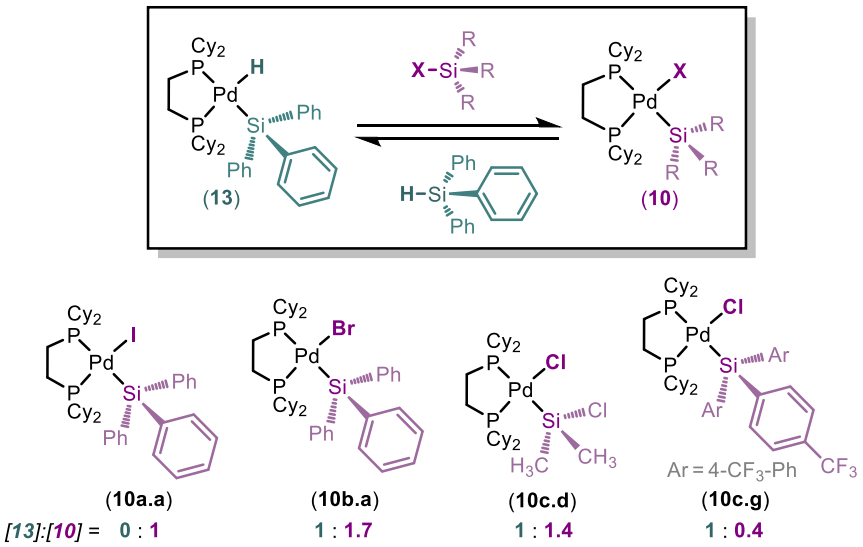

Figure 6.5. Results of competitive equilibrium experiments between $HSiPh_3$ and halosilanes. Experiments were performed in C_6D_6 or C_7D_8 and relative concentrations were determined by ^{31}P NMR integration. Reaction conditions: 1.0 equiv of **5**, 2.05 equiv of $HSiPh_3$, 2.05 equiv of halosilane, 13.33 mM, 5-8 hours.

substituents at silicon. Unexpectedly, when using some halosilanes of different identity than X–$SiPh_3$, such as Br–$SiMe_3$ and Cl–$SiCl_3$, these experiments led to H/X exchange at palladium to give the corresponding (dcpe)Pd(X)($SiPh_3$) (Figure 6.6). This result is especially significant in the case of chlorosilane Cl–$SiCl_3$, as H/X exchange leads to formation of product **10c.a** (and presumably H–$SiCl_3$), which is inaccessible via direct oxidative addition to Cl–$SiPh_3$ under our conditions.

An analogous H/X exchange event was described in early work by Tanaka and co-workers with platinum complexes *trans*-$(PEt_3)_2$PtX($SiMe_3$) in reaction with H–$SiPhMe_2$, though no examples with silyl chlorides were reported.[35] This exchange is proposed to proceed by a sequential oxidative addition-reductive elimination pathway, driven by the formation of more thermodynamically stable M–$SiPh_3$ bonds as compared to M–$SiMe_3$.[35] Similar redistribution processes with halo(hydro)silanes have been explored with *trans*-$(PEt)_2$PtX(H)[29], Vaska-type and Wilkinson's catalysts,[39] and in catalytic reactions with various Ni, Pd, and Pt complexes.[69]

To summarize stoichiometric reaction studies, the results of equilibrium and competition experiments point to the oxidative addition of **5** with halosilanes – and

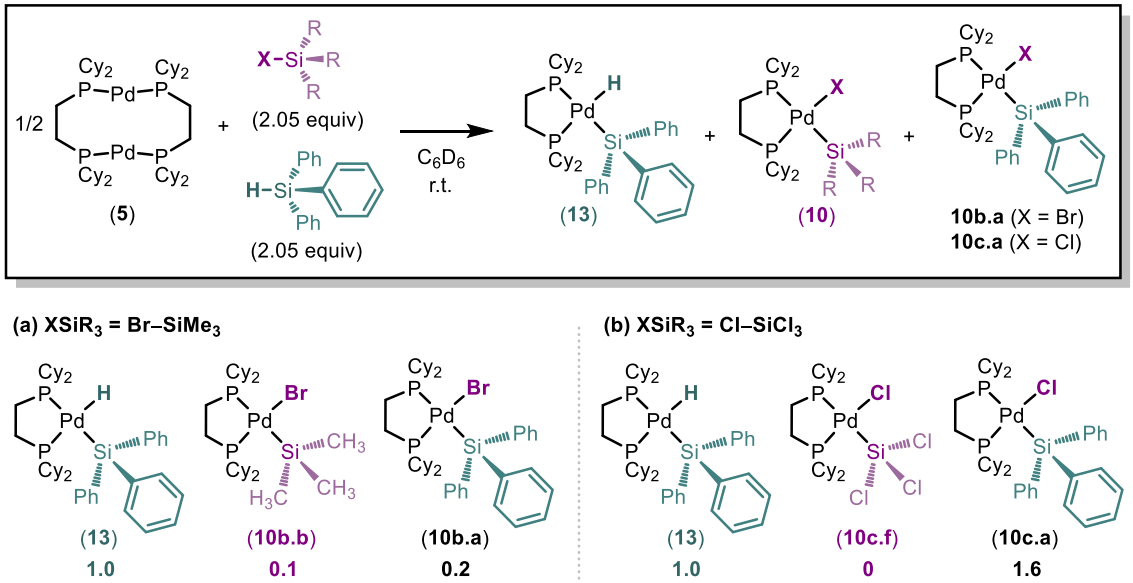

Figure 6.6. Product distributions in competitive equilibrium experiments between $HSiPh_3$ and halosilanes $Br–SiMe_3$ and $Cl–SiCl_3$. Experiments were performed in C_6D_6 and relative concentrations were determined by ^{31}P NMR integration. Reaction conditions: 1.0 equiv of **5**, 2.05 equiv of $HSiPh_3$, 2.05 equiv of halosilane, 13.33 mM, 5-8 hours.

the stability of the resulting complexes **10** – being highly dependent on silyl halide identity and substituents at silicon. An unexpected H/X exchange process is observed in the presenceof both hydrosilane and halosilane to give the corresponding complexes **13** and **10**, yielding even **10c.a** which is unable to form via direct oxidative addition to $Cl–SiPh_3$. Moving forward, we next studied the kinetics of oxidative addition.

Oxidative addition of 5 with halosilanes – kinetic studies

The kinetics of oxidative addition **5** with halosilanes was observed by NMR spectroscopy: a solution of **5**, halosilane, and internal standard in C_7D_8 was mixed at -78 °C and then immediately frozen in liquid nitrogen. The sample was warmed to the desired temperature within the NMR spectrometer pre-cooled to that temperature, and the growth of product was monitored by sequential $^{31}P\{^1H\}$ spectra. Iodosilanes react too quickly at room temperature to collect reliable kinetic

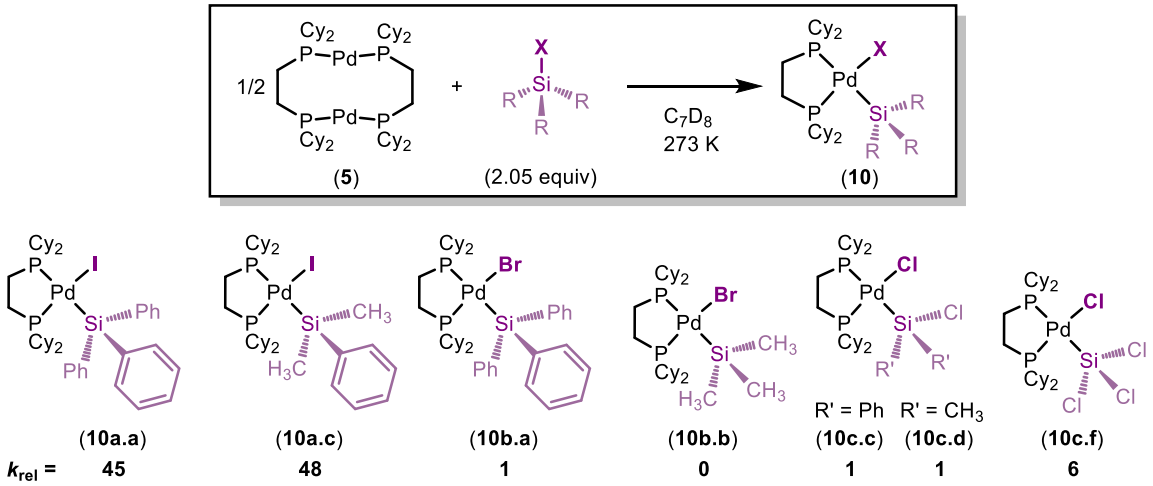

Figure 6.7. Relative initial rates of product formation determined by kinetic studies of the reaction between **5** and halosilanes. Product concentration was determined by ^{31}P NMR integrations against an internal standard. Reaction conditions: 1.0 equiv of **5**, 2.05 equiv of halosilane, 13.33 mM in C_7D_8.

data; thus, trials were conducted at 273 K for preliminary studies. Relative initial rates (k_{obs}) are reported in Figure 6.7.

At 273 K, Br–$SiMe_3$ does not undergo oxidative addition within the time frame of the experiment. Br–$SiPh_3$ shows the slowest rate observed alongside Cl–$SiClR_2$, while the reaction with Cl–$SiCl_3$ is slightly faster. Iodosilanes I–$SiPh_3$ and I–$SiPhMe_2$ undergo oxidative addition rapidly and at essentially the same rate. Interestingly, oxidative addition to Cl–$SiClR_2$ is kinetically equivalent to or more facile than the reaction with either example of Br–SiR_3.

Notably, the rate of oxidative addition with halosilanes is slower than oxidative addition with hydrosilanes, where formation of **13** occurs too quickly to observe even at 233 K. Yet, competitive equilibrium experiments showed the preferential formation of silyl palladium halide products **10** against silyl palladium hydride **13**. We were interested to decouple the kinetic from thermodynamic factors dictating this reaction, and thus performed competitive kinetics experiments. Solutions consisting of equimolar H–$SiPh_3$ and I–$SiPh_3$ were added to **5** and an internal standard, and the reaction was monitored at 273 K.

At t = 60 s, **13** is the dominant product at a relative concentration of 2.5:1 against **10a.a**. Over time, the concentration of **13** decreases at the same rate as

10a.a increases until **10a.a** is the major product of the reaction at t = 20 minutes (Figure 6.8). Raising the temperature to 293 K increases the rate of **10a.a** formation and concomitant **13** consumption. These results are fully in line with previous findings: the formation of **13** is kinetically facile, yet the product is thermodynamically less stable than **10a.a**. At higher temperatures, reductive elimination of H–$SiPh_3$ from **13** is increasingly favored while the rate of oxidative addition to I–$SiPh_3$ is enhanced. Competitive equilibrium experiments represent an extension of this experiment, where full formation of **10a.a** occurs at long time points due to this interplay.

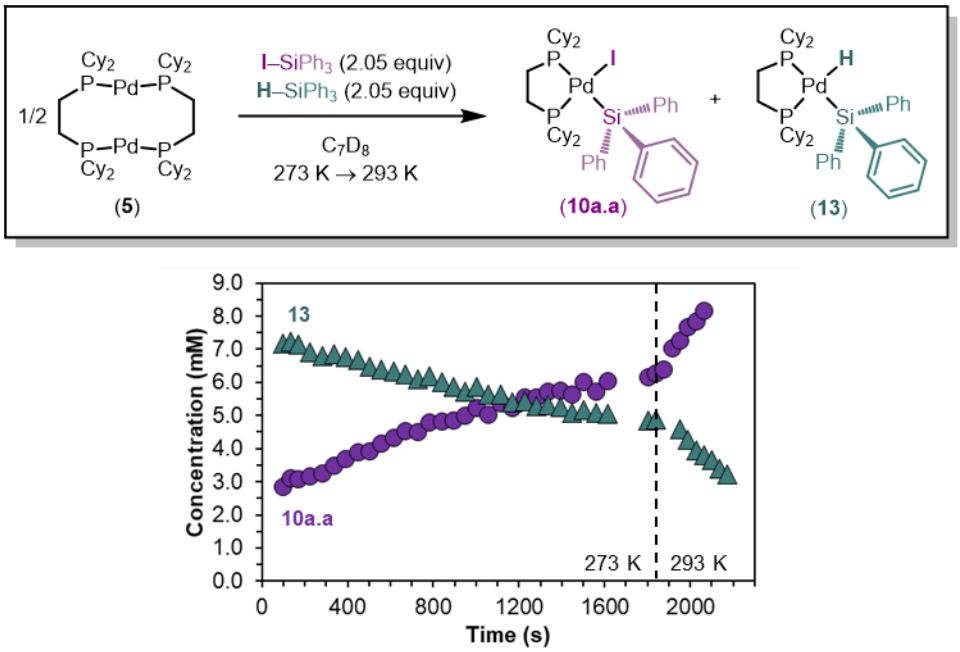

Figure 6.8. Plot of product concentration against time in a competitive kinetics experiment between $HSiPh_3$ and $ISiPh_3$ with **5**. Reaction was conducted at 273 K until ~1800 seconds, at which time the temperature was increased to 293 K. Product concentration was determined by ^{31}P NMR integrations against an internal standard. Reaction conditions: 1.0 equiv of **5**, 2.05 equiv of $HSiPh_3$, 2.05 equiv of $ISiPh_3$, 13.33 mM in C_7D_8.

In good agreement with the observed kinetic favorability of oxidative addition to H–Si against X–Si, previously explored examples in our lab of **5** oxidative addition to chlorinated hydrosilanes $HSiCl_3$ and $HSiClMe_2$ – which effectively behave as substrates for *intra*molecular competition experiments

between the H–Si and Cl–Si bonds – gives exclusively the silyl palladium hydride product with no evidence of oxidative addition to Cl–Si. In this instance, the thermodynamic favorability of (silyl)PdX complexes **10** to (silyl)PdH is not a factor because the Cl–Si bond is rendered inactive towards oxidative addition after the initial reaction with H–Si. This is true even when the silane is properly "activated" towards oxidative addition of the Cl–Si bond with highly electronegative substituents. This helps to explain trends in seminal studies of Pd-catalyzed alkene hydrosilylation first observed by Tsuji and co-workers, where only the H–Si bond of $HSiCl_3$ was activated.[70]

When competitive kinetics experiments with $I–SiPh_3$ and $H–SiPh_3$ were repeated at 253 K, an initial equilibrium was established 2.5:1 between **13** and **10a.a** at t = 60 s, but no change in the concentration of either product was observed thereafter. To investigate how temperature affects the rate and energetics for the formation of **10**, we next conducted variable temperature kinetics experiments.

The reaction rate with each halosilane was studied at a minimum of four different temperatures, and the rates were used to determine the energetics of oxidative addition by Eyring analysis (Figure 6.9). All reactions show large, negative $\Delta S^{‡}$ (~15-40 cal•mol^{-1}•K^{-1}) and positive $\Delta H^{‡}$ (~9-15 kcal•mol^{-1}). $\Delta G^{‡}$ at 273 K is not significantly different between any substrates, though iodosilanes are the least disfavored to a minor degree. The similarity of transition state energies for all halosilanes may indicate that the reaction proceeds via the same mechanism regardless of silyl halide identity and substituents. We sought to further investigate this mechanism.

Oxidative addition of 5 with $I–SiPh_3$ – mechanistic studies

There are three distinct mechanisms possible in non-polar solvents for the oxidative addition of **5'** (generated by dissociation from **5**) to halosilanes: concerted, S_N2-like, or radical (Figure 6.10).[71–73] While we have shown previously that oxidative addition of **5'** to hydrosilanes undergoes a concerted mechanism,[49] the X–Si bond of halosilanes is far more polar than H–Si (for comparison, the Cl– Si bond is more than twice as polar as Cl–C, a classically defined "strongly

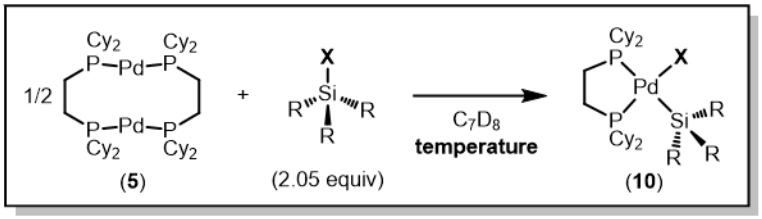

Silane	Product	ΔH‡ kcal•mol^{-1}	ΔS‡ cal•mol^{-1}•K^{-1}	ΔG$_{273}$‡ kcal•mol^{-1}
I–SiPh$_3$	**10a.a**	9.5 ± 0.6	-30 ± 4	18 ± 1
I–SiPhMe$_2$	10a.c	9.1 ± 0.6	-31 ± 4	18 ± 1
Br–SiPh$_3$	**10b.a**	17 ± 2	-13 ± 3	20 ± 3
Br–SiMe$_3$	10b.b	9.4 ± 1	-40 ± 20	21 ± 5
Cl–SiClPh$_2$	10c.c	15 ± 1	-18 ± 2	20 ± 1
Cl–SiClMe$_2$	10c.d	12.1 ± 0.2	-28 ± 1	20.0 ± 0.4
Cl–SiCl$_3$	**10c.f**	9.6 ± 0.6	-34 ± 5	19 ± 1

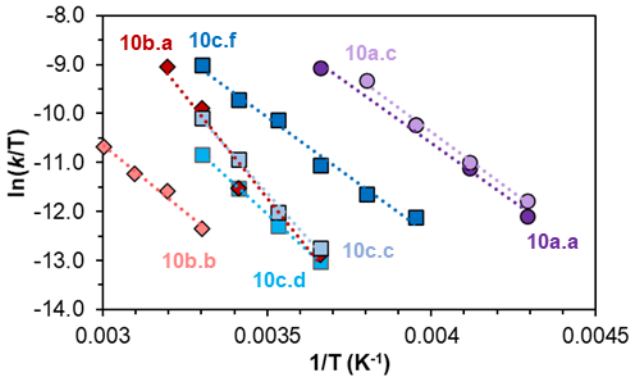

Figure 6.9. Eyring analysis and derived energy parameters from variable temperature kinetics studies of the reaction between **5** and halosilanes. The rate of reaction at each temperature was taken as the average of at least two trials.

polar" bond).[71] S$_N$2-like pathways are regularly observed with polar substrates such as alkyl halides and therefore cannot be dismissed in this system.[72] Radical oxidative additions are characterized by poorly reproducible rates of reaction and high sensitivity to halide identity, giving orders of magnitude faster rates with I–R > Br–R > Cl–R substrates.[72–74] While iodosilanes are favored in our studies, rates differ by only one order of magnitude between examples with I–Si and Cl–Si bonds, and results are reproducible across time and batches of **5**. Additionally, radical oxidative additions are uncommon at coordinatively unsaturated non-first row metal complexes.[73,74] We concluded that a radical mechanism was not operative.

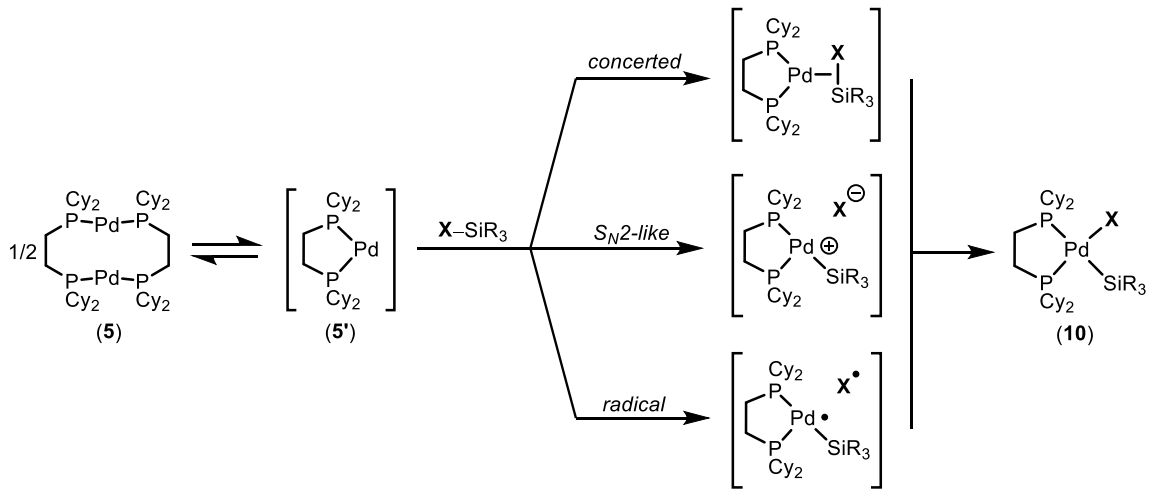

Figure 6.10. Potential pathways for the oxidative addition of **5** to halosilanes via concerted, S_N2-like, or radical mechanisms.

To distinguish between the concerted and S_N2-type mechanisms, we first determined the rate law of the reaction between **5** and I–$SiPh_3$. Samples for kinetics experiments were prepared with varied concentrations of one reagent while the other was kept constant. The order in the reagent of interest was evaluated by plotting the rate of the reaction against the initial concentration of the reagent (Figure 6.11).

From these experiments, the reaction was determined to be 0.5th (0.53 ± 0.03) order in **5**. This is consistent with the proposed dissociation of [(μ-dcpe)Pd]$_2$ into two equivalents of (dcpe)Pd (**5'**) that then undergo oxidative addition. Varying the concentration of the halosilane, we found the reaction to be 1st (0.99 ± 0.08) order in I–$SiPh_3$.The simplified rate law for the reaction can be written (equation 1), showing an overall 1.5th order reaction:

$$Rate = k_{obs}[\mathbf{5}]^{0.5}[\mathrm{ISiPh_3}] \qquad (1)$$

The rate law provides fundamental mechanistic insight into the reaction, yet this result does not inform on the pathway of oxidative addition. For both concerted or S_N2-like pathways, we would expect a 0.5th order dependence on **5** (or a 1st order in **5'**) and a 1st order dependence on I–$SiPh_3$. A large, negative $\Delta S^{\ddagger}$ is also characteristic of both mechanisms.

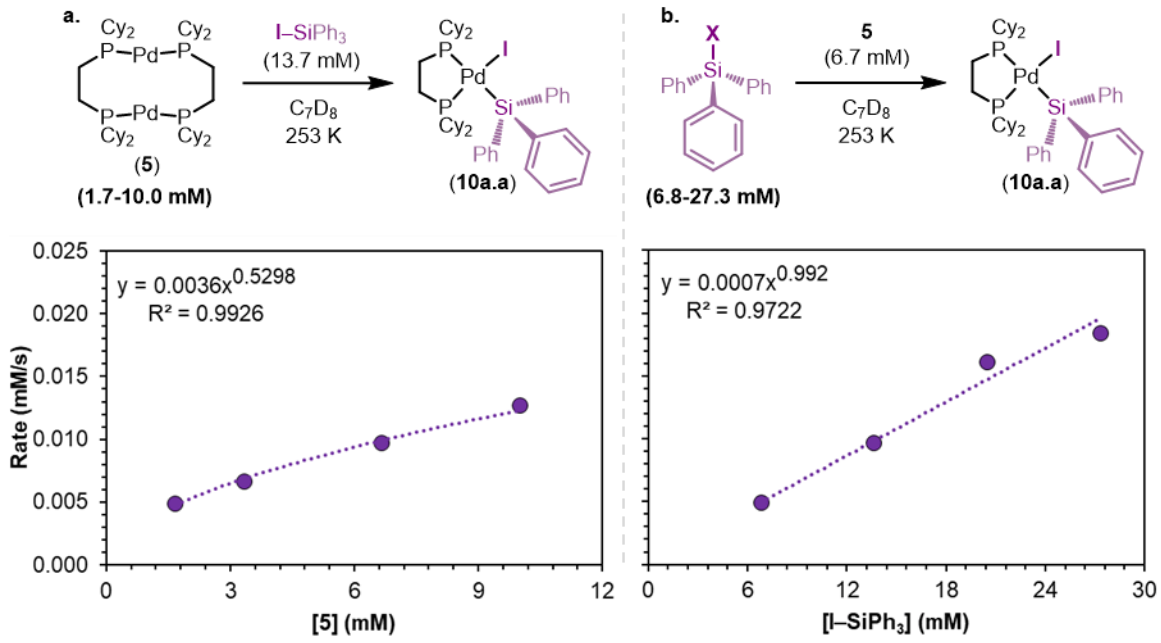

Figure 6.11. (a) plot of initial rate of reaction versus [**5**]. (b) plot of initial rate versus [I–$SiPh_3$]. Kinetics data was collected at 233 K in C_7D_8. Product concentration was determined by ^{31}P NMR integration against an internal standard.

One distinguishing feature of concerted and S_N2-like pathways is their effect on product geometry: concerted reactions generate exclusively the *cis*- product, while S_N2-like reactions can lead to *cis*- or *trans*- products.[73] However, complexes such as **5** with bidentate phosphine ligands are not amenable to the formation of square planar, four-coordinate *trans*- products, as the chelating phosphorus atoms about the metal center are forced in a *cis*- orientation to one another. Due to the inability of the reaction with **5** to form *trans*- products, then, we cannot use product geometry about Pd to lend insight into the mechanism with this complex.

Despite this setback, the two mechanisms of oxidative addition could potentially still be distinguished by probing product stereochemistry and the effect of reaction conditions.[71–73] In concerted oxidative addition, the stereochemistry about a chiral silicon center is preserved, whereas it is inverted under an S_N2-like mechanism. Moreover, concerted reactions tend to be unaffected by solvent polarity, while S_N2-like reactions are faster in polar solvents.

Unfortunately, attempts to synthesize and evaluate the enantiomeric purity of a chiral halosilane were unsuccessful, and the solvent tolerance of **5** is limited

primarily to non-polar hydrocarbons. Thus, the rate of reaction at 253 K was evaluated in a 50:50 mixture of toluene:hexane and compared to a sample prepared side-by-side in 100% toluene (Figure 6.12). While the sample in 50:50 toluene:hexanes showed a slightly slower reaction, the differences in rate and solvent polarity are too minor to draw meaningful conclusions about the mechanism of oxidative addition.

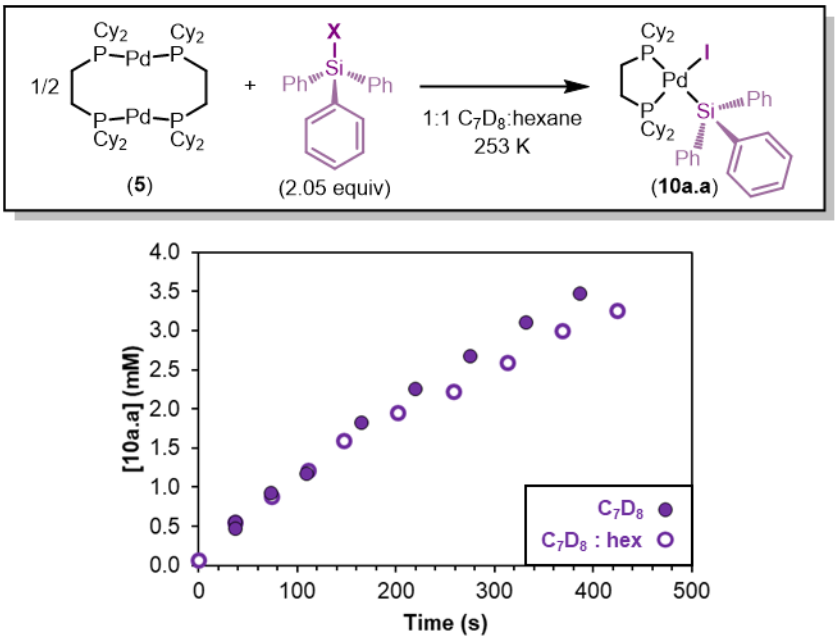

Figure 6.12. Plot of **10a.a** concentration against time for kinetics samples in toluene or 50% hexanes:toluene. Product concentration was determined by ^{31}P NMR integrations against an internal standard.

Absent of spectroscopic handles to evaluate this reaction further, we were not able to elucidate the mechanism for oxidative addition of **5** to I–$SiPh_3$. The rate law of the reaction points to initial dissociation of **5** to two equivalents of active species **5'**, as similarly postulated in studies with hydrosilanes. Oxidative addition at **5'** proceeds through either a concerted or S_N2-like mechanism.

Returning to our preliminary studies on the oxidative addition of diverse Pd precursors with halosilanes, we were interested to explore the complexes in addition to **5** that reacted with Cl–$SiCl_3$. Namely, we wondered how complexes **2a**, **3b**, and **5**, with their vastly different structures, reacted to form similar products **8**, **9b**, and **10**, and if the same mechanism was operative in each instance.

Oxidative addition of 2a, 3b, and 5 with Cl–$SiCl_3$

To begin our mechanistic investigation of **2a** and **3b**, we conducted kinetics studies on their oxidative addition to Cl–$SiCl_3$. Interestingly, **3b** is a novel complex synthesized in our lab and, at the outset of this project, we had not determined whether it was monomeric or dimeric. In C_7D_8 solution, **3b** exists in equilibrium with the free ligand dmespe; upon cooling this solution to 193 K, complicated dynamics are observed by ^{31}P NMR that we were not able to resolve. Studying the kinetics of the reaction of **3b** with Cl–$SiCl_3$ gave us crucial insight in determining the complex as monomeric: upon oxidative addition, one equivalent of free ligand is dissociated from the starting material (Figure 6.13).

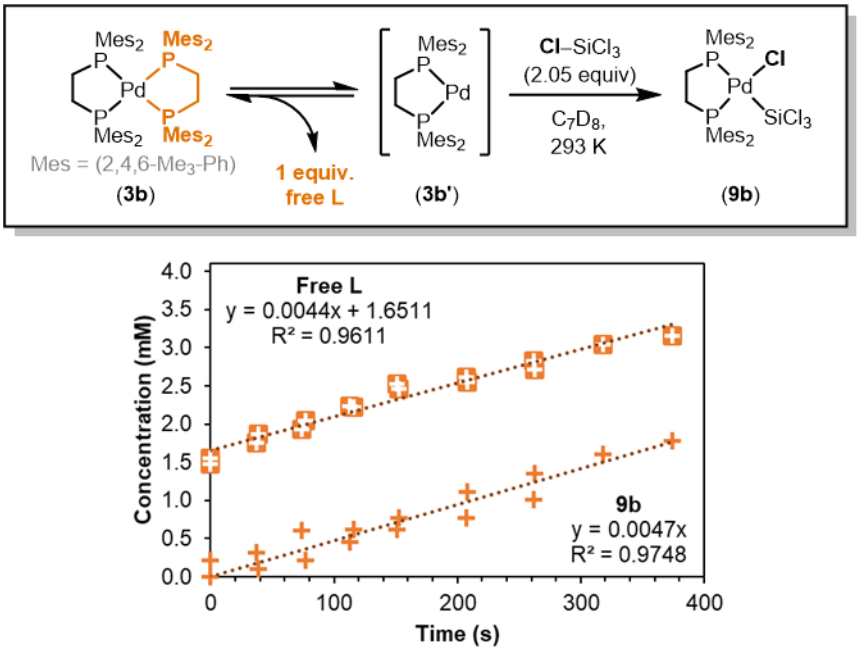

Figure 6.13. Plot of **9b** and free dmespe ligand concentration against time in a kinetics experiment at 293 K. Concentrations were determined by ^{31}P NMR integrations against an internal standard.

The assignment of **3b** as a monomeric species is further supported by the rate law of the reaction (Figure 6.14). Using variable concentration kinetics studies, we determined the reaction to be 1^{st} (1.0 ± 0.1) order in **3b**, indicating that each equivalent of **3b** is transformed to only 1 equivalent of **9b**. This results rules out a dimer dissociation pathway whereby 2 equivalents of **3b'** are generated from **3b**

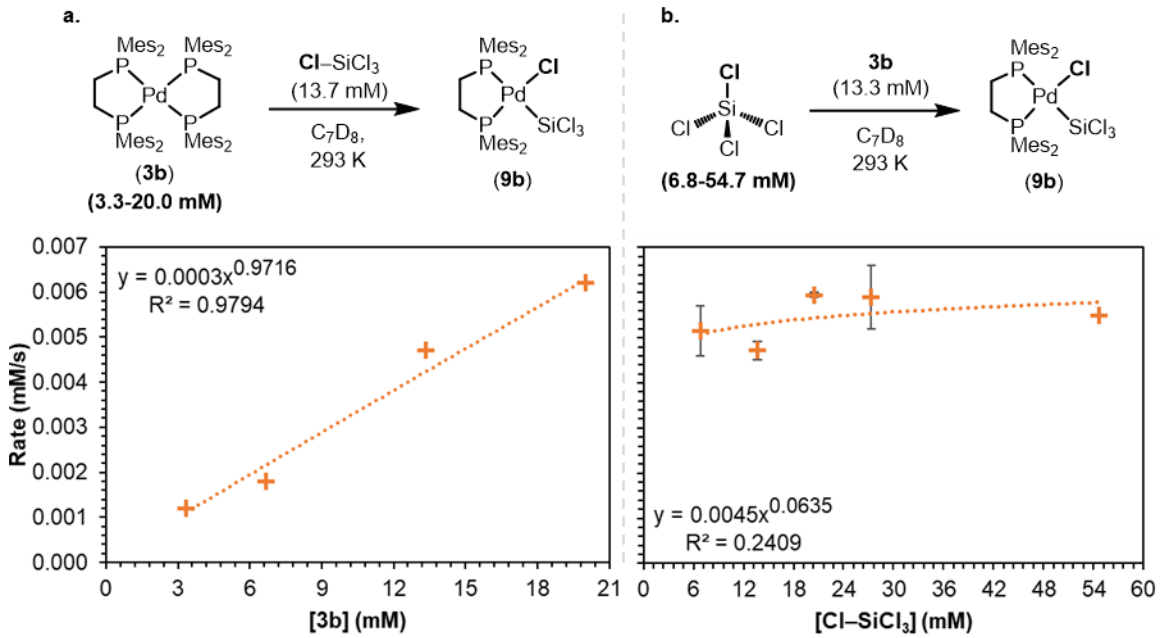

Figure 6.14. (a) plot of initial rate of reaction versus [**3b**]. (b) plot of initial rate versus [Cl–$SiCl_3$] (average of two trials). Kinetics data was collected at 293 K in C_7D_8. Product concentration was determined by ^{31}P NMR integration against an internal standard.

in a manner analogous to **5**. Rather, when paired with the observation of stoichiometric ligand dissociation during the reaction with Cl–$SiCl_3$, these results are fully consistent with the activation of monomeric complex **3b** by dissociation of 1 equivalent of dmespe to form **3b'**, which then undergoes oxidative addition.

Next, varying the concentration of the halosilane, we found the reaction to be 0^{th} (0.06 ± 0.06) order in Cl–$SiCl_3$, This result suggests that the rate-determining step occurs prior to an interaction of **3b** with the halosilane and thus [Cl–$SiCl_3$] is not involved in the rate law. The simplified rate law (equation 2) for the reaction can be written as 1^{st} order:

$$Rate = k_{obs}[\mathbf{3b}] \qquad (2)$$

Unfortunately, a similar side reaction occurs in experiments using **3b** in the presence of excess dmespe ligand. In this case, however, the product of dmespe + Cl–$SiCl_3$ shows two paired triplets (J = 28 Hz) in the $^{31}P\{^1H\}$ NMR spectrum at δ 3 and -19 ppm. Dmespe is an uncommon ligand and, as such, there is a lack of precedent for its reactivity and potential byproducts. Looking at related examples,

the observed byproduct in our studies does not align well with examples of other diaryl(phosphino)ethane ligands dppe (dppe = diphenyl(phosphino)ethane) or potpe (potpe = phenyl(o-tolyl)(phosphino)ethane) chloride adducts $[(P–P)Cl_2]^{2+}[2Cl^-]$ (e.g. $^{31}P\{^1H\}$ NMR δ 72 ppm in $CDCl_3$ at 298 K with potpe)[80] or palladium dichloride complexes $(P–P)PdCl_2$ (e.g. $^{31}P\{^1H\}$ NMR δ 58 ppm in CH_2Cl_3 at 298 K with dppe).[81] This prevalent side reaction precludes determination of the order for added dmespe in the reaction of **3b** with $Cl–SiCl_3$ but does not play a substantial role under standard conditions with no added ligand.

From these studies, we can conclude that the rate-determining step of the reaction is likely dissociation of free dmespe ligand from **3b** to generate **3b'**. This explanation exemplifies a fundamental principle in oxidative addition that "the rates for ligand dissociation that occur prior to oxidative addition affect the rates of the overall addition processes."[71] This is dissimilar to the observed behavior of **5** with $I–SiPh_3$ (and with hydrosilanes), where formation of **5'** occurs with an immeasurably low barrier prior to oxidative addition.

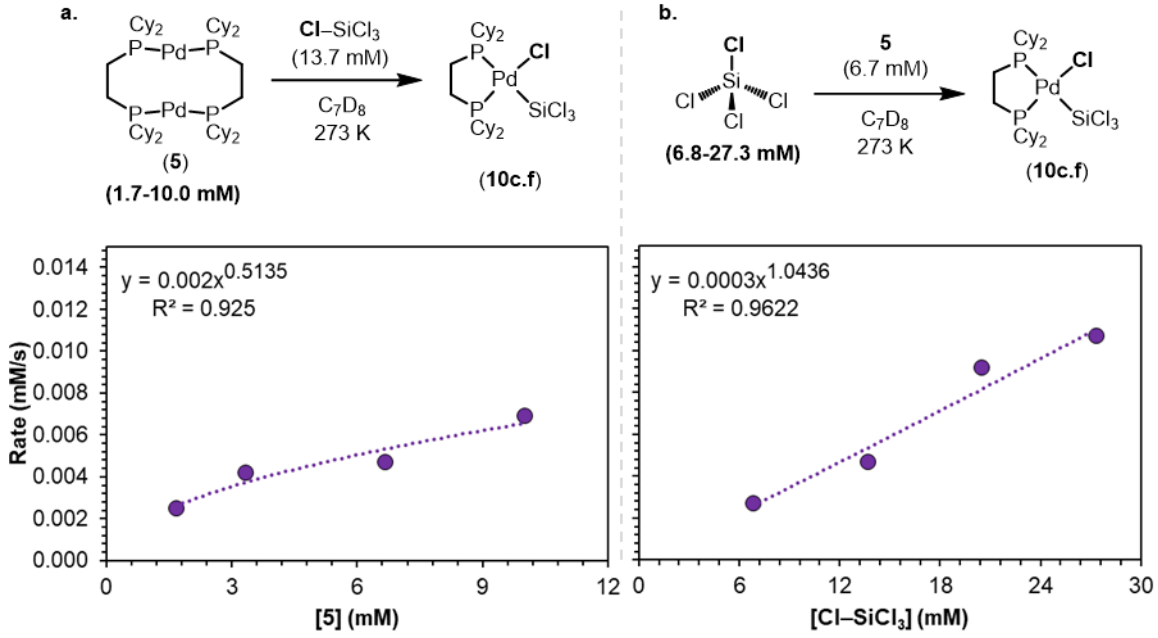

Figure 6.15. (a) plot of initial rate of reaction versus [**5**]. (b) plot of initial rate versus $[Cl–SiCl_3]$. Kinetics data was collected at 273 K in C_7D_8. Product concentration was determined by ^{31}P NMR integration against an internal standard.

There is some precedent for distinct mechanisms arising in oxidative addition of bisphosphine Pd(0) complexes to X–R when the X identity is changed.[75,76] In order to examine whether the mechanism was different in the oxidative addition of **5** to a chlorosilane than in studies with I–$SiPh_3$, the rate law for **5** + Cl–$SiCl_3$ was elucidated (Figure 6.15). As in experiments with the iodosilane, the reaction was determined to be 0.5th (0.51 ± 0.09) order in **5** and 1st order in Cl–$SiCl_3$ (1.0 ± 0.1), which is consistent with interaction of the halosilane occurring at or before the rate-determining step. This discounts the dissociation of **5'** from **5** as rate-limiting. The simplified rate law of the reaction (equation 3) can be written with an overall 1.5th order:

$$Rate = k_{obs}[\mathbf{5}]^{0.5}[\mathrm{ClSiCl_3}] \qquad (3)$$

Finally, we moved on to evaluating the rate law for the oxidative addition of **2a** to Cl–$SiCl_3$ (Figure 6.16). The reaction was determined to be 1st (1.02 ± 0.07) order in **2a**, which is in line with the expected reactivity of **2a** as a monomeric species that can directly undergo oxidative addition. Similarly, a 1st (1.0 ± 0.1) order in Cl–$SiCl_3$ was found. These results suggest that coordinatively unsaturated complex **2a** reacts stoichiometrically with Cl–$SiCl_3$ and is involved at or before the rate-determining step. It has been suggested in theoretical studies that oxidative addition with bisphosphine complexes **2** proceeds by a dissociative oxidative addition mechanism, in which the first step is release of free phosphine ligand to yield monoligated (PR_3)Pd(0) as the active species.[77] In our work, we did not observe the dissociation of PCy_3 ligand by ^{31}P NMR during kinetic trials.

Furthermore, spectroscopic and crystallographic evidence unambiguously identify the product **8** as bisphosphine *trans*-(PCy_3)$_2$PdCl($SiCl_3$) (Figure 2). Therefore, if ligand dissociation were occurring, it must favorably reassociate at a later stage of the reaction pathway, perhaps precluding the spectroscopic observation of free PCy_3 if the reaction occurs at a sufficient rate. In a dissociative mechanism, the presence of excess PCy_3 would severely hinder the rate of reaction as it would stabilize the bis-coordinated complex **2a** and disfavor release of the free ligand.[78] In order to evaluate this hypothesis, the order in free PCy_3 ligand was determined (Figure 17). Kinetics studies were prepared under usual

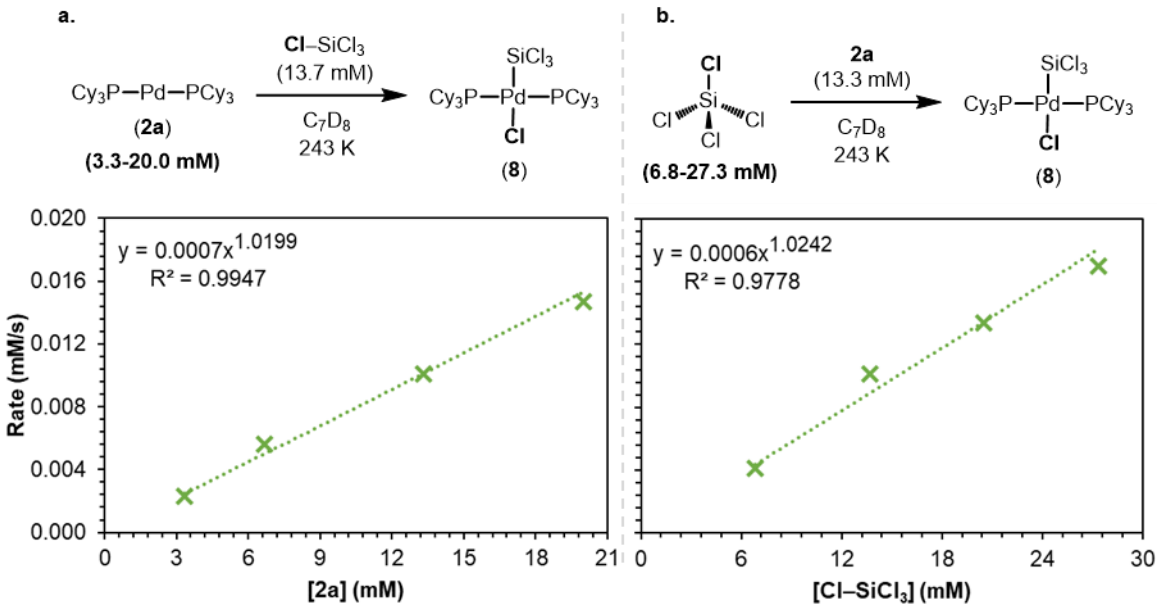

Figure 6.16. (a) plot of initial rate of reaction versus [**2a**]. (b) plot of initial rate versus [Cl–$SiCl_3$]. Kinetics data was collected at 243 K in C_7D_8. Product concentration was determined by ^{31}P NMR integration against an internal standard.

conditions, except that additional PCy_3 (0.5-4.0 equivalents) was added to the reaction mixture.

An inverse correlation in rate was observed with increasing concentration of PCy_3 to give an order of approximately -0.2 (-0.22 ± 0.05). This fractional order in PCy_3 is difficult to interpret but may suggest a stabilization of **2a** by excess ligand in solution. Yet, the concentration of PCy_3 does not change throughout the experiment (Figure 17b). This implies that the interaction of PCy_3 with complex **2a** or Cl–$SiCl_3$ is either fully reversible or occurs entirely within the first seconds of the experiment before spectra are collected.

Notably, the presence of a new product ($^{31}P\{^1H\}$ NMR δ 65 ppm in C_7D_8 at 243 K) was observed in these studies that is not seen in standard kinetics experiments with **2a** and Cl–$SiCl_3$. The chemical shift of this product by $^{31}P\{^1H\}$ NMR is similar to that reported for $[Cl–PCy_3]^+[Cl]^-$ ($^{31}P\{^1H\}$ NMR δ 60 ppm in CD_2Cl_2 at 298 K).[79]

After approximately t = 100 s, the concentration of this byproduct equilibrates, and the final concentration is proportional with the concentration of

added PCy_3. The formation of an unreactive byproduct is also consistent with lower than expected [PCy_3] observed based on the intended stoichiometry of the experiments. Overall, these results suggest that free PCy_3 reacts with Cl–$SiCl_3$ prior to oxidative addition and the resulting species is inactive in the reaction thereafter. Thus, free PCy_3 does not participate in oxidative additionbut indirectly impedes the reaction by lowering the effective concentration of active species Cl–$SiCl_3$. This result is in conflict with the theoretical suggestion of (PR_3)Pd(0) species

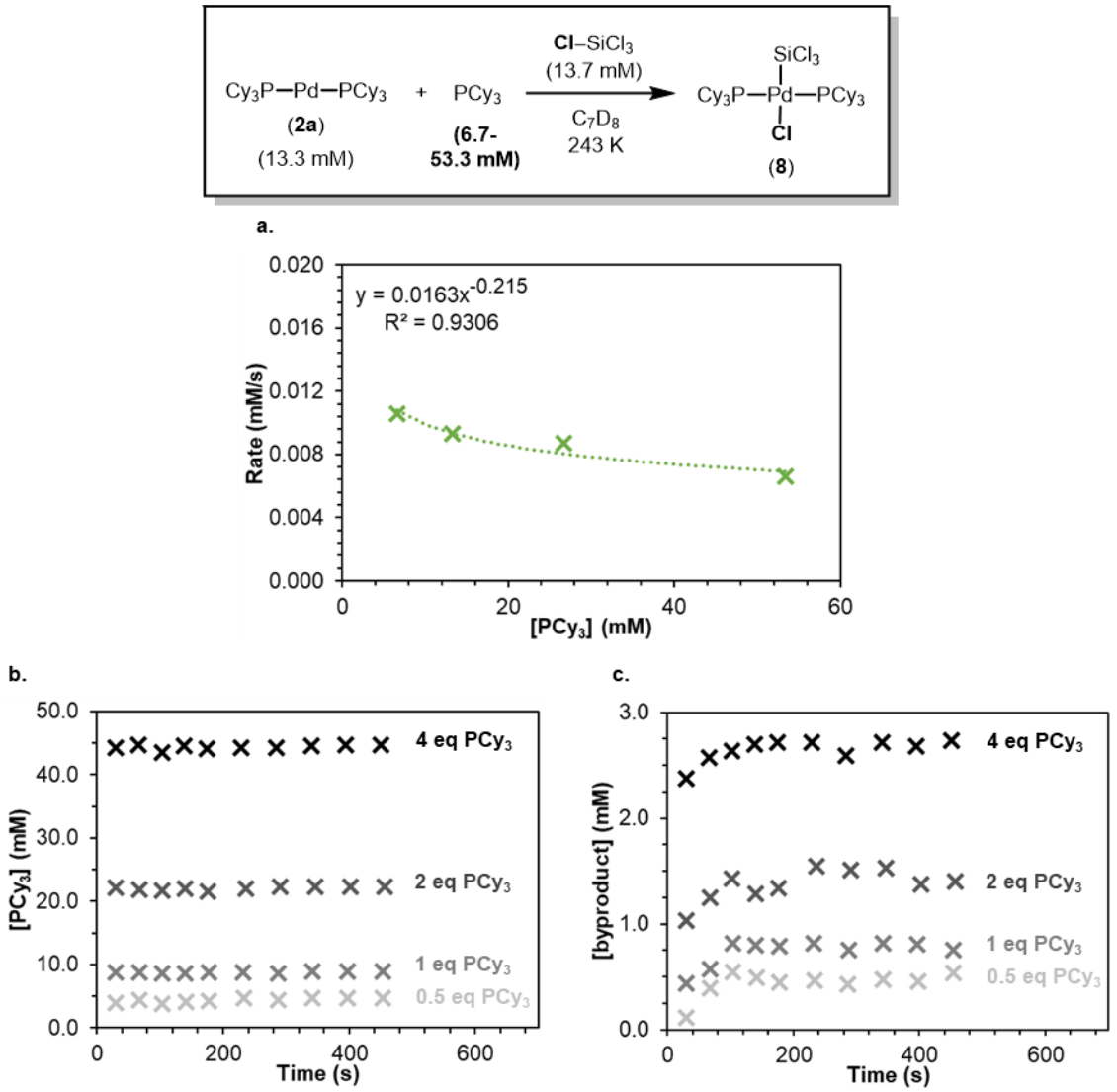

Figure 6.17. (a) plot of initial rate of reaction versus [PCy_3]. (b) plot of PCy_3 concentration against time in a kinetics study conducted at 243 K in C_7D_8. (c) plot of byproduct concentration against time in a kinetics study conducted at 243 K in C_7D_8. Concentrations were determined by ^{31}P NMR integration against an internal standard.

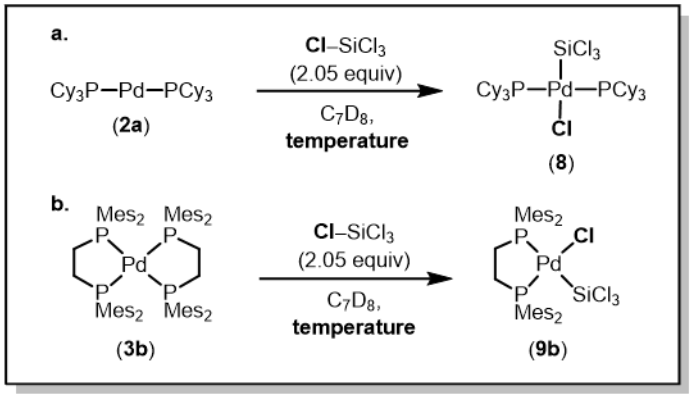

Pd complex	Product	ΔH‡ kcal•mol^{-1}	ΔS‡ cal•mol^{-1}•K^{-1}	ΔG$_{273}$‡ kcal•mol^{-1}
Pd(PCy$_3$)$_2$ (**2a**)	8 ×	5.8 ± 0.2	-43 ± 0.9	17.6 ± 0.3
(dmespe)$_2$Pd (**3b**)	9b +	19 ± 1	-3.5 ± 0.3	20 ± 1
[(μ-dcpe)Pd]$_2$ (**5**)	10c.f ■	9.6 ± 0.6	-34 ± 5	19 ± 1

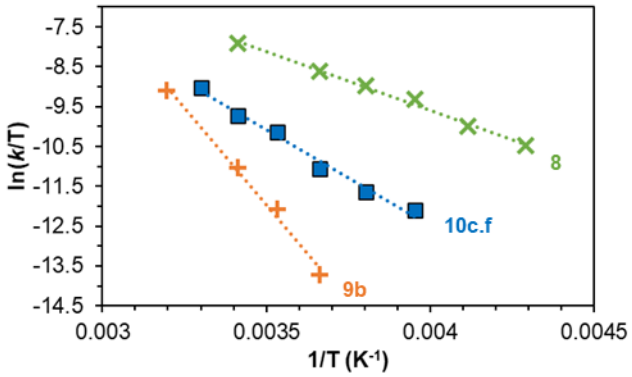

Figure 6.18. Eyring analysis of variable temperature kinetics studies for the reaction of Pd complexes **2a**, **3b**, and **5** with halosilanes and the derived energetic parameters. The rate of reaction at each temperature was taken as the average of at least two trials.

forming in solution prior to oxidative addition, and we suggest ligand dissociation from **2a** is not operative in our system.

Therefore, the rate law for oxidative addition (equation 4) is 2nd order and can be represented without a dependence on [PCy$_3$]:

$$Rate = k_{obs}[\mathbf{2a}][\mathrm{ClSiCl_3}] \qquad (4)$$

Moving forward with this understanding of the stoichiometry and activation pathways of Pd complexes **2a** and **3b**, we next determined the energetics of their

reaction with Cl–$SiCl_3$ by Eyring analysis (Figure 6.18). In comparison to **5**, oxidative addition with **2a** is faster and gives a substantially lower $\Delta H^{\ddagger}$ (5.8 kcal•mol^{-1}); however, this increase in enthalpic favorability is mostly offset by a large, negative $\Delta S^{\ddagger}$ (-43 cal•mol^{-1}•K^{-1}). At 273 K, $\Delta G^{\ddagger}$ of the reaction of **2a** with Cl–$SiCl_3$ is the least disfavored of any complex studied by a small, but statistically significant, amount.

In contrast, **3b** reacts more slowly than **5**, and the activation parameters deviate from the other two complexes. Oxidative addition with **3b** shows a high enthalpic barrier (19 kcal•mol^{-1}) but is essentially entropically neutral. At 273 K, $\Delta G^{\ddagger}$ of the reaction is comparable to that with **5**.

Together, the rate law and $\Delta S^{\ddagger}$ values derived from these reactions give insight into the disparate pathways for activation of Pd complexes **2a**, **3b**, and **5**, as summarized in Scheme 6.3.

Complex **2a** exists as a coordinatively unsaturated monomer that can directly undergo associative oxidative addition without an initial activation process; as a result, the rate-determining step must involve, or come after, an interaction with the halosilane. In line with this finding, the rate law indicates a 1st order dependence on the initial concentration of Cl–$SiCl_3$ in the reaction, and a large negative $\Delta S^{\ddagger}$ suggests a concerted or S_N2-like pathway for oxidative addition. In this system, formation of the *trans*- product isomer may hint at an S_N2-like pathway. However, we cannot rule out a rapid isomerization of the product in solution that could lead to exclusive observation of *trans*-**8** even if *cis*-**8** forms during the reaction; indeed, this isomerization process is precedented with examples of $(PR_3)_2PdRX$ complexes.[82]

Complex **3b** was determined to have a monomeric structure, but it is coordinatively saturated and thus must dissociate an equivalent of dmespe ligand before interacting with Cl–$SiCl_3$. This ligand dissociation comprises the rate-determining step of the reaction, indicated by the rate law being independent of Cl–$SiCl_3$ concentration. This conclusion also agrees well with the energetics of the reaction found by Eyring analysis. Oxidative additions of **2a** and **5** to Cl–$SiCl_3$ are entropically disfavorable, reflecting the loss of disorder in forming one product from

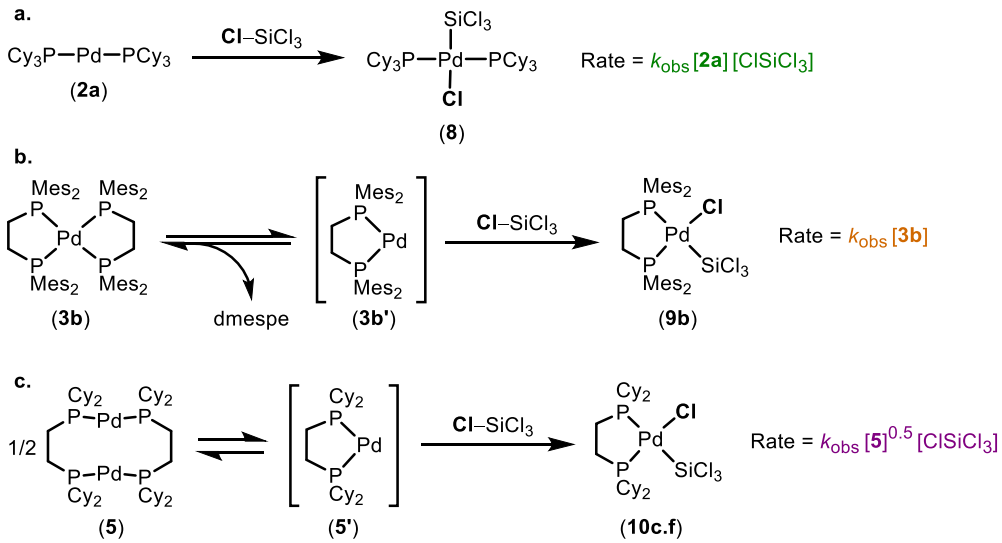

Scheme 6.3. Experimentally determined complex activation pathways for **2a**, **3b**, and **5** en route to oxidative addition with halosilanes.

two starting materials (in the case of **2a** + Cl–$SiCl_3$) or two products from three starting materials (in the case of **5** + 2 equiv Cl–$SiCl_3$). In contrast, the reaction with **3b** is entropically neutral, as the release of free ligand in solution contributes positively to disorder and leads to a net balance of two products (dmespe + **9b**) generated from two starting materials (**3b** + Cl–$SiCl_3$).

Finally, complex **5** dissociates to 2 equivalents of **5'** prior to oxidative addition, and this process is not rate-limiting as determined by the rate law of the reaction. **5'** then reacts stoichiometrically in an associative oxidative addition mechanism with halosilanes I–$SiPh_3$ or Cl–$SiCl_3$ to yield the expected products **10a.a** or **10c.f**. In spite of significant differences in the silyl substituents and halide identity between these substrates, their reactions with **5** give nearly identical energetic parameters by Eyring analysis, and the same rate law was found for both. Overall, the energetics and rate law determined for **2a** and **5** firmly support their proposed oxidative addition through associative mechanisms, while **3b** proceeds by a dissociative mechanism.

Conclusion

In this Chapter, we have described our work on the oxidative addition of Pd complexes to halosilanes X–SiR_3 (X = Cl, Br, I). Initial screening experiments revealed that the reaction is highly sensitive to the ligands and bonding of Pd precursors, proceeding with only three of the tested complexes: **2a**, **3b**, and **5**. Of these complexes, only **5** underwent oxidative addition with diverse halosilane substrates, while **2a** and **3b** reacted exclusively with Cl–$SiCl_3$.

The oxidative addition of **5** to halosilanes was first studied in equilibrium studies, where stoichiometric addition of halosilane to **5** led to varying degrees of product conversion depending on silyl substituents and halide identity. In general, iodosilanes were preferred to bromosilanes > chlorosilanes, and electronegative phenyl substituents were favored against electron-donating methyl substituents. By taking advantage of this substituent electronic effect, we were able to induce the oxidative addition of **5** to a triorgano- chlorosilane, which marks a significant achievement in the activation of halosilanes by transition metals.

We next moved on to studying the kinetics of the reaction of **5** with halosilanes. As in equilibrium studies, oxidative addition to iodosilanes proved the most facile, followed by bromo- and chlorosilanes. For iodosilanes, the rate of oxidative addition is not significantly impacted by changing the silyl substituents from I–$SiPh_3$ to I–$SiPhMe_2$. For bromo- and chlorosilanes, the rate of oxidative addition is less sensitive than K_{eq} to changes in halide identity, and these substrates show comparable rates to one another with appropriate silyl substituents. Competitive kinetics experiments against H–$SiPh_3$ point to the improved thermodynamic favorability of silyl palladium halide product **10a.a** against silyl palladium hydride **13**.

Variable temperature kinetics studies were conducted with **5** and each halosilane, and the rates used in an Eyring analysis to determine the energetics of oxidative addition. Overall, these reactions are characterized by a large, negative $\Delta S^{\ddagger}$ (~15-40 cal•mol^{-1}•K^{-1}) and positive $\Delta H^{\ddagger}$ (~10-15 kcal•mol^{-1}) to give $\Delta G^{\ddagger}_{273}$ = 18-20 kcal•mol^{-1}. The notable similarity of transition state energies in reactions with

diverse halosilane substrates prompted us to investigate the mechanism of the reaction.

Mechanistic studies of the reaction of **5** with I–$SiPh_3$ gave a rate law with 0.5^{th} order dependence on [**5**] and 1^{st} order dependence on [I–$SiPh_3$]. This 0.5^{th} order in **5** supports the proposed dissociation of dimeric **5** into two equivalents of active monomeric species **5'** prior to oxidative addition. Along with a large, negative $\Delta S^{\ddagger}$, the derived 1.5^{th} order rate law is consistent with a concerted or S_N2-like pathway for oxidative addition. However, further attempts to distinguish between these mechanisms were not successful. The oxidative addition of **5** to Cl–$SiCl_3$ proceeds more slowly but gives the same rate law and other mechanistic information as the reaction with I–$SiPh_3$.

Returning to our findings on the scope of Pd complexes competent in oxidative addition to halosilanes, we were interested to study the reaction of **2a** and **3b** with Cl–$SiCl_3$. Oxidative addition of **3b** proceeds with the stoichiometric formation of free dmespe ligand in solution, indicative of ligand dissociation being necessary to activate the coordinatively saturated complex. Accordingly, the rate law was determined to show a 1^{st} order dependence on [**3b**] and 0^{th} order dependence on [Cl–$SiCl_3$], suggesting this intramolecular ligand dissociation step to be rate-limiting. This assignment is supported by energetic parameters determined via Eyring analysis that show the reaction to be entropically neutral, likely due to an increase in disorder resulting from the release of free ligand in solution.

Complex **2a** undergoes oxidative addition directly with Cl–$SiCl_3$ to give **8** without an initial complex activation, which may explain why it proceeds with the fastest rate of any complex studied here. While exogenous PCy_3 ligand leads to slightly diminished rates of oxidative addition, this is due to side reactivity of Cl–$SiCl_3$ and PCy_3 and not an inherent effect on the oxidative addition pathway. The rate law for the reaction of **2a** with Cl–$SiCl_3$ is overall second order, with a 1^{st} order dependence found for each reagent. As in studies with complex **5**, understanding the precise mechanism operative in the oxidative addition of **2a** to Cl–$SiCl_3$ is precluded by experimental and structural challenges in studying these reactions.

In this work, we have extensively studied the formation of silyl palladium halide complexes to generate novel products **8**, **9b**, and **10**. The oxidative addition of halosilanes was studied fundamentally and mechanistically, to give trends in reactivity with regard to silane halide identity, silane substituents, and Pd(0) complex ligands and bonding. Given the lack of study in this area, we posit that this work represents a meaningful contribution to the understanding of fundamental organometallic chemistry.

Perspective and Outlook

Overall, this work provides the first fundamental and mechanistic insights into the oxidative addition of Pd complexes to halosilanes with diverse substituents and halide identity. By developing an understanding of the factors dictating this reactivity, we hope to contribute to the effective design of catalytic systems employing halosilanes. Moving forward, the results of this study will prove useful in expanding the application of halosilanes with late transition metals, including in reactions with readily available, industrially relevant chlorosilanes. We envision that this work will contribute to opening avenues for the powerful transformation of these under-utilized precursors in transition metal catalysis to organosilicon compounds and polymers.

7. SYNTHESIS OF SILICA-SUPPORTED PALLADIUM HYDRIDE CATALYSTS

The synthesis and catalysis described in this section were performed by me. The project was conceptualized by Dr. Amanda Cook. X-ray photoelectron spectra were collected by Tawney Knecht. Solid-state NMR spectra were collected by Dr. Shiva Moaven. The writing was done solely by me.

Introduction

The field of chemical catalysis is commonly divided into (at least) two subfields: homogeneous and heterogeneous catalysis. While the development of homogeneous catalysts can be dynamic and powerful towards achieving transformations with high efficiency, selectivity, and other metrics, the use of homogeneous metal complexes in industry is limited.[1] Rather, reactions conducted on manufacturing scale commonly employ heterogeneous catalysis.[2] indeed, estimates suggest that up to 90% of all chemical processes use heterogeneous catalysts.[3]

Some of the reasons for the predominance of heterogeneous catalysts in industry include their robustness compared to homogeneous catalysts and their easy recyclability from a reaction mixture for use in later transformations, making them highly cost efficient and potentially "green."[4] Additionally, the most heavily used heterogeneous catalysts are synthesized by impregnation or high temperature annealing of metal precursors onto a material support, obliviating the need for the design of expensive and finicky ligand scaffolds.[1] Yet, these same strengths that make heterogeneous catalysts so popular also lead to some of their shortfalls.

One of the main challenges in heterogeneous metal catalysis is catalyst design.[3] Although the activity of a given catalyst can easily be monitored, and some systems can be optimized to high levels of efficiency based on engineering and reaction development, mechanistic understanding of the active species is often complicated by the imprecise nature of the synthesized material. An inability to identify the active site among many other inactive (or deleteriously active) sites on

the material precludes mechanistic study and thus rational optimization or troubleshooting in catalysis.[5]

While not widely applied (yet) for catalysts that find use on an industrial scale, other methods are known to synthesize surface-supported metal species. Surface Organometallic Chemistry (SOMC) involves the use of a metal oxide such as silica that will bind oxophilic metals through a reaction with surface silanols.[6] Yet, this method does not solely circumvent the issue of non-specificity in metal

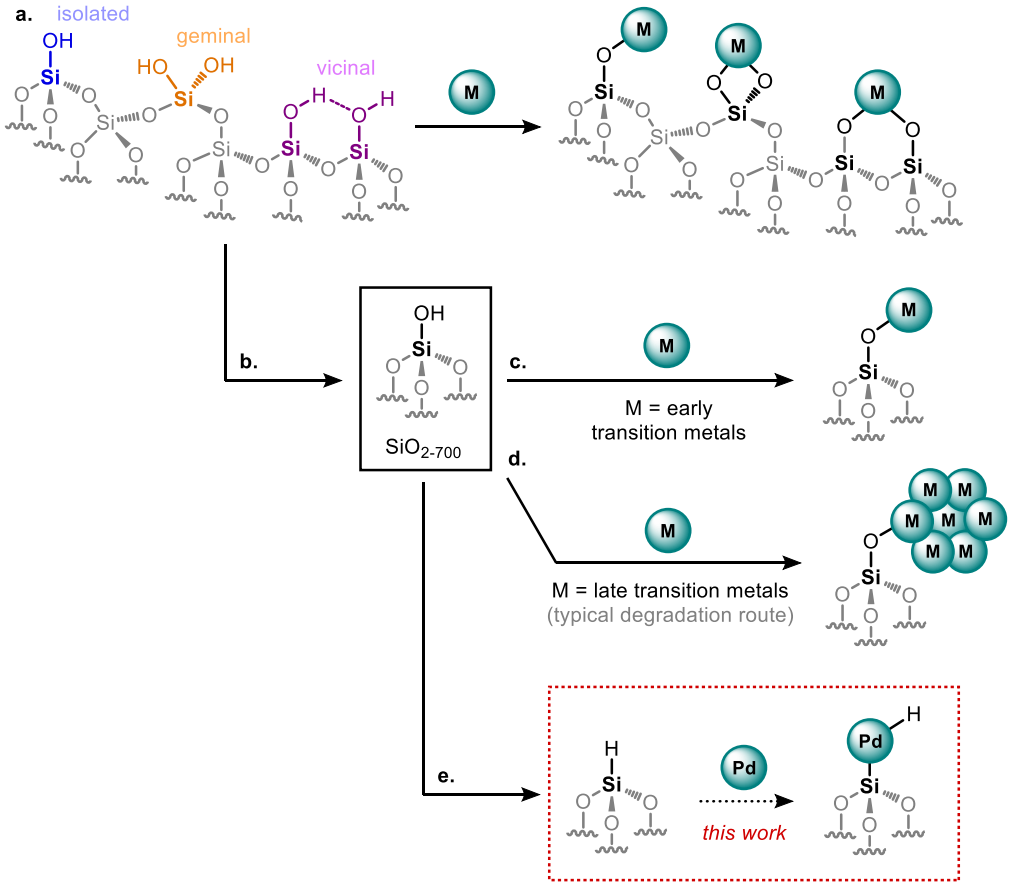

Figure 7.1. (a) various types of silanols on the surface of silica lead to imprecise grafting of metal complexes. (b) treatment of bulk silica at 700 °C leads to SiO2-700, which contains almost exclusively isolated silanols. (c) early transition metals can be supported through an oxo-bridge to the silica surface. (d) late transition metal-oxygen bonds are easily cleaved to give other types of supported metal clusters. (e) this work proposes to synthesize a new type of heterogeneous catalyst by oxidative addition to Si–H on the surface of silica.

species formation, as silica too contains a variety of silanol sites (isolated, geminal, and vicinal) on the surface, each of which could lead to formation of a different complex upon reaction with a metal precursor (Figure 7.1a). Instead, silica can be treated at high temperatures and vacuum to dehydroxylate the surface and form high concentrations of strictly “isolated” silanols. These silanols are present at a low concentration on the surface of the synthesized silica material and react with metal precursors in predictable ways.[7,8] The extent of dehydroxylation is dependent on the temperature used; commonly, this treatment will be conducted at 700 °C to make $SiO_{2\text{-}700}$, which contains up to 95% isolated silanols (Figure 7.1b).[6]

The use of this strategy to form heterogenous materials from early transition metals is well-explored (Figure 7.1c). However, late transition metals (LTMs), including those that play important roles in catalysis like Pd and Ni, are not amenable to grafting through an Si–O–LTM linkage to the surface due to their low oxophilicity.[9,10] Thus, the formed O–LTM bond is easily cleaved to release metal species into solution, which further degrade under harsh reaction conditions (Figure 7.1d). One precedented decomposition pathway for Pd complexes bonded through this motif is to form nanoparticles[11–14] that can exhibit divergent reactivity from the desired grafted catalyst; though, this decomposition pathway has also been used to purposefully generate supported nanoparticles, which have merit for other reasons.[11,14] To synthesize stable and molecularly-defined surface species, however, this pathway is deleterious. Therefore, we sought to develop an alternate route to graft metal complexes onto silica and other metal oxides that does not result in the formation of an LTM-oxygen interaction.

In previous Chapters and publications,[15,16] I have discussed the work we have done to understand the oxidative addition of Pd(0) complexes to the Si–H bond of molecular silanes. The insight gained through those studies, including the effect of silane electronics and sterics, metal complex tolerance, reaction conditions, and spectroscopic handles, lay the foundation for the development of a new class of heterogeneous catalyst materials formed through oxidative addition to surface Si–H (Figure 7.1e). Using Pd, this will lead to unique surface-bound silyl

palladium hydride species, in analogy to the molecular silyl palladium hydrides described in Chapters 3-5.

To our knowledge, only a couple of examples of grafting with a late transition metal via oxidative addition to silica surface X–H have been reported, to graft platinum complex $Pt(P\textit{t}\text{-}Bu_3)_2$[17] or a bidentate phosphine-ruthenium dihydride[18] the Si–OH bonds of silica. Yet, the support of metal complexes through oxidative addition provides several profound benefits to traditional heterogeneous catalyst synthesis; primarily, a desired active site structure can be installed by proper design of molecular precursors to grafting, and those features stay intact after bonding to the surface. Thus, catalytic reactivity will be precisely tunable by the choice of ligands on the metal center and the functionalization of silica sites that can introduced in the starting materials.

Separately, we are aware of only one report of silanized silica used as a support for late transition metals, also using ruthenium. However, in this case, the formation of surface metal hydrides was not observed, and concomitant H_2 gas formation occurred to consume the surface Si–H.[19] Otherwise, silanized silica surface are commonly known for their application as substrates in hydrosilylation reactions[20,21] or as modified stationary phases for high-performance liquid chromatography.[22–24] Thus, the work here describes the novel use of silanized silica as a platform for the oxidative addition of Pd(0) complexes to generate unprecedented surface Si–Pd–H.

Results and Discussion

Preliminary studies with "bulk" silica

To begin studying the grafting of Pd(0) complex $[(\mu\text{-dcpe})Pd]_2$ (**1**) to silica, we first needed to synthesize our desired support materials. Although our ultimate goal is to achieve precise grafting at low concentrations to diffuse Si–H sites (i.e. those formed on $SiO_{2\text{-}700}$), we were interested initially to explore the fundamental feasibility of Pd(0) oxidative addition to surface Si–H, as this is a novel route to supporting Pd complexes on silica and an understudied reaction even with molecular silanes. Therefore, we started our investigation by synthesizing a

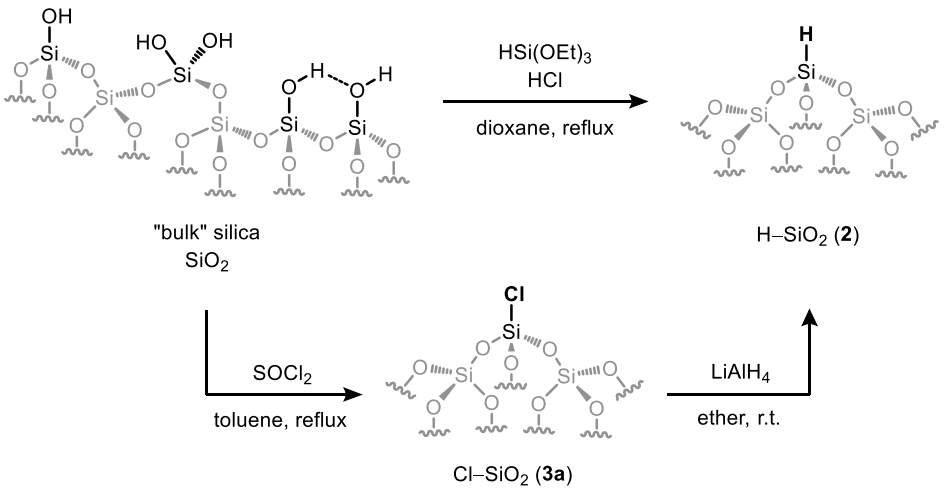

Scheme 7.1. Synthetic routes to H–SiO_2 (**2**) and Cl–SiO_2 (**3a**) with bulk silica.

material with high concentrations of Si–H, silanized "bulk" silica, H–SiO_2 (**2**). In contrast to $SiO_{2\text{-}700}$, bulk silica has not been heat treated to dehydroxylate the surface, and consequentially there remains a variety of silanol moieties.

Nonetheless, procedures are known for the generation of abundant Si–H sites on the surface of bulk silica (Scheme 7.1). Early work in this area was conducted by Sandoval and Pesek; the pioneering (and now somewhat outdated) method reported for the silanization of silica proceeds first by chlorination of the surface by thionyl chloride to give Cl–SiO_2 (**3a**).[25,26] This intermediate can be isolated and then reacted with lithium aluminum hydride to form **2**. Variations are known, for example using hydrogen gas as the redutant other than $LiAlH_4$.[27] An alternative, and commonly preferred, pathway proceeds in one step by a sequential acid-catalyzed hydrolysis and condensation of triethoxysilane.[20,28] Although the clear generation of surface Si–H moieties is observed at high surface coverages via the latter method (modern estimates suggest a coverage of ~5 Si–H per nm^{-2}, very near the silanol content of hydrated silica),[20] the exact structure of **2** and the fate of all silanols has not been determined quantitatively. Indeed, residual Si–OH surface species are confirmed by IR and NMR spectroscopy, and the authors note an uncertainty in the formation of monolayer Si–H or polymeric Si–H compounds of the structure $(HSiO_{3/2})_n$.[28]

The chlorination/reduction sequence to form **2** also presents several challenges: namely, low surface coverage and difficulty in removing the reactive aluminum byproducts. However, our previous studies into oxidative addition of **1** to halosilanes suggests some potential for supporting Pd complexes through a Si–Pd–Cl linkage from **3a**. Thus, we pursued the synthesis of **2** via triethoxysilane condensation, and the synthesis of **3a** via chlorination of SiO_2 with $SOCl_2$.

Looking first at the synthesis of **2**, we carried out a hydrolysis/condensation of triethoxysilane with bulk silica and aqueous HCl. The collected, free-flowing white powder shows an IR spectrum fully consistent with the expected transformation (Figure 7.2). In comparison to unmodified silica, there is a growth of a peak at 2260 cm^{-1} corresponding to Si–H, which matches exactly with the literature value.[28] Residual Si–OH are observed from ~4000–3000 cm^{-1}, and the broadness indicates the presence of multiple types of silanols remaining on the surface. A qualitative comparison of this IR spectrum to one published by Sandoval and Pesek shows a similar extent of silanization based on the height of Si–OH to Si–H vibrations. The peaks from ~2000-1500 cm^{-1} arise from siloxane bridges in the silica matrix, and nothing at lower wavenumbers is observable due to the intensity of absorbance from the subsurface structure of silica (which, by definition, makes up the bulk of the material).

Moving next to the synthesis of **3a**, we conducted a chlorination of the surface using $SOCl_2$. During the reaction, a pronounced color change occurred from white to violet, and the isolated product is a light purple solid. This observation is in line with literature reports[25] and provides a useful handle to determine the success of the reaction, as the produced Cl–Si gives IR vibrations only at low wavenumbers (~600 cm^{-1}) where they are obscured by the strong absorbance of silica. In our preliminary experiments, we also tried bromination of SiO_2 with $SOBr_2$ to give **3b**; in this case, a color change of the solution to red was observed during the reaction, but the collected material had no significant coloration. Characterization of the product by IR spectroscopy was precluded for the same reasons as for **3a**.

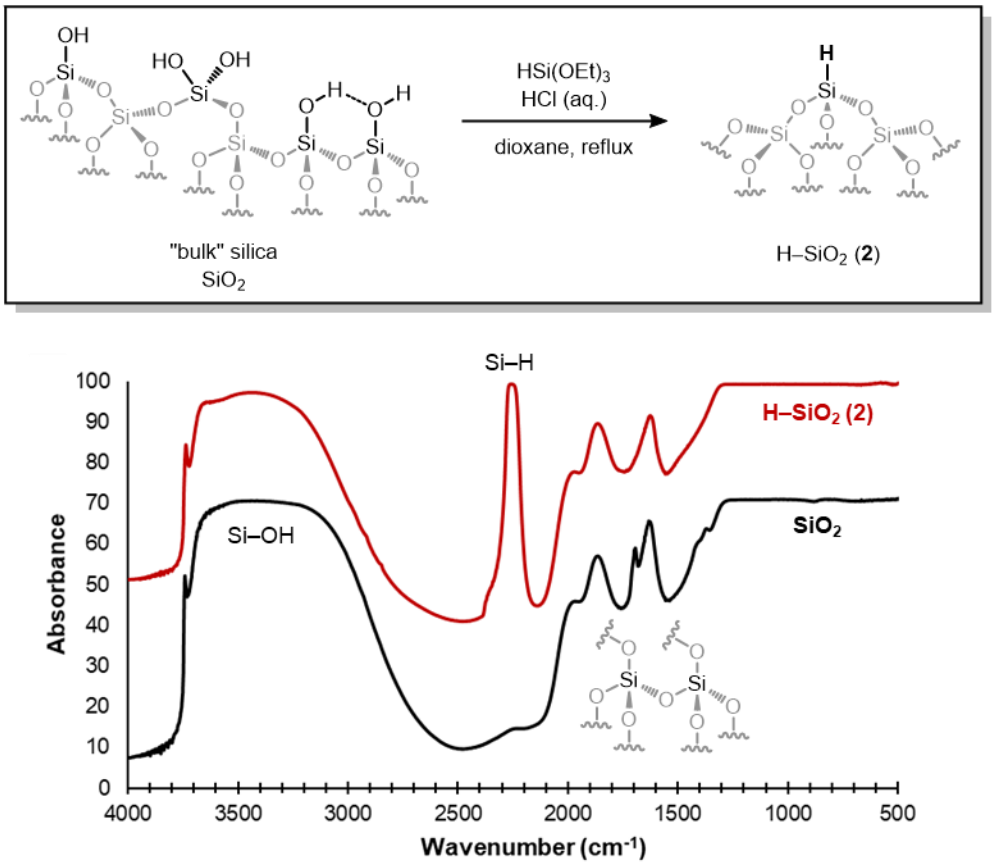

Figure 7.2. IR spectra of bulk silica and H–SiO_2 (**2**)

To better identify and quantify the success of these silica halogenation reactions, we turned to X-ray photoelectron spectroscopy (XPS). XPS is a powerful technique to identify and quantify the elements present within approximately 10 nanometers depth of a material sample and does not require dissolution or digestion beforehand.[29,30] This makes it an excellent tool for the analysis of materials with air-sensitive or otherwise unstable functional groups, such as our silyl halides or transition metal complexes. Additionally, it provides information that is limited primarily to surface species, so data is not obscured by the overwhelming spectroscopic response of the silica substructure. Unfortunately, hydrogen atoms are not observable, and therefore XPS could not supplement IR evidence for the formation of **2**.

XPS spectra were recorded on the solids collected from silica halogenation reactions after they were thoroughly washed under an inert (N_2) atmosphere and

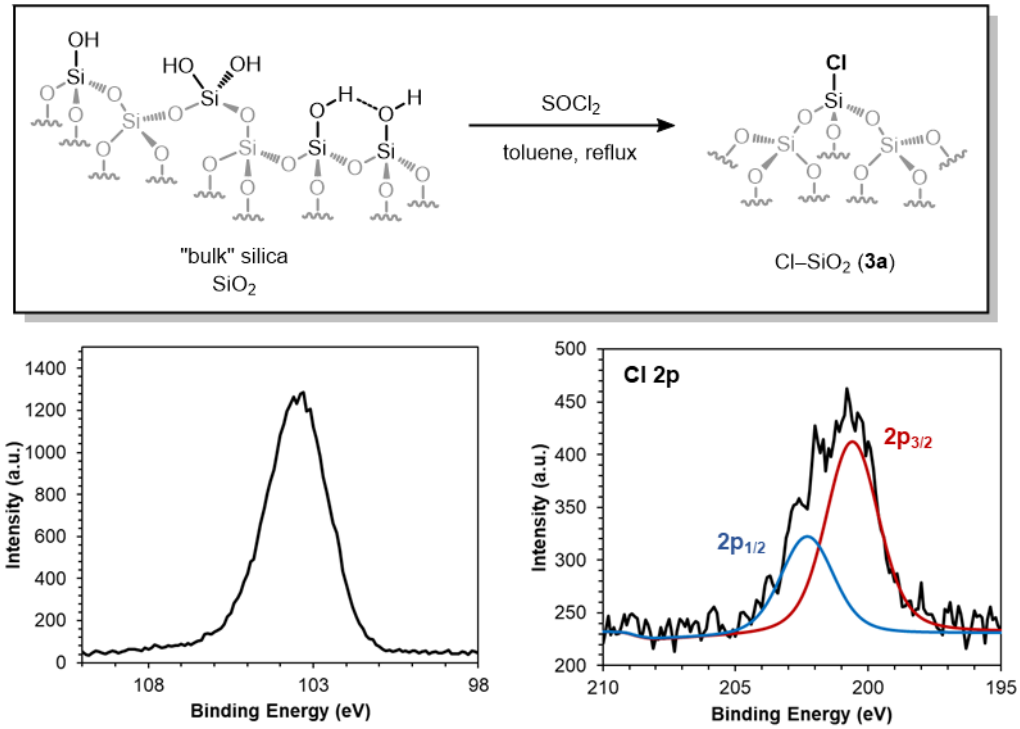

Figure 7.3. Plots of XPS spectra in regions corresponding to energies for silicon and chlorine. Peak fitting was modelled for the chlorine spectrum to identify contributions from $2p_{1/2}$ and $2p_{3/2}$ states. XPS spectra were collected with Tawney Knecht.

dried on vacuum. The presence of chlorine in a sample of **3a** gives strong evidence for the successful installation of Si–Cl on the surface (Figure 7.3); on the other hand, no bromine was observed in the sample of **3b**. Correcting for inherent differences in sensitivity between atoms of different elements, the signal response in XPS can be used to quantify the presence of each. Calculating relative chlorine to silicon concentration, we find a ratio of approximately 9:91. Thus, we have achieved ~9% coverage of Si–Cl sites on the surface of silica. A small portion of this material was taken forward to silanize the surface with $LiAlH_4$; however, the resulting product showed a lower concentration of Si–H than **2** formed from $HSi(OEt)_3$ condensation, as is generally reported in literature.[20] Therefore, we did not further explore **3a** as a synthetic intermediate for **2**.

With these modified silica materials **2** and **3a** in hand, we next explored their reactivity with Pd(0) complex **1**. In analogy to our and others' previous work with

molecular silanes,[31–33,15,16] we hypothesized that **1** would dissociate into two equivalents of (dcpe)Pd monomer **1'** that would then undergo oxidative addition to the Si–X bond. This pathway would allow access to materials with unique Si–Pd linkages to the surface of SiO_2, which we propose will be more tolerant to harsh reaction conditions than Si–O–LTM (LTM = late transition metal) moieties. Perhaps the paramount benefit to this method is that it would enable molecular level tunability in the choice of Pd ligand structure and silyl X group to effectively optimize the catalytic performance across many applications.

To initially test this hypothesis, we conducted grafting reactions with **1** and one of the modified silica substrates **2** or **3a**. The mixtures were left to stir in toluene under an inert atmosphere overnight and then the solids were collected, washed, and dried under vacuum. IR spectroscopy was used to evaluate the identity of the collected solid in the reaction with **2** (since signals for **3a** and the corresponding product are obscured) and ^{31}P NMR spectroscopy was used to analyze the residual metal complex(es) in the wash solution from grafting (Figure 7.4).

In both experiments, the $^{31}P\{^{1}H\}$ NMR spectra show remaining **1** in solution. This is unsurprising, as excess **1** was used; however, it is a positive sign that there was no degradation of the complex through undesired side reactions. The IR spectrum of the solids collected from the reaction with **2** is more telling. Although a large Si–H peak remains, and a Pd–H peak is not visible under the siloxane overtones, C–H stretching (3000-2800 cm^{-1}) and bending (1500 cm^{-1}) resemblant of **1** are present in the product. These are likely from the cyclohexyl groups of dcpe ligand, indicating the adsorption or oxidative addition of **1** to the surface. This assignment is supported by comparison to the IR spectrum of an analogous molecular silyl palladium hydride, (dcpe)PdH(Si(OEt)$_3$) (**6a**) (Figure 7.5). Unlike the grafted product **4**, the formation of this molecular complex can be confirmed by solution $^{31}P\{^{1}H\}$ and ^{1}H NMR. This well-defined molecular complex then provides a useful spectroscopic comparison to the grafted material **4** because they share similar (dcpe)PdH(Si(OR)$_3$) environments. Indeed, good agreement is observed in C–H features of the IR spectra for **4** and **6**, though other diagnostic signals are obscured by the vibrations of silica.

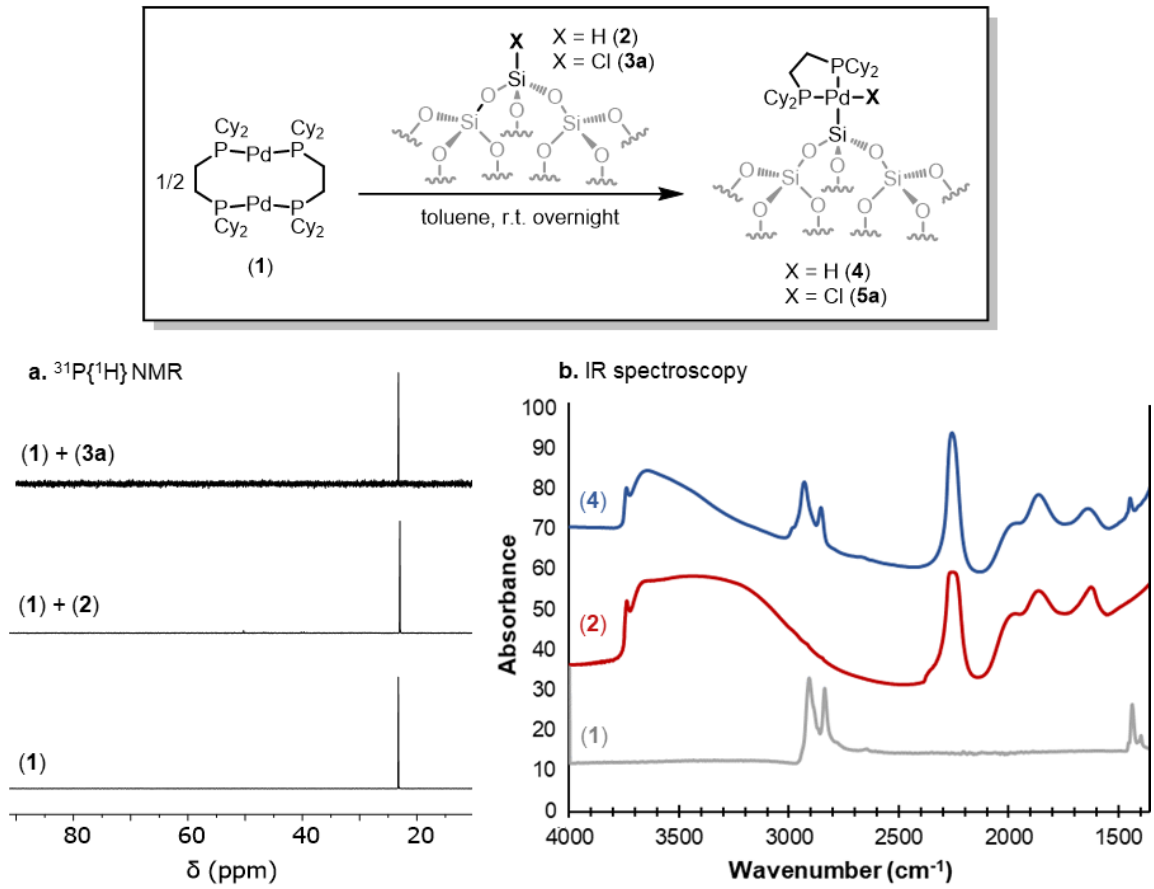

Figure 7.4. (a) $^{31}P\{^{1}H\}$ NMR spectra of the wash solution after grafting reactions. (b) IR spectra of the solids collected from grafting reactions.

We again turned to XPS for verification of the surface species. The collected solids in the reaction of **1** and **3a** did not show the presence of Pd, signaling that no grafting took place to the surface Si–Cl bonds. On the other hand, the XPS spectrum of **4** shows a peak at energies characteristic of Pd(II) (Figure 7.6). Encouragingly, the relative concentrations of phosphorus and palladium can be quantified, and they are present in approximately a 2:1 ratio as expected for product **4**. Further, the Pd:Si ratio is approximately 8:92, suggesting a surface coverage of 8%. Although hydrogen is not directly observable by XPS and thus an unambiguous assignment of Pd–H species has not yet been possible, these results are fully in line with the successful oxidative addition of **1** to Si–H on the surface of silica. With convincing evidence we had formed one of our desired materials, we next sought to apply it in catalysis.

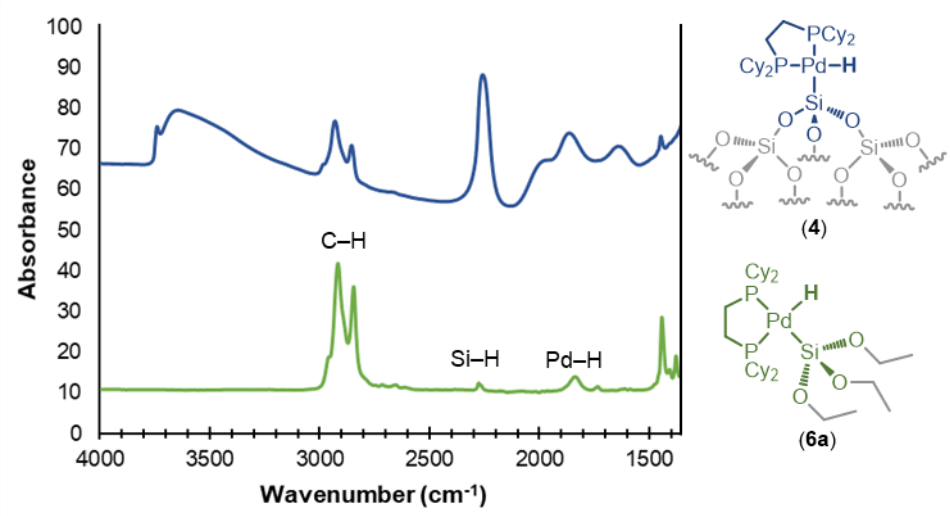

Figure 7.5. IR spectra comparison of **4** against molecular silyl palladium hydride **6a**.

For preliminary catalytic studies, we chose to target the isomerization of alkenes. This is a prime system to test the activity of surface palladium hydrides, as a prominent mechanism in alkene isomerization is catalyzed by metal hydrides (Figure 7.7).[34] Whereas in many cases these metal hydride active catalysts are generated *in situ*, particularly with late transition metals, the synthesized grafted

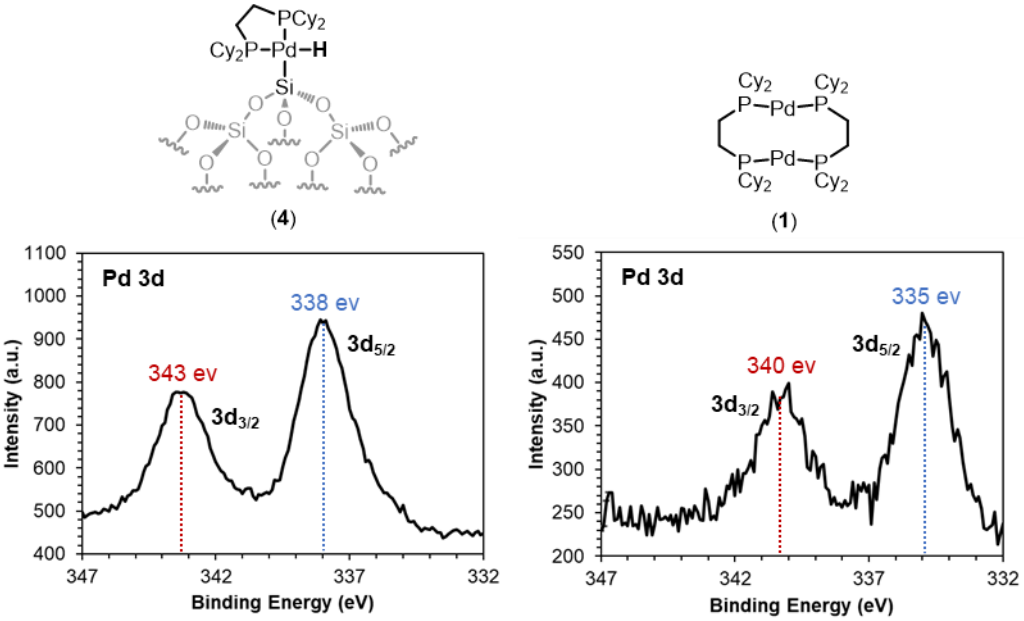

Figure 7.6. XPS spectra of **4** and **1**, zoomed in to energies corresponding to Pd.

material **4** allows direct access to this important species. During isomerization, the Pd–H bond is reformed to regenerate **4** after each turnover, which, along with the heterogeneous nature of the catalyst, should allow for its recyclability across multiple reactions. Additionally, alkene isomerization is a meaningful catalytic target because it is widely applied across industry, such as in the Dupont adiponitrile process.[35]

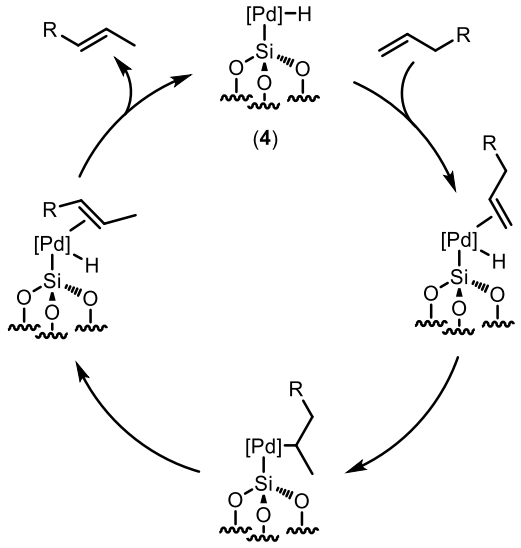

Figure 7.7. Established mechanism for alkene isomerization catalyzed by metal hydrides.

We evaluated the catalytic activity of **4** in the isomerization of allylbenzene (Figure 7.8). Control reactions were conducted using silanized silica **2** or molecular silyl palladium hydride (dcpe)PdH($SiPh_3$) (**6b**) (formed *in situ* from $HSiPh_3$ + **1**). These controls show no or little reaction, respectively. Pd(0) complex **1** on its own is a middling catalyst for allylbenzene isomerization, showing approximately 45% yield after overnight at room temperature. Unfortunately, grafted complex **4** performed even worse to give only 10% yield under the same conditions. Despite these poor catalytic results, however, this set of experiments served as a proof of concept for the grafting of palladium complexes through oxidative addition to Si–H on the surface of silica. Instead of optimizing further upon this model system, we sought to translate this work towards our primary goal of grafting to finely tuned silica surfaces prepared from $SiO_{2\text{-}700}$.

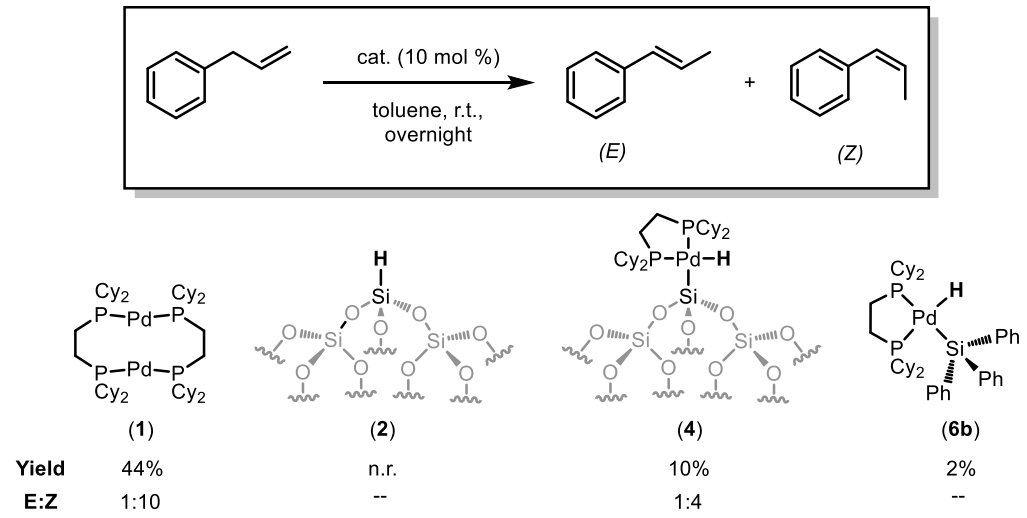

Figure 7.8. Results of catalytic alkene isomerization with studied materials. Reaction conditions: 1.0 equiv allylbenzene, 0.1 equiv catalyst, 40 mM in toluene. Catalyst concentration was based on quantification of Pd surface coverage by XPS. Product formation was determined by GC against an internal standard.

Synthesis of Pd complexes grafted to silanized metal oxides

We therefore moved on to synthesizing these advanced materials, beginning with $SiO_{2\text{-}700}$ (**7**). Treating bulk silica at 700 °C under vacuum or a flow of dry air drives off surface water and encourages chemical dehydration of the surface to give 90-95% “isolated” silanol species. This results in a characteristic change in the energies of Si–OH vibrations observed in the IR spectrum: for untreated silica, Si–OH vibrations appear as a broad signal across 4000-3000 cm^{-1}, while the spectrum of **7** shows only a single, sharp Si–OH peak at approximately 3800 cm^{-1} (Figure 7.9).[6,36]

In addition to IR spectroscopy, the extent of dehydroxylation can be quantified by titration. This method involves the addition of a well-defined benzyl Grignard reagent to a suspension of $SiO_{2\text{-}700}$. The acidic Si–OH sites of silica will rapidly cleave the Mg–C bond to release an organic analyte (toluene) into solution in a predictable manner (Scheme 7.2); the concentration of this formed analyte can then be observed spectroscopically by ^1H NMR. In the presence of an internal

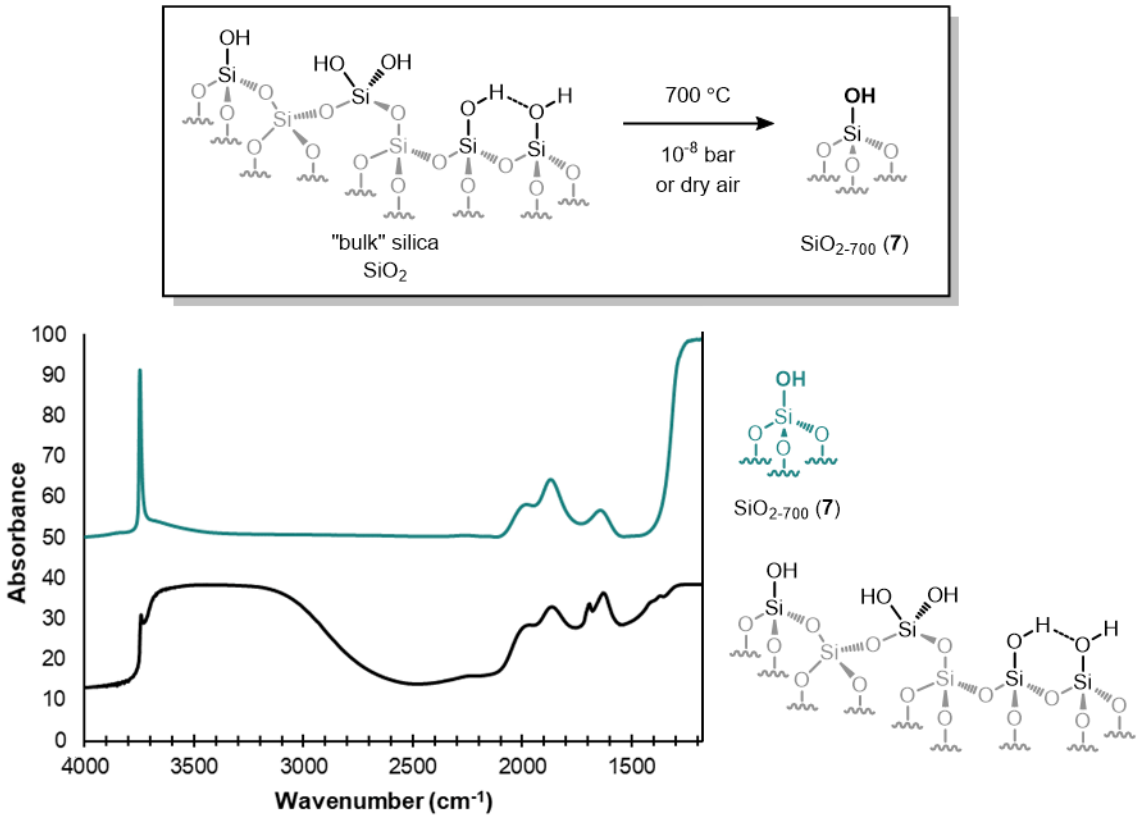

Figure 7.9. IR spectra comparison of bulk silica against $SiO_{2\text{-}700}$ (**7**). Spectrum of **7** courtesy of Dr. Shiva Moaven.

standard, the amount of generated toluene is quantified by peak integration, and the concentration then used in a calculation to determine Si–OH content in the material of interest. In contrast to bulk silica which can have concentrations of Si–OH as high as ~1.6 mmol Si–OH/g SiO_2, the expected value for **7** is around 0.30 Si–OH/g SiO_2. Titrations in our laboratory commonly give near this expected concentration of Si–OH/g SiO_2.

With fully dehydrated **7** in hand, we moved on to the installation of Si–H groups on the surface. The same procedure was followed as for the

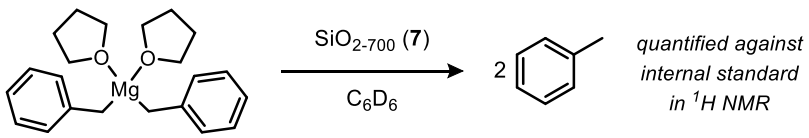

Scheme 7.2. Titration of $SiO_{2\text{-}700}$ to determine the surface concentration of Si–OH.

functionalization of bulk silica to **2**, with the important modification that all steps were done under an inert nitrogen atmosphere and no aqueous reagents were used (i.e. aqueous HCl was substituted for dry HCl in dioxane). This is due to the extraordinary sensitivity of **7** towards atmospheric moisture, which will rapidly rehydrate to reform an assortment of silanol moieties on the surface – effectively reversing the rigorous heat treatment involved in synthesizing **7**. Additionally, the stoichiometry in the silanization reaction was adjusted to account for the lower concentration of surface Si–OH on **7** vs bulk silica.

Unlike in the previous silanization of bulk silica, the solids collected from the silanization reaction with **7** via hydrolysis/condensation of $HSi(OEt)_3$ gave an IR spectrum with strong C–H stretching vibrations (Figure 7.10). Exhaustive drying under vacuum did not decrease the proportion of these vibrations in comparison to the other species present, suggesting that this signal is not due to adventitious solvent or another adsorbed volatile compound. Yet, silanization is clearly successful, as indicated by the growth of a strong vibration corresponding to Si–H.

In fact, the formed product can be identified as $H–Si(OEt_2)–O–SiO_{2\text{-}700}$ (**8a**), in line with literature precedent by Busca and Turturro.[37,38] In these fundamental studies, the silanization of metal oxides was conducted entirely within a vacuum- and air- tight chamber equipped with *in situ* IR spectroscopy instrumentaiton, and $HSi(OEt)_3$ was transferred onto $SiO_{2\text{-}700}$ via diffusion in the gas phase. In contrast, our synthesis employs classical “wet” methods to silanization. Nonetheless, our results are consistent with the formation of the same surface species proposed by Busca and Turturro as **8a**. This assignment explains the persistence of C–H stretching in the IR spectrum, as two ethoxy groups are still present on the bound silane, while one has been cleaved to form to an Si–O–Si linkage to the surface. A necessary byproduct generated in this reaction would be ethanol (EtOH) and, indeed, ethanol is observed in ^{1}H NMR spectra of the reaction mixture during silanization. By IR spectroscopy, our isolated material matches closely with that reported in literature, and the diagnostic Si–H stretching vibration appears at 2235 cm^{-1} (compared to the reported value: 2230 cm^{-1}).[37,38]

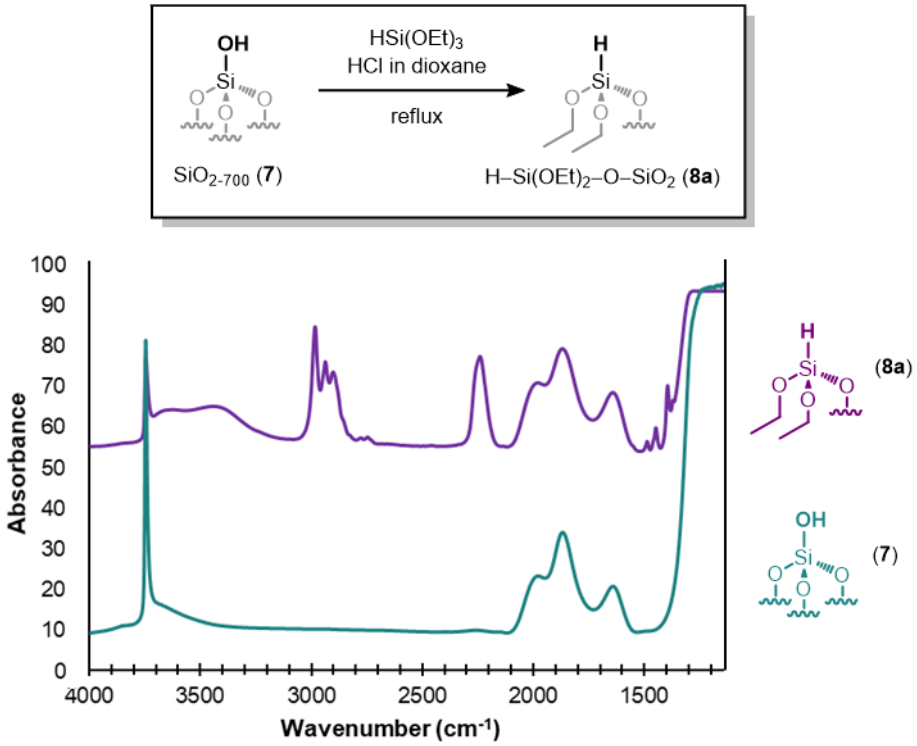

Figure 7.10. IR spectra comparison of **7** and **8a**.

Promisingly, not only can **8a** behave as a desired surface Si–H, but it can also be treated as a synthetic intermediate to **9**. Upon heating **8a** to 500 °C under vacuum, further reaction takes place to give the fully condensed product **9**. This process is proposed to occur with the release of two equivalents of ethylene and the reformation of isolated silanols in the vicinity of the reaction site.[37,38] We observe the disappearance of C–H stretching in the IR spectrum along with concomitant growth of the Si–OH stretching frequency at ~3800 cm^{-1}, consistent with this transformation (Figure 7.11). Further, the Si–H vibration shifts to higher wavenumber (2279 cm^{-1}), in agreement with the literature precedent (reported value: 2280 cm^{-1}). Taken together, these results give strong support for the formation of the desired silanized materials **8a** and **9**.

We were interested to expand this silanization method to allow for tuning of the electronics at Si–H. Specifically, in our previous studies, we observed that silyl palladium hydrides formed from the oxidative addition of **1** to silanes with electron-withdrawing substituents were more stable than those with electron-donating

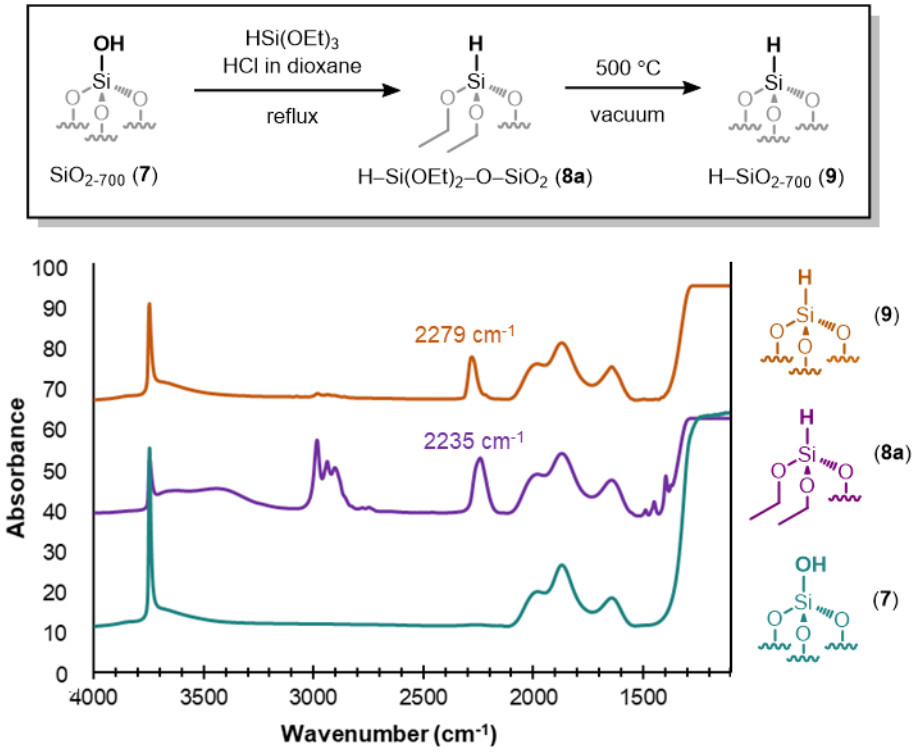

Figure 7.11. IR spectra comparison of **7**, **8a**, and **9**.

substituents.[15] We hoped to apply this insight to favor oxidative addition to surface Si–H species. The stepwise reaction pathway from **7** to **9** allows for the isolation of singly oxo-bridged surface silanes **8** with different substituents at silicon, so long as at least one of them is an alkoxy group in the precursor. We thus undertook the synthesis and application of substituted alkoxysilanes to silanize the surface of $SiO_{2\text{-}700}$.

In studies with molecular silanes, triaryl silanes were highly compatible partners for the oxidative addition of **1**, and the most favorable example we tested was electron-poor $HSi(4\text{-}CF_3\text{-}Ph)_3$.[15] This precedent formed the basis for our initial experiments in changing the identity of alkoxysilanes used in silanization. $HSiPh_2(OEt)$ and $HSi(4\text{-}CF_3\text{-}Ph)_2O$*t*-Bu were synthesized from the corresponding dihydrosilanes and alcohols and used in the silanization reaction with **7** (Figure 7.12).

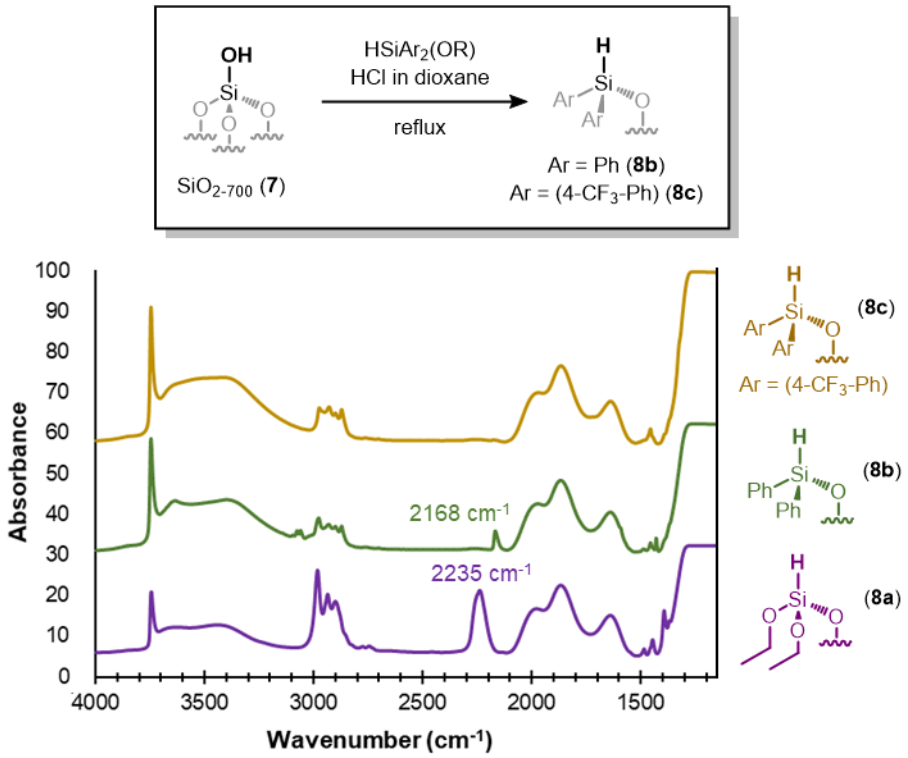

Figure 7.12. IR spectra comparison of **8a**, **8b**, and **8c**.

In both reactions to form **8b** and **8c**, the IR spectra of the collected solids show the growth of new C–H stretching vibrations. In the case of **8b**, a new Si–H peak is also apparent at 2168 cm^{-1}, albeit at a far lower relative concentration to Si–OH compared to **8a**. Although the C–H stretching and bending (ca 1500 cm^{-1}) bands of **8c** suggest the formation of a surface-bound species, no peak for Si–H is observed. A significant shift in the position of Si–H is observed going from **8a** to **8b**; given the other indications of a successful reaction to synthesize **8c**, it may be that substitution of highly electron withdrawing groups at silicon caused a shift of the Si–H peak to lower wavenumbers, where it is obscured under the siloxane overtones of silica.

One other route for tuning the reactivity of surface Si–H is in the choice of support. Although our work focuses primarily on silica, other metal oxides can undergo similar reaction pathways to give supported Si–H species. Briefly, we applied the silanization procedure with $HSi(OEt)_3$ on dehydroxylated alumina, $Al_2O_{3\text{-}500}$, to give a material postulated as $H–Si(OEt)_2–O–Al_2O_3$ (**10**). A portion of

this material was heated to 500 °C under vacuum to further condense the ethoxy groups and give H–SiO_2–O–Al_2O_3 (**11**). Generally, the spectroscopic evidence for the formation of this product echoes that observed with silica (Figure 7.13); the isolated product **10** shows residual C–H stretching in the IR spectrum that disappears upon treatment at 500 °C, and the Si–H peak shifts from 2232 cm^{-1} for **10** to 2277 cm^{-1} for **11**. In analogy to the reformation of isolated silanols on the surface of silica upon condensation at 500 °C, new M–OH (M = Si or Al) vibrations are observed in the spectrum of **11** at ~3800-3700 cm^{-1}.

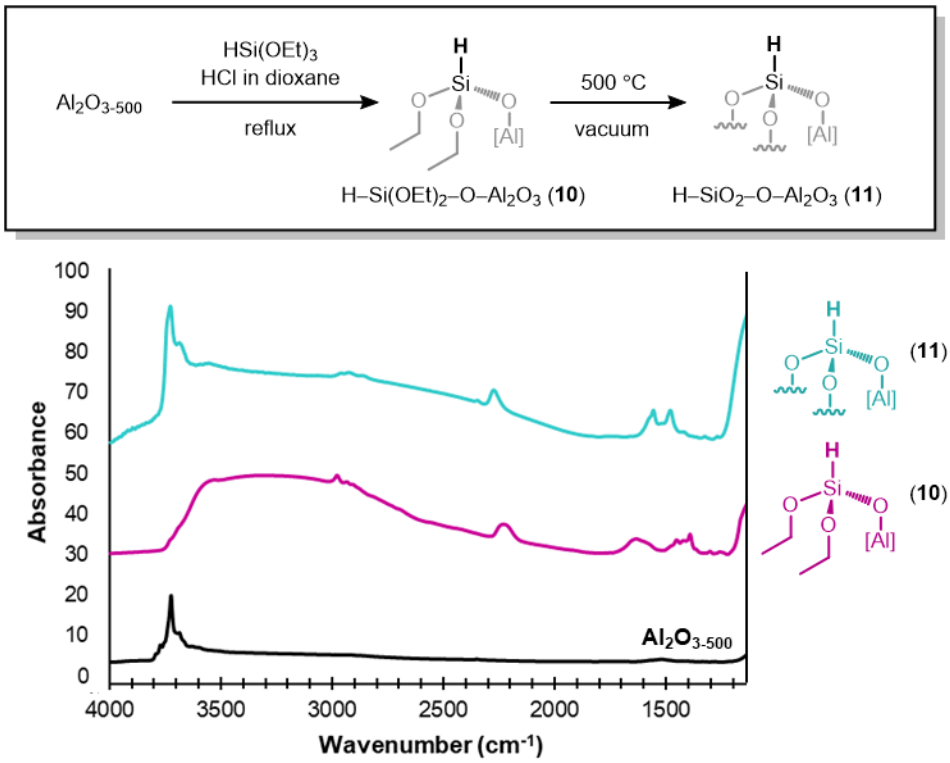

Figure 7.13. IR spectra comparison of Al_2O_{3-500} with silanized alumina materials **10** and **11**.

Finally, these synthesized materials **8**, **9**, **10**, and **11** were subjected to grafting reactions with Pd(0) complex **1**. These reactions were conducted in a similar manner as with bulk silica, and analysis was carried out accordingly. Solution $^{31}P\{^1H\}$ NMR spectra of the wash solutions from grafting reactions show only starting material **1** with negligible side reaction or decomposition. IR spectra of the collected solids in reactions with SiO_{2-700} materials resemble the products

formed from the grafting of **1** to **2**; specifically, C–H stretching and bending vibrations characteristic of the cyclohexyl groups of dcpe ligands are apparent, but no Pd–H peaks can be observed as their expected frequencies (~1800 cm^{-1} based on studies of molecular silyl palladium hydrides) are obscured by the siloxane overtones of silica (Figure 7.14). Notably, however, these reactions show full consumption of the Si–H peak of the starting materials **8** or **9**. Grafting with silanized alumina materials **10** and **11** gives similar results, though some Si–H remains after the reaction. Overall, these spectra are in line with the successful grafting of **1** to the surface of metal oxides by oxidative addition to Si–H, but do not provide positive evidence for the formation of Pd–H. To attempt a better assignment of this surface species, we turned to solid state NMR (SSNMR).

By $^{31}P\{^{1}H\}$ SSNMR, the growth of a peak at approximately 75 ppm is observed, shifted downfield from approximately 35 ppm in the starting material (Figure 7.15). This change in chemical shift is comparable to that observed from **1**

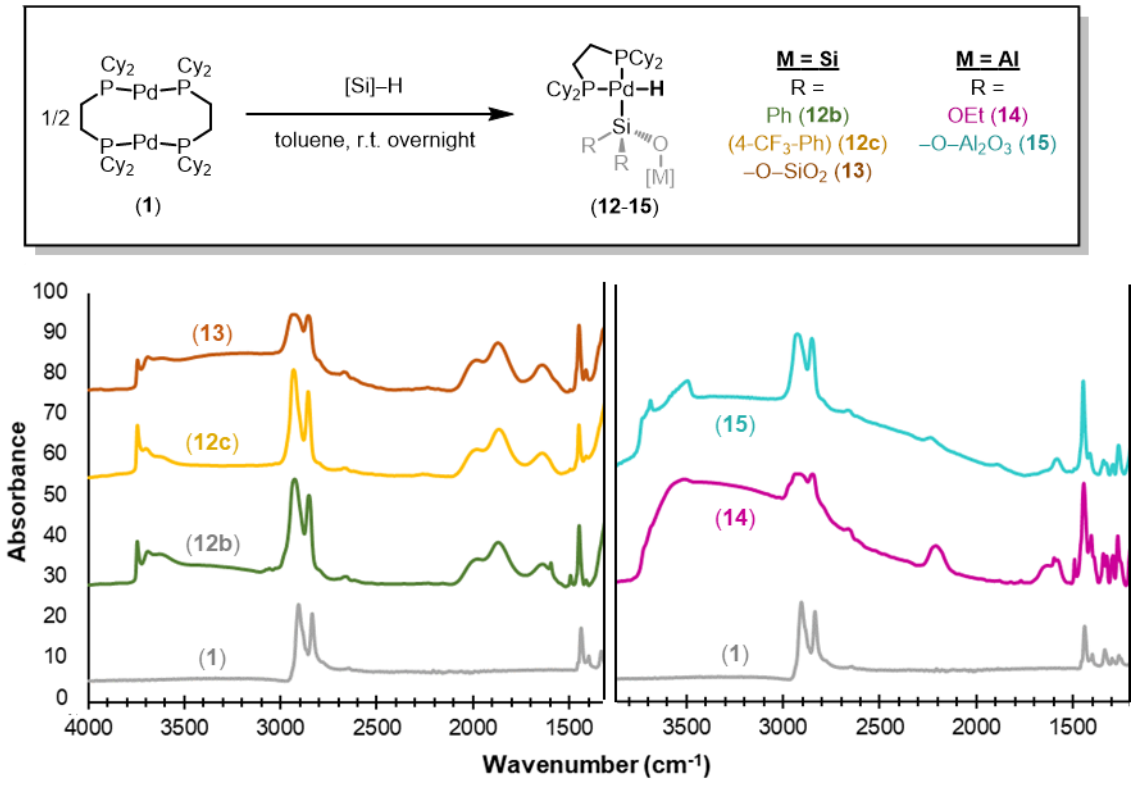

Figure 7.14. IR spectra comparisons of grafted silica materials (left) and grafted alumina materials (right) with **1**.

($^{31}P\{^{1}H\}$ NMR δ in C_6D_6: 23 ppm) to molecular silyl palladium hydrides **6** ($^{31}P\{^{1}H\}$ NMR δ in C_6D_6: 60-70 ppm) in solution. Based on this assignment of the product peak by NMR, the results of grafting to **8b** or **9** can be compared. Normalizing for the peak height of **1**, the grafted material **12b** shows a higher concentration of the desired product than **13**, though at least slight evidence of grafting is observed for both materials. Supplementing IR data, this allows for greater confidence in determining the success of grafting reactions of **1** to surface Si–H via oxidative addition.

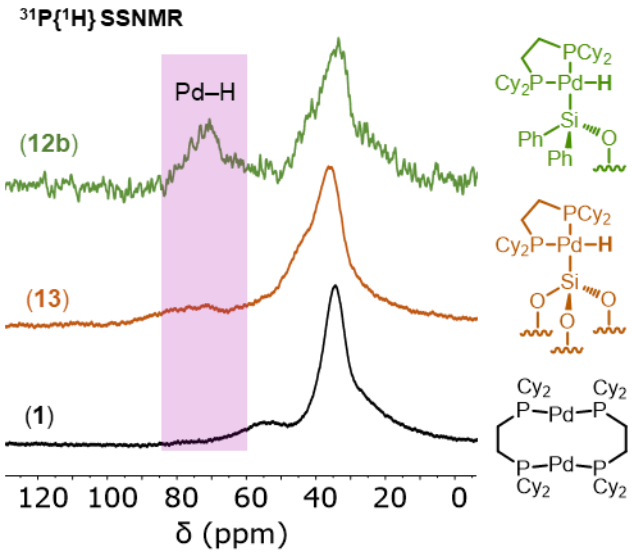

Figure 7.15. $^{31}P\{^{1}H\}$ SSNMR spectra comparison of **12b** to **13**. SSNMR spectra collected by Dr. Shiva Moaven.

Catalytic studies – isomerization of 4-allylanisole

To explore the activity of these newly synthesized materials as heterogeneous catalysts, we returned to alkene isomerization. Using 4-allylanisole (**16**) as the alkene substrate, reactions were conducted with catalytic loading of each of the previously synthesized $SiO_{2\text{-}700}$ and $Al_2O_{3\text{-}500}$ materials, including ungrafted silica. The concentration of active species was approximated to be 0.30 mmol Si–H/g for silica samples **7**-**9** and 0.15 mmol Pd–H/g for grafted samples **12**-**15**, and these concentrations were used to achieve a catalyst loading of 5 mol %.

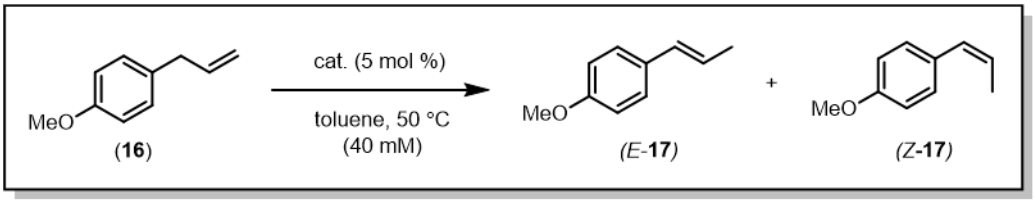

Catalyst	Time	Yield of **17**	E : Z
none	18 h	n.r.	--
1	18 h	91%	9 : 1
6b (**1** + $HSiPh_3$)	18 h	33%	45 : 1
$HSiPh_3$	18 h	n.r.	--
7	26 h	n.r.	--
8a	18 h	n.r.	--
8b	18 h	n.r.	--
8c	18 h	n.r.	--
9	24 h	n.r.	--
12b	18 h	35%	6 : 1
12c	18 h	37%	6 : 1
13	18 h	52%	6 : 1
14	20 h*	27%	4 : 1
15	20 h*	27%	5 : 1

Figure 7.16. Results of catalytic reactions in the isomerization of **16** with materials studied throughout this project. Reaction conditions: 1.0 equiv **16**, 0.05 equiv catalyst, 40 mM in toluene. For heterogeneous catalysts, concentration of active species was approximated from Si–OH in $SiO_{2\text{-}700}$ starting material. Product concentration was monitored by GC against an internal standard. *20 mM.

The reaction was mildly heated to 50 °C to encourage isomerization. Results are given in Figure 7.16.

Conducting the reaction at high concentrations and 50 °C, **1** is a good catalyst for alkene isomerization and gives above 90% yield of the product **17** with fair E:Z ratio. As observed in earlier studies with allylbenzene, addition of $HSiPh_3$ with **1** – to form silyl palladium hydride **6b** *in situ* – impedes the reaction. Yet, this catalyst combination is quite selective for the (*E*) product despite low yields. $HSiPh_3$ itself is not active under the reaction conditions, nor are any of the ungrafted silica materials.

Encouragingly, all of the grafted materials catalyze the isomerization of **16**. There does not appear to be a significant difference in activity based on varied aryl groups in **12b** and **12c** or the extent of condensation in alumina materials **14** and **15**. The best performing material is **13**, though still it is not an effective catalyst for the reaction. In addition to further developing this catalyst, we were interested to evaluate the behavior of **1**. Thus, we carried **13** forward to optimization studies, and ran concurrent experiments to investigate **1** as a homogeneous catalyst for the isomerization of 4-allylanisole.

We first tested the effect of temperature on the reaction. Trials were conducted at varied temperatures – 0 °C, 25 °C, 50 °C, and 70 °C – and the rate of product formation was monitored by gas chromatography (GC) against an internal standard (Figure 7.17).

Surprisingly, although **1** leads to higher yields of **17** at long reaction times, the rate of isomerization is initially faster with **13** at 70 °C. Indeed, the activity of **13** is more sensitive to temperature than **1**, and the **13**-catalyzed reaction is

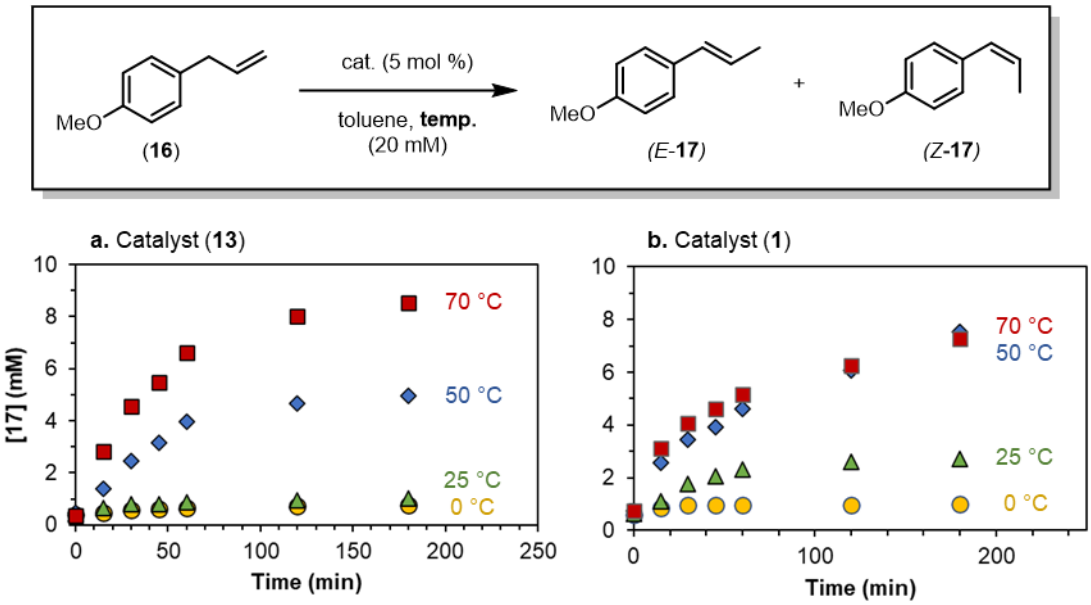

Figure 7.17. Results of isomerization of **16** with **1** and **13** at various temperatures. Reaction conditions: 1.0 equiv **16**, 0.05 equiv catalyst, 40 mM in toluene. For **13**, concentration of active species was approximated from Si–OH in $SiO_{2\text{-}700}$ starting material. Product concentration was monitored by GC against an internal standard.

exceedingly sluggish at and below room temperature. As observed in earlier studies with allylbenzene, **1** is poorly capable of isomerization at room temperature, but does proceed to low yields. Under more favorable conditions, the same profile is observed regardless of whether the **1**-catalyzed reaction is warmed to 50 °C or 70 °C. For these reasons, we chose to continue optimization studies at 50 °C.

We next evaluated the impact of catalyst loading on the isomerization. We prepared reactions with varied concentrations of catalyst – 1 mol %, 2.5 mol %, 5 mol %, and 10 mol % – and monitored product formation (Figure 7.18). While the reaction with **1** was not strongly affected by the catalyst loading, the concentration of **13** had a significant impact on the rate and overall yield. However, the benefit of increased catalyst loading in this case is outweighed by practical considerations. Using twice as much catalyst in the reaction leads only to the formation of twice as much product before the isomerization stops at approximately 50% conversion. Following with this logic, a catalyst loading of up to 20-40 mol % would be required

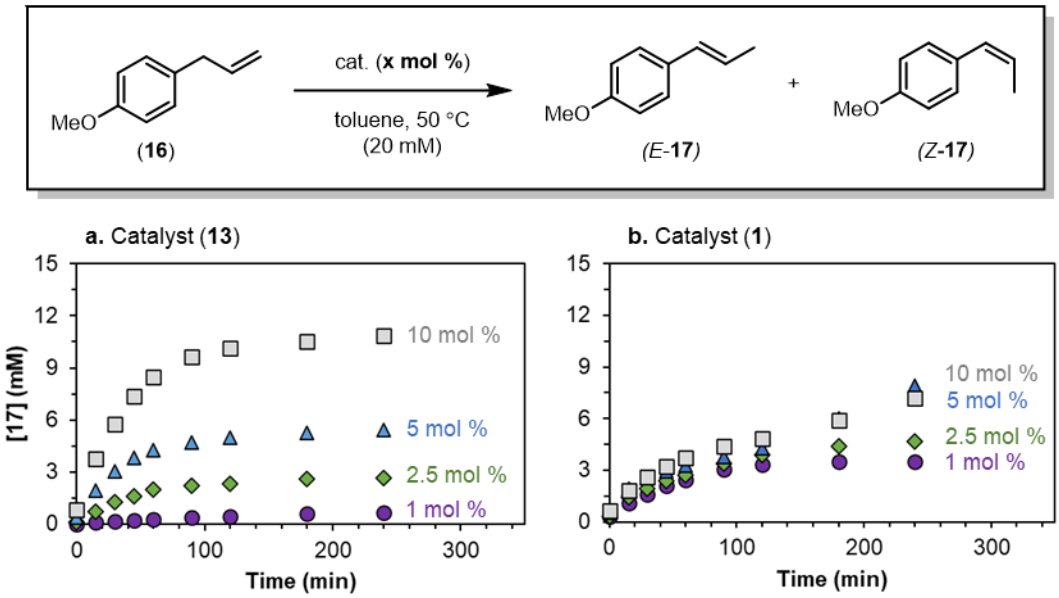

Figure 7.18. Results of isomerization of **16** with **1** and **13** at various catalyst loading. Reaction conditions: 1.0 equiv **16**, 0.05-0.20 equiv catalyst, 40 mM in toluene. For **13**, concentration of active species was approximated from Si–OH in $SiO_{2\text{-}700}$ starting material. Product concentration was monitored by GC against an internal standard.

to drive the reaction to full conversion. Thus, we determined that optimization in catalyst loading is an effective avenue to developing **13**, and we moved forward with 5 mol % as our standard conditions.

Finally, we investigated the role of solvent on the isomerization of 4-allylanisole. Previous trials were all conducted in toluene; in this experiment, reactions were set up in acetone, acetonitrile, hexanes, and THF, as well as a control sample in toluene (Figure 7.19). Acetonitrile is a poor solvent with either catalyst. **1** performs well in all of the other solvents tested, showing the best activity in hexanes or THF. The reaction with **13** in acetone is somewhat hindered, and the reaction in THF is comparable to the trials in toluene. For **13**, the most non-polar solvent examined in this experiment, hexanes, leads to the highest yield and an above average E:Z ratio (average across all previous trials in toluene is ~5:1). Indeed, continued trials using hexanes as a solvent outperform those run alongside in toluene.

Throughout these studies, the tolerance of catalysts **1** and **13** to different reaction conditions was tested. In each experiment, disparate trends were observed in the behavior of **1** and the behavior of **13**. This is an important consideration in evaluating whether **13** is truly a heterogeneous catalyst, as an alternate pathway to the desired transformation could be dissociation of Pd from the surface to generate the active species **1'** in solution – in which case catalysis would be expected to proceed similarly as if **1'** were generated from **1**. However, the unique behavior of each of these catalyst systems under identical reaction conditions inspires confidence in the assignment of **13** as heterogeneous, or at least signals that a different active catalyst is generated from **13** than from **1**.

To get a better handle on the homo- or heterogeneity of the catalyst **13** during the isomerization of 4-allylanisole, a hot filtration experiment was performed. In this experiment, a reaction mixture was prepared under standard conditions, and isomerization was monitored until it reached approximately 20% conversion at 30 minutes. At this time, the reaction mixture was cannula filtered into a separate flask while keeping the system under nitrogen, and the reaction in both flasks was monitored thereafter. The purpose of this experiment is to evaluate

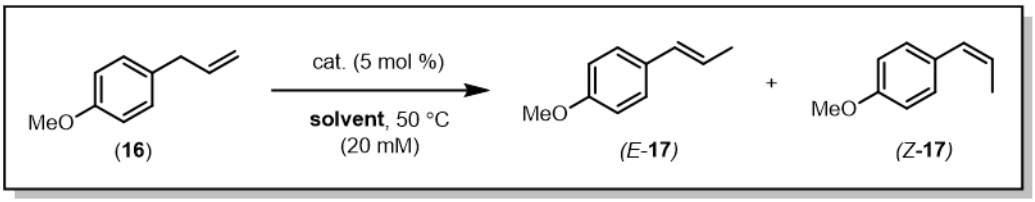

Catalyst	Solvent	Yield of **17**	E : Z
1	Acetone	69%	7 : 1
	MeCN	30%	6 : 1
	Hexanes	84%	7 : 1
	THF	85%	9 : 1
	Toluene	66%	6 : 1
13	Acetone	30%	5 : 1
	MeCN	27%	4 : 1
	Hexanes	70%	8 : 1
	THF	39%	5 : 1
	Toluene	45%	6 : 1

Figure 7.19. Results of isomerization of **16** with **1** and **13** in various solvents. Reaction conditions: 1.0 equiv **16**, 0.05 equiv catalyst, 40 mM. For **13**, concentration of active species was approximated from Si–OH in $SiO_{2\text{-}700}$ starting material. Product concentration was monitored by GC against an internal standard.

how a filtration of the reaction mixture impacts catalysis; if filtering the solids from the reaction leads to the termination of isomerization, this supports that the active catalyst is associated with the surface of the solids and was not carried with the solvent into the second flask. However, if both reactions proceed at a similar rate after filtration, then it must be concluded that the active species was dissolved in solution, and that the catalyst is not heterogeneous.

Our results support the heterogeneity of **13** (Figure 7.20). Upon filtration of the reaction mixture, the filtrate shows nearly no further conversion of **16** ($\mathbf{16}_{\text{filtrate}}$) to **17** ($\mathbf{17}_{\text{filtrate}}$) even with exposure to the reaction conditions overnight. On the other hand, the residue left with the solids in the original flask continues to proceed in catalysis. In fact, the rate of $\mathbf{17}_{\mathbf{solids}}$ formation is even slightly enhanced by the effective increase in catalyst concentration induced by removing a portion of the reaction solution to leave behind **13**. Overall, the results in this study provide

promising ground to further develop **13** as a heterogeneous catalyst for alkene isomerization, among other reactions.

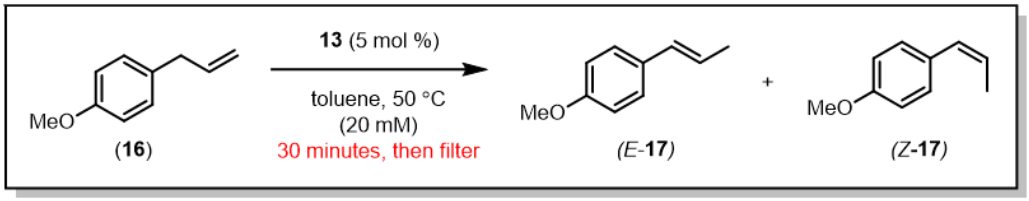

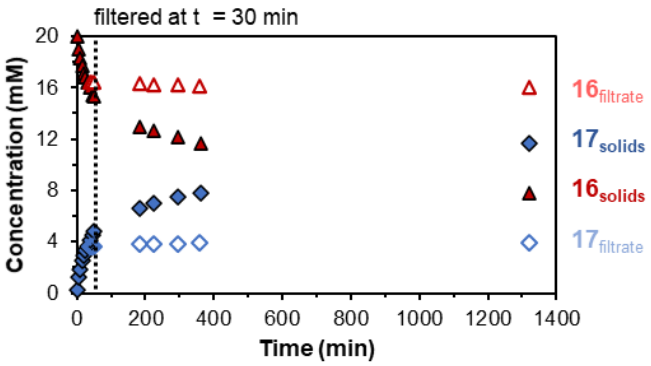

Sample	Time (min)	Yield of **17**
Filtrate	30	18.2%
	185	18.9%
	1320	19.8%
Solids	30	18.2%
	185	33.7%
	1320	59.8%

Figure 7.20. Results of a hot filtration experiment during the isomerization of **16** with **1** and **13** . Reaction conditions: 1.0 equiv **16**, 0.05 equiv catalyst, 40 mM in toluene. For **13**, concentration of active species was approximated from Si–OH in $SiO_{2\text{-}700}$ starting material. Product concentration was monitored by GC against an internal standard.

Conclusion

In this Chapter, we have described our work to develop a new class of heterogeneous catalysts based on the oxidative addition of palladium into Si – H bonds installed on the surface of silica. This project follows our thorough work on understanding the oxidative addition reaction with molecular silanes and elucidating factors that influence the desired reactivity. Our first trials to evaluate oxidative addition to the surface of silica used “bulk” silica that was silanized by the hydrolysis and condensation of $HSi(OEt)_3$. After a grafting reaction with Pd(0) complex 1, IR spectra were indicative of the association of the complex. XPS results suggest the formed species is oxidized to Pd(II) and has a Pd:P ratio of 1:2. These results are in line with the expected reaction, and this evidence leads to our

optimistic conclusion that the grafting reaction was successful. Upon applying the formed materials as catalysts in the isomerization of alkenes, though, only poor activity was observed.

We then moved to studying the silanization and grafting to dehydroxylated silica and alumina surfaces. Using similar methods as in the modification of bulk silica surfaces, we were able to install a variety of Si–H moieties to the surface of metal oxides. This allows for the effective tuning of the Si–H bond both through choice of substituents at silicon and at the metal oxide, which we hope can be used to bias the oxidative addition of **1** and stabilize the corresponding surface silyl palladium hydride species.

These modified $SiO_{2\text{-}700}$ and $Al_2O_{3\text{-}500}$ surfaces were evaluated in grafting reactions with **1**, and tentatively result in successful grafting based on IR spectroscopy. The synthesized materials were then used as heterogeneous catalysts for the isomerization of 4-allylanisole. **1** grafted to a fully condensed H–Si(O–)$_3$ showed the best activity (though still only fair at ~50% conversion overnight) and was carried forward in optimization studies. Studies at variable temperature and catalyst loading show faster and more complete reactions at high temperature and catalyst loading. Non-polar solvents seem to be most compatible with **13** for alkene isomerization.

In comparison to the catalytic activity and profile in the isomerization of 4-allylanisole, it seems that different active species are operative. This is promising in the assignment of **13** as a heterogeneous catalyst. This assignment was supported by hot filtration experiments, which showed the complete termination of reaction upon removal of the reaction solution from **13** solids, indicating the active catalyst to be associated with the surface. This represents a significant achievement in the research conducted in our laboratory: based on thorough background and understanding of the oxidative addition reaction with Pd(0), we now have promising results towards accessing a new class of heterogeneous catalyst. This provides a strong motivation for the study of fundamental mechanisms in the rational development of functional materials.

Perspective and Outlook

Heterogeneous catalysis is ubiquitous in industrial chemical processes yet suffers from fundamental challenges in catalyst design as a result of imprecise synthetic methods. In this Chapter, we have described our investigation into the synthesis of well-defined palladium complexes supported on the surface of silica through oxidative addition to Si–H. The resulting Si–Pd–H species were applied in catalysis and show fair activity for alkene isomerization without intensive optimization. This work provides proof of concept for the formation of new heterogeneous catalysts through this method and lays the foundation for a further exploration of this field. Building upon these results has promise to aid in the development of a new class of efficient, highly tunable heterogeneous catalysts.

8. CONCLUSION

In this dissertation we have reported the results of our extensive studies on the oxidative addition of Pd(0) to hydro- and halo- silanes. A common thread running through each Chapter contained herein is a specific focus on elucidating and understanding reaction mechanisms. Ultimately, this work has contributed to our ongoing studies into homogeneous and heterogeneous catalysis, and it lays the foundation for future studies to come.

In Chapter 1, we gave a general overview of the activation of hydro- and halo- silanes by late transition metals, and contextualized this importance with examples of silane activation in catalysis.

In Chapter 2, we hypothesized and systematically supported a mechanism for the oxidative addition of Pd(0) to hydrosilanes. This experimental work allowed for a rich analysis of the reaction, to give the full energy profile of the reaction and allow us to ascertain of the rate determining step: silane coordination.

In Chapter 3, we continued study into the oxidative addition of Pd(0) to hydrosilanes by modifying the electronics of the silane. Utilizing many of the same experimental tools as in Chapter 3, we identify a pronounced electronic trend favoring electron-poor silanes in oxidative addition.

In Chapter 4, we expanded our study into the effect of silane substituents to probe the influence of steric bulk. Our results show an excellent correlation with empirically derived Charton parameters for steric bulk, trending to disfavor hindered silanes.

In Chapter 5, we explored the further transformations of silyl palladium hydrides by applying them in the hydrosilylation of arylacetylenes. Preliminary studies into electronic and steric effects are in good agreement with trends in oxidative addition, and initial mechanistic experiments suggest interesting interactions between the metal complex and substrates.

In Chapter 6, we examined the oxidative addition of Pd(0) complexes to halosilanes. In these studies, silyl iodides were both kinetically and thermodynamically favored to silyl bromides, and silyl chlorides only underwent oxidative addition with strongly electronegative substituents (i.e. $SiCl_4$). The

mechanistic investigation of this reaction with three different Pd(0) complexes suggests disparate activation pathways for each.

Finally, in Chapter 7, we combine the knowledge gained in previous studies to develop new heterogeneous catalysts by the oxidative addition of Pd(0) to Si–H on the surface of silica. Various forms of silanized silica are synthesized and examined in grafting reactions, and the grafted materials used to catalyze alkene isomerization. These early results show promise for this novel method of heterogeneous catalyst preparation.

APPENDIX

MATERIALS AND METHODS

General Experimental

All syntheses and manipulations were carried out under nitrogen using standard Schlenk (vacuum 10^{-2} mbar) technique or in a nitrogen-filled glovebox unless otherwise indicated. All reagents and solvents were used after drying and stored under nitrogen, unless otherwise indicated. Tetrahydrofuran (THF; Fisher Chemical; HPLC grade, unstabilized), hexanes (Fisher Chemical; HPLC grade), diethyl ether (Et_2O; B&J Brand; HPLC grade, unstabilized) and acetonitrile (MeCN; Fisher Chemical; HPLC grade) were dispensed under nitrogen from an LC Technology SP-1 solvent system. Benzene (ACS grade) was refluxed overnight with CaH_2 and distilled under nitrogen before use. The dried solvents were thereafter stored on activated 4Å molecular sieves under nitrogen. $CDCl_3$, CD_3CN, C_6D_6 and C_7D_8 were purchased from Cambridge Isotope Laboratories, degassed by freeze-pump-thaw, and thereafter stored on activated 4Å molecular sieves under nitrogen. All stock solutions were prepared by mass and were dispensed into reaction vessel by difference from syringe, as detailed in the procedure for each experiment.

Nuclear magnetic resonance (NMR) spectra were collected at room temperature (298 K) unless otherwise stated on a Bruker AV-III HD 600 NMR (600.13 MHz for ^{1}H; 150.90 MHz for ^{13}C; 564.69 MHz for ^{19}F; 119.23 MHz for ^{29}Si; 232.94 MHz for ^{31}P), Bruker Avance-III HD 500 NMR (499.90 MHz for ^{1}H; 126 MHz for ^{13}C; 471 MHz for ^{19}F; 99 MHz for ^{29}Si; 202.46 MHz for ^{31}P), or Varian Inova 500 NMR (499.90 MHz for ^{1}H; 126 MHz for ^{13}C; 471 MHz for ^{19}F; 99 MHz for ^{29}Si; 202.46 MHz for ^{31}P). ^{1}H and ^{13}C spectra were referenced to residual solvent peaks (C_6D_6: ^{1}H δ = 7.16 ppm, ^{13}C δ = 128.06 ppm; C_7D_8: ^{1}H δ = 2.08, 6.97, 7.01, 7.09 ppm, ^{13}C δ = 137.48, 128.87, 127.96, 125.13, 20.43 ppm). Chemical shifts are reported in parts per million (ppm, δ) relative to tetramethylsilane at 0.00 ppm. Peaks are characterized as follows: s (singlet), d (doublet), t (triplet), q (quartet),

pent (pentet), hept (heptet), m (multiplet), br (broad), app (apparent), and/or ms (multiple signals). Coupling constants, *J*, are reported in Hz. Infrared spectroscopy was performed on a Bruker Alpha II FT-IR spectrometer or an Agilent Nicolet 6700 FT-IR, and peaks are reported in cm^{-1}. For catalytic reactions, yields were determined using Gas Chromatography-Mass Spectrometry (GCMS) against an internal standard. GCMS was carried out on a Shimadzu GC-2010 Plus/GCMS-QP2010 SE using a Restek Rtx®-5 (Crossbond 5% diphenyl – 95% dimethyl polysiloxane; 15 m, 0.25 mm ID, 0.25 μm df) column. High-resolution mass spectrometry (HRMS) was carried out on a Waters XEVO G2-XS TOF mass spectrometer.

Chapters 2 and 3

From Hurst, M.R., Zakharov, L.N., Cook, A.K. “The Mechanism of Oxidative Addition of Pd(0) to Si–H Bonds: Electronic Effects, Reaction Mechanism, and Hydrosilylation.” *Chem. Sci.* **2021**, 12, 13045-13060.

Synthesis of palladium complex, [(μ-dcpe)Pd]$_2$

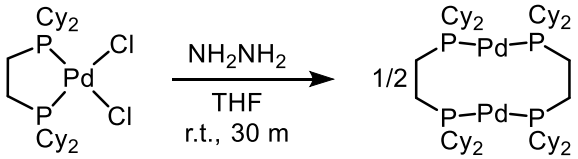

[(μ-dcpe)Pd]$_2$ was synthesized via modified literature procedure:[1] to a 20 mL scintillation vial in a glovebox was added (dcpe)PdCl$_2$ (1.0 equiv) and THF (5 mL) with stirring. To the suspension, anhydrous NH_2NH_2 (20 equiv) was added at once by syringe, and the reaction was stirred for 30 minutes. Hexanes (10 mL) was added and the reaction mixture filtered over a Celite plug to collect a deep red solution, which was concentrated under reduced pressure to yield crude [(μ-dcpe)Pd]$_2$. The material was re-dissolved in hexanes and extracted with MeCN to remove impurities; the hexanes fraction was then concentrated to yield a pure, microcrystalline red solid.

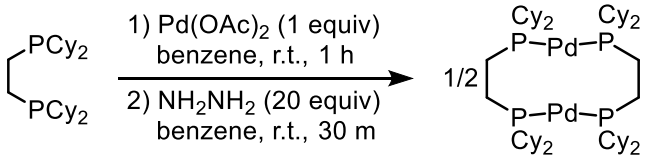

Alternatively, the complex was synthesized in a one-pot procedure: to a 20 mL scintillation vial in the glovebox was added Pd(OAc)$_2$ (1.0 equiv), dcpe (1.0 equiv), and benzene (5 mL) with stirring. The reaction was stirred for 1 hour, and anhydrous NH_2NH_2 (20 equiv) was added all at once by syringe. The reaction was stirred for 30 minutes more before hexanes (10 mL) was added and the reaction mixture was filtered over a Celite plug to collect a deep red solution. The solution was extracted with MeCN and the hexanes layer concentrated under reduced pressure to yield a pure, microcrystalline red solid.

Synthesis of triaryl silanes

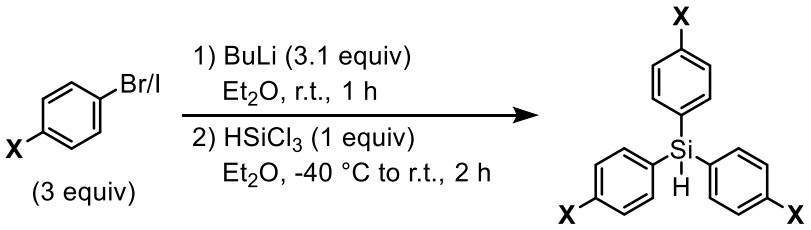

Triaryl silanes were synthesized via modified literature procedure:[2] an oven-dried Schlenk flask was charged with the aryl iodide or aryl bromide (3.33 equiv), which was dissolved in Et_2O. BuLi (2.5 M in hexanes, 3.41 equiv) was added dropwise and the reaction was left to stir at room temperature for 1 hour. The reaction was cooled to -40 °C in a dry ice/MeCN bath. $HSiCl_3$ (1.0 equiv) was slowly added, and the reaction allowed to stir for 1 hour at -40 °C, then warmed to room temperature and stirred for an additional 1 hour. The flask was cooled to 0 °C, opened to air, and quenched with NH_4Cl (saturated aqueous solution). The organic layer was separated, and the aqueous layer extracted twice with Et_2O. The combined organic layers were dried over $MgSO_4$ and filtered, and the filtrate was concentrated under reduced pressure to yield the corresponding crude product. Purification was carried out by column chromatography yield the silanes as clear, colorless oils or colorless solids.

Synthesis of aryldimethyl silanes

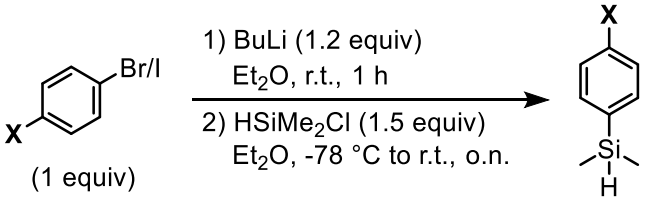

Aryl dimethyl silanes were synthesized via modified literature procedure:[3] an oven-dried Schlenk flask was charged with aryl iodide or aryl bromide (1.0 equiv.), which was dissolved in Et_2O. BuLi (2.5 M in hexanes, 1.2 equiv.) was added dropwise and the reaction was left to stir at room temperature for 1 hour, after which it was cooled to -78 °C in a dry ice/acetone bath. $HSiMe_2Cl$ (1.5 equiv.) was added slowly and the reaction mixture stirred at -78 °C while slowly warming

to room temperature overnight. The flask was cooled to 0 °C, opened to air, and quenched with NH_4Cl (saturated aqueous solution). The organic layer was separated, and the aqueous layer was extracted twice with Et_2O. The combined organic layers were dried over $MgSO_4$ and filtered, and the filtrate was concentrated under reduced pressure to yield the corresponding products as clear, colorless liquids. Purification was performed by column chromatography or distillation.

Synthesis of deuterated silanes

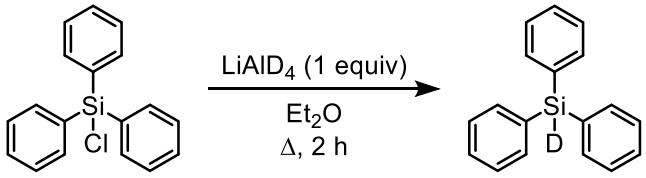

$DSiPh_3$ was prepared via modified literature procedure:[4] to an oven-dried Schlenk flask was added $ClSiPh_3$ (1.0 equiv) and degassed Et_2O (15 mL) with stirring. $LiAlD_4$ (1.0 equiv) was added to the reaction, and the flask was equipped with a reflux condenser. The reaction mixture was heated to reflux and stirred overnight. The reaction was cooled to room temperature and quenched with H_2O. The reaction mixture was extracted with Et_2O and the organics filtered through Celite. The collected clear liquid was concentrated under reduced pressure to yield $DSiPh_3$ as a viscous, clear, colorless oil.

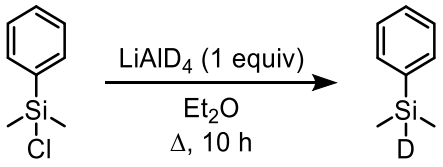

$DSiPhMe_2$ was prepared according to literature procedure:[5] to an oven-dried Schlenk flask was added $LiAlD_4$ (2.7 equiv) and Et_2O (15 mL) with stirring. $PhMe_2SiCl$ (1.0 equiv) was added to the suspension via syringe, and the flask was equipped with a reflux condenser. The reaction mixture was heated to reflux and stirred overnight. The reaction was cooled to room temperature and quenched by slow addition of 10 wt% NaOH (aqueous solution). The product was then extracted

into Et_2O, and the organic layer was separated, dried over $MgSO_4$, filtered, and concentrated under reduced pressure. The crude product was purified via vacuum distillation (room temperature, 1 Torr) into a collection flask cooled with an acetone/dry ice bath to give $DSiPhMe_2$ as a clear colorless oil.

Equilibrium studies at room temperature – General Procedure 3A

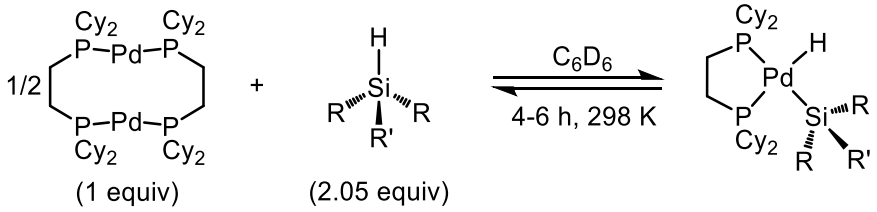

In a nitrogen-filled glovebox, stock solutions of $[(\mu\text{-dcpe})Pd]_2$ (13.3 mM) and silane (54.7 mM) were prepared by weighing out the reagents and diluting with C_6D_6. $[(\mu\text{-dcpe})Pd]_2$ (0.30 mL of stock solution, 0.0040 mmol, 1.0 equiv), the appropriate silane (0.15 mL of stock solution, 0.0082 mmol, 2.05 equiv), and additional C_6D_6 (0.15 mL) were added to an NMR tube using disposable 1-mL syringes. Then, the NMR tube was capped and the reaction was allowed to react for 4-6 hours in the glovebox, after which it was further sealed with Teflon tape to prevent exposure to air and moisture and removed from the glovebox for analysis by NMR. The integrations of each $^{31}P\{^1H\}$ NMR peak corresponding to the product and $[(\mu\text{-dcpe})Pd]_2$ were used to determine percent conversion in each reaction.

Equilibrium studies at variable temperature – General Procedure 3B

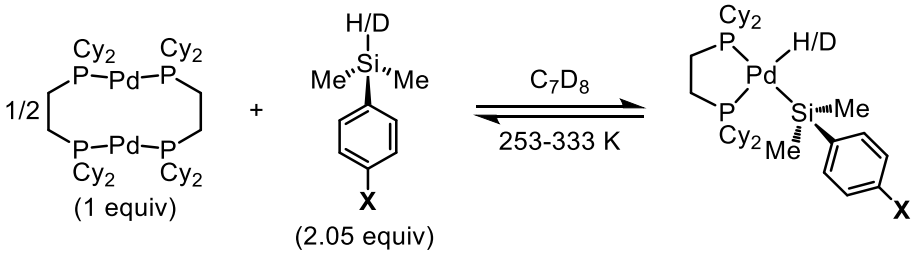

In a nitrogen-filled glovebox, stock solutions of $[(\mu\text{-dcpe})Pd]_2$ (13.3 mM) and silane (54.7 mM) were prepared by weighing out the reagents and diluting with C_7D_8. $[(\mu\text{-dcpe})Pd]_2$ (0.30 mL of stock solution, 0.004 mmol, 1.0 equiv), the

appropriate silane (0.15 mL of stock solution, 0.0082 mmol, 2.05 equiv), and additional C_7D_8 (0.15 mL) were added to a screw-top NMR tube using disposable 1-mL syringes. The NMR tube was capped and the reaction was allowed to react at room temperature for 4 h. Then, the NMR tube was removed from the glovebox for analysis by NMR. The sample was inserted into the NMR at -40 °C, and initial $^{31}P\{^1H\}$ and ^1H spectra were collected after sample was sufficiently cooled. The sample was gradually warmed in 20 °C increments, allowing 10 minutes to equilibrate at each temperature before spectra were collected. The effect of temperature was qualitatively evaluated by observing changes in ^{31}P and ^1H peak shape. Additionally, if both $[(\mu\text{-dcpe})Pd]_2$ and silyl palladium hydride products are present at equilibrium, the integrations of each $^{31}P\{^1H\}$ NMR peak were used to determine relative concentrations and K_{eq} values.

Reversibility with respect to temperature

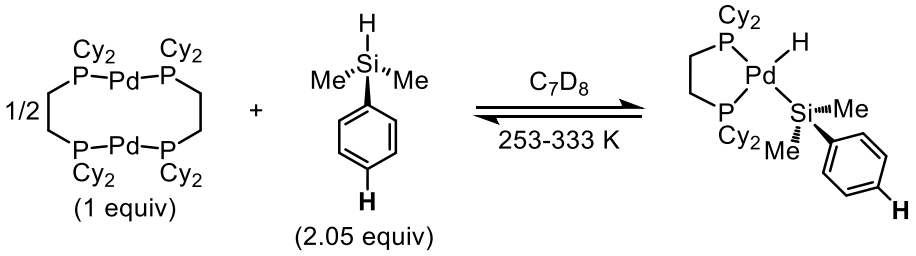

In a nitrogen-filled glovebox, stock solutions of $[(\mu\text{-dcpe})Pd]_2$ (13.3 mM) and silane (54.7 mM) were prepared by weighing out the reagents and diluting with C_7D_8. $[(\mu\text{-dcpe})Pd]_2$ (0.30 mL of stock solution, 0.004 mmol, 1.0 equiv), silane (0.15 mL of stock solution, 0.0082 mmol, 2.05 equiv), and additional C_7D_8 (0.15 mL) were added to a screw-top NMR tube using disposable 1-mL syringes. The NMR tube was capped and the reaction was allowed to react at room temperature for 4 h. Then, the NMR tube was removed from the glovebox for analysis by NMR. The sample was inserted into the NMR which was precooled to -40 °C, and initial $^{31}P\{^1H\}$ and ^1H spectra were collected after sample was sufficiently cooled. The sample was gradually warmed in 20 °C increments to 60 °C, allowing 10 minutes to equilibrate at each temperature before spectra were collected. Then, the sample was allowed to cool back down to room temperature (298 K), and spectra were

recorded. The integrations of the peaks corresponding to starting materials and products by $^{31}P\{^{1}H\}$ NMR were used to determine conversion.

Reversibility with respect to product distribution

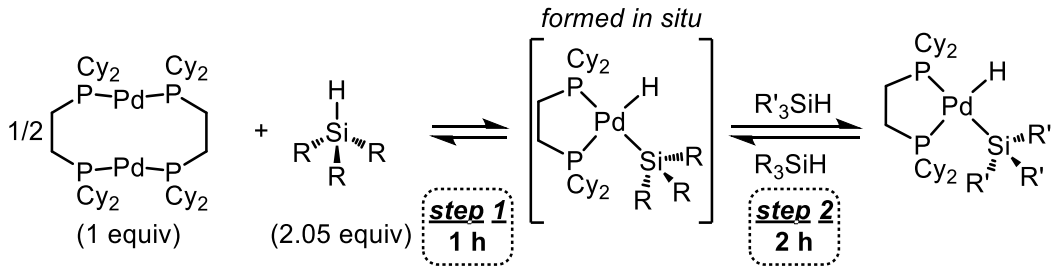

In a nitrogen-filled glovebox, stock solutions of $[(\mu\text{-dcpe})Pd]_2$ (13.3 mM), $HSiR_3$ (54.7 mM) and $HSiR'_3$ (54.7 mM) were prepared by weighing out the reagents and diluting with C_7D_8. $[(\mu\text{-dcpe})Pd]_2$ (0.30 mL of stock solution, 0.004 mmol, 1.0 equiv) and one of the silanes (0.15 mL of stock solution, 0.0082 mmol, 2.05 equiv) were added to a screw-top NMR tube using disposable 1-mL syringes. The NMR tube was capped and the reaction was allowed to react at room temperature for 1 h. Then, the NMR tube was removed from the glovebox for analysis by NMR. The integrations of the peaks corresponding to starting materials and product by $^{31}P\{^{1}H\}$ NMR were used to determine relative concentrations of each species. Then, the NMR tube was brought back into the glovebox, and a different silane was added to the NMR tube (0.15 mL of stock solution, 0.0082 mmol, 2.05 equiv) via a disposable 1-mL syringe. The reaction was allowed to react at room temperature for 2 h. The NMR tube was removed from the glovebox for analysis by NMR. The integrations of the peaks corresponding to the silyl palladium hydrides formed from each silane by $^{31}P\{^{1}H\}$ NMR were used to determine relative concentrations of each species.

Competition studies – General Procedure 3C

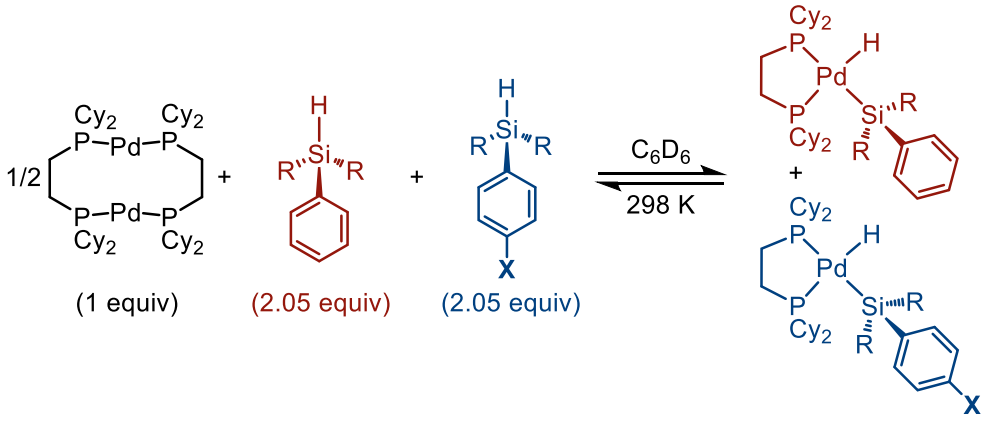

In a nitrogen-filled glovebox, stock solutions of $[(\mu\text{-dcpe})Pd]_2$ (13.3 mM), the parent silane (red; 54.7 mM), and the 4-substituted silane (blue; 54.7 mM) were prepared by weighing out the reagents and diluting with C_6D_6. $[(\mu\text{-dcpe})Pd]_2$ (0.30 mL of stock solution, 0.004 mmol, 1.0 equiv), parent silane (0.15 mL of stock solution, 0.0082 mmol, 2.05 equiv), and the 4-substituted silane (0.15 mL of stock solution, 0.0082 mmol, 2.05 equiv) were added to a screw-top NMR tube using disposable 1-mL syringes. The NMR tube was capped and the reaction was allowed to react at room temperature for 4-6 h. Then, the NMR tube was removed from the glovebox for analysis by NMR. The integrations of the peaks corresponding to starting materials and products by $^{31}P\{^1H\}$ NMR were used to determine conversion.

Kinetic studies – General Procedure 3D

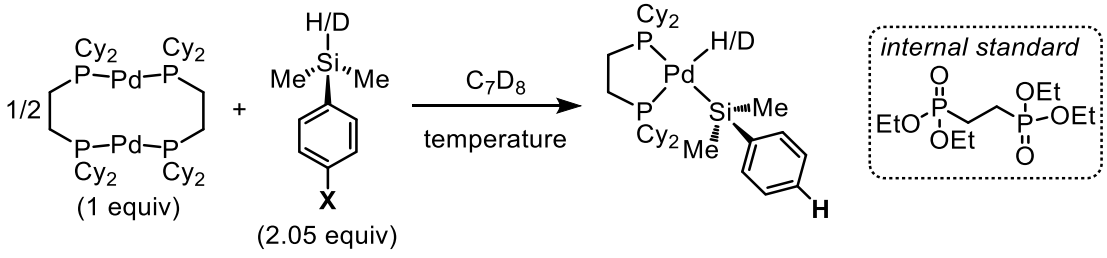

In a nitrogen-filled glovebox, stock solutions of $[(\mu\text{-dcpe})Pd]_2$ (13.3 mM), silane (54.7 mM), and internal standard (tetraethyl(ethylene)bisphosphonate, 26.67 mM) were prepared by weighing out the reagents and diluting with C_7D_8. [(μ-

dcpe)Pd]$_2$ (0.30 mL of stock solution, 0.0040 mmol, 1.0 equiv) and internal standard (0.15 mL of stock solution, 0.0040 mmol, 1.0 equiv) were added to a screw-top NMR tube using disposable 1-mL syringes. The NMR tube was capped with a septum cap and then removed from glovebox. The tube was then cooled to -78 °C in a dry ice/acetone bath. In the glovebox, 0.15 mL of the silane solution (0.0082 mmol, 2.05 equiv) was pulled into a 1.0 mL plastic syringe, which was inverted, and the plunger pulled back completely to collect ample head space of nitrogen. The syringe was removed from the glovebox and injected quickly into the NMR tube while it is still submerged in the dry ice/acetone bath. The NMR tube was then briefly shaken to homogenize the solutions, and then quickly frozen in a liquid nitrogen bath. The samples were stored in the liquid nitrogen bath until analysis.

The NMR probe was pre-cooled to the desired temperature and was locked, tuned, and shimmed at temperature to a dummy sample of C_7D_8. The experimental sample was removed from liquid nitrogen dewar and quickly inserted into the instrument, and $^{31}P\{^1H\}$ NMR scans were collected immediately upon the sample lock. Product concentration was determined by relative peak integrations against internal standard.

Kinetics data was analyzed using MestreNova v14.0. Integrations of product against internal standard were used to determine concentration of product as a function of time. The method of initial rates was used to determine the rate of reaction. We chose this method to prevent complications from the backwards reaction interfering with analysis and interpretation of data. At least two separate trials were run, and all the data points from each trial were used collectively to determine the rate of the reaction.

Kinetics to measure the order in [(μ-dcpe)Pd]$_2$

General procedure 2D was followed using $HSiPhMe_2$ to form (dcpe)PdH($SiPhMe_2$) at 233 K with the following difference:

- 26.7 mM stock solution of [(μ-dcpe)Pd]$_2$ was used, and the following amounts were added to each NMR tube:

Final conc. $[(\mu\text{-dcpe})Pd]_2$ (mM)	Volume stock solution of $[(\mu\text{-dcpe})Pd]_2$ added	mmol $[(\mu\text{-dcpe})Pd]_2$ added	Volume of extra C_7D_8 added
1.67	38 µL	0.0010	0.26 mL
3.33	75 µL	0.0020	0.23 mL
6.67	150 µL	0.0040	0.15 mL
13.3	300 µL	0.0080	0 mL

Kinetics to measure the order in $HSiPhMe_2$

General procedure 2D was followed using $HSiPhMe_2$ to form (dcpe)PdH($SiPhMe_2$) at 233 K with the following difference:

- Four different stock solutions of $HSiPhMe_2$ were prepared, as detailed below, and the following amounts were added to each NMR tube:

Final conc. $HSiPhMe_2$ (mM)	Concentration stock solution of $HSiPhMe_2$	Volume stock solution of $HSiPhMe_2$ added	mmol $HSiPhMe_2$ added
3.42 mM	13.7 mM	0.15 mL	0.0020
6.83 mM	27.3 mM	0.15 mL	0.0041
13.7 mM	54.7 mM	0.15 mL	0.0082
27.3 mM	109.3 mM	0.15 mL	0.0016

Dynamic behavior

General procedure 2B was followed to generate the (silyl)Pd(H) species in solution with the exception that larger temperature ranges were examined. Activation parameters were estimated by the bandwidth method.[6,7]

At cold temperatures, the exchange of ligand environments is slow on the NMR timescale, and two distinct peaks can be observed in $^{31}P\{^1H\}$ NMR spectra. The rate of such slow exchange can be approximated as:

$$k = \pi[(\Delta v_e)_{1/2} - (\Delta v_0)_{1/2}]$$

Where $(\Delta v_e)_{1/2}$ is the width at half-height (WHH) of a peak that is broadened as a consequence of exchange at low temperatures, and $(\Delta v_0)_{1/2}$ is the WHH of the same peak at a temperature where broadening due to exchange is negligible.

At slightly warmer temperatures, the rate of exchange begins to transition from slow on the NMR timescale to fast on the NMR timescale. Between those two regimes is the point of coalescence, at which $^{31}P\{^{1}H\}$ NMR spectra changes from two distinct peaks to one broad, ill-defined peak that is not resolved from the baseline. At this temperature, which varies based on the silane examined, rate can be approximated:

$$k = \frac{\pi \Delta v_0}{\sqrt{2}}$$

Where Δv_0 is the separation (in Hz) between the two distinct peaks present in NMR spectra of a system in slow exchange. At temperatures above coalescence, exchange enters a regime that is fast on the NMR timescale and spectra show only a single peak. Within this regime, rate can be approximated:

$$k = \frac{\pi \Delta v_0^2}{2}[(\Delta v_e)_{1/2} - (\Delta v_0)_{1/2}]^{-1}$$

At a temperature within the fast regime, the peak of interest will be the least broadened due to exchange. At this temperature, the rate is simplified and can be approximated as:

$$k = \frac{\pi \Delta v_0^2}{2}$$

Using these equations in analysis of $^{31}P\{^{1}H\}$ NMR spectra, the rate of exchange was determined for a range of temperatures, and Eyring plots were constructed to determine the activation parameters for this dynamic exchange process.

Chapter 4

From Hurst, M. R.; Davis, A. G.; Cook, A. K. The Influence of Silane Steric Bulk on the Formation and Dynamic Behavior of Silyl Palladium Hydrides. *Organometallics* **2022** *(accepted)*.

Synthesis of aryldiphenyl silanes, $HSiPh_2$(2-R-Ph) (R = Me, Et, ^{i}Pr)

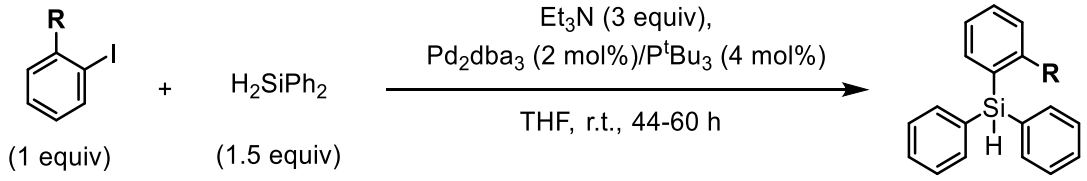

Aryldiphenyl silanes were synthesized via modified literature procedure.[8] In a nitrogen-filled glovebox, a 40 mL scintillation vial was charged with Pd_2dba_3 (2 mol%) and P^tBu_3 (4 mol%), which were suspended in 10 mL THF. Into a separate vial was charged the aryl iodide (1 equiv.) and diphenylsilane (1.5 equiv), which were dissolved in 10 mL THF, and the solution added to the catalyst mixture with stirring. The vial was capped with a septum-lid and removed from the glovebox, where Et_3N (3.0 equiv) was added via syringe under N_2. The reaction was allowed to stir at room temperature under N_2 while product formation was monitored via GC-MS. When product formation ceased, the vial was opened to air, and the reaction quenched by addition of H_2O (5 mL). The organic layer was filtered through a plug of $MgSO_4/SiO_2$ (1:5) to remove residual Pd. The aqueous layer was extracted twice with dichloromethane (2 x 5 mL) and the organics filtered through the $MgSO_4/SiO_2$ plug. The combined organics were concentrated under reduced pressure to yield the corresponding crude product. Purification was conducted by column chromatography.

Synthesis of mesityldiphenylsilane, $HSiPh_2$(2,4,6-Me_3-Ph)

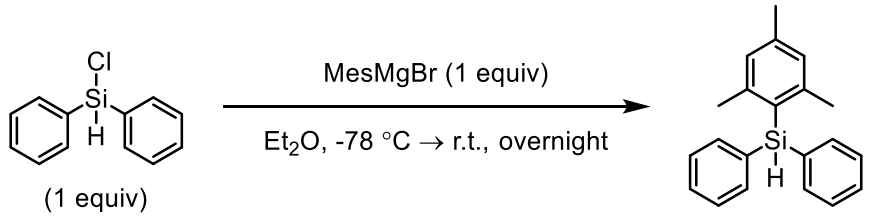

An oven-dried Schlenk flask was charged with diphenylchlorosilane (1 equiv), which was dissolved in 20 mL degassed, anhydrous Et_2O with stirring. The solution was cooled to -78 °C in a dry ice/acetone bath. MesMgBr (1.0 equiv) was slowly added via syringe as a 1 M solution in THF. The reaction was allowed to slowly warm to room temperature with stirring overnight. After overnight, the flask was opened to air, and the reaction quenched by addition of H_2O (~5 mL). The organic layer was separated, and aqueous layer extracted twice more with Et_2O (2 x 10 mL). The combined organics were dried over $MgSO_4$ and filtered, and the filtrate was concentrated under reduced pressure to yield the corresponding crude product as an oil. The crude material was purified by column chromatography on silica using hexanes as an eluent. The pure product was isolated as a clear, colorless, viscous oil.

Synthesis of bis(2-tolyl)phenylsilane, $HSiPh(2\text{-}Me\text{-}Ph)_2$

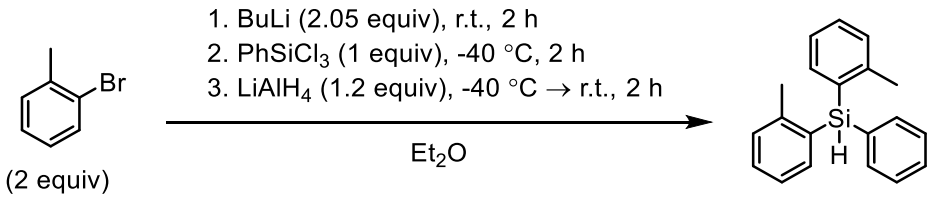

An oven-dried Schlenk flask was charged with 2-bromotoluene (2.0 equiv), which was dissolved in 20 mL degassed, anhydrous Et_2O with stirring. BuLi (2.05 equiv) was added slowly via syringe as a 2.5 M solution in hexanes. The reaction was allowed to stir at room temperature for 2 hours. A second oven-dried Schlenk flask was charged with $PhSiCl_3$ (1.0 equiv), which was dissolved in 10 mL degassed, anhydrous Et_2O with stirring. This Schlenk flask was cooled to -40 °C

in a dry ice/acetonitrile bath and equipped with an addition funnel. The solution of 2-tolyl-lithium was cannula transferred under positive pressure N_2 into the addition funnel, and then was added dropwise to $PhSiCl_3$ over 10 minutes. The combined mixture was allowed to stir at -40 °C for two hours, at which time $LiAlH_4$ (1.2 equiv) was added. The reaction was warmed to room temperature and stirred for 2 hours, then opened to air and slowly poured over ice. The organic layer was separated, and the aqueous layer extracted twice more with Et_2O (2 x 10 mL). The combined organics were dried over $MgSO_4$ and filtered, and the filtrate was concentrated under reduced pressure to yield the corresponding crude product as a yellowish oil. The crude material was purified by column chromatography on silica using hexanes as an eluent. The pure product was isolated as a colorless solid.

Synthesis of tris(2-tolyl)silane, $HSi(2\text{-}Me\text{-}Ph)_3$

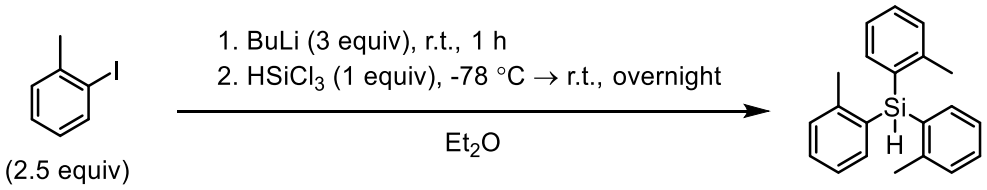

An oven-dried Schlenk flask was charged with 2-iodotoluene (2.5 equiv), which was dissolved in 15 mL degassed, anhydrous Et_2O. BuLi (3.0 equiv). was added slowly via syringe as a 2.5 M solution in hexanes. The reaction was allowed to stir at room temperature for 1 hour before the flask was cooled to -78 °C in a dry ice/acetone bath. $HSiCl_3$ (1.0 equiv) was added slowly via syringe and the solution allowed to slowly warm to room temperature overnight. After overnight, the flask was opened to air and H_2O (~5 mL) was added to quench the reaction. The organic layer was separated, and the aqueous layer extracted twice with Et_2O (2 x 10 mL). The combined organics were dried over $MgSO_4$ and filtered, and the filtrate was concentrated under reduced pressure to yield the corresponding crude product as an off-white solid. The crude material was run through a silica plug with Et_2O as an eluent, then the solution concentrated to saturation under reduced pressure and placed in freezer at -20 °C. The pure product was isolated by crystallization as a waxy, colorless solid.

Equilibrium studies at room temperature – General Procedure 3A

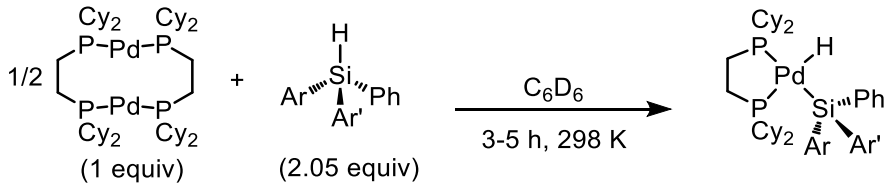

Equilibrium studies were conducted as previously described.[9] In a nitrogen-filled glovebox, a stock solution of [(μ-dcpe)Pd]$_2$ (13.33 mM) was prepared by massing 4.2 mg (0.004 mmol, 1 equiv) into a scintillation vial and dissolving in 0.30 mL C_6D_6. A stock solution of the silane (27.33 mM) was prepared by massing 0.0082 mmol (2.05 equiv) into a scintillation vial and dissolving in 0.30 mL C_6D_6. The solutions were combined and transferred to an NMR tube via glass pipet. The NMR tube was capped and the reaction allowed to stand for 3-5 hours in the glovebox. Before removing for analysis by NMR, the sample was sealed with Teflon tape to prevent exposure to air. The integrations of each $^{31}P\{^1H\}$ NMR peak corresponding to the product and [(μ-dcpe)Pd]$_2$ were used to determine percent conversion in each reaction.

Equilibrium studies at variable temperature – General Procedure 3B

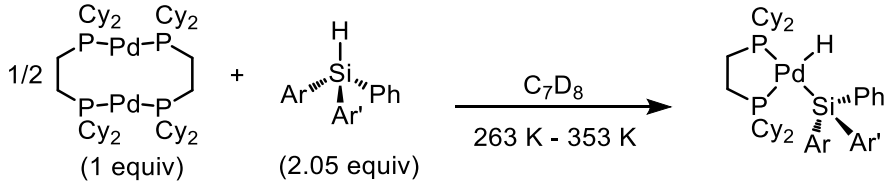

Variable temperature equilibrium studies were conducted as previously described.[9] In a nitrogen-filled glovebox, a stock solution of [(μ-dcpe)Pd]$_2$ (13.33 mM) was prepared by massing 4.2 mg (0.004 mmol, 1 equiv) into a scintillation vial and dissolving in 0.30 mL C_7D_8. A stock solution of the silane (27.33 mM) was prepared by massing 0.0082 mmol (2.05 equiv) into a scintillation vial and dissolving in 0.30 mL C_7D_8. The solutions were combined and transferred to an NMR tube via glass pipet. The NMR tube was capped and the reaction allowed to stand for 3-5 hours in the glovebox. Before removing for analysis by NMR, the

sample was sealed with Teflon tape to prevent exposure to air. The sample was inserted into the NMR at a desired temperature, and initial $^{31}P\{^{1}H\}$ and ^{1}H spectra were collected after the sample was sufficiently cooled. The sample was gradually warmed in 10 °C or 20 °C increments, allowing 10 minutes to equilibrate at each temperature before spectra were collected. At temperatures where both starting materials and products are present at equilibrium, the integrations of each $^{31}P\{^{1}H\}$ NMR peak were used to determine relative concentrations and K_{eq} values.

Kinetics studies – General Procedure 3C

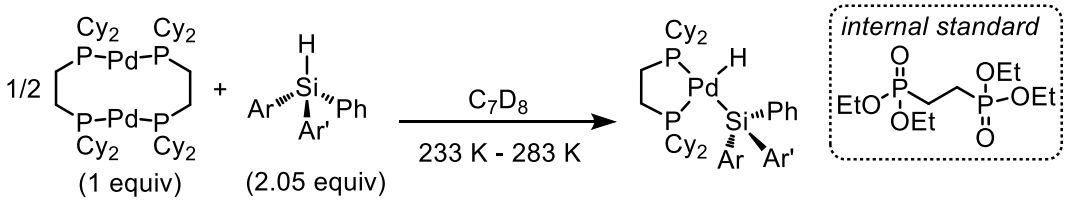

Kinetics experiments were conducted as previously described.[9] In a nitrogen-filled glovebox, stock solutions of $[(\mu\text{-dcpe})Pd]_2$ (13.3 mM), silane (54.7 mM), and internal standard (tetraethyl(ethylene)bisphosphonate, 26.67 mM) were prepared by weighing out the reagents and diluting with C_7D_8. **1** (0.30 mL of stock solution, 0.0040 mmol, 1.0 equiv) and **S1** (0.15 mL of stock solution, 0.0040 mmol, 1.0 equiv) were mixed, then the solution added to a screw-top NMR tube by glass pipet. The NMR tube was capped with a septum cap and removed from glovebox. The tube was then cooled to -78 °C in a dry ice/acetone bath. In the glovebox, 0.15 mL of the silane solution (0.0082 mmol, 2.05 equiv) was pulled into a 1.0 mL plastic syringe, which was inverted, and the plunger pulled back completely to collect ample head space of nitrogen. The syringe was removed from the glovebox and injected quickly into the NMR tube while it is still submerged in the dry ice/acetone bath. The NMR tube was then briefly shaken to homogenize the solutions, and then quickly frozen in a liquid nitrogen bath. The samples were stored in the liquid nitrogen bath until analysis.

The NMR probe was pre-cooled to the desired temperature and was locked, tuned, and shimmed at temperature to a dummy sample of C_7D_8. The experimental sample was removed from liquid nitrogen dewar and quickly inserted into the

instrument, and $^{31}P\{^{1}H\}$ NMR scans were collected immediately upon the sample lock. Product concentration was determined by relative peak integrations against internal standard.

Kinetics data was analyzed using MestreNova v14.0. Integrations of products and internal standard were used to determine concentrations of products as a function of time. The method of initial rates was used to determine the rate of reaction. For each silane at each temperature, at least two trials were conducted on *separate days with fresh stock solutions*, and data points from each trial were used collectively to determine the rate of the reaction.

Dynamic behavior

Dynamic behavior experiments were conducted as previously described.[9] General procedure 3B was followed to generate the (silyl)Pd(H) species in solution, then record $^{31}P\{^{1}H\}$, ^{31}P, and ^{1}H NMR spectra of them over a broad temperature range. Activation parameters were estimated by the linewidth method.[6,7]

Chapter 5

Partially from Hurst, M.R., Zakharov, L.N., Cook, A.K. “The Mechanism of Oxidative Addition of Pd(0) to Si–H Bonds: Electronic Effects, Reaction Mechanism, and Hydrosilylation.” *Chem. Sci.* **2021**, 12, 13045-13060.

Note: synthesis of $[(\mu\text{-dcpe})Pd]_2$, electronically and sterically varied silanes, and $DSiPh_3$ described above (Appendix: Materials and Methods – Chapters 2 and 3, Chapter 4)

Synthesis of deuterated phenylacetylene

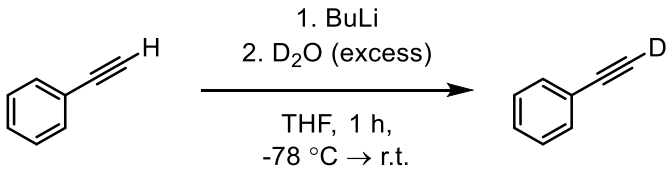

Deuterated phenylacetylene was synthesized according to literature procedure.[10] An oven-dried Schlenk flask was charged with phenylacetylene (1 equiv), which was dissolved in 20 mL degassed, anhydrous THF with stirring. The solution was cooled to -78 °C in a dry ice/acetone bath. nBuLi (1.0 equiv) was slowly added via syringe as a 2.5 M solution in hexanes. The reaction was allowed to stir at -78 °C for 1 hour and then warmed to room temperature for an additional hour. Next, degassed D_2O (excess) was added by syringe. The mixture was stirred for 30 minutes, then poured over $MgSO_4$, filtered, and the filtrate concentrated under reduced pressure to give deuterated phenylacetylene as a light-yellow oil. This crude product was passed through a silica plug eluted by hexanes to give the pure product as a clear liquid.

Catalytic studies – varied silane electronics and steric bulk

General Procedure 5A

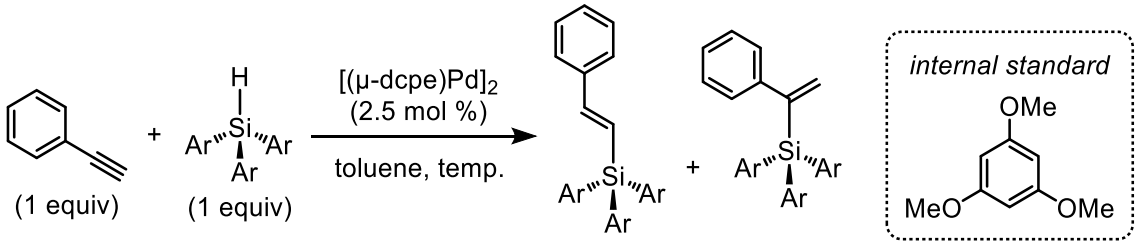

Prior to conducting catalytic studies, $[(\mu\text{-dcpe})Pd]_2$ was further purified. In the glovebox, cold diethyl ether (-30 °C) was added to $[(\mu\text{-dcpe})Pd]_2$ in a scintillation vial. The resulting dark red solution was immediately filtered through celite, and the collected filtrate was concentrated to dryness under vacuum to give a deep red, microcrystalline powder.

For studies with electronically varied silanes: In a nitrogen-filled glovebox, a 4 mM solution of $[(\mu\text{-dcpe})Pd]_2$ was prepared by dissolving $[(\mu\text{-dcpe})Pd]_2$ (0.0010 mmol, 0.025 equiv) in 0.25 mL toluene. 160 mM stock solutions of the silanes (0.040 mmol, 1.0 equiv), phenylacetylene (0.040 mmol, 1.0 equiv), and 1,3,5-trimethoxybenzene (TMB; internal standard; 0.040 mmol, 1.0 equiv) were similarly prepared. To a 4 mL scintillation vial was added 0.25 mL of the stock solution of $[(\mu\text{-dcpe})Pd]_2$, followed by 0.25 mL of the silane solution, 0.25 mL phenylacetylene solution, and finally 0.25 mL TMB solution, for a total volume of 1.0 mL. The reaction vial was sealed with a septum-adapted lid, then removed from glovebox and placed onto a vial block preheated to 40 °C. At determined timepoints, a 25 μL syringe was used to remove 10 μL aliquots, which were filtered through silica and then flushed thoroughly with dichloromethane into a GCMS vial of 1.5 mL total volume. The product concentration was determined via relative integration (by GCMS) of the product peaks against internal standard, in accordance with calibration curves prepared independently using the isolated products. All trials reported were run in duplicate.

For studies with sterically varied silanes, a similar procedure was followed: in a nitrogen-filled glovebox, a 8 mM solution of $[(\mu\text{-dcpe})Pd]_2$ was prepared by dissolving $[(\mu\text{-dcpe})Pd]_2$ (0.0020 mmol, 0.050 equiv) in 0.25 mL toluene. 160 mM

stock solutions of the silanes (0.040 mmol, 1.0 equiv), phenylacetylene (0.040 mmol, 1.0 equiv), and 1,3,5-trimethoxybenzene (TMB; internal standard; 0.040 mmol, 1.0 equi) were similarly prepared. To a 4 mL scintillation vial was added 0.25 mL of the stock solution of $[(\mu\text{-dcpe})Pd]_2$, followed by 0.25 mL of the silane solution, 0.25 mL phenylacetylene solution, and finally 0.25 mL TMB solution, for a total volume of 1.0 mL. The reaction vial was sealed with a septum-adapted lid, then removed from glovebox and placed onto a vial block preheated to the desired temperature (313 K or 333 K). At determined timepoints, a 25 µL syringe was used to remove 10 µL aliquots, which were filtered through silica and then flushed thoroughly with dichloromethane into a GCMS vial of 1.5 mL total volume. The product concentration was determined via relative integration (by GCMS) of the product peaks against internal standard, in accordance with calibration curves prepared independently using the isolated products. All trials reported were run in duplicate.

Catalytic studies – initial rates

General Procedure 5B

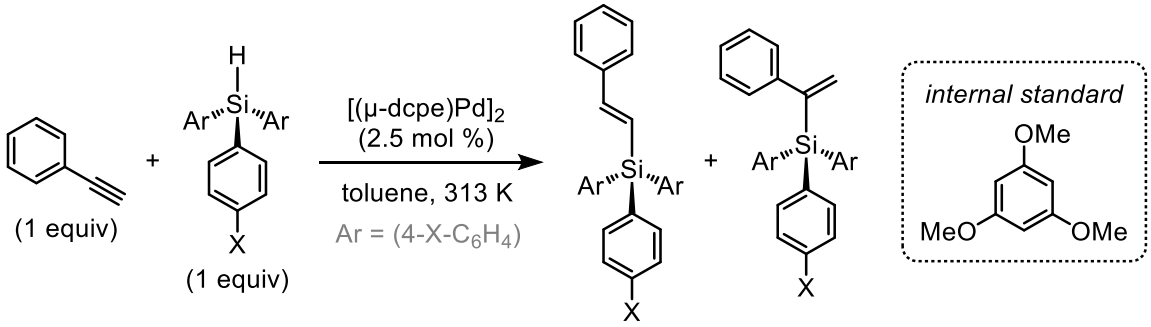

To evaluate the initial rates of reaction, slight modification was necessary for cases where the reaction proceeds too quickly to collect satisfactory data at early timepoints (due to product formation prior to initial data collection). Stock solutions were prepared as described above and were mixed as described above *excluding the phenylacetylene solution*. Instead, 0.25 mL of the phenylacetylene stock solution was taken into a 1 mL plastic syringe, which was inverted and the plunger pulled back to collect a head space of N_2. The reaction vials were sealed with septum lids and removed from the glovebox alongside the syringes prepared

with phenylacetylene stock solution. The phenylacetylene solution was added to each reaction vial at room temperature, then the vials were placed on a vial block warmed to 313 K and monitored as described above.

In situ NMR reaction monitoring

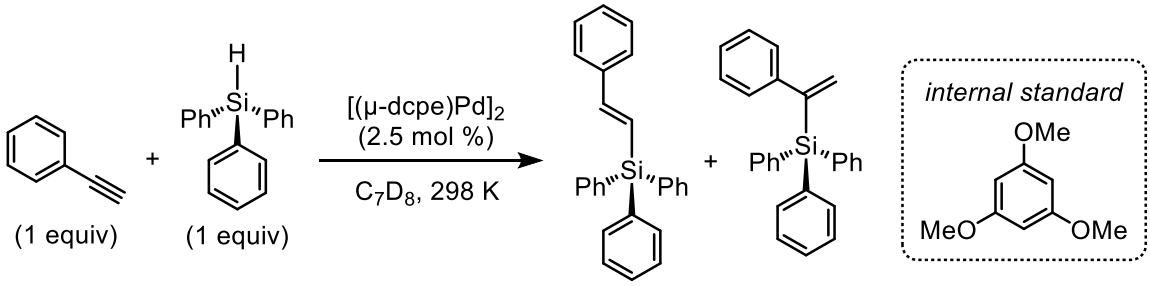

To evaluate the hydrosilylation reaction by NMR, General Procedure 5A was modified slightly: in a nitrogen-filled glovebox, a 6.67 mM solution of [(μ-dcpe)Pd]$_2$ was prepared by dissolving [(μ-dcpe)Pd]$_2$ (0.0010 mmol, 0.025 equiv) in 0.15 mL C_7D_8. 267 mM stock solutions of triphenylsilane (0.040 mmol, 1.0 equiv), phenylacetylene (0.040 mmol, 1.0 equiv), and 1,3,5-trimethoxybenzene (TMB; internal standard; 0.040 mmol, 1.0 equiv) were similarly prepared. To a J-Young NMR tube was added 0.15 mL of the stock solution of [(μ-dcpe)Pd]$_2$, followed by 0.15 mL of the silane solution, 0.15 mL phenylacetylene solution, and finally 0.15 mL TMB solution, for a total volume of 0.60 mL. The NMR tube was then sealed and removed from the glovebox for periodic analysis by ^{31}P and ^{1}H NMR; relative concentrations of the metal species were determined by relative peak integration in ^{31}P NMR spectra, while product formation from the hydrosilylation reaction was quantified against TMB internal standard in ^{1}H NMR spectra.

Independent synthesis of intermediates observed during hydrosilylation

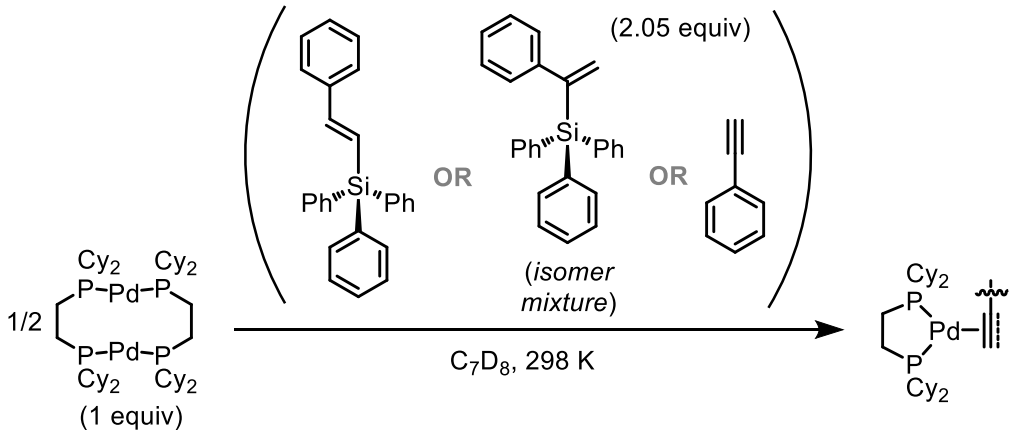

In a nitrogen-filled glovebox, a 16.4 mM stock solution of alkene or alkyne substrate was prepared by dissolving 0.0082 mmol (2.05 equiv) in 0.5 mL C_7D_8. This solution was then added to $[(\mu\text{-dcpe})Pd]_2$ (0.004 mmol, 1.0 equiv), and the resulting mixture was transferred to an NMR tube and sealed. The mixtures were allowed to stand for approximately an hour, though we consistently observed the reaction with any of these substrates to occur nearly instantly. The sample was then removed from the glovebox and analyzed by ^{31}P and ^{1}H NMR. To support the formation of species present during catalysis, the corresponding spectra were compared to those collected during the in situ reaction monitoring study described above.

Coordination reversibility studies

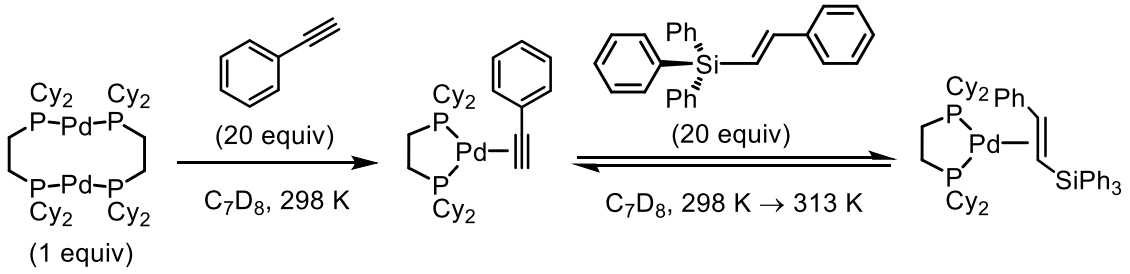

In a nitrogen-filled glovebox, 80 mM stock solutions of each phenylacetylene and 1-phenyl-2-(triphenylsilyl)ethene were prepared by dissolving 0.020 mmol (20 equiv) in 0.25 mL C_7D_8. The stock solution of phenylacetylene was first added to $[(\mu\text{-dcpe})Pd]_2$ (0.001 mmol, 1.0 equiv) and the reaction mixture was

allowed to stand for approximately 30 minutes. The stock solution of 1-phenyl-2-(triphenylsilyl)ethene was then added and the NMR tube was capped and allowed to stand at room temperature for 6 hours, then was warmed to 313 K. The relative concentration of metal species was determined by relative peak integrations in ^{31}P NMR spectra.

Kinetics to determine the rate law

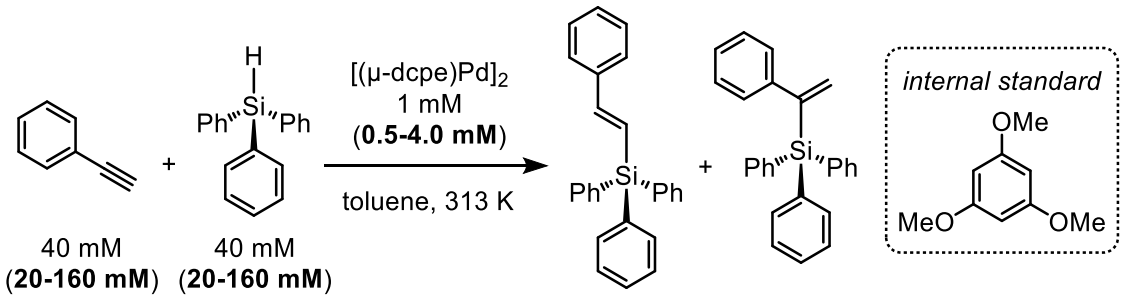

To determine the rate law of the reaction, kinetics experiments were conducted following General Procedure 5A or General Procedure 5B, with the modification that stock solutions of the reagent of interest were prepared at varied concentration.

For example, to evaluate the order in phenylacetylene, stock solutions of phenylacetylene were prepared at 20 mM, 40 mM, 80 mM, and 160 mM concentrations. After preparing reaction vials with the catalytic mixture containing $HSiPh_3$, $[(\mu\text{-dcpe})Pd]_2$, and internal standard, 0.25 mL of a phenylacetylene stock solution was added to each vial. The initial rates of the reactions were then monitored by GC as described above. In these experiments, the reagents not-of-interest are at standard concentrations: 40 mM for internal standard, 40 mM for phenylacetylene, 40 mM for $HSiPh_3$, and 1 mM for $[(\mu\text{-dcpe})Pd]_2$.

Stock solutions and catalytic samples were prepared at the following concentrations to determine the order in each reagent.

Order in phenylacetylene:

Final conc. phenylacetylene	Concentration stock solution of phenylacetylene	Vol. stock solution phenylacetylene added	mmol phenylacetylene added
20 mM	80 mM	0.25 mL	0.020
40 mM	160 mM	0.25 mL	0.040
80 mM	320 mM	0.25 mL	0.080
160 mM	640 mM	0.25 mL	0.160

Order in silane:

Final conc. $HSiPh_3$	Concentration stock solution of $HSiPh_3$	Vol. stock solution of $HSiPh_3$ added	mmol $HSiPh_3$ added
20 mM	80 mM	0.25 mL	0.020
40 mM	160 mM	0.25 mL	0.040
80 mM	320 mM	0.25 mL	0.080
160 mM	640 mM	0.25 mL	0.160

Order in $[(\mu\text{-dcpe})Pd]_2$:

Final conc. $[(\mu\text{-dcpe})Pd]_2$	Concentration stock solution of $[(\mu\text{-dcpe})Pd]_2$	Vol. stock solution of $[(\mu\text{-dcpe})Pd]_2$ added	mmol $[(\mu\text{-dcpe})Pd]_2$ added
0.5 mM	2 mM	0.25 mL	0.0005
1.0 mM	4 mM	0.25 mL	0.001
2.0 mM	8 mM	0.25 mL	0.002
4.0 mM	16 mM	0.25 mL	0.004

KIE and deuterium incorporation studies

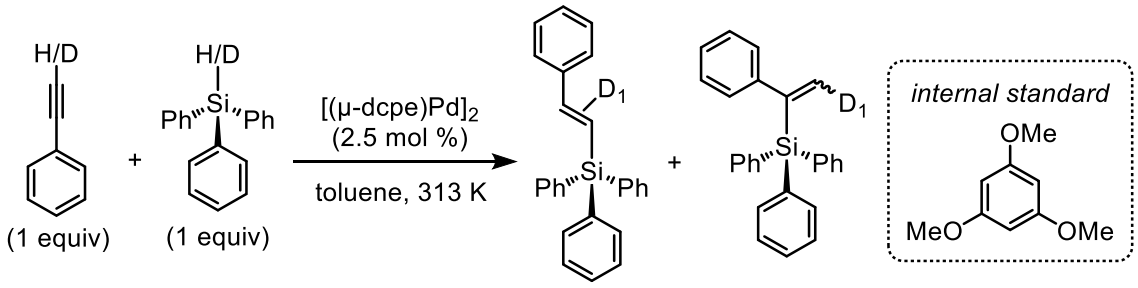

Kinetics experiments with deuterium-labeled substrates were performed as described in General Procedure 5A and General Procedure 5B. The reaction mixtures were worked up afterwards by diluting with hexanes and running the reaction mixture through a plug of $MgSO_4$:SiO_2 (1:10), then flushing the plug with dichloromethane. The collected organics were dried on vacuum and the whole crude mixtures dissolved in CD_3CN for ^1H and ^2H NMR.

Chapter 6

Note: metal precursor complexes were synthesized as reported in literature – $(NHC)_2Pd$,[11,12] $Pd(PR_3)_2$,[13] $[(P–P)Pd]_2$,[9,14,15] $(P–P)PdMe_2$[14,16] – unless reported otherwise. Halosilanes were purchased commercially unless reported otherwise.

Synthesis of dmespe and $(dmespe)_2Pd$
(dmespe = dimesityl(phosphino)ethane)

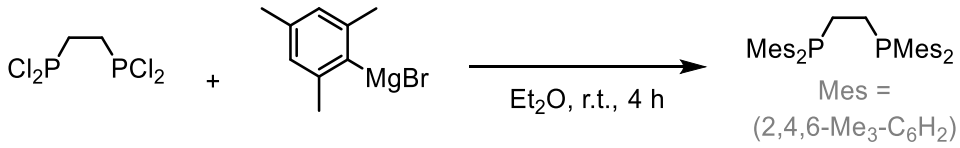

In a nitrogen-filled glovebox, an oven-dried Schlenk flask was charged with $Cl_2P(C_2H_4)PCl_2$ (1.0 mmol, 1 equiv) , which was dissolved in 20 mL Et_2O with stirring. The Schlenk flask was sealed and removed from glovebox and placed under nitrogen on the Schlenk line. MesMgBr (1.0 M in THF; 6.0 mmol, 6 equiv) was added slowly by syringe and an immediate precipitation of white solid was observed. The reaction was stirred for 4 hours, at which time it was opened to air and quenched by addition of water (~5 mL). The biphasic mixture was filtered over a fritted funnel to collect the product as a pure white solid. Higher yields can be achieved by collecting the organic filtrate layer, drying over $MgSO_4$, filtering, and concentrating on vacuum. If purification is necessary, trituration with hexanes or Et_2O is effective.

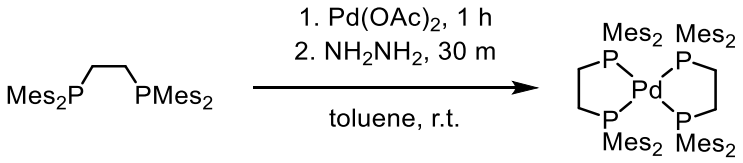

In a nitrogen-filled glovebox, dmespe (0.6 mmol, 2.0 equiv) and $Pd(OAc)_2$ (0.3 mmol, 1.0 equiv) were dissolved/suspended in toluene (5 mL) with stirring. A yellow opaque mixture was observed to form; after an hour, NH_2NH_2 (6.0 mmol, 20 equiv) was added at once. Within a minute, a color change to pinkish-red was observed, and this color deepened over the course of 30 minutes. The reaction

mixture was diluted with hexanes (3 x 10 mL) and filtered over a celite plug. To the organic filtrate was added MeCN to form a biphasic mixture. The hexanes layer was decanted and concentrated on vacuum to give a deep red solid product that is pinkish-red in dilute solution.

Synthesis of halosilanes

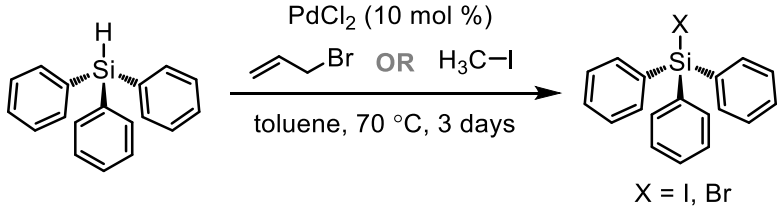

$ISiPh_3$ and $BrSiPh_3$ were synthesized in analogy to literature procedures:[17,18] In an oven-dried Schlenk flask was added $HSiPh_3$ (3.5 mmol, 1.0 equiv) and toluene (20 mL) with stirring under an atmosphere of N_2. Next, allyl bromide or iodomethane (3.9 mmol, 1.1 equiv) was added, followed by $PdCl_2$ (0.04 mmol, 0.01 equiv), and the reaction was warmed to 70 °C with an oil bath. The reaction was allowed to stir for 3 days, at which time it was cooled to room temperature and the mixture concentrated on vacuum. The evacuated flask was brought into a nitrogen-filled glovebox and opened. The solids were suspended in hexanes and the solution filtered over a celite plug. The solids were then suspended/dissolved in toluene and also filtered over celite. The combined organics were concentrated on vacuum until approximately three-quarters of the solvent had evaporated, at which time a large amount of white crystalline material had precipitated ($BrSiPh_3$ has a slight tan hue). The solution was decanted, and the solids washed with minimal hexanes, which was then removed by pipet. Further crystallization is possible from these washes. The crystalline solids were dried on vacuum to give pure $ISiPh_3$ or $BrSiPh_3$.

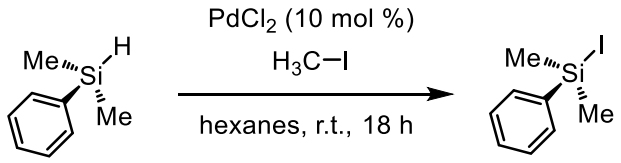

To synthesize $ISiPhMe_2$, the same procedure was followed as described for $ISiPh_3$, but the reaction was conducted at room temperature, in hexanes, and only for 18 hours. Afterwards, the reaction mixture was concentrated under reduced pressure to remove hexanes, then the reaction flask was connected directly to a distillation apparatus. The crude product was distilled at 30-35 °C (ca. 100 mTorr) to collect a light brown oil in the receiving flask. This flask was brought into the glovebox and the oil was dissolved in hexanes, filtered over celite, and concentrated on vacuum. The oil was then dissolved in MeCN, filtered over celite, and then extracted with hexanes. The hexanes layer was decanted and concentrated under vacuum to give pure product.

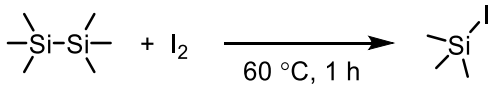

$ISiMe_3$ was synthesized according to literature procedure.[19] In a nitrogen-filled glovebox, a vial was charged with a stir bar, $Me_3Si–SiMe_3$ (1.0 equiv) and I_2 (1.0 equiv). The vial was sealed, then removed from the glovebox and warmed to 60 °C. The reaction was stirred at 60 °C for an hour, then cooled to room temperature and brought back into glovebox. The resulting clear liquid product requires no further purification.

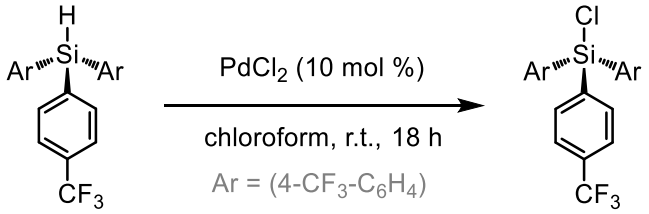

$ClSi(4\text{-}CF_3\text{-}Ph)_3$ was synthesized by a similar method to iodo- and bromo-silanes above. In an oven-dried Schlenk flask was added $HSi(4\text{-}CF_3\text{-}Ph)_3$ (0.25 mmol, 1.0 equiv) which was dissolved in dry, degassed chloroform with stirring. $PdCl_2$ was added (0.003 mmol, 0.01 equiv) and the reaction allowed to stir at room temperature overnight. Afterwards, the reaction mixture was concentrated on vacuum and the evacuated flask brought into a nitrogen-filled glovebox. The solids were dissolved in hexanes, filtered over celite, and the filtrate concentrated under reduced pressure.

Screening for oxidative addition with Pd complexes

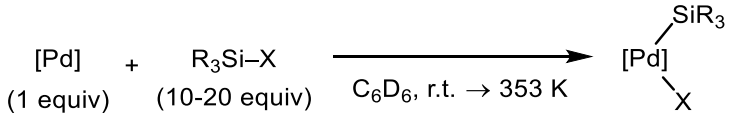

In a nitrogen-filled glovebox, a 133 mM stock solution of halosilane was prepared by dissolving 0.04 mmol (10 equiv) in 0.30 mL C_6D_6. A 13.3 mM stock solution of Pd complex was prepared by dissolving 0.004 mmol (1 equiv) in 0.30 mL C_6D_6, and then 0.30 mL of both stock solutions were combined into an NMR tube. After sealing and allowing to stand for 4 hours, the NMR tubes were removed from the glovebox for analysis. The reaction was monitored by periodically collecting ^{1}H and ^{31}P NMR spectra. After standing at room temperature overnight, the samples were warmed to 353 K in an oil bath for 6-8 hours and monitored further by NMR.

Equilibrium studies with [(μ-dcpe)Pd]$_2$ – General Procedure 6A

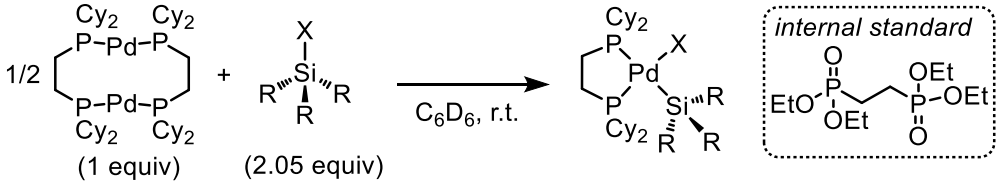

In a nitrogen-filled glovebox, 54.7 mM stock solutions of halosilanes were prepared by dissolving 0.0082 mmol (2.05 equiv) in 0.15 mL C_6D_6. A 26.7 mM stock solution of internal standard was prepared by dissolving 0.004 (1.0 equiv) mmol in 0.15 mL C_6D_6. A 13.33 mM stock solution of [(μ-dcpe)Pd]$_2$ was prepared by dissolving 0.004 mmol (1.0 equiv) in 0.30 mL C_6D_6. Next, 0.15 mL of each the halosilane and internal standard stock solutions were combined with 0.30 mL of [(μ-dcpe)Pd]$_2$ stock solution in an NMR tube for a total volume of 0.6 mL (note: in samples where an internal standard solution was not included, 0.15 mL of C_6D_6 was added instead). The reactions were sealed and allowed to stand in the glovebox for 4-6 hours, at which time they were removed from the glovebox for analysis. The product conversion was determined by relative peak integrations in ^{31}P NMR spectra of the product against internal standard or starting material.

Equilibrium competition studies with [(μ-dcpe)Pd]$_2$

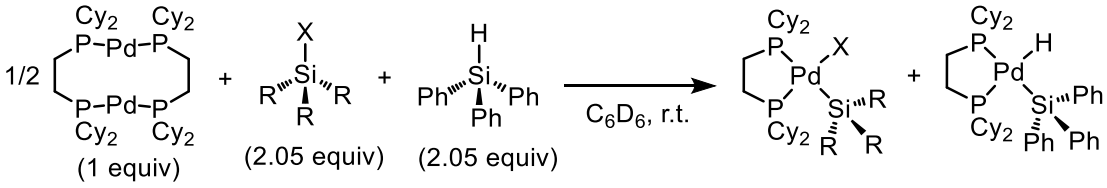

To conduct equilibrium competition studies with [(μ-dcpe)Pd]$_2$, halosilanes, and a representative hydrosilane ($HSiPh_3$), General Procedure 6A was followed with slight modification. In these studies, no internal standard was included, and a 54.7 mM stock solution of $HSiPh_3$ was prepared by dissolving 0.0082 mmol (2.05 equiv) in 0.15 mL C_6D_6. Solutions of [(μ-dcpe)Pd]$_2$ (0.30 mL) and $HSiPh_3$ (0.15 mL) were mixed first into an NMR tube, then 0.15 mL stock solution of halosilane was added. The reactions were allowed to equilibrate for 6 hours, and then removed

from the glovebox. ^{1}H and ^{31}P NMR spectra were collected, and relative peak integrations in ^{31}P spectra were used to determine relative product formation.

Kinetic studies with [(μ-dcpe)Pd]$_2$ – General Procedure 6B

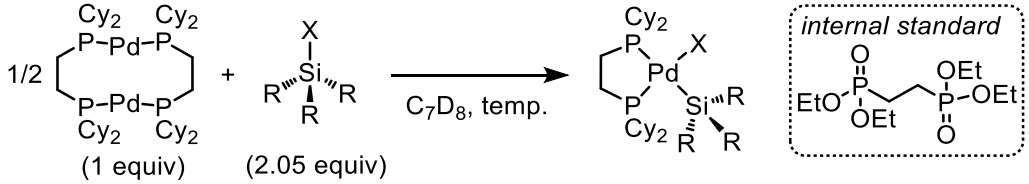

In a nitrogen-filled glovebox, stock solutions were prepared analogously to General Procedure 6A, but using C_7D_8 as the solvent rather than C_6D_6. Into a screw-top NMR tube was added 0.30 mL of [(μ-dcpe)Pd]$_2$ stock solution (13.33 mM; 0.004 mmol) followed by 0.15 mL of internal standard stock solution (26.7 mM; 0.004 mmol). The NMR tube was sealed with a septum lid. Next, 0.15 mL of the halosilane solution (54.7 mM; 0.0082 mmol) was taken into a 1 mL syringe, which was inverted and the plunger pulled back to collect a headspace of nitrogen gas in the syringe barrel. The sealed NMR tube and syringe containing halosilane were removed from the glovebox, and the NMR tube placed directly into a dry ice/acetone bath. The halosilane solution was added through the NMR tube septum lid and the sample was briefly shaken and placed immediately in a dewar of liquid nitrogen. The sample was kept frozen in liquid nitrogen until analysis.

The NMR probe was cooled to the desired temperature and was locked, tuned, and shimmed to a dummy sample of C_7D_8 equilibrated at that temperature. A kinetics sample was removed from liquid nitrogen and quickly inserted into the NMR. Sequential ^{31}P spectra were collected immediately upon sample lock; peak integrations of the product against internal standard were used to quantify product formation.

Kinetic competition studies with [(μ-dcpe)Pd]$_2$

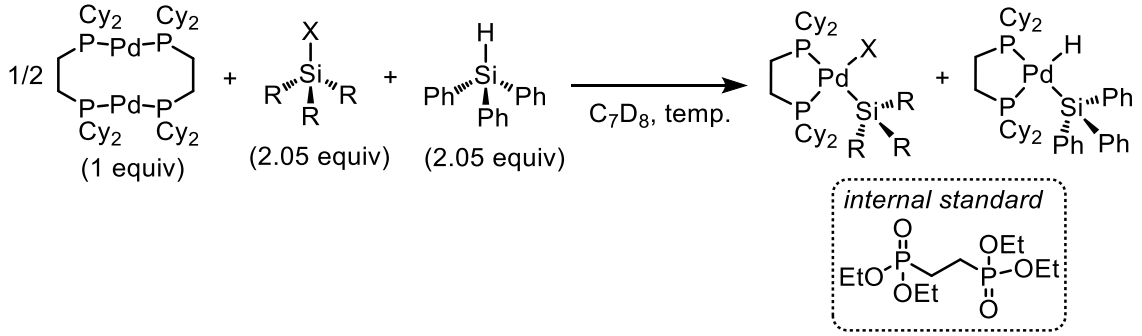

To conduct kinetic competition studies with [(μ-dcpe)Pd]$_2$, halosilanes, and a representative hydrosilane ($HSiPh_3$), General Procedure 6B was followed with slight modification. In a nitrogen-filled glovebox, stock solutions were prepared using C_7D_8 as the solvent. Into a screw-top NMR tube was added 0.15 mL of [(μ-dcpe)Pd]$_2$ stock solution (26.7 mM; 0.004 mmol) followed by 0.15 mL of internal standard stock solution (26.7 mM; 0.004 mmol). The NMR tube was sealed with a septum lid. Next, 0.15 mL of the halosilane solution (54.7 mM; 0.0082 mmol) was mixed with 0.15 mL of a solution of $HSiPh_3$ (54.7 mM, 0.0082 mmol), then the volume of 0.30 mL was taken into a 1 mL syringe, which was inverted and the plunger pulled back to collect a headspace of nitrogen gas in the syringe barrel. The samples were treated analogously to General Procedure 6B thereafter. The formation of both products was monitored by ^{31}P NMR spectra, using peak integrations for the products against internal standard.

Determination of rate law with [(μ-dcpe)Pd]$_2$ – General Procedure 6C

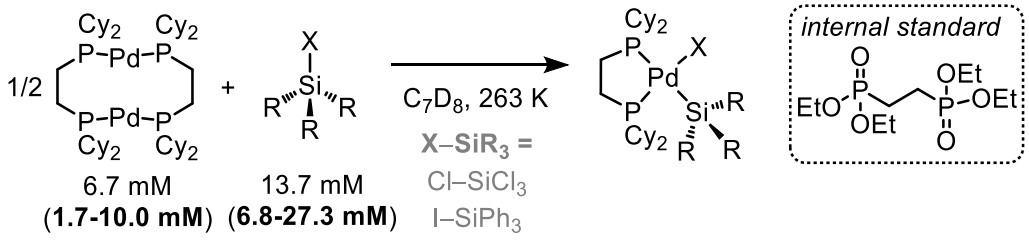

To determine the rate law of the reaction with respect to [(μ-dcpe)Pd]$_2$ or X–SiR_3, General Procedure 6B was followed with slight modification. The

concentration of stock solution for the reagent of interest was modified in accord with the desired concentration of the reagent in the kinetic sample; for example, stock solutions of I–$SiPh_3$ were prepared at concentrations of 6.8 mM, 13.6 mM, 27.3 mM, and 54.6 mM in C_7D_8, and then 0.15 mL of these solutions were used to prepare kinetics samples as described in General Procedure 6B. The concentrations of stock solutions and experimental samples were as follows:

Order in halosilane:

Final conc. halosilane	Concentration stock solution of halosilane	Vol. stock solution of halosilane added	mmol halosilane added
6.8 mM	27.3 mM	0.15 mL	0.0041
13.6 mM	54.7 mM	0.15 mL	0.0082
20.5 mM	82.0 mM	0.15 mL	0.0123
27.3 mM	109.4 mM	0.15 mL	0.0164

Order in [(μ-dcpe)Pd]$_2$:

Final conc. [(μ-dcpe)Pd]$_2$	Concentration stock solution of [(μ-dcpe)Pd]$_2$	Volume stock solution of [(μ-dcpe)Pd]$_2$ added	mmol [(μ-dcpe)Pd]$_2$ added
1.7 mM	6.7 mM	0.15 mL	0.0010
3.3 mM	13.3 mM	0.15 mL	0.0020
6.7 mM	26.7 mM	0.15 mL	0.0040
13.3 mM	53.3 mM	0.15 mL	0.0080

Determination of rate law with $(dmespe)_2Pd$

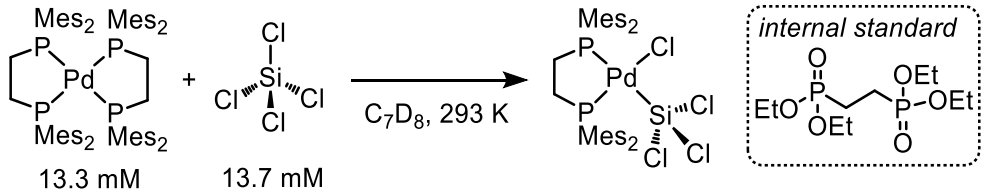

13.3 mM (**3.3-20.0 mM**) 13.7 mM (**6.8-27.3 mM**)

To determine the rate law of the reaction with $(dmespe)_2Pd$, General Procedure 6C was followed with slight modifications: $(dmespe)_2Pd$ was used rather than $[(\mu\text{-dcpe})Pd]_2$, the concentration of the metal complex was increased by a factor of two to account for the monomeric (as opposed to dimeric $[(\mu\text{-dcpe})Pd]_2$) nature of the complex, and only the reaction with $SiCl_4$ was examined. With those modifications, samples were prepared at the following concentrations:

Order in $SiCl_4$:

Final conc. $SiCl_4$	Concentration stock solution of $SiCl_4$	Vol. stock solution of $SiCl_4$ added	mmol $SiCl_4$ added
6.8 mM	27.3 mM	0.15 mL	0.0041
13.6 mM	54.7 mM	0.15 mL	0.0082
20.5 mM	82.0 mM	0.15 mL	0.0123
27.3 mM	109.4 mM	0.15 mL	0.0164

Order in $(dmespe)_2Pd$:

Final conc. $(dmespe)_2Pd$	Concentration stock solution of $(dmespe)_2Pd$	Volume stock solution of $(dmespe)_2Pd$ added	mmol $(dmespe)_2Pd$ added
3.3 mM	13.3 mM	0.15 mL	0.0020
6.7 mM	26.7 mM	0.15 mL	0.0040
13.3 mM	53.3 mM	0.15 mL	0.0080
20.0 mM	80.0 mM	0.15 mL	0.0120

Determination of rate law with $(PCy_3)_2Pd$

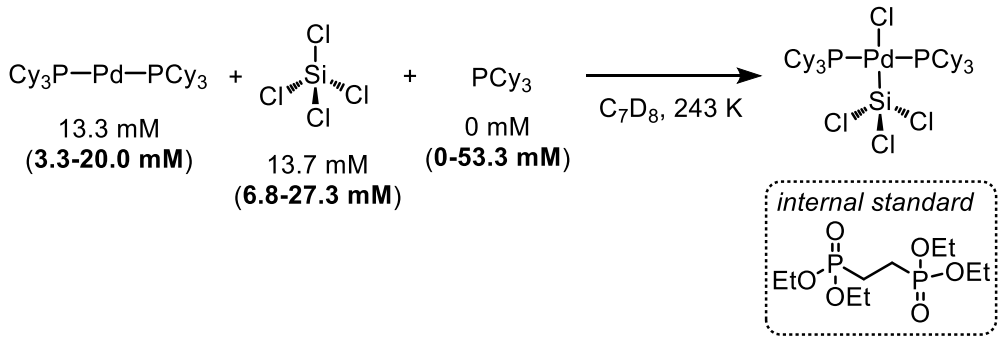

To determine the rate law of the reaction with $Pd(PCy_3)_2$, the same procedure was followed as for $(dmespe)_2Pd$ except that $Pd(PCy_3)_2$ was used. With these modifications, samples were prepared at the following concentrations**:**

Order in $SiCl_4$:

Final conc. $SiCl_4$	Concentration stock solution of $SiCl_4$	Vol. stock solution of $SiCl_4$ added	mmol $SiCl_4$ added
6.8 mM	27.3 mM	0.15 mL	0.0041
13.6 mM	54.7 mM	0.15 mL	0.0082
20.5 mM	82.0 mM	0.15 mL	0.0123
27.3 mM	109.4 mM	0.15 mL	0.0164

Order in $Pd(PCy_3)_2$:

Final conc. $Pd(PCy_3)_2$	Concentration stock solution of $Pd(PCy_3)_2$	Volume stock solution of $Pd(PCy_3)_2$ added	mmol $Pd(PCy_3)_2$ added
3.3 mM	13.3 mM	0.15 mL	0.0020
6.7 mM	26.7 mM	0.15 mL	0.0040
13.3 mM	53.3 mM	0.15 mL	0.0080
20.0 mM	80.0 mM	0.15 mL	0.0120

Chapter 7

Silanization and chlorination of bulk silica

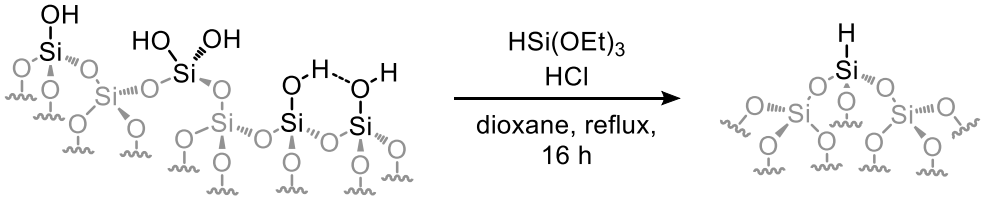

Bulk silica was silanized following a modified literature procedure.[20] In an oven-dried Schlenk flask was added SiO_2 (oven-dried) under nitrogen gas, which was suspended in dry, degassed dioxanes with stirring. HCl (4 N in dioxanes; 3.2 mmol, 1.0 equiv) was added to the reaction mixture and it was warmed to 80 °C. While warming, $HSi(OEt)_3$ (4.5 mmol, 1.4 equiv) was dissolved in dry, degassed dioxanes under nitrogen gas and added to the flask. The reaction mixture was allowed to stir overnight at 80 °C, after which time it was concentrated under reduced pressure. The evacuated flask was brought into a nitrogen-filled glovebox and the white solid material suspended in Et_2O, filtered, and then dried on vacuum to give silanized bulk silica as a free-flowing white powder.

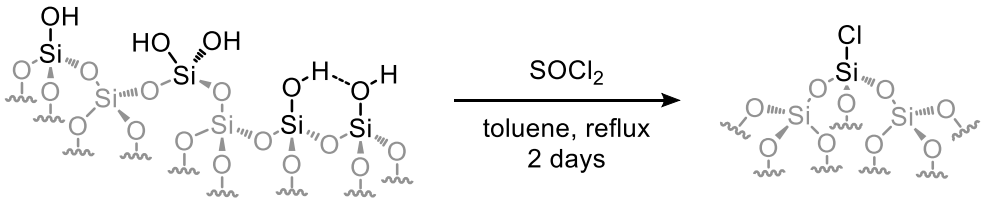

Bulk silica was chlorinated following a modified literature procedure.[21] In an oven-dried Schlenk flask was added SiO_2 (oven-dried) under nitrogen gas, which was suspended in dry, degassed toluene with stirring. $SOCl_2$ (10.0 equiv) was added to the reaction mixture and it was warmed to reflux. The reaction mixture was allowed to stir for two days at refluxing temperature, forming a purple solution. After two days, the mixture was concentrated under reduced pressure. The evacuated flask was brought into a nitrogen-filled glovebox and the purple solid material suspended in Et_2O, filtered, and then dried on vacuum to give silanized bulk silica as a free-flowing white powder.

Synthesis of $SiO_{2\text{-}700}$

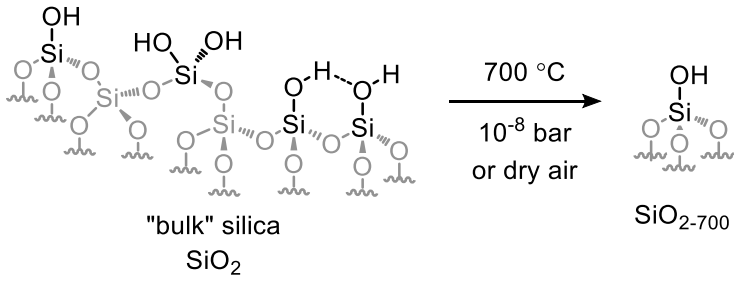

Bulk silica was transformed to $SiO_{2\text{-}700}$ following modified literature procedures.[22] Bulk silica was suspended in H_2O and then dried in an oven at 150 C for 2 days. The dried material was placed inside of a quartz flow reaction tube with in-line fritted filter. The quartz tube was then connected to a gas cylinder of dry air, and air was flowed through the SiO_2 sitting atop the fritted filter. An oil bubbler was placed on the other end of the reaction tube to prevent the entry of atmospheric air and contaminants. The reaction tube was placed inside of a furnace and warmed to 700 °C for 2 days. After this time, the quartz tube was removed from the furnace and cooled to approximately 150 °C before it was sealed and immediately moved into a nitrogen-filled glovebox. The extent of dehydroxylation achieved in this process was determined by titration.

Titration of $SiO_{2\text{-}700}$ to determine silanol concentration

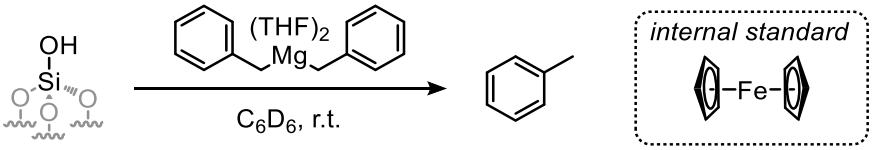

SiO2-700 was titrated following literature procedures.[22] In a nitrogen-filled glovebox, $SiO_{2\text{-}700}$ (24.2 mg) was weighed into a J. Young NMR tube. A 36.7 mM solution of ferrocene (0.022 mmol in 0.6 mmol C_6D_6, 1.0 equiv) was prepared and then added to $Bn_2Mg(THF)_2$ (0.022 mmol, 1.0 equiv). The resulting solution was then added directly to $SiO_{2\text{-}700}$ in the NMR tube. The sample was shaken briefly to ensure all $SiO_{2\text{-}700}$ was submerged in solvent, then the sample was sealed and removed from the glovebox. The concentration of Si–OH sites on the surface per gram of $SiO_{2\text{-}700}$ was determined by quantifying the amount of toluene generated

in the reaction by peak integration in ^{1}H NMR against ferrocene as an internal standard.

Synthesis of H–SiR_2–O–$SiO_{2\text{-}700}$ and H–$SiO_{2\text{-}700}$

General Procedure 7A

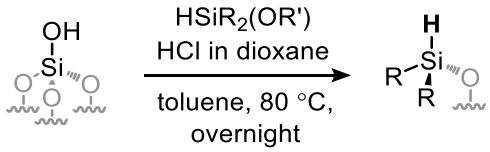

Synthesis of silanized silica materials was achieved by modifying literature procedure.[23,24] In a nitrogen-filled glovebox, $SiO_{2\text{-}700}$ (1.0 g, approximately 0.30 mmol Si–OH/g) was added to a Schlenk flask and suspended in toluene with stirring. The flask was sealed and removed from the glovebox. Dry, degassed HCl (4 N in dioxanes, 0.64 mmol, 1.0 equiv) was added under nitrogen and the flask was warmed to 80 °C. Back in the glovebox, a solution was prepared of $HSiR_2(OR')$ (0.90 mmol, 1.4 equiv) in dioxanes, which was taken into a syringe. The syringe was inverted and the plunger pulled back to collect a headspace of nitrogen gas, then it was removed from the glovebox and immediately added to the reaction flask. The mixture was allowed to stir overnight at 80 °C. After overnight, the reaction mixture was concentrated under reduced pressure, and the evacuated flask was brought into the glovebox. The crude material was suspended in hexanes and then filtered over a fritted funnel to collect the products as white powders which were washed thoroughly with hexanes and toluene, then dried on vacuum.

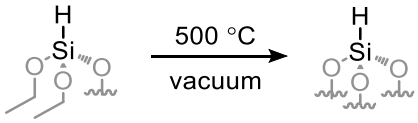

The material synthesized as above (R = OEt) was subjected to further treatment as described in literature. In a nitrogen-filled glovebox, the white powder was added to a borosilicate reaction tube, which was then sealed and removed from the glovebox and connected to vacuum (at or below 1 Torr). The reaction

tube was placed inside of a tube furnace and warmed to 500 °C while evacuated overnight. After this time, the quartz tube was removed from the furnace and cooled to approximately 150 °C before it was sealed and immediately moved into a nitrogen-filled glovebox.

Synthesis of silanized $Al_2O_{3\text{-}500}$

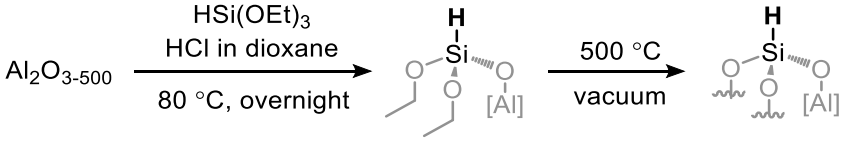

To synthesize silanized alumina materials, General Procedure 7A was followed except that $Al_2O_{3\text{-}500}$ was used rather than $SiO_{2\text{-}700}$. All other methods were identical to those employed with $SiO_{2\text{-}700}$; this applies as well to grafting and catalytic reactions (*vide infra*).

Grafting to modified bulk silica materials

General Procedure 7B

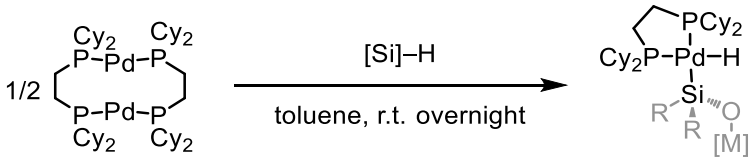

In a nitrogen-filled glovebox, a 4.5 mM solution of $[(\mu\text{-dcpe})Pd]_2$ was prepared by dissolving 0.045 mmol (1.0 equiv) in 10 mL toluene. This solution was added to silanized metal oxide material (0.090 mmol, 2.0 equiv) and the suspension was allowed to stir gently at room temperature in the glovebox overnight. After overnight, the reaction mixture was filtered over a fritted funnel and the collected beige solid was washed thoroughly with hexanes and toluene. The solids were transferred to a scintillation vial and dried under vacuum, while the filtrate was concentrated on vacuum to recollect starting material.

Catalysis with modified bulk silica materials

General Procedure 7C

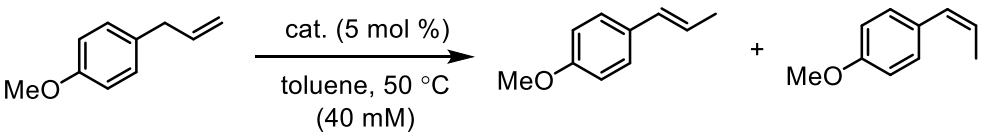

In a nitrogen-filled glovebox, catalyst (0.001 mmol, 0.05 equiv) was weighed into a 4 mL vial with stir bar. 4-allylanisole (0.040 mmol, 1.0 equiv) and internal standard (durene; 0.040 mmol, 1.0 equiv) were each dissolved in 0.50 mL toluene. These solutions were combined for a total volume of 1.0 mL, and then added to the vial containing catalyst. The vial was quickly capped and then removed from the glovebox and placed in vial block warmed to 50 °C. The reaction was monitored by removing a 20-30 µL of the reaction mixture and filtering it over a plug of celite, which was then washed through with DCM. These collected aliquots were then analyzed by GC and integrations were used to quantify product concentration against the internal standard.

Alkene isomerization with varied conditions

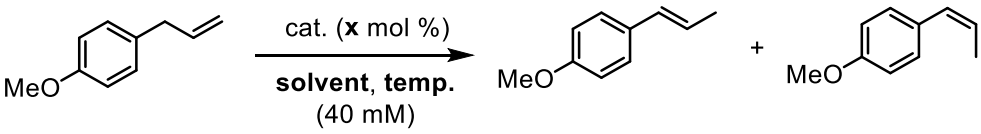

To evaluate the role of conditions on the reaction, General Procedure 7C was followed with slight modifications. To alter the catalyst loading, each vial was charged with a variable amount of Pd catalyst (0.0002 mmol, 0.0005 mmol, 0.001 mmol, or 0.002 mmol), and then the experiment was prepared analogously thereafter. To alter the reaction temperature, samples were prepared as described above and then placed into a vial block at a different desired temperature. To alter the reaction solvent, stock solutions were prepared as described but using the desired solvent. Reaction progress for all experiments was monitored as described in General Procedure 7C.

REFERENCES CITED

Chapter 1

(1) *Silicon-Based Polymer Science: A Comprehensive Resource*; Zeigler, J. M., Fearon, F. W. G., Eds.; Advances in Chemistry; American Chemical Society: Washington, DC, 1989; Vol. 224.

(2) *Organosilicon Materials*; Chandra, G., Allen, R. B., Hutzinger, O., Eds.; The handbook of environmental chemistry / ed. by O. Hutzinger Vol. 3, Anthropogenic compounds; Springer: Berlin, 1997.

(3) Lukin, R. Y.; Kuchkaev, A. M.; Sukhov, A. V.; Bekmukhamedov, G. E.; Yakhvarov, D. G. Platinum-Catalyzed Hydrosilylation in Polymer Chemistry. *Polymers* **2020**, 22.

(4) Tacke, R.; Zilch, H. Sila-Substitution — a Useful Strategy for Drug Design? *Endeavour* **1986**, *10*, 191–197.

(5) Englebienne, P.; Hoonacker, A.; Herst, C. The Place of the Bioisosteric Sila-Substitution in Drug Design. *DDRO* **2005**, *2*, 467–483.

(6) Franz, A. K.; Wilson, S. O. Organosilicon Molecules with Medicinal Applications. *J. Med. Chem.* **2013**, *56*, 388–405.

(7) Denmark, S. E.; Sweis, R. F. Organosilicon Compounds in Cross-Coupling Reactions. In *Metal-Catalyzed Cross-Coupling Reactions*; de Meijere, A., Diederich, F., Eds.; Wiley-VCH Verlag GmbH: Weinheim, Germany, 2004;

(8) Organosilicon Compounds for Industrial Applications - Part 1. In *Organosilicon Chemistry Set*; Auner, N., Weis, J., Eds.; Wiley-VCH Verlag GmbH: Weinheim, Germany, 2005; pp 600–686.

(9) Denmark, S. E.; Liu, J. H.-C. Silicon-Based Cross-Coupling Reactions in the Total Synthesis of Natural Products. *Angewandte Chemie International Edition* **2010**, *49*, 2978–2986.

(10) Kalchauer, W.; Pachaly, B. Müller−Rochow Synthesis: The Direct Process to Methylchlorosilanes. In *Handbook of Heterogeneous Catalysis*; Wiley-VCH Verlag GmbH & Co. KGaA: Weinheim, Germany, 2008; p hetcat0134.

(11) Larson, G. L. Recent Synthetic Applications of Organosilanes. In *The Chemistry of Functional Groups*; Patai, S., Rappoport, Z., Eds.; John Wiley & Sons, Ltd: Chichester, UK, 1989; pp 763–808.

(12) Nilsson, M. Product Subclass 12: Haloogranosilanes. In *Category 1, Organometallics: Compounds of Groups 15 (As, Sb, Bi) and Silicon Compounds*; Fleming, Ley, Eds.; Georg Thieme Verlag: Stuttgart, 2002; pp 247–268.

(13) *Biocatalysis and Biomimetics*; Burrington, J. D., Clark, D. S., Eds.; ACS Symposium Series; American Chemical Society: Washington, DC, 1989; Vol. 392.

(14) Zelisko, P. M. Silicon in a Biological Environment. In *Bio-Inspired Silicon-Based Materials*; Zelisko, P. M., Ed.; Advances in Silicon Science; Springer Netherlands: Dordrecht, 2014; Vol. 5, pp 1–18.

(15) Russell, J. Sealed with Care - A Q&A. National Aeronautics and Space Administration. August 3, 2020.

(16) Finholt, A. E.; Bond, A. C.; Wilzbach, K. E.; Schlesinger, H. I. The Preparation and Some Properties of Hydrides of Elements of the Fourth Group of the Periodic System and of Their Organic Derivatives. *J. Am. Chem. Soc.* **1947**, *69*, 2692–2696.

(17) Wilt, J. W.; Belmonte, F. G.; Zieske, P. A. Reduction of Halosilanes by Organotin Hydrides. *J. Am. Chem. Soc.* **1983**, *105*, 5665–5675.

(18) Ito, M.; Itazaki, M.; Abe, T.; Nakazawa, H. Hydrogenation of Chlorosilanes by $NaBH_4$. *Chem. Lett.* **2016**, *45*, 1434–1436.

(19) Neumeyer, F.; Auner, N. One-Step Synthesis of Siloxanes from the Direct Process Disilane Residue. *Chem. Eur. J.* **2016**, *22*, 17165–17168.

(20) Sturm, A. G.; Santowski, T.; Schweizer, J. I.; Meyer, L.; Lewis, K. M.; Felder, T.; Auner, N.; Holthausen, M. C. Making Use of the Direct Process Residue: Synthesis of Bifunctional Monosilanes. *Chem. Eur. J.* **2019**, *25*

(21) Tsushima, D.; Igarashi, M.; Sato, K.; Shimada, S. Ir-Catalyzed Hydrogenolysis Reaction of Silyl Triflates and Halides with H_2. *Chem. Lett.* **2017**, *46*, 1532–1534.

(22) Beppu, T.; Sakamoto, K.; Nakajima, Y.; Matsumoto, K.; Sato, K.; Shimada, S. Hydrosilane Synthesis via Catalytic Hydrogenolysis of Halosilanes Using a Metal-Ligand Bifunctional Iridium Catalyst. *Journal of Organometallic Chemistry* **2018**, *869*, 75–80.

(23) Glüer, A.; Schweizer, J. I.; Karaca, U. S.; Würtele, C.; Diefenbach, M.; Holthausen, M. C.; Schneider, S. Hydrosilane Synthesis by Catalytic Hydrogenolysis of Chlorosilanes and Silyl Triflates. *Inorg. Chem.* **2018**, *57*, 13822–13828.

(24) Durin, G.; Berthet, J.-C.; Nicolas, E.; Cantat, T. Unlocking the Catalytic Hydrogenolysis of Chlorosilanes into Hydrosilanes with Superbases. *ACS Catal.* **2021**, *11*, 10855–10861.

(25) Corey, J. Y.; Braddock-Wilking, J. Reactions of Hydrosilanes with Transition-Metal Complexes: Formation of Stable Transition-Metal Silyl Compounds. *Chem. Rev.* **1999**, *99*, 175–292.

(26) Corey, J. Y. Reactions of Hydrosilanes with Transition Metal Complexes and Characterization of the Products. *Chem. Rev.* **2011**, *111*, 863–1071.

(27) Corey, J. Y. Reactions of Hydrosilanes with Transition Metal Complexes. *Chem. Rev.* **2016**, *116*, 11291–11435.

(28) Fleming-Tamao Oxidation: (Tamao Oxidation, Tamao-Fleming Oxidation). In *Comprehensive Organic Name Reactions and Reagents*; John Wiley & Sons, Inc.: Hoboken, NJ, USA, 2010; p conrr241.

(29) Cartledge, F. K. Steric Effects on Reactivity in Silicon Chemistry. *Organometallics* **1983**, *2*, 425–430.

(30) Komiyama, T.; Minami, Y.; Hiyama, T. Recent Advances in Transition-Metal-Catalyzed Synthetic Transformations of Organosilicon Reagents. *ACS Catal.* **2017**, *7*, 631–651.

(31) *Comprehensive Handbook on Hydrosilylation*; Marciniec, B., Ed.; Pergamon Press: Oxford ; New York, 1992.

(32) Roy, A. K. A Review of Recent Progress in Catalyzed Homogeneous Hydrosilation (Hydrosilylation). In *Advances in Organometallic Chemistry*; Elsevier, 2007; Vol. 55, pp 1–59.

(33) Nakajima, Y.; Shimada, S. Hydrosilylation Reaction of Olefins: Recent Advances and Perspectives. *RSC Adv.* **2015**, *5*, 20603–20616.

(34) Wang, D.; Klein, J.; Mejía, E. Catalytic Systems for the Cross-Linking of Organosilicon Polymers. *Chem. Asian J.* **2017**, *12*, 1180–1197.
(35) Schubert, U. H2 Coordination of Si–H σ Bonds to Transition Metals. In *Advances in Organometallic Chemistry*; Elsevier, 1990; Vol. 30, pp 151–187.

(36) Crabtree, R. H. Transition Metal Complexation Ofσ Bonds. *Angew. Chem. Int. Ed. Engl.* **1993**, *32*, 789–805.

(37) Kubas, G. J. *Metal Dihydrogen and [Sigma]-Bond Complexes: Structure, Theory, and Reactivity*; Modern inorganic chemistry; Kluwer Academic: New York, 2001.

(38) Nikonov, G. I. Recent Advances in Nonclassical Interligand Si--H Interaction. In *Advances in Organometallic Chemistry*; Academic Press, 2005; pp 217–304.

(39) Scherer, W.; Meixner, P.; Batke, K.; Barquera-Lozada, J. E.; Ruhland, K.; Fischer, A.; Eickerling, G.; Eichele, K. J(Si,H) Coupling Constants in Nonclassical Transition-Metal Silane Complexes. *Angew. Chem. Int. Ed.* **2016**, *55*, 11673–11677.

(40) Meixner, P.; Batke, K.; Fischer, A.; Schmitz, D.; Eickerling, G.; Kalter, M.; Ruhland, K.; Eichele, K.; Barquera-Lozada, J. E.; Casati, N. P. M.; Montisci, F.; Macchi, P.; Scherer, W. *J* (Si,H) Coupling Constants of Activated Si–H Bonds. *J. Phys. Chem. A* **2017**, *121*, 7219–7235.

(41) Jacobsen, H.; Fink, M. J. Tuning the Palladium−Silicon Bond: Bond Analysis of Bisphosphine Silyl Palladium Hydrides. *Organometallics* **2006**, *25*, 1945–1952.

(42) *Hydrosilylation*; Marciniec, B., Ed.; Advances In Silicon Science; Springer Netherlands: Dordrecht, 2009; Vol. 1.

(43) Marciniec, B.; Maciejewski, H.; Pietraszuk, C.; Pawluc, P.; Gulinski, J. Hydrosilylation. In *Encyclopedia of Catalysis*; Horváth, I., Ed.; John Wiley & Sons, Inc.: Hoboken, NJ, USA, 2010

(44) Chalk, A. J.; Harrod, J. F. Homogeneous Catalysis. II. The Mechanism of the Hydrosilation of Olefins Catalyzed by Group VIII Metal Complexes [1].

(45) Sakaki, S.; Mizoe, N.; Sugimoto, M. Theoretical Study of Platinum(0)-Catalyzed Hydrosilylation of Ethylene. Chalk−Harrod Mechanism or Modified Chalk−Harrod Mechanism. *Organometallics* **1998**, *17*, 2510–2523.

(46) Meister, T. K.; Riener, K.; Gigler, P.; Stohrer, J.; Herrmann, W. A.; Kühn, F. E. Platinum Catalysis Revisited—Unraveling Principles of Catalytic Olefin Hydrosilylation. *ACS Catal.* **2016**, *6*, 1274–1284.

(47) Miller, Z. D.; Li, W.; Belderrain, T. R.; Montgomery, J. Regioselective Allene Hydrosilylation Catalyzed by *N* -Heterocyclic Carbene Complexes of Nickel and Palladium. *J. Am. Chem. Soc.* **2013**, *135*, 15282–15285.

(48) Xie, H.; Zhao, L.; Yang, L.; Lei, Q.; Fang, W.; Xiong, C. Mechanisms and Origins of Switchable Regioselectivity of Palladium- and Nickel-Catalyzed Allene Hydrosilylation with N-Heterocyclic Carbene Ligands: A Theoretical Study. *J. Org. Chem.* **2014**, *79*, 4517–4527.

(49) Schneider, J. J. SiH and CH Activation by Transition Metal Complexes: A Step Towards Isolable Alkane Complexes? *Angew. Chem. Int. Ed. Engl.* **1996**, *35*, 1068–1075.

(50) Lersch, M.; Tilset, M. Mechanistic Aspects of C−H Activation by Pt Complexes. *Chem. Rev.* **2005**, *105*, 2471–2526.

(51) Wencel-Delord, J.; Dröge, T.; Liu, F.; Glorius, F. Towards Mild Metal-Catalyzed C–H Bond Activation. *Chem. Soc. Rev.* **2011**, *40*, 4740.

(52) Ma, Z.; Zaera, F. Heterogeneous Catalysis by Metals. In *Encyclopedia of Inorganic Chemistry*; King, R. B., Crabtree, R. H., Lukehart, C. M., Atwood, D. A., Scott, R. A., Eds.; John Wiley & Sons, Ltd: Chichester, UK, 2006; p ia084.

(53) Dumesic, J. A.; Huber, G. W.; Boudart, M. Principles of Heterogeneous Catalysis. In *Handbook of Heterogeneous Catalysis*; Ertl, G., Knzinger, H., Schth, F., Weitkamp, J., Eds.; Wiley-VCH Verlag GmbH & Co. KGaA: Weinheim, Germany, 2008

(54) Heterogeneously Catalyzed Processes in Industry. In *Industrial Catalysis*; Wiley-VCH Verlag GmbH & Co. KGaA: Weinheim, Germany, 2015; pp 261–298.

(55) Copéret, C.; Comas-Vives, A.; Conley, M. P.; Estes, D. P.; Fedorov, A.; Mougel, V.; Nagae, H.; Núñez-Zarur, F.; Zhizhko, P. A. Surface Organometallic and Coordination Chemistry toward Single-Site Heterogeneous Catalysts: Strategies, Methods, Structures, and Activities. *Chem. Rev.* **2016**, *116*, 323–421.

(56) Copéret, C.; Fedorov, A.; Zhizhko, P. A. Surface Organometallic Chemistry: Paving the Way Beyond Well-Defined Supported Organometallics and Single-Site Catalysis. *Catal Lett* **2017**, *147*, 2247–2259.

(57) Samantaray, M. K.; Mishra, S. K.; Saidi, A.; Basset, J.-M. Surface Organometallic Chemistry: A Sustainable Approach in Modern Catalysis. *Journal of Organometallic Chemistry* **2021**, *945*, 121864.

(58) Vansant, E. F.; Voort, P. van der, Vrancken, K. C. *Characterization and Chemical Modification of the Silica Surface*; Elsevier: Amsterdam; New York, 1995.

(59) Copéret, C.; Estes, D. P.; Larmier, K.; Searles, K. Isolated Surface Hydrides: Formation, Structure, and Reactivity. *Chem. Rev.* **2016**, *116*, 8463–8505.

(60) Hurst, M. R.; Zakharov, L. N.; Cook, A. K. The Mechanism of Oxidative Addition of Pd(0) to Si–H Bonds: Electronic Effects, Reaction Mechanism, and Hydrosilylation. *Chem. Sci.* **2021**, *12*, 13045–13060.

(61) Hurst, M. R.; Davis, A. G.; Cook, A. K. The Influence of Silane Steric Bulk on the Formation and Dynamic Behavior of Silyl Palladium Hydrides. *Organometallics* **2022** *(accepted)*.

Chapter 2

(1) Grushin, V. V. Hydrido Complexes of Palladium. *Chem. Rev.* **1996**, *96* (6), 2011–2034.

(2) Hii, K. K. M. In *Handbook of Organopalladium Chemistry for Organic Synthesis: Volume 1 and Volume 2*; Negishi, E., Ed.; Wiley., 2003; pp 81–90.

(3) Heck, R. F. Palladium-Catalyzed Reactions of Organic Halides with Olefins. *Acc. Chem. Res.* **1979**, *12*, 146–151.

(4) Beletskaya, I. P.; Cheprakov, A. V. The Heck Reaction as a Sharpening Stone of Palladium Catalysis. *Chem. Rev.* **2000**, *100*, 3009–3066.

(5) Hills, I. D.; Fu, G. C. Elucidating Reactivity Differences in Palladium-Catalyzed Coupling Processes: The Chemistry of Palladium Hydrides. *J. Am. Chem. Soc.* **2004**, *126*, 13178–13179.

(6) Sigman, M. S.; Jensen, D. R. Ligand-Modulated Palladium-Catalyzed Aerobic Alcohol Oxidations. *Acc. Chem. Res.* **2006**, *39*, 221–229.

(7) Wang, D.; Weinstein, A. B.; White, P. B.; Stahl, S. S. Ligand-Promoted Palladium-Catalyzed Aerobic Oxidation Reactions. *Chem. Rev.* **2018**, *118*, 2636–2679.

(8) Mann, S.; Benhamou, L.; Sheppard, T. Palladium(II)-Catalysed Oxidation of Alkenes. *Synthesis* **2015**, *47*, 3079–3117.

(9) Hartwig, J. F. *Organotransition Metal Chemistry: From Bonding to Catalysis*; University Science Books: Sausalito, Calif, 2010.

(10) Cavinato, G.; Toniolo, L. Carbonylation of Ethene Catalysed by Pd(II)-Phosphine Complexes. *Molecules* **2014**, *19*, 15116–15161.

(11) Chen, Z.; Brookhart, M. Exploring Ethylene/Polar Vinyl Monomer Copolymerizations Using Ni and Pd α-Diimine Catalysts. *Acc. Chem. Res.* **2018**, *51*, 1831–1839.

(12) Trost, B. M. Palladium-Catalyzed Cycloisomerizations of Enynes and Related Reactions. *Acc. Chem. Res.* **1990**, *23*, 34–42.

(13) Larionov, E.; Li, H.; Mazet, C. Well-Defined Transition Metal Hydrides in Catalytic Isomerizations. *Chem. Commun.* **2014**, *50*, 9816.

(14) Molloy, J. J.; Morack, T.; Gilmour, R. Positional and Geometrical Isomerisation of Alkenes: The Pinnacle of Atom Economy. *Angew. Chem. Int. Ed.* **2019**, *58*, 13654–13664.

(15) Moretto, H.-H.; Schulze, M.; Wagner, G. Silicones. In *Ullmann's Encyclopedia of Industrial Chemistry*; Wiley-VCH, 2012; Vol. 32, pp 675–712.

(16) Lukin, R. Yu.; Kuchkaev, A. M.; Sukhov, A. V.; Bekmukhamedov, G. E.; Yakhvarov, D. G. Platinum-Catalyzed Hydrosilylation in Polymer Chemistry. *Polymers* **2020**, *12*, 2174.

(17) Kan, S. B. J.; Lewis, R. D.; Chen, K.; Arnold, F. H. Directed Evolution of Cytochrome c for Carbon–Silicon Bond Formation: Bringing Silicon to Life. *Science* **2016**, *354*, 1048–1051.

(18) Showell, G. A.; Mills, J. S. Chemistry Challenges in Lead Optimization: Silicon Isosteres in Drug Discovery. *Drug Discovery Today* **2003**, *8*, 551–556.

(19) Franz, A. K.; Wilson, S. O. Organosilicon Molecules with Medicinal Applications. *J. Med. Chem.* **2013**, *56*, 388–405.

(20) Rémond, E.; Martin, C.; Martinez, J.; Cavelier, F. Silicon-Containing Amino Acids: Synthetic Aspects, Conformational Studies, and Applications to Bioactive Peptides. *Chem. Rev.* **2016**, *116*, 11654–11684.

(21) Marciniec, B. Catalysis by Transition Metal Complexes of Alkene Silylation–Recent Progress and Mechanistic Implications. *Coord. Chem. Rev.* **2005**, *249*, 2374–2390.

(22) Roy, A. K. A Review of Recent Progress in Catalyzed Homogeneous Hydrosilation (Hydrosilylation). In *Advances in Organometallic Chemistry*; Elsevier, 2007; Vol. 55, pp 1–59.

(23) *Hydrosilylation*; Marciniec, B., Ed.; Advances In Silicon Science; Springer Netherlands: Dordrecht, 2009; Vol. 1.

(24) Troegel, D.; Stohrer, J. Recent Advances and Actual Challenges in Late Transition Metal Catalyzed Hydrosilylation of Olefins from an Industrial Point of View. *Coord. Chem. Rev.* **2011**, *255*, 1440–1459.

(25) Nakajima, Y. Hydrosilylation Reaction of Olefins: Recent Advances and Perspectives. *RSC Adv.* **2015**, 5, 20603-20616.

(26) Meister, T. K.; Riener, K.; Gigler, P.; Stohrer, J.; Herrmann, W. A.; Kühn, F. E. Platinum Catalysis Revisited—Unraveling Principles of Catalytic Olefin Hydrosilylation. *ACS Catal.* **2016**, *6*, 1274–1284.

(27) Horn, K. A. Regio- and Stereochemical Aspects of the Palladium-Catalyzed Reactions of Silanes. *Chem. Rev.* **1995**, *95*, 1317–1350.

(28) Zaranek, M.; Pawluc, P. Markovnikov Hydrosilylation of Alkenes: How an Oddity Becomes the Goal. *ACS Catal.* **2018**, *8*, 9865–9876.

(29) Hayashi, T. Chiral Monodentate Phosphine Ligand MOP for Transition-Metal-Catalyzed Asymmetric Reactions. *Acc. Chem. Res.* **2000**, *33*, 354–362.
(30) Tietze, L. F.; Ila, H.; Bell, H. P. Enantioselective Palladium-Catalyzed Transformations. *Chem. Rev.* **2004**, *104*, 3453–3516.

(31) Gibson, S. E.; Rudd, M. The Role of Secondary Interactions in the Asymmetric Palladium-Catalysed Hydrosilylation of Olefins with Monophosphane Ligands. *Adv. Synth. Catal.* **2007**, *349*, 781–795.

(32) Han, J. W.; Hayashi, T. Palladium-Catalyzed Asymmetric Hydrosilylation of Styrenes with Trichlorosilane. *Tetrahedron: Asymmetry* **2014**, *25*, 479–484.

(33) Corey, J. Y.; Braddock-Wilking, J. Reactions of Hydrosilanes with Transition-Metal Complexes: Formation of Stable Transition-Metal Silyl Compounds. *Chem. Rev.* **1999**, *99*, 175–292.

(34) Corey, J. Y. Reactions of Hydrosilanes with Transition Metal Complexes and Characterization of the Products. *Chem. Rev.* **2011**, *111*, 863–1071.

(35) Corey, J. Y. Reactions of Hydrosilanes with Transition Metal Complexes. *Chem. Rev.* **2016**, *116*, 11291–11435.

(36) Ebsworth, E. A. V.; Marganian, V. M.; Reed, F. J. S.; Gould, R. O. Platinum Hydrides Containing Silyl or Germyl Ligands. Crystal Structure of Trans-Hydridosilylbis(Tricyclohexylphosphine)Platinum(II). *J. Chem. Soc., Dalton Trans.* **1978**, No. 9, 1167.

(37) Paonessa, R. S.; Prignano, A. L.; Trogler, W. C. Photochemical Generation of Bis(Phosphine)Palladium and Bis(Phosphine)Platinum Equivalents. *Organometallics* **1985**, *4*, 647–657.

(38) Packett, D. L.; Syed, A.; Trogler, W. C. Associative Reactions of Dihydridobis(Trimethylphosphine)Platinum(II). Molecular Structures of (Diphenylacetylene)Bis(Trimethylphosphine)Platinum and Hydridotris(Trimethylphosphine)Platinum(II) Tetraphenylborate. *Organometallics* **1988**, *7*, 159–166.

(39) Mullica, D. F.; Sappenfield, E. L.; Hampden-Smith, M. J. Synthesis and X-Ray Structural Investigation of Cis-Hydrido(Triphenylsilyl)-1,4-Butanediyl-Bis-(Dicyclohexylphosphine)Platinum(II). *Polyhedron* **1991**, *10*, 867–872.

(40) Boardman, L. D. (.Eta.5-Cyclopentadienyl)Trialkylplatinum Photohydrosilylation Catalysts. Mechanism of Active Catalyst Formation and Preparation of a Novel Bis(Silyl)Platinum Hydride. *Organometallics* **1992**, *11*, 4194–4201.

(41) Grumbine, S. D.; Tilley, T. D.; Arnold, F. P.; Rheingold, A. L. A Fischer-Type Silylene Complex of Platinum: [Trans-(Cy3P)2(H)Pt:Si(SEt)2]BPh4. *J. Am. Chem. Soc.* **1993**, *115*, 7884–7885.

(42) Latif, L. A.; Eaborn, C.; Pidcock, A. P.; Weng, N. S. Square Planar Platinum(II) Complexes. Crystal Structures of Cis-Bis(Triphenylphosphine)Hydro (Triphenylstannyl)Platinum(II) and Cis-Bis(Triphenylphosphine)Hydro(Triphenylsilyl)Platinum(II). *J. of Organomet. Chem.* **1994**, *474*, 217–221.

(43) Koizumi, T.; Osakada, K.; Yamamoto, T. Intermolecular Transfer of Triarylsilane from RhCl(H)(SiAr $_3$)[P(*i* -Pr) $_3$] $_2$ to a Platinum(0) Complex, Giving *Cis* -PtH(SiAr $_3$)(PEt $_3$) $_2$ (Ar = C $_6$ H $_5$, C $_6$ H $_4$ F- *p* , C $_6$ H $_4$ Cl- *p*). *Organometallics* **1997**, *16*, 6014–6016.

(44) Feldman, J. D.; Mitchell, G. P.; Nolte, J.-O.; Tilley, T. D. Isolation and Characterization of Neutral Platinum Silylene Complexes of the Type (R $_3$ P) $_2$ PtSiMes $_2$ (Mes = 2,4,6-Trimethylphenyl). *J. Am. Chem. Soc.* **1998**, *120*, 11184–11185.

(45) Simons, R. S.; Sanow, L. M.; Galat, K. J.; Tessier, C. A.; Youngs, W. J. Synthesis and Structural Characterization of the Mono(Silyl)Platinum(II) Complex *Cis*- (2,6-Mes $_2$ C $_6$ H $_3$ (H) $_2$ Si)Pt(H)(PPr $_3$) $_2$. *Organometallics* **2000**, *19*, 3994–3996.

(46) Chan, D.; Duckett, S. B.; Heath, S. L.; Khazal, I. G.; Perutz, R. N.; Sabo-Etienne, S.; Timmins, P. L. Platinum Bis(Tricyclohexylphosphine) Silyl Hydride Complexes. *Organometallics* **2004**, *23*, 5744–5756.

(47) Takaya, J.; Iwasawa, N. Reaction of Bis(o-Phosphinophenyl)Silane with M(PPh3)4 (M = Ni, Pd, Pt): Synthesis and Structural Analysis of H2-(Si–H) Metal(0) and Pentacoordinate Silyl Metal(Ii) Hydride Complexes of the Ni Triad Bearing a PSiP-Pincer Ligand. *Dalton Trans.* **2011**, *40*, 8814.

(48) Nakata, N.; Kato, N.; Sekizawa, N.; Ishii, A. Si–H Bond Activation of a Primary Silane with a Pt(0) Complex: Synthesis and Structures of Mononuclear (Hydrido)(Dihydrosilyl) Platinum(II) Complexes. *Inorganics* **2017**, *5*, 72.

(49) Naka, A.; Mihara, T.; Kobayashi, H.; Ishikawa, M. Platinum-Catalyzed Reactions of 2,3-Bis(Diisopropylsilyl)Thiophene with Alkynes. *ACS Omega* **2017**, *2*, 8517–8525.

(50) Keipour, H.; Carreras, V.; Ollevier, T. Recent Progress in the Catalytic Carbene Insertion Reactions into the Silicon–Hydrogen Bond. *Org. Biomol. Chem.* **2017**, *15*, 5441–5456.

(51) Bergstrom, B. D.; Nickerson, L. A.; Shaw, J. T.; Souza, L. W. Transition Metal Catalyzed Insertion Reactions with Donor/Donor Carbenes. *Angew. Chem. Int. Ed.* **2021**, *60*,

(52) Liu, Z.; Huo, J.; Fu, T.; Tan, H.; Ye, F.; Hossain, M. L.; Wang, J. Palladium(0)-Catalyzed C(Sp^3)–Si Bond Formation *via* Formal Carbene Insertion into a Si–H Bond. *Chem. Commun.* **2018**, *54*, 11419–11422.

(53) Xu, Z.; Huang, W.-S.; Zhang, J.; Xu, L.-W. Recent Advances in Transition-Metal-Catalyzed Silylations of Arenes with Hydrosilanes: C–X Bond Cleavage or C–H Bond Activation- Synchronized with Si–H Bond Activation. *Synthesis* **2015**, *47*, 3645–3668.

(54) Alonso, F.; Beletskaya, I. P.; Yus, M. Metal-Mediated Reductive Hydrodehalogenation of Organic Halides. *Chem. Rev.* **2002**, *102*, 4009–4092.
(55) Bähr, S.; Xue, W.; Oestreich, M. C(Sp^3)–Si Cross-Coupling. *ACS Catal.* **2019**, *9*, 16–24.

(56) Noonan, G. M.; Hayter, B. R.; Campbell, A. D.; Gorman, T. W.; Partridge, B. E.; Lamont, G. M. Expanding the Scope of Silane-Mediated Hydrodehalogenation Reactions. *Tetrahedron Letters* **2013**, *54*, 4518–4521.

(57) Iwata, A.; Toyoshima, Y.; Hayashida, T.; Ochi, T.; Kunai, A.; Ohshita, J. PdCl2 and NiCl2-Catalyzed Hydrogen–Halogen Exchange for the Convenient Preparation of Bromo- and Iodosilanes and Germanes. *J. of Organomet. Chem.* **2003**, *667*, 90–95.

(58) Boukherroub, R.; Chatgilialoglu, C.; Manuel, G. $PdCl_2$-Catalyzed Reduction of Organic Halides by Triethylsilane. *Organometallics* **1996**, *15*, 1508–1510.

(59) Kunai, A.; Sakurai, T.; Toyoda, E.; Ishikawa, M.; Yamamoto, Y. Versatile Method for the Synthesis of Iodosilanes. *Organometallics* **1994**, *13*, 3233–3236.

(60) Mirza-Aghayan, M.; Boukherroub, R.; Bolourtchian, M.; Hoseini, M.; Tabar-Hydar, K. A Novel and Efficient Method for Double Bond Isomerization. *J. Organomet. Chem.* **2003**, *678*, 1–4.

(61) Mirza-Aghayan, M.; Boukherroub, R.; Bolourtchian, M. A Mild and Efficient Palladium–Triethylsilane System for Reduction of Olefins and Carbon–Carbon Double Bond Isomerization. *Appl. Organometal. Chem.* **2006**, *20*, 214–219.

(62) Mirza-Aghayan, M.; Boukherroub, R.; Rahimifard, M. Efficient Method for the Reduction of Carbonyl Compounds by Triethylsilane Catalyzed by PdCl2. *J. Organomet. Chem.* **2008**, *693*, 3567–3570.

(63) Bai, X.-F.; Xu, L.-W.; Zheng, L.-S.; Jiang, J.-X.; Lai, G.-Q.; Shang, J.-Y. Aromatic-Amide-Derived Olefins as a Springboard: Isomerization-Initiated Palladium-Catalyzed Hydrogenation of Olefins and Reductive Decarbonylation of Acyl Chlorides with Hydrosilane. *Chem. Eur. J.* **2012**, *18*, 8174–8179.

(64) Bai, X.-F.; Song, T.; Deng, W.-H.; Wei, Y.-L.; Li, L.; Xia, C.-G.; Xu, L.-W. (EtO)3SiH-Promoted Palladium-Catalyzed Isomerization of Olefins: Convenient Synthesis of Internal Alkenes from Terminal Alkenes. *Synlett* **2013**, *25*, 417–422.

(65) Matsumura, T.; Niwa, T.; Nakada, M. Pd-Catalyzed Reductive Cleavage of Alkyl Aryl Sulfides with Triethylsilane That Is Accelerated by Trialkylsilyl Chloride. *Tetrahedron Lett.* **2012**, *53*, 4313–4316.

(66) Boyle, R. C.; Mague, J. T.; Fink, M. J. The First Stable Mononuclear Silyl Palladium Hydrides. *J. Am. Chem. Soc.* **2003**, *125*, 3228–3229.

(67) Boyle, R. C.; Pool, D.; Jacobsen, H.; Fink, M. J. Dynamic Processes in Silyl Palladium Complexes: Evidence for Intermediate Si−H and Si−Si σ-Complexes. *J. Am. Chem. Soc.* **2006**, *128*, 9054–9055.

(68) Nakata, N.; Fukazawa, S.; Kato, N.; Ishii, A. Palladium(II) Hydrido Complexes Having a Primary Silyl or Germyl Ligand: Synthesis, Crystal Structures, and Dynamic Behavior. *Organometallics* **2011**, *30*, 4490–4493.

(69) Barrett, B. J.; Iluc, V. M. An Adaptable Chelating Diphosphine Ligand for the Stabilization of Palladium and Platinum Carbenes. *Organometallics* **2017**, *36*, 730–741.

(70) Barrett, B. J.; Iluc, V. M. Metal-Ligand Cooperation between Palladium and a Diphosphine Ligand with an Olefinic Backbone. *Inorganica Chimica Acta* **2017**, *460*, 35–42.

(71) Jones, W. D. Isotope Effects in C−H Bond Activation Reactions by Transition Metals. *Acc. Chem. Res.* **2003**, *36*, 140–146.
(72) Parkin, G. Temperature-Dependent Transitions Between Normal and Inverse Isotope Effects Pertaining to the Interaction of H−H and C−H Bonds with Transition Metal Centers. *Acc. Chem. Res.* **2009**, *42*, 315–325.

(73) Wolfsberg, M. Theoretical Evaluation of Experimentally Observed Isotope Effects. *Acc. Chem. Res.* **1972**, *5*, 225–233.

(74) Churchill, D. G.; Janak, K. E.; Wittenberg, J. S.; Parkin, G. Normal and Inverse Primary Kinetic Deuterium Isotope Effects for C−H Bond Reductive Elimination and Oxidative Addition Reactions of Molybdenocene and Tungstenocene Complexes: Evidence for Benzene σ-Complex Intermediates. *J. Am. Chem. Soc.* **2003**, *125*, 1403–1420.

(75) Raebiger, J. W.; Miedaner, A.; Curtis, C. J.; Miller, S. M.; Anderson, O. P.; DuBois, D. L. Using Ligand Bite Angles To Control the Hydricity of Palladium Diphosphine Complexes. *J. Am. Chem. Soc.* **2004**, *126*, 5502–5514.

(76) Buncel, E.; Venkatachalam, T. K. Carbanion Mechanisms XXI. Solution Acidity of Triphenylsilane. *J. Organomet. Chem.* **2000**, *604*, 208–210.

(77) Reid, S. M.; Fink, M. J. Reductive Routes to Dinuclear d^{10} −d^{10} Palladium(0) Complexes and Their Redistribution Equilibria in Solution. *Organometallics* **2001**, *20*, 2959–2961.

(78) Gómez-Gallego, M.; Sierra, M. A. Kinetic Isotope Effects in the Study of Organometallic Reaction Mechanisms. *Chem. Rev.* **2011**, *111*, 4857–4963.

(79) Tsuji, Y.; Obora, Y. Structure and Fluxional Behavior of Platinum and Palladium Complexes Having M□Si or M□Sn (M=Pt or Pd) Inter-Element Linkages. *J. Organomet. Chem.* **2000**, *611*, 343–348.

(80) Vyboishchikov, S. F.; Nikonov, G. I. Rhodium Silyl Hydrides in Oxidation State +5: Classical or Nonclassical? †. *Organometallics* **2007**, *26*, 4160–4169.

(81) Ramey, K. C.; Louick, D. J.; Whitehurst, P. W.; Wise, W. B.; Mukherjee, R.; Moriarty, R. M. A Line Width Method for Determining Chemical Exchange Rates from NMR Spectra. *Org. Magn. Reson.* **1971**, *3*, 201–216.

(82) Gasparro, F. P.; Kolodny, N. H. NMR Determination of the Rotational Barrier in N,N-Dimethylacetamide. A Physical Chemistry Experiment. *J. Chem. Educ.* **1977**, *54*, 258.

Chapter 3

(1) Grushin, V. V. Hydrido Complexes of Palladium. *Chem. Rev.* **1996**, *96* (6), 2011–2034.

(2) Hii, K. K. M. In *Handbook of Organopalladium Chemistry for Organic Synthesis: Volume 1 and Volume 2*; Negishi, E., Ed.; Wiley., 2003; pp 81–90.

(3) Corey, J. Y.; Braddock-Wilking, J. Reactions of Hydrosilanes with Transition-Metal Complexes: Formation of Stable Transition-Metal Silyl Compounds. *Chem. Rev.* **1999**, *99*, 175–292.

(4) Corey, J. Y. Reactions of Hydrosilanes with Transition Metal Complexes and Characterization of the Products. *Chem. Rev.* **2011**, *111*, 863–1071.

(5) Corey, J. Y. Reactions of Hydrosilanes with Transition Metal Complexes. *Chem. Rev.* **2016**, *116*, 11291–11435.

(6) Keipour, H.; Carreras, V.; Ollevier, T. Recent Progress in the Catalytic Carbene Insertion Reactions into the Silicon–Hydrogen Bond. *Org. Biomol. Chem.* **2017**, *15*, 5441–5456.

(7) Bergstrom, B. D.; Nickerson, L. A.; Shaw, J. T.; Souza, L. W. Transition Metal Catalyzed Insertion Reactions with Donor/Donor Carbenes. *Angew. Chem. Int. Ed.* **2021**, *60*, 6864–6878.

(8) Liu, Z.; Huo, J.; Fu, T.; Tan, H.; Ye, F.; Hossain, M. L.; Wang, J. Palladium(0)-Catalyzed C(Sp^3)–Si Bond Formation *via* Formal Carbene Insertion into a Si–H Bond. *Chem. Commun.* **2018**, *54*, 11419–11422.

(9) Xu, Z.; Huang, W.-S.; Zhang, J.; Xu, L.-W. Recent Advances in Transition-Metal-Catalyzed Silylations of Arenes with Hydrosilanes: C–X Bond Cleavage or C–H Bond Activation- Synchronized with Si–H Bond Activation. *Synthesis* **2015**, *47*, 3645–3668.

(10) Xu, Z.; Xu, L.-W. Silylations of Arenes with Hydrosilanes: From Transition-Metal-Catalyzed C□X Bond Cleavage to Environmentally Benign Transition-Metal-Free C□H Bond Activation. *ChemSusChem* **2015**, *8*, 2176–2179.

(11) Alonso, F.; Beletskaya, I. P.; Yus, M. Metal-Mediated Reductive Hydrodehalogenation of Organic Halides. *Chem. Rev.* **2002**, *102*, 4009–4092.

(12) Bähr, S.; Xue, W.; Oestreich, M. C(Sp^3)–Si Cross-Coupling. *ACS Catal.* **2019**, *9*, 16–24.

(13) Noonan, G. M.; Hayter, B. R.; Campbell, A. D.; Gorman, T. W.; Partridge, B. E.; Lamont, G. M. Expanding the Scope of Silane-Mediated Hydrodehalogenation Reactions. *Tetrahedron Letters* **2013**, *54* (34), 4518–4521.

(14) Iwata, A.; Toyoshima, Y.; Hayashida, T.; Ochi, T.; Kunai, A.; Ohshita, J. PdCl2 and NiCl2-Catalyzed Hydrogen–Halogen Exchange for the Convenient Preparation of Bromo- and Iodosilanes and Germanes. *Journal of Organometallic Chemistry* **2003**, *667*, 90–95.

(15) Boukherroub, R.; Chatgilialoglu, C.; Manuel, G. $PdCl_2$ -Catalyzed Reduction of Organic Halides by Triethylsilane. *Organometallics* **1996**, *15*, 1508–1510.

(16) Kunai, A.; Sakurai, T.; Toyoda, E.; Ishikawa, M.; Yamamoto, Y. Versatile Method for the Synthesis of Iodosilanes. *Organometallics* **1994**, *13*, 3233–3236..

(17) Larionov, E.; Li, H.; Mazet, C. Well-Defined Transition Metal Hydrides in Catalytic Isomerizations. *Chem. Commun.* **2014**, *50*, 9816.

(18) *Comprehensive Handbook on Hydrosilylation*; Marciniec, B., Ed.; Pergamon Press: Oxford ; New York, 1992.

(19) Hydrosilylation. In *Homogeneous Catalysis: Understanding the Art*; van Leeuwen, P. W. N. M., Ed.; Springer Netherlands: Dordrecht, 2004; pp 371–385.

(20) Roy, A. K. A Review of Recent Progress in Catalyzed Homogeneous Hydrosilation (Hydrosilylation). In *Advances in Organometallic Chemistry*; Elsevier, 2007; Vol. 55, pp 1–59.

(21) Marciniec, B.; Maciejewski, H.; Pietraszuk, C.; Pawluc, P.; Gulinski, J. Hydrosilylation. In *Encyclopedia of Catalysis*; Horváth, I., Ed.; John Wiley & Sons, Inc.: Hoboken, NJ, USA, 2010; p eoc117.

(22) Troegel, D. Recent Advances and Actual Challenges in Late Transition Metal Catalyzed Hydrosilylation of Olefins from an Industrial Point of View. *Coordination Chem. Rev.* **2011**, 20.

(23) Nakajima, Y. Hydrosilylation Reaction of Olefins: Recent Advances and Perspectives. *RSC Adv.* **2015**, 14.

(24) *Organosilicon Materials*; Chandra, G., Allen, R. B., Hutzinger, O., Eds.; The handbook of environmental chemistry / ed. by O. Hutzinger Vol. 3, Anthropogenic compounds; Springer: Berlin, 1997.

(25) Organosilicon Compounds for Industrial Applications - Part 1. In *Organosilicon Chemistry Set*; Auner, N., Weis, J., Eds.; Wiley-VCH Verlag GmbH: Weinheim, Germany, 2005; pp 600–686.

(26) Moretto, H.-H.; Schulze, M.; Wagner, G. Silicones. In *Ullmann's Encyclopedia of Industrial Chemistry*; Wiley-VCH, 2012; Vol. 32, pp 675–712.

(27) Lukin, R. Yu.; Kuchkaev, A. M.; Sukhov, A. V.; Bekmukhamedov, G. E.; Yakhvarov, D. G. Platinum-Catalyzed Hydrosilylation in Polymer Chemistry. *Polymers* **2020**, *12*, 2174.

(28) Englebienne, P.; Hoonacker, A.; Herst, C. The Place of the Bioisosteric Sila-Substitution in Drug Design. *DDRO* **2005**, *2*, 467–483.

(29) K. Pooni, P.; A. Showell, G. Silicon Switches of Marketed Drugs. *MRMC* **2006**, *6*, 1169–1177.

(30) Franz, A. K.; Wilson, S. O. Organosilicon Molecules with Medicinal Applications. *J. Med. Chem.* **2013**, *56*, 388–405.

(31) Kan, S. B. J.; Lewis, R. D.; Chen, K.; Arnold, F. H. Directed Evolution of Cytochrome c for Carbon–Silicon Bond Formation: Bringing Silicon to Life. *Science* **2016**, *354*, 1048–1051.

(32) Komiyama, T.; Minami, Y.; Hiyama, T. Recent Advances in Transition-Metal-Catalyzed Synthetic Transformations of Organosilicon Reagents. *ACS Catal.* **2017**, *7*, 631–651.

(33) Marciniec, B. Catalysis by Transition Metal Complexes of Alkene Silylation–Recent Progress and Mechanistic Implications. *Coordination Chemistry Reviews* **2005**, *249*, 2374–2390.

(34) *Hydrosilylation*; Marciniec, B., Ed.; Advances In Silicon Science; Springer Netherlands: Dordrecht, 2009; Vol. 1.

(35) Meister, T. K.; Riener, K.; Gigler, P.; Stohrer, J.; Herrmann, W. A.; Kühn, F. E. Platinum Catalysis Revisited—Unraveling Principles of Catalytic Olefin Hydrosilylation. *ACS Catal.* **2016**, *6*, 1274–1284.

(36) Horn, K. A. Regio- and Stereochemical Aspects of the Palladium-Catalyzed Reactions of Silanes. *Chem. Rev.* **1995**, *95*, 1317–1350.

(37) Zaranek, M.; Pawluc, P. Markovnikov Hydrosilylation of Alkenes: How an Oddity Becomes the Goal. *ACS Catal.* **2018**, *8*, 9865–9876.

(38) Hayashi, T. Chiral Monodentate Phosphine Ligand MOP for Transition-Metal-Catalyzed Asymmetric Reactions. *Acc. Chem. Res.* **2000**, *33*, 354–362.

(39) Gibson, S. E.; Rudd, M. The Role of Secondary Interactions in the Asymmetric Palladium-Catalysed Hydrosilylation of Olefins with Monophosphane Ligands. *Adv. Synth. Catal.* **2007**, *349*, 781–795.

(40) Han, J. W.; Hayashi, T. Palladium-Catalyzed Asymmetric Hydrosilylation of Styrenes with Trichlorosilane. *Tetrahedron: Asymmetry* **2014**, *25*, 479–484.

(41) Tietze, L. F.; Ila, H.; Bell, H. P. Enantioselective Palladium-Catalyzed Transformations. *Chem. Rev.* **2004**, *104*, 3453–3516.

(42) Boyle, R. C.; Mague, J. T.; Fink, M. J. The First Stable Mononuclear Silyl Palladium Hydrides. *J. Am. Chem. Soc.* **2003**, *125*, 3228–3229.

(43) Boyle, R. C.; Pool, D.; Jacobsen, H.; Fink, M. J. Dynamic Processes in Silyl Palladium Complexes: Evidence for Intermediate Si−H and Si−Si σ-Complexes. *J. Am. Chem. Soc.* **2006**, *128*, 9054–9055.

(44) Nakata, N.; Fukazawa, S.; Kato, N.; Ishii, A. Palladium(II) Hydrido Complexes Having a Primary Silyl or Germyl Ligand: Synthesis, Crystal Structures, and Dynamic Behavior. *Organometallics* **2011**, *30*, 4490–4493.

(45) Barrett, B. J.; Iluc, V. M. Metal-Ligand Cooperation between Palladium and a Diphosphine Ligand with an Olefinic Backbone. *Inorganica Chimica Acta* **2017**, *460*, 35–42.

(46) Barrett, B. J.; Iluc, V. M. An Adaptable Chelating Diphosphine Ligand for the Stabilization of Palladium and Platinum Carbenes. *Organometallics* **2017**, *36*, 730–741.

(47) Jacobsen, H.; Fink, M. J. Tuning the Palladium−Silicon Bond: Bond Analysis of Bisphosphine Silyl Palladium Hydrides. *Organometallics* **2006**, *25*, 1945–1952.

(48) Sakaki, S.; Ogawa, M.; Kinoshita, M. A Theoretical Study on the Oxidative Addition of an Si-X Bond (X = H or Si) to M(PH3)2 (M = Pd or Pt). A Comparison of the Reactivity between Pt(PH3)2 and Pd(PH3)2. *J. Phys. Chem.* **1995**, *99*, 9933–9939.

(49) Mullay, J. Atomic and Group Electronegativities. *J. Am. Chem. Soc.* **1984**, *106*, 5842–5847.

(50) Yang, L.; Powell, D. R.; Houser, R. P. Structural Variation in Copper(I) Complexes with Pyridylmethylamide Ligands: Structural Analysis with a New Four-Coordinate Geometry Index, τ_4. *Dalton Trans.* **2007**, No. 9, 955–964.

(51) Okuniewski, A.; Rosiak, D.; Chojnacki, J.; Becker, B. Coordination Polymers and Molecular Structures among Complexes of Mercury(II) Halides with Selected 1-Benzoylthioureas. *Polyhedron* **2015**, *90*, 47–57
.
(52) Chatt, J.; Eaborn, C.; Ibekwe, S. Silicon, a Ligand Atom of Exceptionally High Trans-Effect. *Chem. Commun. (London)* **1966**, No. 19, 700.

(53) Hartley, F. R. The Cis- and Trans-Effects of Ligands. *Chem. Soc. Rev.* **1973**, *2*, 163.

(54) Appleton, T. G.; Clark, H. C.; Manzer, L. E. The Trans-Influence: Its Measurement and Significance. *Coordination Chemistry Reviews* **1973**, *10*, 335–422.

(55) Hansch, Corwin.; Leo, A.; Taft, R. W. A Survey of Hammett Substituent Constants and Resonance and Field Parameters. *Chem. Rev.* **1991**, *91*, 165–195.

(56) Ramey, K. C.; Louick, D. J.; Whitehurst, P. W.; Wise, W. B.; Mukherjee, R.; Moriarty, R. M. A Line Width Method for Determining Chemical Exchange Rates from NMR Spectra. *Org. Magn. Reson.* **1971**, *3*, 201–216.

(57) Gasparro, F. P.; Kolodny, N. H. NMR Determination of the Rotational Barrier in N,N-Dimethylacetamide. A Physical Chemistry Experiment. *J. Chem. Educ.* **1977**, *54*, 258.

Chapter 4

(1) Organosilicon Compounds for Industrial Applications - Part 1. In *Organosilicon Chemistry Set: From Molecules to Materials*, Auner, N.; Weis, J., Eds. WILEY-VCH Verlag GmbH & Co. KGaA: Weinheim, 2005; pp 600-686.

(2) Moretto, H.-H.; Schulze, M.; Wagner, G. Silicones. *Ullmann's Encycl. Ind. Chem.* **2012**, 675-715.

(3) Hiyama, T., Organosilicon Compounds in Cross-Coupling Reactions. In *Metal-Catalyzed Cross-Coupling Reactions*, 1998; pp 421-453.

(4) Denmark, S. E.; Sweis, R. F., Organosilicon Compounds in Cross-Coupling Reactions. In *Metal-Catalyzed Cross-Coupling Reactions*, 2004; pp 163-216.

(5) Komiyama, T.; Minami, Y.; Hiyama, T. Recent Advances in Transition-Metal-Catalyzed Synthetic Transformations of Organosilicon Reagents. *ACS Catal.* **2017,** *7*, 631-651.

(6) Jones, G. R.; Landais, Y. The oxidation of the carbon-silicon bond. *Tetrahedron* **1996,** *52*, 7599-7662.

(7) Franz, A. K.; Wilson, S. O. Organosilicon Molecules with Medicinal Applications. *J. Med. Chem.* **2013,** *56*, 388-405.

(8) Kan, S. B. J.; Lewis, R. D.; Chen, K.; Arnold, F. H. Directed evolution of cytochrome c for carbon–silicon bond formation: Bringing silicon to life. *Science* **2016,** *354*, 1048-1051.

(9) Roy, A. K. A Review of Recent Progress in Catalyzed Homogeneous Hydrosilation (Hydrosilylation). *Adv. Organomet. Chem.* **2007,** *55*, 1-59.

(10) Troegel, D.; Stohrer, J. Recent advances and actual challenges in late transition metal catalyzed hydrosilylation of olefins from an industrial point of view. *Coord. Chem. Rev.* **2011,** *255*, 1440-1459.

(11) Nakajima, Y.; Shimada, S. Hydrosilylation reaction of olefins: recent advances and perspectives. *RSC Adv.* **2015,** *5*, 20603-20616.

(12) Chalk, A. J.; Harrod, J. F. Homogeneous Catalysis. II. The Mechanism of the Hydrosilation of Olefins Catalyzed by Group VIII Metal Complexes1. *J. Am. Chem. Soc.* **1965,** *87*, 16-21.

(13) Meister, T. K.; Riener, K.; Gigler, P.; Stohrer, J.; Herrmann, W. A.; Kühn, F. E. Platinum Catalysis Revisited—Unraveling Principles of Catalytic Olefin Hydrosilylation. *ACS Catal.* **2016,** *6*, 1274-1284.

(14) Horn, K. A. Regio- and Stereochemical Aspects of the Palladium-Catalyzed Reactions of Silanes. *Chem. Rev.* **1995,** *95*, 1317-1350.

(15) Magistrato, A.; Woo, T. K.; Togni, A.; Rothlisberger, U. Enantioselective Palladium-Catalyzed Hydrosilylation of Styrene: Detailed Reaction Mechanism from First-Principles and Hybrid QM/MM Molecular Dynamics Simulations. *Organometallics* **2004,** *23*, 3218-3227.

(16) Han, J. W.; Hayashi, T. Palladium-catalyzed asymmetric hydrosilylation of styrenes with trichlorosilane. *Tetrahedron: Asymmetry* **2014,** *25*, 479-484.

(17) Corey, J. Y.; Braddock-Wilking, J. Reactions of Hydrosilanes with Transition-Metal Complexes: Formation of Stable Transition-Metal Silyl Compounds. *Chem. Rev.* **1999,** *99*, 175-292.

(18) Corey, J. Y. Reactions of Hydrosilanes with Transition Metal Complexes and Characterization of the Products. *Chem. Rev.* **2011,** *111*, 863-1071.

(19) Corey, J. Y. Reactions of Hydrosilanes with Transition Metal Complexes. *Chem. Rev.* **2016,** *116*, 11291-11435.

(20) Boyle, R. C.; Mague, J. T.; Fink, M. J. The First Stable Mononuclear Silyl Palladium Hydrides. *J. Am. Chem. Soc.* **2003,** *125*, 3228-3229.

(21) Jacobsen, H.; Fink, M. J. Tuning the Palladium−Silicon Bond: Bond Analysis of Bisphosphine Silyl Palladium Hydrides. *Organometallics* **2006,** *25*, 1945-1952.

(22) Nakata, N.; Fukazawa, S.; Kato, N.; Ishii, A. Palladium(II) Hydrido Complexes Having a Primary Silyl or Germyl Ligand: Synthesis, Crystal Structures, and Dynamic Behavior. *Organometallics* **2011,** *30*, 4490-4493.

(23) Barrett, B. J.; Iluc, V. M. Metal-ligand cooperation between palladium and a diphosphine ligand with an olefinic backbone. *Inorg. Chim. Acta* **2017,** *460*, 35-42.

(24) Hurst, M. R.; Zakharov, L. N.; Cook, A. K. The mechanism of oxidative addition of Pd(0) to Si–H bonds: electronic effects, reaction mechanism, and hydrosilylation. *Chem. Sci.* **2021,** *12*, 13045-13060.

(25) Kunai, A.; Sakurai, T.; Toyoda, E.; Ishikawa, M.; Yamamoto, Y. Versatile Method for the Synthesis of Iodosilanes. *Organometallics* **1994,** *13*, 3233-3236.

(26) Boukherroub, R.; Chatgilialoglu, C.; Manuel, G. PdCl2-Catalyzed Reduction of Organic Halides by Triethylsilane. *Organometallics* **1996,** *15*, 1508-1510.

(27) Takaya, J.; Kirai, N.; Iwasawa, N. Efficient Synthesis of Diborylalkenes from Alkenes and Diboron by a New PSiP-Pincer Palladium-Catalyzed Dehydrogenative Borylation. *J. Am. Chem. Soc.* **2011,** *133*, 12980-12983.

(28) Kirai, N.; Takaya, J.; Iwasawa, N. Two Reversible σ-Bond Metathesis Pathways for Boron–Palladium Bond Formation: Selective Synthesis of Isomeric Five-Coordinate Borylpalladium Complexes. *J. Am. Chem. Soc.* **2013,** *135*, 2493-2496.

(29) Kirai, N.; Iguchi, S.; Ito, T.; Takaya, J.; Iwasawa, N. PSiP-Pincer Type Palladium-Catalyzed Dehydrogenative Borylation of Alkenes and 1,3-Dienes. *Bull. Chem. Soc. Jpn.* **2013,** *86*, 784-799.

(30) Takaya, J.; Iwasawa, N. Hydrocarboxylation of Allenes with CO2 Catalyzed by Silyl Pincer-Type Palladium Complex. *J. Am. Chem. Soc.* **2008,** *130*, 15254-15255.

(31) Takaya, J.; Iwasawa, N. Bis(o-phosphinophenyl)silane as a Scaffold for Dynamic Behavior of H−Si and C−Si Bonds with Palladium(0). *Organometallics* **2009,** *28*, 6636-6638.

(32) Takaya, J.; Sasano, K.; Iwasawa, N. Efficient One-to-One Coupling of Easily Available 1,3-Dienes with Carbon Dioxide. *Org. Lett.* **2011,** *13*, 1698-1701.

(33) Suh, H.-W.; Schmeier, T. J.; Hazari, N.; Kemp, R. A.; Takase, M. K. Experimental and Computational Studies of the Reaction of Carbon Dioxide with Pincer-Supported Nickel and Palladium Hydrides. *Organometallics* **2012,** *31*, 8225-8236.

(34) Liu, Z.; Huo, J.; Fu, T.; Tan, H.; Ye, F.; Hossain, M. L.; Wang, J. Palladium(0)-catalyzed C(sp3)–Si bond formation via formal carbene insertion into a Si–H bond. *Chem. Commun.* **2018,** *54*, 11419-11422.

(35) Murata, M.; Suzuki, K.; Watanabe, S.; Masuda, Y. Synthesis of Arylsilanes via Palladium(0)-Catalyzed Silylation of Aryl Halides with Hydrosilane. *J. Org. Chem.* **1997,** *62*, 8569-8571.

(36) Manoso, A. S.; DeShong, P. Improved Synthesis of Aryltriethoxysilanes via Palladium(0)-Catalyzed Silylation of Aryl Iodides and Bromides with Triethoxysilane. *J. Org. Chem.* **2001,** *66*, 7449-7455.

(37) Yamanoi, Y. Palladium-Catalyzed Silylations of Hydrosilanes with Aryl Halides Using Bulky Alkyl Phosphine. *J. Org. Chem.* **2005,** *70*, 9607-9609.

(38) Yamanoi, Y.; Taira, T.; Sato, J.-i.; Nakamula, I.; Nishihara, H. Efficient Preparation of Monohydrosilanes Using Palladium-Catalyzed Si−C Bond Formation. *Org. Lett.* **2007,** *9*, 4543-4546.

(39) Lesbani , A.; Kondo, H.; Yabusaki, Y.; Nakai, M.; Yamanoi, Y.; Nishihara, H. Integrated Palladium-Catalyzed Arylation of Heavier Group 14 Hydrides. *Chem. - Eur. J.* **2010,** *16*, 13519-13527.

(40) Iranpoor, N.; Firouzabadi, H.; Azadi, R. Diphenylphosphinite ionic liquid (IL-OPPh2): A solvent and ligand for palladium-catalyzed silylation and dehalogenation reaction of aryl halides with triethylsilane. *J. Organomet. Chem.* **2010,** *695*, 887-890.

(41) Kurihara, Y.; Yamanoi, Y.; Nishihara, H. Pd-catalyzed synthesis of symmetrical and unsymmetrical siloxanes. *Chem. Commun.* **2013,** *49*, 11275-11277.

(42) Mirza-Aghayan, M.; Boukherroub, R.; Bolourtchian, M.; Hoseini, M.; Tabar-Hydar, K. A novel and efficient method for double bond isomerization. *J. Organomet. Chem.* **2003,** *678*, 1-4.

(43) Mirza-Aghayan, M.; Boukherroub, R.; Bolourtchian, M. A mild and efficient palladium–triethylsilane system for reduction of olefins and carbon–carbon double bond isomerization. *Appl. Organomet. Chem.* **2006,** *20*, 214-219.

(44) Bai, X.-F.; Song, T.; Deng, W.-H.; Wei, Y.-L.; Li, L.; Xia, C.-G.; Xu, L.-W. (EtO)3SiH-Promoted Palladium-Catalyzed Isomerization of Olefins: Convenient Synthesis of Internal Alkenes from Terminal Alkenes. *Synlett* **2014,** *25*, 417-422.

(45) Keinan, E.; Greenspoon, N. Zinc chloride-mediated conjugate reduction with silicon hydrides and palladium(O) catalyst. *Tetrahedron Lett.* **1985,** *26*, 1353-1356.

(46) Keinan, E.; Greenspoon, N. Highly chemoselective palladium-catalyzed conjugate reduction of .alpha.,.beta.-unsaturated carbonyl compounds with silicon hydrides and zinc chloride cocatalyst. *J. Am. Chem. Soc.* **1986,** *108*, 7314-7325.

(47) Mirza-Aghayan, M.; Boukherroub, R.; Rahimifard, M. Efficient method for the reduction of carbonyl compounds by triethylsilane catalyzed by PdCl2. *J. Organomet. Chem.* **2008,** *693*, 3567-3570.

(48) Mirza-Aghayan, M.; Kalantari, M.; Boukherroub, R. Palladium oxide nanoparticles supported on graphene oxide: A convenient heterogeneous catalyst for reduction of various carbonyl compounds using triethylsilane. *Appl. Organomet. Chem.* **2019,** *33*, e4837.

(49) Naka, A.; Okada, T.; Ishikawa, M. Palladium-catalyzed reactions of 1,1,2,2-tetraethyl- and 1,1,2,2-tetra(isopropyl)-3,4-benzo-1,2-disilacyclobut-3-ene with alkynes. *J. Organomet. Chem.* **1996,** *521*, 163-170.

(50) Matsumura, T.; Niwa, T.; Nakada, M. Pd-catalyzed reductive cleavage of alkyl aryl sulfides with triethylsilane that is accelerated by trialkylsilyl chloride. *Tetrahedron Lett.* **2012,** *53*, 4313-4316.

(51) Chouthaiwale, P. V.; Rawat, V.; Sudalai, A. Pd-catalyzed selective hydrosilylation of aryl ketones and aldehydes. *Tetrahedron Lett.* **2012,** *53*, 148-150.

(52) Takaya, J.; Nakamura, S.; Iwasawa, N. Synthesis, Structure, and Catalytic Activity of Palladium Complexes Bearing a Tridentate PXP-Pincer Ligand of Heavier Group 14 Element (X = Ge, Sn). *Chem. Lett.* **2012,** *41*, 967-969.

(53) Takaya, J.; Iwasawa, N. Silyl Ligand Mediated Reversible β-Hydrogen Elimination and Hydrometalation at Palladium. *Chem. - Eur. J.* **2014,** *20*, 11812-11819.

(54) Cartledge, F. K. Steric effects on reactivity in silicon chemistry. *Organometallics* **1983,** *2*, 425-430.

(55) Ploom, A.; Tuulmets, A.; Järv, J. Structure-reactivity relationships in organosilicon chemistry revisited. *Open Chem.* **2011,** *9*, 910-916.

(56) Boutevin, B.; Guida-Pietrasanta, F.; Ratsimihety, A., Side Group Modified Polysiloxanes. In *Silicon-Containing Polymers: The Science and Technology of Their Synthesis and Applications*, Jones, R. G.; Ando, W.; Chojnowski, J., Eds. Springer Netherlands: Dordrecht, 2000; pp 79-112.

(57) Dvornic, P. R., Thermal Properties of Polysiloxanes. In *Silicon-Containing Polymers: The Science and Technology of Their Synthesis and Applications*, Jones, R. G.; Ando, W.; Chojnowski, J., Eds. Springer Netherlands: Dordrecht, 2000; pp 185-212.

(58) Madkour, T. M.; Mohamed, S. K.; Barakat, A. M. Interplay of the polymer stiffness and the permeability behavior of silane and siloxane polymers. *Polymer* **2002,** *43*, 533-539.

(59) Zalewski, K.; Chyłek, Z.; Trzciński, W. A. A Review of Polysiloxanes in Terms of Their Application in Explosives. *Polymers* **2021,** *13*, 1080.

(60) Gentle, T. E.; Snow, S. A. Absorption of Small Silicone Polyether Surfactants at the Air/Water Surface. *Langmuir* **1995,** *11*, 2905-2910.

(61) Hao, C.; Cui, Y.; Yang, P.; Zhang, H.; Mao, D.; Cui, X.; Li, J. Effect of siloxane spacer length on organosilicon bi-quaternary ammonium amphiphiles. *Colloids Surf., B* **2015,** *128*, 528-536.

(62) Tan, J.; He, Z.; Miao, Y.; Zhou, D. Effect of Steric Hindrance on the Aggregation Behavior of Cationic Silicone Surfactants in Aqueous Solutions. *J. Solution Chem.* **2019,** *48*, 891-904.

(63) Tan, J.; Xiong, X.; He, Z.; Cao, F.; Sun, D. Aggregation Behavior of Polyether Based Siloxane Surfactants in Aqueous Solutions: Effect of Alkyl Groups and Steric Hindrance. *J. Phys. Chem. B* **2019,** *123*, 1390-1399.

(64) Tan, J.; He, Z.; Miao, Y.; Lin, M. Synthesis and Surface Properties of Polyether-Based Silicone Surfactants with Different Siloxane Groups. *J. Surfactants Deterg.* **2019,** *22*, 875-883.

(65) Guo, X.; Farwaha, R.; Rempel, G. L. Catalytic hydrosilylation of diene-based polymers. 1. Hydrosilylation of polybutadiene. *Macromolecules* **1990,** *23*, 5047-5054.

(66) McGrath, M. P.; Sall, E. D.; Tremont, S. J. Functionalization of Polymers by Metal-Mediated Processes. *Chem. Rev.* **1995,** *95*, 381-398.

(67) Kowalewska, A.; Stańczyk, W. A.; Boileau, S.; Lestel, L.; Smith, J. D. Novel polymer systems with very bulky organosilicon side chain substituents. *Polymer* **1999,** *40*, 813-818.

(68) Kowalewska, A.; Stańczyk, W. A. Highly Thermally Resistant UV-Curable Poly(siloxane)s Bearing Bulky Substituents. *Chem. Mater.* **2003,** *15*, 2991-2997.

(69) Chauhan, B. P. S.; Balagam, B. Silyl Functionalization of Polyolefins. *Macromolecules* **2006,** *39*, 2010-2012.

(70) Kowalewska, A. Hybrid polymeric systems bearing bulky derivatives of tris(trimethylsilyl)methane. *RSC Adv.* **2014,** *4*, 9622-9631.

(71) Mohanty, A. D.; Bae, C., Chapter One - Transition Metal-Catalyzed Functionalization of Polyolefins Containing CC, CC, and CH Bonds. In *Adv. Organomet. Chem.*, Pérez, P. J., Ed. Academic Press: 2015; Vol. 64, pp 1-39.

(72) Januszewski, R.; Kownacki, I.; Maciejewski, H.; Marciniec, B. Transition metal-catalyzed hydrosilylation of polybutadiene – The effect of substituents at silicon on efficiency of silylfunctionalization process. *J. Catal.* **2019,** *371*, 27-34.

(73) Januszewski, R.; Dutkiewicz, M.; Kownacki, I.; Marciniec, B. The effect of organosilicon modifier structure on the efficiency of the polybutadiene hydrosilylation process. *Catal. Sci. Technol.* **2020,** *10*, 7240-7248.

(74) Chauhan, M.; Hauck, B. J.; Keller, L. P.; Boudjouk, P. Hydrosilylation of alkynes catalyzed by platinum on carbon. *J. Organomet. Chem.* **2002,** *645*, 1-13.

(75) De Bo, G.; Berthon-Gelloz, G.; Tinant, B.; Markó, I. E. Hydrosilylation of Alkynes Mediated by N-Heterocyclic Carbene Platinum(0) Complexes. *Organometallics* **2006,** *25*, 1881-1890.

(76) Berthon-Gelloz, G.; Schumers, J.-M.; De Bo, G.; Markó, I. E. Highly β-(E)-Selective Hydrosilylation of Terminal and Internal Alkynes Catalyzed by a (IPr)Pt(diene) Complex. *J. Org. Chem.* **2008,** *73*, 4190-4197.

(77) Sanchez, J. C.; Urbas, S. A.; Toal, S. J.; DiPasquale, A. G.; Rheingold, A. L.; Trogler, W. C. Catalytic Hydrosilylation Routes to Divinylbenzene Bridged Silole and Silafluorene Polymers. Applications to Surface Imaging of Explosive Particulates. *Macromolecules* **2008,** *41*, 1237-1245.

(78) McLaughlin, M. G.; Cook, M. J. Highly diastereoselective hydrosilylations of allylic alcohols. *Chem. Commun.* **2014,** *50*, 3501-3504.

(79) Dierick, S.; Vercruysse, E.; Berthon-Gelloz, G.; Markó, I. E. User-Friendly Platinum Catalysts for the Highly Stereoselective Hydrosilylation of Alkynes and Alkenes. *Chem. - Eur. J.* **2015,** *21*, 17073-17078.

(80) Perch, N. S.; Kisanga, P.; Widenhoefer, R. A. Reductive Cyclization of Dimethyl Diallylmalonate Catalyzed by Palladium−Bisoxazoline Complexes in the Presence of Silane and Water. *Organometallics* **2000,** *19*, 2541-2545.

(81) Li, K.; Nie, M.; Tang, W. Synthesis of α-tertiary allylsilanes by palladium-catalyzed hydrosilylation of 1,1-disubstituted allenes. *Green Synthesis and Catalysis* **2020,** *1*, 171-174.

(82) Pei, T.; Widenhoefer, R. A. Palladium-Catalyzed Asymmetric Diene Cyclization/Hydrosilylation Employing Functionalized Silanes and Disiloxanes. *J. Org. Chem.* **2001,** *66*, 7639-7645.

(83) Tafazolian, H.; Schmidt, J. A. R. Highly efficient regioselective hydrosilylation of allenes using a [(3IP)Pd(allyl)]OTf catalyst; first example of allene hydrosilylation with phenyl- and diphenylsilane. *Chem. Commun.* **2015,** *51*, 5943-5946.

(84) Hossain, I.; Schmidt, J. A. R. Cationic Nickel(II)-Catalyzed Hydrosilylation of Alkenes: Role of P, N-Type Ligand Scaffold on Selectivity and Reactivity. *Organometallics* **2020,** *39*, 3441-3451.

(85) Ojima, I.; Clos, N.; Donovan, R. J.; Ingallina, P. Hydrosilylation of 1-hexyne catalyzed by rhodium and cobalt-rhodium mixed-metal complexes. Mechanism of apparent trans addition. *Organometallics* **1990,** *9*, 3127-3133.

(86) Török, B.; Felföldi, K.; Molnár, Á.; Bartók, M. Transformation of organic compounds in the presence of metal complexes: VII. Selective reduction of diketones by hydrosilylation in the presence of rhodium(I) complexes. *J. Organomet. Chem.* **1993,** *460*, 111-115.

(87) Takeuchi, R.; Yasue, H. Cationic Rhodium Complex-Catalyzed Highly Selective Dehydrogenative Silylation of Styrene. *Organometallics* **1996,** *15*, 2098-2102.

(88) Corma, A.; Isabel de Dios, M.; Iglesias, M.; Sánchez, F., Regiospecific hydrosilylation of styrene by rhodium complexes heterogenised on modified USY-zeolites. In *Studies in Surface Science and Catalysis*, Blaser, H. U.; Baiker, A.; Prins, R., Eds. Elsevier: 1997; Vol. 108, pp 501-507.

(89) Ojima, I.; Li, Z.; Zhu, J., Recent Advances in the Hydrosilylation and Related Reactions. In *The Chemistry of Organic Silicon Compounds*, 1998; pp 1687-1792.

(90) Solomonsz, W. A.; Rance, G. A.; Suyetin, M.; La Torre, A.; Bichoutskaia, E.; Khlobystov, A. N. Controlling the Regioselectivity of the Hydrosilylation Reaction in Carbon Nanoreactors. *Chem. - Eur. J.* **2012,** *18*, 13180-13187.

(91) Iglesias, M.; Sanz Miguel, P. J.; Polo, V.; Fernández-Alvarez, F. J.; Pérez-Torrente, J. J.; Oro, L. A. An Alternative Mechanistic Paradigm for the β-Z Hydrosilylation of Terminal Alkynes: The Role of Acetone as a Silane Shuttle. *Chem. - Eur. J.* **2013,** *19*, 17559-17566.

(92) Panyam, P. K. R.; Atwi, B.; Ziegler, F.; Frey, W.; Nowakowski, M.; Bauer, M.; Buchmeiser, M. R. Rh(I)/(III)-N-Heterocyclic Carbene Complexes: Effect of Steric Confinement Upon Immobilization on Regio- and Stereoselectivity in the Hydrosilylation of Alkynes. *Chem. - Eur. J.* **2021,** *27*, 17220-17229.

(93) Apple, D. C.; Brady, K. A.; Chance, J. M.; Heard, N. E.; Nile, T. A. Iridium complexes as hydrosilylation catalysts. *J. Mol. Catal.* **1985,** *29*, 55-64.

(94) Jun, C.-H.; Crabtree, R. H. Dehydrogenative silation, isomerization and the control of syn- vs. anti-addition in the hydrosilation of alkynes. *J. Organomet. Chem.* **1993,** *447*, 177-187.

(95) Kawanami, Y.; Sonoda, Y.; Mori, T.; Yamamoto, K. Ruthenium-Catalyzed Hydrosilylation of 1-Alkynes with Novel Regioselectivity. *Org. Lett.* **2002,** *4*, 2825-2827.

(96) Ding, S.; Song, L.-J.; Wang, Y.; Zhang, X.; Chung, L. W.; Wu, Y.-D.; Sun, J. Highly Regio- and Stereoselective Hydrosilylation of Internal Thioalkynes under Mild Conditions. *Angew. Chem., Int. Ed.* **2015,** *54*, 5632-5635.

(97) Xie, X.; Zhang, X.; Gao, W.; Meng, C.; Wang, X.; Ding, S. Iridium-catalyzed Markovnikov hydrosilylation of terminal alkynes achieved by using a trimethylsilyl-protected trihydroxysilane. *Commun. Chem.* **2019,** *2*, 101.

(98) Wang, D.; Lai, Y.; Wang, P.; Leng, X.; Xiao, J.; Deng, L. Markovnikov Hydrosilylation of Alkynes with Tertiary Silanes Catalyzed by Dinuclear Cobalt Carbonyl Complexes with NHC Ligation. *J. Am. Chem. Soc.* **2021,** *143*, 12847-12856.

(99) Zell, T.; Schaub, T.; Radacki, K.; Radius, U. Si-H Activation of hydrosilanes leading to hydrido silyl and bis(silyl) nickel complexes. *Dalton Trans.* **2011,** *40*, 1852-1854.

(100) Schmidt, D.; Zell, T.; Schaub, T.; Radius, U. Si-H bond activation at {(NHC)2Ni0} leading to hydrido silyl and bis(silyl) complexes: a versatile tool for catalytic Si-H/D exchange, acceptorless dehydrogenative coupling of hydrosilanes, and hydrogenation of disilanes to hydrosilanes. *Dalton Trans.* **2014,** *43*, 10816-10827.

(101) Pan, Y.; Mague, J. T.; Fink, M. J. Stable bis(silyl)palladium complexes: synthesis, structure, and bis-silylation of acetylenes. *Organometallics* **1992,** *11*, 3495-3497.

(102) Pan, Y.; Mague, J. T.; Fink, M. J. Synthesis, structure, and unusual reactivity of a d10-d10 palladium(0) dimer. *J. Am. Chem. Soc.* **1993,** *115*, 3842-3843.

(103) Boyle, R. C.; Pool, D.; Jacobsen, H.; Fink, M. J. Dynamic Processes in Silyl Palladium Complexes: Evidence for Intermediate Si−H and Si−Si σ-Complexes. *J. Am. Chem. Soc.* **2006,** *128*, 9054-9055.

(104) Chatt, J.; Eaborn, C.; Kapoor, P. N. Preparation of compounds containing platinum–silicon bonds from silicon hydrides and platinum(0) complexes. *J. Chem. Soc. A* **1970**, 881-884.

(105) Eaborn, C.; Pidcock, A.; Ratcliff, B. The interaction of organosilicon hydrides and dimethyl-bis(phosphine)platinum(II) complexes. *J. Organomet. Chem.* **1974,** *66*, 23-28.

(106) Shimada, S.; Tanaka, M. Group 10 transition-metal complexes with metal–silicon bonds derived from 1,2-disilylbenzenes and bis(2-silylphenyl)silane. *Coord. Chem. Rev.* **2006,** *250*, 991-1011.

(107) Nakata, N.; Kato, N.; Sekizawa, N.; Ishii, A. Si–H Bond Activation of a Primary Silane with a Pt(0) Complex: Synthesis and Structures of Mononuclear (Hydrido)(dihydrosilyl) Platinum(II) Complexes. *Inorganics* **2017,** *5*, 72.

(108) Nakata, N.; Aoyama, M.; Takahashi, S.; Kato, N.; Ishii, A. Synthesis, Structure, and Dynamic Behavior of Hydrido(dihydrosilyl) Platinum(II) Complex Having Me3P Ligands. *Chem. Lett.* **2020,** *49*, 1043-1046.

(109) Duczmal, W.; Maciejewska, B.; Śliwińska, E.; Marciniec, B. Effect of substituents at silicon on the oxidative addition of trisubstituted silanes to [RhCl(cod)PPh3]. *Transition Metal Chemistry* **1995,** *20*, 162-165.

(110) Duczmal, W.; Śliwińska, E.; Maciejewska, B.; Marciniec, B.; Maciejewski, H. Stereoelectronic effects of substituents at silicon on the hydrosilylation of 1-hexene catalysed by [RhCl(cod)(1-hexene)]. *Transition Metal Chemistry* **1995,** *20*, 435-439.

(111) Schubert, U., η2 Coordination of Si–H σ Bonds to Transition Metals. In *Adv. Organomet. Chem.*, Stone, F. G. A.; West, R., Eds. Academic Press: 1990; Vol. 30, pp 151-187.

(112) Nikonov, G. I. New types of non-classical interligand interactions involving silicon based ligands. *J. Organomet. Chem.* **2001,** *635*, 24-36.

(113) Nikonov, G. I., Recent Advances in Nonclassical Interligand Si…H Interactions. In *Adv. Organomet. Chem.*, West, R.; Hill, A. F.; Stone, F. G. A., Eds. Academic Press: 2005; Vol. 53, pp 217-309.

(114) Scherer, W.; Meixner, P.; Batke, K.; Barquera-Lozada, J. E.; Ruhland, K.; Fischer, A.; Eickerling, G.; Eichele, K. J(Si,H) Coupling Constants in Nonclassical Transition-Metal Silane Complexes. *Angew. Chem., Int. Ed.* **2016,** *55*, 11673-11677.

(115) Dubberley, S. R.; Ignatov, S. K.; Rees, N. H.; Razuvaev, A. G.; Mountford, P.; Nikonov, G. I. Are J(Si−H) NMR Coupling Constants Really a Probe for the Existence of Nonclassical H−Si Interactions? *J. Am. Chem. Soc.* **2003,** *125*, 642-643.

(116) Lachaize, S.; Sabo-Etienne, S. σ-Silane Ruthenium Complexes: The Crucial Role of Secondary Interactions. *Eur. J. Inorg. Chem.* **2006,** *2006*, 2115-2127.

(117) Hammett, L. P. Some Relations between Reaction Rates and Equilibrium Constants. *Chem. Rev.* **1935,** *17*, 125-136.

(118) Shorter, J., The Separation of Polar, Steric, and Resonance Effects by the Use of Linear Free Energy Relationships. In *Advances in Linear Free Energy Relationships*, Chapman, N. B.; Shorter, J., Eds. Springer US: Boston, MA, 1972; pp 71-117.

(119) Hansch, C.; Leo, A.; Taft, R. W. A survey of Hammett substituent constants and resonance and field parameters. *Chem. Rev.* **1991,** *91*, 165-195.

(120) Taft, R. W. Linear Free Energy Relationships from Rates of Esterification and Hydrolysis of Aliphatic and Ortho-substituted Benzoate Esters. *J. Am. Chem. Soc.* **1952,** *74*, 2729-2732.

(121) Taft, R. W. Linear Steric Energy Relationships. *J. Am. Chem. Soc.* **1953,** *75*, 4538-4539.

(122) Charton, M. Nature of the ortho effect. II. Composition of the Taft steric parameters. *J. Am. Chem. Soc.* **1969,** *91*, 615-618.

(123) Charton, M. Nature of the ortho effect. V. Ortho-substituent constants. *J. Am. Chem. Soc.* **1969,** *91*, 6649-6654.

(124) Charton, M. Steric effects. 7. Additional V constants. *J. Org. Chem.* **1976,** *41*, 2217-2220.

(125) Ramey, K. C.; Louick, D. J.; Whitehurst, P. W.; Wise, W. B.; Mukherjee, R.; Moriarty, R. M. A line width method for determining chemical exchange rates from NMR spectra. *Org. Magn. Reson.* **1971,** *3*, 201-216.

(126) Gasparro, F. P.; Kolodny, N. H. NMR determination of the rotational barrier in N,N-dimethylacetamide. A physical chemistry experiment. *J. Chem. Educ* **1977,** *54*, 258.

(127) Reid, S. M.; Fink, M. J. Reductive Routes to Dinuclear d10−d10 Palladium(0) Complexes and Their Redistribution Equilibria in Solution. *Organometallics* **2001,** *20*, 2959-2961.

Chapter 5

(1) Ojima, I.; Li, Z.; Zhu, J. Recent Advances in the Hydrosilylation and Related Reactions. In *The Chemistry of Functional Groups*; Rappoport, Z., Apeloig, Y., Eds.; John Wiley & Sons, Ltd: Chichester, UK, 1998; Vol. 2, pp 1687–1792.

(2) Roy, A. K. A Review of Recent Progress in Catalyzed Homogeneous Hydrosilation (Hydrosilylation). In *Advances in Organometallic Chemistry*; Elsevier, 2007; Vol. 55, pp 1–59.

(3) *Hydrosilylation*; Marciniec, B., Ed.; Advances In Silicon Science; Springer Netherlands: Dordrecht, 2009; Vol. 1.

(4) Obligacion, J. V.; Chirik, P. J. Earth-Abundant Transition Metal Catalysts for Alkene Hydrosilylation and Hydroboration. *Nat Rev Chem* **2018**, *2*, 15–34.

(5) Lukin, R. Yu.; Kuchkaev, A. M.; Sukhov, A. V.; Bekmukhamedov, G. E.; Yakhvarov, D. G. Platinum-Catalyzed Hydrosilylation in Polymer Chemistry. *Polymers* **2020**, *12*, 2174.

(6) Troegel, D. Recent Advances and Actual Challenges in Late Transition Metal Catalyzed Hydrosilylation of Olefins from an Industrial Point of View. *Coord. Chem. Rev.* **2011**, 20.

(7) Meister, T. K.; Riener, K.; Gigler, P.; Stohrer, J.; Herrmann, W. A.; Kühn, F. E. Platinum Catalysis Revisited—Unraveling Principles of Catalytic Olefin Hydrosilylation. *ACS Catal.* **2016**, *6*, 1274–1284.

(8) Speier, J. L. Homogeneous Catalysis of Hydrosilation by Transition Metals. In *Advances in Organometallic Chemistry*; Elsevier, 1979; Vol. 17, pp 407–447.

(9) Meals, R. N. Hydrosilation in the Synthesis of Organosilanes. *Pure and Applied Chemistry* **1966**, *13*, 141–158.

(10) Stein, J.; Lewis, L. N.; Gao, Y.; Scott, R. A. In Situ Determination of the Active Catalyst in Hydrosilylation Reactions Using Highly Reactive Pt(0) Catalyst Precursors. *J. Am. Chem. Soc.* **1999**, *121*, 3693–3703.

(11) Markó, I. E.; Stérin, S.; Buisine, O.; Mignani, G.; Branlard, P.; Tinant, B.; Declercq, J.-P. Selective and Efficient Platinum(0)-Carbene Complexes As Hydrosilylation Catalysts. *Science* **2002**, *298*, 204–206.

(12) Chalk, A. J.; Harrod, J. F. Homogeneous Catalysis. II. The Mechanism of the Hydrosilation of Olefins Catalyzed by Group VIII Metal Complexes. *J. Am. Chem. Soc.* **1965**, *87*, 16–21.

(13) Sakaki, S.; Mizoe, N.; Sugimoto, M. Theoretical Study of Platinum(0)-Catalyzed Hydrosilylation of Ethylene. Chalk−Harrod Mechanism or Modified Chalk−Harrod Mechanism. *Organometallics* **1998**, *17*, 2510–2523.

(14) Marciniec, B. Hydrosilylation of Alkynes and Their Derivatives. In *Hydrosilylation*; Marciniec, B., Ed.; Advances In Silicon Science; Springer Netherlands: Dordrecht, 2009; Vol. 1, pp 53–86.

(15) Hiyama, T. Organosilicon Compounds in Cross-Coupling Reactions. In *Metal-Catalyzed Cross-Coupling Reactions*; Diederich, F., Stang, P. J., Eds.; Wiley-VCH Verlag GmbH: Weinheim, Germany, 1998; pp 421–453.

(16) Denmark, S. E.; Sweis, R. F. Organosilicon Compounds in Cross-Coupling Reactions. In *Metal-Catalyzed Cross-Coupling Reactions*; de Meijere, A., Diederich, F., Eds.; Wiley-VCH Verlag GmbH: Weinheim, Germany, 2004; pp 163–216.

(17) Blumenkopf, T. A.; Overman, L. E. Vinylsilane- and Alkynylsilane-Terminated Cyclization Reactions. *Chem. Rev.* **1986**, *86*, 857–873.

(18) Fleming-Tamao Oxidation: (Tamao Oxidation, Tamao-Fleming Oxidation). In *Comprehensive Organic Name Reactions and Reagents*; John Wiley & Sons, Inc.: Hoboken, NJ, USA, 2010; p conrr241.

(19) Munslow, I. J. Alkyne Reductions. In *Modern Reduction Methods*; Andersson, P. G., Munslow, I. J., Eds.; Wiley-VCH Verlag GmbH & Co. KGaA: Weinheim, Germany, 2008; pp 363–385.

(20) Marciniec, B. Hydrosilylation of Carbon—Carbon Multiple Bonds in Organic Synthesis. In *Hydrosilylation*; Marciniec, B., Ed.; Advances In Silicon Science; Springer Netherlands: Dordrecht, 2009; Vol. 1, pp 87–123.

(21) Corey, J. Y.; Braddock-Wilking, J. Reactions of Hydrosilanes with Transition-Metal Complexes: Formation of Stable Transition-Metal Silyl Compounds. *Chem. Rev.* **1999**, *99*, 175–292.

(22) Corey, J. Y. Reactions of Hydrosilanes with Transition Metal Complexes and Characterization of the Products. *Chem. Rev.* **2011**, *111*, 863–1071.

(23) Corey, J. Y. Reactions of Hydrosilanes with Transition Metal Complexes. *Chem. Rev.* **2016**, *116*, 11291–11435.

(24) Hurst, M. R.; Zakharov, L. N.; Cook, A. K. The Mechanism of Oxidative Addition of Pd(0) to Si–H Bonds: Electronic Effects, Reaction Mechanism, and Hydrosilylation. *Chem. Sci.* **2021**, *12*, 13045–13060.

(25) Hurst, M. R.; Davis, A. G.; Cook, A. K. The Influence of Silane Steric Bulk on the Formation and Dynamic Behavior of Silyl Palladium Hydrides. *Organometallics* **2022** *(accepted)*.

(26) Hansch, Corwin.; Leo, A.; Taft, R. W. A Survey of Hammett Substituent Constants and Resonance and Field Parameters. *Chem. Rev.* **1991**, *91*, 165–195.

(27) Taft, R. W. Linear Steric Energy Relationships. *J. Am. Chem. Soc.* **1953**, *75*, 4538–4539.

(28) Charton, M. The Upsilon Steric Parameter — Definition and Determination. In *Steric Effects in Drug Design*; Topics in Current Chemistry; Springer Berlin Heidelberg: Berlin, Heidelberg, 1983; Vol. 114, pp 57–91.

(29) Motoda, D.; Shinokubo, H.; Oshima, K. Efficient Pd(0)-Catalyzed Hydrosilylation of Alkynes with Triorganosilanes. *Synlett* **2002**, *2002*, 1529–1531.

(30) Sumida, Y.; Kato, T.; Yoshida, S.; Hosoya, T. Palladium-Catalyzed Regio- and Stereoselective Hydrosilylation of Electron-Deficient Alkynes. *Org. Lett.* **2012**, *14*, 1552–1555.

(31) Jun, C.-H.; Crabtree, R. H. Dehydrogenative Silation, Isomerization and the Control of Syn- vs. Anti-Addition in the Hydrosilation of Alkynes. *Journal of Organometallic Chemistry* **1993**, *447*, 177–187.

(32) Ojima, I.; Clos, N.; Donovan, R. J.; Ingallina, P. Hydrosilylation of 1-Hexyne Catalyzed by Rhodium and Cobalt-Rhodium Mixed-Metal Complexes. Mechanism of Apparent Trans Addition. *Organometallics* **1990**, *9*, 3127–3133.

(33) Pan, Y.; Mague, J. T.; Fink, M. J. Stable Bis(Silyl)Palladium Complexes: Synthesis, Structure, and Bis-Silylation of Acetylenes. *Organometallics* **1992**, *11*, 3495–3497.

(34) Pan, Y.; Mague, J. T.; Fink, M. J. Synthesis, Structure, and Unusual Reactivity of a D10-D10 Palladium(0) Dimer. *J. Am. Chem. Soc.* **1993**, *115*, 3842–3843.

(35) Reid, S. M.; Fink, M. J. Reductive Routes to Dinuclear d^{10}–d^{10} Palladium(0) Complexes and Their Redistribution Equilibria in Solution. *Organometallics* **2001**, *20*, 2959–2961.

(36) Boyle, R. C.; Mague, J. T.; Fink, M. J. The First Stable Mononuclear Silyl Palladium Hydrides. *J. Am. Chem. Soc.* **2003**, *125*, 3228–3229.

(37) Gómez-Gallego, M.; Sierra, M. A. Kinetic Isotope Effects in the Study of Organometallic Reaction Mechanisms. *Chem. Rev.* **2011**, *111*, 4857–4963.

(38) Wolfsberg, M. Theoretical Evaluation of Experimentally Observed Isotope Effects. *Acc. Chem. Res.* **1972**, *5*, 225–233.

(39) Parkin, G. Temperature-Dependent Transitions Between Normal and Inverse Isotope Effects Pertaining to the Interaction of H−H and C−H Bonds with Transition Metal Centers. *Acc. Chem. Res.* **2009**, *42* (2), 315–325.

Chapter 6

(1) Sauer, R. O.; Patnode, W. Derivatives of the Methylchlorosilanes. II. 2-Chloroethoxysilanes. *J. Am. Chem. Soc.* **1945**, *67*, 1548–1549.

(2) Olah, G. A.; Narang, S. C. Iodotrimethylsilane—a Versatile Synthetic Reagent. *Tetrahedron* **1982**, *38* , 2225–2277..

(3) Larson, G. L. Recent Synthetic Applications of Organosilanes. In *The Chemistry of Functional Groups*; Patai, S., Rappoport, Z., Eds.; John Wiley & Sons, Ltd: Chichester, UK, 1989; pp 763–808.

(4) Nilsson, M. Product Subclass 12: Haloogranosilanes. In *Category 1, Organometallics: Compounds of Groups 15 (As, Sb, Bi) and Silicon Compounds*; Fleming, Ley, Eds.; Georg Thieme Verlag: Stuttgart, 2002; pp 247–268.

(5) Prasad, H. Organosilicon Reagents in Natural Product Synthesis. *Reson* **2002**, *7* , 48–64.

(6) Crouch, R. D. Recent Advances in Silyl Protection of Alcohols. *Synthetic Communications* **2013**, *43*, 2265–2279.

(7) Ajvazi, N.; Stavber, S. Direct Halogenation of Alcohols with Halosilanes under Catalyst- and Organic Solvent-Free Reaction Conditions. *Tetrahedron Lett.* **2016**, *57*, 2430–2433.

(8) Kalchauer, W.; Pachaly, B. Müller−Rochow Synthesis: The Direct Process to Methylchlorosilanes. In *Handbook of Heterogeneous Catalysis*; Wiley-VCH Verlag GmbH & Co. KGaA: Weinheim, Germany, 200.

(9) Seyferth, D. Dimethyldichlorosilane and the Direct Synthesis of Methylchlorosilanes. The Key to the Silicones Industry. *Organometallics* **2001**, *20*, 4978–4992.

(10) Schmidt, A. H. Bromotrimethylsilane and Iodotrimethylsilane - Versatile Reagents for Organic Synthesis. In *Aldrichimica Acta*; 1981; Vol. 14, pp 31–38.

(11) Walsh, R. Thermochemistry. In *The Chemistry of Functional Groups*; Patai, S., Rappoport, Z., Eds.; John Wiley & Sons, Ltd: Chichester, UK, 1989; pp 371–391.

(12) *Silicon-Based Polymer Science: A Comprehensive Resource*; Zeigler, J. M., Fearon, F. W. G., Eds.; Advances in Chemistry; American Chemical Society: Washington, DC, 1989; Vol. 224.

(13) Korch, K. M.; Watson, D. A. Cross-Coupling of Heteroatomic Electrophiles. *Chem. Rev.* **2019**, *119*, 8192–8228.

(14) Chatani, N.; Amishiro, N.; Murai, S. A New Catalytic Reaction Involving Oxidative Addition of Iodotrimethylsilane (Me3SiI) to Palladium(0). Synthesis of Stereodefined Enynes by the Coupling of Me3SiI, Acetylenes, and Acetylenic Tin Reagents. *J. Am. Chem. Soc.* **1991**, *113*, 7778–7780.

(15) Yamashita, H.; Kobayashi, T.; Hayashi, T.; Tanaka, M. Heck-Type Reaction of Lodotrimethylsilane with Olefins Affording Alkenyltrimethylsilanes. *Chem. Lett.* **1991**, *20*, 761–762.

(16) Chatani, N.; Amishiro, N.; Morii, T.; Yamashita, T.; Murai, S. Pd-Catalyzed Coupling Reaction of Acetylenes, Iodotrimethylsilane, and Organozinc Reagents for the Stereoselective Synthesis of Vinylsilanes. *J. Org. Chem.* **1995**, *60*, 1834–1840.

(17) McAtee, J. R.; Martin, S. E. S.; Cinderella, A. P.; Reid, W. B.; Johnson, K. A.; Watson, D. A. The First Example of Nickel-Catalyzed Silyl-Heck Reactions: Direct Activation of Silyl Triflates without Iodide Additives. *Tetrahedron* **2014**, *70*, 4250–4256.

(18) McAtee, J. R.; Yap, G. P. A.; Watson, D. A. Rational Design of a Second Generation Catalyst for Preparation of Allylsilanes Using the Silyl-Heck Reaction. *J. Am. Chem. Soc.* **2014**, *136*, 10166–10172.

(19) McAtee, J. R.; Krause, S. B.; Watson, D. A. Simplified Preparation of Trialkylvinylsilanes *via* the Silyl-Heck Reaction Utilizing a Second Generation Catalyst. *Adv. Synth. Catal.* **2015**, *357*, 2317–2321.

(20) Cinderella, A. P.; Vulovic, B.; Watson, D. A. Palladium-Catalyzed Cross-Coupling of Silyl Electrophiles with Alkylzinc Halides: A Silyl-Negishi Reaction. *J. Am. Chem. Soc.* **2017**, *139*, 7741–7744.

(21) Krause, S. B.; McAtee, J. R.; Yap, G. P. A.; Watson, D. A. A Bench-Stable, Single-Component Precatalyst for Silyl–Heck Reactions. *Org. Lett.* **2017**, *19*, 5641–5644.

(22) Yamashita, H.; Kawamoto, A. M.; Tanaka, M.; Goto, M. Oxidative Addition of Halo(Methyl)Silanes to an In Situ Generated Ir(I) Complex and β-Hydride Elimination Reaction of the Resulting (Methylsilyl)Iridium Complexes. *Chem. Lett.* **1990**, *19*, 2107–2110.

(23) McAtee, J. R.; Martin, S. E. S.; Ahneman, D. T.; Johnson, K. A.; Watson, D. A. Preparation of Allyl and Vinyl Silanes by the Palladium-Catalyzed Silylation of Terminal Olefins: A Silyl-Heck Reaction. *Angew. Chem. Int. Ed.* **2012**, *51*, 3663–3667.

(24) Martin, S. E. S.; Watson, D. A. Preparation of Vinyl Silyl Ethers and Disiloxanes via the Silyl-Heck Reaction of Silyl Ditriflates. *J. Am. Chem. Soc.* **2013**, *135*, 13330–13333.

(25) Corey, J. Y.; Braddock-Wilking, J. Reactions of Hydrosilanes with Transition-Metal Complexes: Formation of Stable Transition-Metal Silyl Compounds. *Chem. Rev.* **1999**, *99*, 175–292.

(26) Corey, J. Y. Reactions of Hydrosilanes with Transition Metal Complexes and Characterization of the Products. *Chem. Rev.* **2011**, *111*, 863–1071.

(27) Corey, J. Y. Reactions of Hydrosilanes with Transition Metal Complexes. *Chem. Rev.* **2016**, *116*, 11291–11435.

(28) Clemmit, A. F.; Glockling, F. Trimethyl-Silyl, -Germyl and -Stannyl Complexes of Platinum. *J. Chem. Soc., A* **1971**, 1164.

(29) Bentham, J. E.; Cradock, S.; Ebsworth, E. A. V. Silyl and Germyl Compounds of Platinum and Palladium. Part I. Platinum Derivatives of Monosilane and Monogermane. *J. Chem. Soc., A* **1971**, 587.

(30) Clark, H. C.; Hampden-Smith, M. J. Ligand Interactioins in Crowded Molecules. *Coord. Chem. Rev.* **1987**, *79*, 229–255.

(31) Yamashita, Hiroshi.; Hayashi, Teruyuki.; Kobayashi, Toshiaki.; Tanaka, Masato.; Goto, Midori. Oxidative Addition of Halosilanes to Zero-Valent Platinum Complexes. *J. Am. Chem. Soc.* **1988**, *110*, 4417–4418.

(32) Yamashita, H.; Kobayashi, T.; Hayashi, T.; Tanaka, M. Dichotomous Reactivity of Halodisilanes in Oxidative Addition with $Pt(PEt_3)_3$. Formation of Bis(Silyl)- or (Disilanyl)Platinum Complexes. *Chem. Lett.* **1990**, *19*, 1447–1450.

(33) Levy, C. J.; Puddephatt, R. J.; Vittal, J. J. The Halogen Effect in Oxidative Addition of Trimethylsilyl and Trimethyltin Halides to Platinum(II): Synthesis and Characterization of Silylplatinum(IV) Complexes. *Organometallics* **1994**, *13*, 1559–1560.

(34) Levy, C. J.; Vittal, J. J.; Puddephatt, R. J. Synthesis and Characterization of Group 14−Platinum(IV) Complexes. *Organometallics* **1996**, *15*, 2108–2117.

(35) Yamashita, H.; Tanaka, M.; Goto, M. Oxidative Addition of Silicon−Halogen Bonds to Platinum(0) Complexes and Reactivities of the Resulting Silylplatinum Species. *Organometallics* **1997**, *16*, 4696–4704.

(36) Mitton, S. J.; Turculet, L. Mild Reduction of Carbon Dioxide to Methane with Tertiary Silanes Catalyzed by Platinum and Palladium Silyl Pincer Complexes. *Chem. Eur. J.* **2012**, *18*, 15258–15262.

(37) Uson, R.; Oro, L. A.; Fernandez, M. J. Preparation, Reactions and Catalytic Activity of Complexes of the Type [Ir(COD){P(p-RC6H4)3}2]A (R □ Cl, F, H, CH3 OR CH3O; A □ ClO4− OR B(C6H5)4−). *J. Organomet. Chem.* **1980**, *193*, 127–133.

(38) Usón, R.; Oro, L. A.; Ciriano, M. A.; Gonzalez, R. 8-Oxyquinolate Iridium(I) Complexes and Their Oxidative-Addition Reactions. *Journal of Organometallic Chemistry* **1981**, *205*, 259–271.

(39) Yamashita, H.; Kobayashi, T.; Hayashi, T.; Tanaka, M. Novel Halogen Exchange Reactions between Halosilanes and Rh(I) or Ir(I) Complexes. *Chem. Lett.* **1989**, *18*, 471–474.

(40) Zlota, A. A.; Frolow, F.; Milstein, D. Oxidative Addition of Si–Cl Bonds to Electron-Rich Ir ^{I} Complexes. *J. Chem. Soc., Chem. Commun.* **1989**, 1826–1827.

(41) Kameo, H.; Ikeda, K.; Sakaki, S.; Takemoto, S.; Nakazawa, H.; Matsuzaka, H. Experimental and Theoretical Studies of Si–Cl and Ge–Cl σ-Bond Activation Reactions by Iridium-Hydride. *Dalton Trans.* **2016**, *45*, 7570–7580.

(42) Gatard, S.; Chen, C.-H.; Foxman, B. M.; Ozerov, O. V. Oxidative Addition Reactions of Silyl Halides with the (PNP)Rh Fragment. *Organometallics* **2008**, *27*, 6257–6263.

(43) Kim, Yongseong; Woo, Han Young; Hwang, Sungu. Density Functional Theoretical Study on the Oxidative Additions of Silyl Halides to the Rh Pincer Complex. *Bulletin of the Korean Chemical Society* **2011**, *32*, 2479–2481.

(44) Lukevics, E.; Arsenyan, P.; Pudova, O. MOLECULAR STRUCTURE OF ORGANOSILICON COMPOUNDS WITH Si - Ru, Si - Rh and Si - Pd BONDS. *Main Group Met. Chem.* **2002**, *25* .

(45) Lukevics, E.; Arsenyan, P.; Pudova, O. MOLECULAR STRUCTURE OF ORGANOSILICON COMPOUNDS WITH Si - Os, Si - Ir, and Si - Pt BONDS. *Main Group Met. Chem.* **2002**, *25*.

(46) Lukevics, E.; Pudova, O. MOLECULAR STRUCTURE OF ORGANOSILICON COMPOUNDS WITH Si-Fe, Si-Co AND Si-Ni BONDS. *Main Group Met. Chem.* **2000**, *23*.

(47) Ozawa, F.; Sugawara, M.; Hasebe, K.; Hayashi, T. Reactions of Bis(Silyl)Palladium(II) Complexes with Allyl Halides. Synthesis of Mono(Silyl)Palladium(II) Halides and X-Ray Structure of Trans-PdCl(SiF2Ph)(PMe2Ph)2. *Inorganica Chimica Acta* **1999**, *296*, 19–25.

(48) Esposito, O.; Roberts, D. E.; Cloke, F. G. N.; Caddick, S.; Green, J. C.; Hazari, N.; Hitchcock, P. B. Carbon–Silicon Bond Activation by [Pd(I *t* Bu) $_2$] – the Molecular Structures of [Pd(Me $_3$ Si)(I *t* Bu)(M-I)] $_2$ and [Pd(CH $_2$ I *t* Bu)I $_2$]. *Eur. J. Inorg. Chem.* **2009**, *2009*, 1844–1850.

(49) Hurst, M. R.; Zakharov, L. N.; Cook, A. K. The Mechanism of Oxidative Addition of Pd(0) to Si–H Bonds: Electronic Effects, Reaction Mechanism, and Hydrosilylation. *Chem. Sci.* **2021**, *12*, 13045–13060.

(50) Boyle, R. C.; Mague, J. T.; Fink, M. J. The First Stable Mononuclear Silyl Palladium Hydrides. *J. Am. Chem. Soc.* **2003**, *125*, 3228–3229.

(51) Boyle, R. C.; Pool, D.; Jacobsen, H.; Fink, M. J. Dynamic Processes in Silyl Palladium Complexes: Evidence for Intermediate Si−H and Si−Si σ-Complexes. *J. Am. Chem. Soc.* **2006**, *128*, 9054–9055.

(52) Yang, L.; Powell, D. R.; Houser, R. P. Structural Variation in Copper(I) Complexes with Pyridylmethylamide Ligands: Structural Analysis with a New Four-Coordinate Geometry Index, τ $_4$. *Dalton Trans.* **2007**, No. 9, 955–964.

(53) Okuniewski, A.; Rosiak, D.; Chojnacki, J.; Becker, B. Coordination Polymers and Molecular Structures among Complexes of Mercury(II) Halides with Selected 1-Benzoylthioureas. *Polyhedron* **2015**, *90*, 47–57.

(54) Kirss, R. U. Trimethylsilyl Halide Adducts of Dinuclear Phosphine-Bridged Palladium Halide Complexes: Synthesis, Spectroscopy, and Reactions of Pd2X2(Dppm)2.Cntdot.Me3SiX' (X, X' = Cl, Br, I). *Inorg. Chem.* **1992**, *31*, 3451–3458.

(55) Pamplin, C. B.; Rettig, S. J.; Patrick, B. O.; James, B. R. Solution Behavior and Structural Diversity of Bis(Dialkylphosphino)Methane Complexes of Palladium. *Inorg. Chem.* **2003**, *42*, 4117–4126.

(56) Reid, S. M.; Mague, J. T.; Fink, M. J. Facile Reductive Elimination of Ethane from Strained Dimethylpalladium(II) Complexes. *J. Am. Chem. Soc.* **2001**, *123*, 4081–4082.

(57) Shimada, S.; Tanaka, M.; Shiro, M. The First Silylpalladium(IV) Complex. *Angew. Chem. Int. Ed. Engl.* **1996**, *35*, 1856–1858.

(58) Pfeiffer, J.; Kickelbick, G.; Schubert, U. Transition Metal Silyl Complexes. 62. [1] Platinum Dimethyl Complexes with Hemilabile P,N-Chelating Ligands: Synthesis, Structure, and Reactions with Iodotrimethylsilane and 1,2-Bis(Dimethylsilyl)Benzene. *Organometallics* **2000**, *19*, 62–71.

(59) Stöhr, F.; Sturmayr, D.; Kickelbick, G.; Schubert, U. C−Cl and Si−Cl Activation ByP,N-Chelated PtII Complexes. *Eur. J. Inorg. Chem.* **2002**, 2305–2311.

(60) Schubert, U.; Pfeiffer, J.; Stöhr, F.; Sturmayr, D.; Thompson, S. Transformations of Organosilanes by Pt(II) Complexes with Hemilabile P,N-Chelating Ligands. *Journal of Organometallic Chemistry* **2002**, *646*, 53–58.

(61) Pan, Y.; Mague, J. T.; Fink, M. J. Synthesis, Structure, and Unusual Reactivity of a D10-D10 Palladium(0) Dimer. *J. Am. Chem. Soc.* **1993**, *115*, 3842–3843.

(62) Waterman, R. σ-Bond Metathesis: A 30-Year Retrospective. *Organometallics* **2013**, *32*, 7249–7263.

(63) Suginome, M.; Oike, H.; Ito, Y. Macrocycles with Regularly Arranged Si-Si Bonds: Ring-Enlargement Oligomerization of Cyclic Disilanes via Palladium-Catalyzed Si-Si .Sigma.-Bond Metathesis. *J. Am. Chem. Soc.* **1995**, *117*, 1665–1666.

(64) Siegbahn, P. E. M.; Crabtree, R. H. Modeling the Solvent Sphere: Mechanism of the Shilov Reaction. *J. Am. Chem. Soc.* **1996**, *118*, 4442–4450.

(65) Milet, A.; Dedieu, A.; Kapteijn, G.; van Koten, G. σ-Bond Metathesis Reactions Involving Palladium(II) Hydride and Methyl Complexes: A Theoretical Assessment. *Inorg. Chem.* **1997**, *36*, 3223–3231.

(66) Perutz, R. N.; Sabo-Etienne, S. The σ-CAM Mechanism: σ Complexes as the Basis of σ-Bond Metathesis at Late-Transition-Metal Centers. *Angew. Chem. Int. Ed.* **2007**, *46*, 2578–2592.

(67) Igarashi, M.; Kubo, K.; Matsumoto, T.; Sato, K.; Ando, W.; Shimada, S. Pd/C-Catalyzed Cross-Coupling Reaction of Benzyloxysilanes with Halosilanes for Selective Synthesis of Unsymmetrical Siloxanes. *RSC Adv.* **2014**, *4*, 19099.

(68) Vulovic, B.; Cinderella, A. P.; Watson, D. A. Palladium-Catalyzed Cross-Coupling of Monochlorosilanes and Grignard Reagents. *ACS Catal.* **2017**, *7*, 8113–8117.

(69) Curtis, M. D.; Epstein, P. S. Redistribution Reactions on Silicon Catalyzed by Transition Metal Complexes. In *Advances in Organometallic Chemistry*; Elsevier, 1981; Vol. 19, pp 213–255.

(70) Tsuji, J.; Hara, M.; Ohno, K. Organic Synthesis by Means of Noble Metal Complexes—XCIV. *Tetrahedron* **1974**, *30*, 2143–2146.

(71) Hartwig, J. F. Chapter 6: Oxidative Addition of Nonpolar Reagents. In *Organotransition metal chemistry: from bonding to catalysis*; University Science Books, 2010; pp 263–300.

(72) Hartwig, J. F. Chapter 7: Oxidative Addition of Polar Reagents. In *Organotransition metal chemistry: from bonding to catalysis*; University Science Books, 2010; pp 301–320.

(73) Oxidative Addition and Reductive Elimination. In *The Organometallic Chemistry of the Transition Metals*; Crabtree, R. H., Ed.; John Wiley & Sons, Inc.: Hoboken, NJ, USA, 2014; pp 163–184.

(74) Labinger, J. A. Tutorial on Oxidative Addition. *Organometallics* **2015**, *34*, 4784–4795.

(75) Barrios-Landeros, F.; Hartwig, J. F. Distinct Mechanisms for the Oxidative Addition of Chloro-, Bromo-, and Iodoarenes to a Bisphosphine Palladium(0) Complex with Hindered Ligands. *J. Am. Chem. Soc.* **2005**, *127*, 6944–6945.

(76) Barrios-Landeros, F.; Carrow, B. P.; Hartwig, J. F. Effect of Ligand Steric Properties and Halide Identity on the Mechanism for Oxidative Addition of Haloarenes to Trialkylphosphine Pd(0) Complexes. *J. Am. Chem. Soc.* **2009**, *131*, 8141–8154.

(77) Ahlquist, M.; Fristrup, P.; Tanner, D.; Norrby, P.-O. Theoretical Evidence for Low-Ligated Palladium(0): [Pd−L] as the Active Species in Oxidative Addition Reactions. *Organometallics* **2006**, *25*, 2066–2073.

(78) Hartwig, J. F. Chapter 5: Ligand Substitution Reactions. In *Organotransition metal chemistry: from bonding to catalysis*; University Science Books, 2010; pp 217–260.

(79) Kapuśniak, Ł.; Plessow, P. N.; Trzybiński, D.; Woźniak, K.; Hofmann, P.; Jolly, P. I. A Mild One-Pot Reduction of Phosphine(V) Oxides Affording Phosphines(III) and Their Metal Catalysts. *Organometallics* **2021**, *40*, 693–701.

(80) Rajendran, K. V.; Gilheany, D. G. Simple Unprecedented Conversion of Phosphine Oxides and Sulfides to Phosphine Boranes Using Sodium Borohydride. *Chem. Commun.* **2012**, *48*, 817–819.

(81) Padia, J. K.; Barnard, C. F. J.; Colacot, T. J. Dichloro[1,2-Bis(Diphenylphosphino)Ethane]Palladium(II). In *Encyclopedia of Reagents for Organic Synthesis*; John Wiley & Sons, Ltd, Ed.; John Wiley & Sons, Ltd: Chichester, UK, 2009

(82) Casado, A. L.; Espinet, P. On the Configuration Resulting from Oxidative Addition of RX to Pd(PPh $_3$) $_4$ and the Mechanism of the *Cis* -to- *Trans* Isomerization of [PdRX(PPh $_3$) $_2$] Complexes (R = Aryl, X = Halide). *Organometallics* **1998**, *17*, 954–959.

Chapter 7

(1) Ma, Z.; Zaera, F. Heterogeneous Catalysis by Metals. In *Encyclopedia of Inorganic Chemistry*; King, R. B., Crabtree, R. H., Lukehart, C. M., Atwood, D. A., Scott, R. A., Eds.; John Wiley & Sons, Ltd: Chichester, UK, 2006

(2) Heterogeneously Catalyzed Processes in Industry. In *Industrial Catalysis*; Wiley-VCH Verlag GmbH & Co. KGaA: Weinheim, Germany, 2015; pp 261–298
.

(3) Dumesic, J. A.; Huber, G. W.; Boudart, M. Principles of Heterogeneous Catalysis. In *Handbook of Heterogeneous Catalysis*; Ertl, G., Knzinger, H., Schth, F., Weitkamp, J., Eds.; Wiley-VCH Verlag GmbH & Co. KGaA: Weinheim, Germany, 2008

(4) Hu, X.; Yip, A. C. K. Heterogeneous Catalysis: Enabling a Sustainable Future. *Front. Catal.* **2021**, *1*, 667675.

(5) Pan, Y.; Shen, X.; Yao, L.; Bentalib, A.; Peng, Z. Active Sites in Heterogeneous Catalytic Reaction on Metal and Metal Oxide: Theory and Practice. *Catalysts* **2018**, *8*, 478.

(6) Copéret, C.; Comas-Vives, A.; Conley, M. P.; Estes, D. P.; Fedorov, A.; Mougel, V.; Nagae, H.; Núñez-Zarur, F.; Zhizhko, P. A. Surface Organometallic and Coordination Chemistry toward Single-Site Heterogeneous Catalysts: Strategies, Methods, Structures, and Activities. *Chem. Rev.* **2016**, *116*, 323–421.

(7) Copéret, C.; Fedorov, A.; Zhizhko, P. A. Surface Organometallic Chemistry: Paving the Way Beyond Well-Defined Supported Organometallics and Single-Site Catalysis. *Catal Lett* **2017**, *147*, 2247–2259.

(8) Samantaray, M. K.; Mishra, S. K.; Saidi, A.; Basset, J.-M. Surface Organometallic Chemistry: A Sustainable Approach in Modern Catalysis. *Journal of Organometallic Chemistry* **2021**, *945*, 121864.

(9) Kepp, K. P. A Quantitative Scale of Oxophilicity and Thiophilicity. *Inorg. Chem.* **2016**, *55*, 9461–9470.

(10) Kayode, G. O.; Montemore, M. M. *Factors Controlling Oxophilicity and Carbophilicity of Transition Metals and Main Group Metals*; preprint; Chemistry, 2021.

(11) Mori, K.; Hara, T.; Mizugaki, T.; Ebitani, K.; Kaneda, K. Hydroxyapatite-Supported Palladium Nanoclusters: A Highly Active Heterogeneous Catalyst for Selective Oxidation of Alcohols by Use of Molecular Oxygen. *J. Am. Chem. Soc.* **2004**, *126*, 10657–10666.

(12) Phan, N. T. S.; Van Der Sluys, M.; Jones, C. W. On the Nature of the Active Species in Palladium Catalyzed Mizoroki–Heck and Suzuki–Miyaura Couplings – Homogeneous or Heterogeneous Catalysis, A Critical Review. *Adv. Synth. Catal.* **2006**, *348*, 609–679.

(13) Hackett, S. F. J.; Brydson, R. M.; Gass, M. H.; Harvey, I.; Newman, A. D.; Wilson, K.; Lee, A. F. High-Activity, Single-Site Mesoporous Pd/Al $_2$ O $_3$ Catalysts for Selective Aerobic Oxidation of Allylic Alcohols. *Angew. Chem. Int. Ed.* **2007**, *46*, 8593–8596.

(14) Choi, Y. S.; Moschetta, E. G.; Miller, J. T.; Fasulo, M.; McMurdo, M. J.; Rioux, R. M.; Tilley, T. D. Highly Dispersed Pd-SBA15 Materials from Tris(*Tert* -Butoxy)Siloxy Complexes of Pd(II). *ACS Catal.* **2011**, *1*, 1166–1177.

(15) Hurst, M. R.; Zakharov, L. N.; Cook, A. K. The Mechanism of Oxidative Addition of Pd(0) to Si–H Bonds: Electronic Effects, Reaction Mechanism, and Hydrosilylation. *Chem. Sci.* **2021**, *12*, 13045–13060.

(16) Hurst, M. R.; Davis, A. G.; Cook, A. K. The Influence of Silane Steric Bulk on the Formation and Dynamic Behavior of Silyl Palladium Hydrides. *Organometallics* **2022** *(accepted)*.

(17) Maier, S.; Cronin, S. P.; Vu Dinh, M.-A.; Li, Z.; Dyballa, M.; Nowakowski, M.; Bauer, M.; Estes, D. P. Immobilized Platinum Hydride Species as Catalysts for Olefin Isomerizations and Enyne Cycloisomerizations. *Organometallics* **2021**, *40*, 1751–1757.

(18) Kaplan, A. W.; Bergman, R. G. Nitrous Oxide Mediated Synthesis of Monomeric Hydroxoruthenium Complexes. Reactivity of (DMPE) $_2$ Ru(H)(OH) and the Synthesis of a Silica-Bound Ruthenium Complex. *Organometallics* **1998**, *17*, 5072–5085.

(19) Rascón, F.; Berthoud, R.; Wischert, R.; Lukens, W.; Coperet, C. Access to Well-Defined Ruthenium Mononuclear Species Grafted via a Si−Ru Bond on Silane Functionalized Silica. *J. Phys. Chem. C* **2011**, *115*, 1150–1155.

(20) Copéret, C.; Estes, D. P.; Larmier, K.; Searles, K. Isolated Surface Hydrides: Formation, Structure, and Reactivity. *Chem. Rev.* **2016**, *116*, 8463–8505.

(21) Sandoval, J. E.; Pesek, J. J. Hydrolytically Stable Bonded Chromatographic Phases Prepared through Hydrosilylation of Olefins on a Hydride-Modified Silica Intermediate. *Anal. Chem.* **1991**, *63*, 2634–2641.

(22) Pesek, J. J.; Matyska, M. T. Our Favorite Materials: Silica Hydride Stationary Phases: Liquid Chromatography. *J. Sep. Science* **2009**, *32*, 3999–4011.

(23) Gomez, J. E.; Sandoval, J. E. New Approaches to Prepare Hydride Silica. *Anal. Chem.* **2010**, *82*, 7444–7451.

(24) Matyska, M.; Pesek, J. The Development of Silica Hydride Stationary Phases for High-Performance Liquid Chromatography from Conception to Commercialization. *Separations* **2019**, *6*, 27.

(25) Sandoval, J. E.; Pesek, J. J. Synthesis and Characterization of a Hydride-Modified Porous Silica Material as an Intermediate in the Preparation of Chemically Bonded Chromatographic Stationary Phases. *Anal. Chem.* **1989**, *61*, 2067–2075.

(26) Chapter 9 Modification with Silicon Compounds: Mechanistic Studies. In *Studies in Surface Science and Catalysis*; Elsevier, 1995; Vol. 93, pp 193–297.

(27) Plumeré, N.; Speiser, B.; Mayer, H. A.; Joosten, D.; Wesemann, L. High-Temperature Chlorination-Reduction Sequence for the Preparation of Silicon Hydride Modified Silica Surfaces. *Chem. Eur. J.* **2009**, *15*, 936–946.

(28) Chu, C. Hau.; Jonsson, Elisabet.; Auvinen, Mirva.; Pesek, J. J.; Sandoval, J. E. A New Approach for the Preparation of a Hydride-Modified Substrate Used as an Intermediate in the Synthesis of Surface-Bonded Materials. *Anal. Chem.* **1993**, *65*, 808–816.

(29) Shard, A. G. Practical Guides for X-Ray Photoelectron Spectroscopy: Quantitative XPS. *Journal of Vacuum Science & Technology A* **2020**, *38*, 041201.

(30) Greczynski, G.; Hultman, L. X-Ray Photoelectron Spectroscopy: Towards Reliable Binding Energy Referencing. *Progress in Materials Science* **2020**, *107*, 100591.

(31) Pan, Y.; Mague, J. T.; Fink, M. J. Synthesis, Structure, and Unusual Reactivity of a D10-D10 Palladium(0) Dimer. *J. Am. Chem. Soc.* **1993**, *115*, 3842–3843.

(32) Reid, S. M.; Fink, M. J. Reductive Routes to Dinuclear d^{10}–d^{10} Palladium(0) Complexes and Their Redistribution Equilibria in Solution. *Organometallics* **2001**, *20*, 2959–2961.

(33) Boyle, R. C.; Mague, J. T.; Fink, M. J. The First Stable Mononuclear Silyl Palladium Hydrides. *J. Am. Chem. Soc.* **2003**, *125*, 3228–3229.

(34) Biswas, S. Mechanistic Understanding of Transition-Metal-Catalyzed Olefin Isomerization: Metal-Hydride Insertion-Elimination vs. π-Allyl Pathways. *Comments on Inorganic Chemistry* **2015**, *35*, 300–330.

(35) *Applied Homogeneous Catalysis with Organometallic Compounds: A Comprehensive Handbook in Four Volumes*, 1st ed.; Cornils, B., Herrmann, W. A., Beller, M., Paciello, R., Eds.; Wiley, 2017.

(36) Vansant, E. F.; Voort, P. van der, Vrancken, K. C. *Characterization and Chemical Modification of the Silica Surface*; Elsevier: Amsterdam; New York, 1995.

(37) Marrone, M.; Montanari, T.; Busca, G.; Conzatti, L.; Costa, G.; Castellano, M.; Turturro, A. A Fourier Transform Infrared (FTIR) Study of the Reaction of Triethoxysilane (TES) and Bis[3-Triethoxysilylpropyl]Tetrasulfane (TESPT) with the Surface of Amorphous Silica. *J. Phys. Chem. B* **2004**, *108*, 3563–3572.

(38) Riccio, M.; Montanari, T.; Castellano, M.; Turturro, A.; Negroni, F. M.; Busca, G. An IR Study of the Chemistry of Triethoxysilane at the Surface of Metal Oxides. *Colloids and Surfaces A: Physicochemical and Engineering Aspects* **2007**, *294*, 181–190.

Appendix (Materials and Methods)

(1) Reid, S. M.; Fink, M. J. Reductive Routes to Dinuclear d^{10} −d^{10} Palladium(0) Complexes and Their Redistribution Equilibria in Solution. *Organometallics* **2001**, *20*, 2959–2961.

(2) Akhani, R. K.; Moore, M. I.; Pribyl, J. G.; Wiskur, S. L. Linear Free-Energy Relationship and Rate Study on a Silylation-Based Kinetic Resolution: Mechanistic Insights. *J. Org. Chem.* **2014,** *79*, 2384-2396.

(3) Nakagawa, Y.; Chanthamath, S.; Fujisawa, I.; Shibatomi, K.; Iwasa, S. Ru(ii)-Pheox-catalyzed Si–H insertion reaction: construction of enantioenriched carbon and silicon centers. *Chem. Commun.* **2017,** *53*, 3753-3756.

(4) Savela, R.; Zawartka, W.; Leino, R. Iron-Catalyzed Chlorination of Silanes. *Organometallics* **2012,** *31*, 3199-3206.

(5) Gandhamsetty, N.; Park, S.; Chang, S. Selective Silylative Reduction of Pyridines Leading to Structurally Diverse Azacyclic Compounds with the Formation of sp3 C–Si Bonds. *J. Am. Chem. Soc.* **2015,** *137*, 15176-15184

(6) Ramey, K. C.; Louick, D. J.; Whitehurst, P. W.; Wise, W. B.; Mukherjee, R.; Moriarty, R. M. A line width method for determining chemical exchange rates from NMR spectra. *Org. Magn. Reson.* **1971,** *3*, 201-216.

(7) Gasparro, F. P.; Kolodny, N. H. NMR determination of the rotational barrier in N,N-dimethylacetamide. A physical chemistry experiment. *J. Chem. Educ* **1977,** *54*, 258.

(8) Yamanoi, Y.; Taira, T.; Sato, J.; Nakamula, I.; Nishihara, H. Efficient Preparation of Monohydrosilanes Using Palladium-Catalyzed Si−C Bond Formation. *Org. Lett.* **2007**, *9*, 4543–4546.

(9) Hurst, M. R.; Zakharov, L. N.; Cook, A. K. The Mechanism of Oxidative Addition of Pd(0) to Si–H Bonds: Electronic Effects, Reaction Mechanism, and Hydrosilylation. *Chem. Sci.* **2021**, *12*, 13045–13060.

(10) Zhao, J.; Zheng, X.; Tao, S.; Zhu, Y.; Yi, J.; Tang, S.; Li, R.; Chen, H.; Fu, H.; Yuan, M. Selective Rhodium-Catalyzed Hydroformylation of Terminal Arylalkynes and Conjugated Enynes to (Poly)Enals Enabled by a π-Acceptor Biphosphoramidite Ligand. *Org. Lett.* **2021**, *23*, 6067–6072.

(11) Konnick, M. M.; Guzei, I. A.; Stahl, S. S. Characterization of Peroxo and Hydroperoxo Intermediates in the Aerobic Oxidation of *N* -Heterocyclic-Carbene-Coordinated Palladium(0). *J. Am. Chem. Soc.* **2004**, *126*, 10212–10213.

(12) Fantasia, S.; Nolan, S. P. A General Synthetic Route to Mixed NHC-Phosphane Palladium(0) Complexes (NHC=N-Heterocyclic Carbene). *Chem. Eur. J.* **2008**.

(13) Li, H.; Grasa, G. A.; Colacot, T. J. A Highly Efficient, Practical, and General Route for the Synthesis of (R 3 P) 2 Pd(0): Structural Evidence on the Reduction Mechanism of Pd(II) to Pd(0). *Org. Lett.* **2010**, *12*, 3332–3335.

(14) Reid, S. M.; Mague, J. T.; Fink, M. J. Facile Reductive Elimination of Ethane from Strained Dimethylpalladium(II) Complexes. *J. Am. Chem. Soc.* **2001**, *123*, 4081–4082.

(15) Lumbreras, E.; Sisler, E. M.; Shelby, Q. D. Synthesis, X-Ray Crystal Structure, and Reactivity of Pd2(μ-Dotpm)2 (Dotpm=bis(Di-Ortho-Tolylphosphino)Methane). *J. Organomet. Chem.* **2010**, *695*, 201–205.

(16) Spaniel, T.; Schmidt, H.; Wagner, C.; Merzweiler, K.; Steinborn, D. (Phenylalkyl)Palladium Complexes Containing β-Hydrogen Atoms: Synthesis and Characterization of [PdR2(Dppe)], [PdR(SPh)(Dppe)] (R = CH2CH2Ph, CH2CH2CH2Ph, CH2CHMePh), and [Pd(CH2CH2CH2Ph)X(Dppe)] (X = I, Br, Cl). *Eur. J. Inorg. Chem.* **2002**, *2002*, 2868–2877.

(17) Kunai, A.; Sakurai, T.; Toyoda, E.; Ishikawa, M.; Yamamoto, Y. Versatile Method for the Synthesis of Iodosilanes. *Organometallics* **1994**, *13*, 3233–3236.

(18) Iwata, A.; Toyoshima, Y.; Hayashida, T.; Ochi, T.; Kunai, A.; Ohshita, J. PdCl2 and NiCl2-Catalyzed Hydrogen–Halogen Exchange for the Convenient Preparation of Bromo- and Iodosilanes and Germanes. *J. of Organomet. Chem.* **2003**, *667*, 90–95.

(19) Wappes, E. A.; Nakafuku, K. M.; Nagib, D. A. Directed β C–H Amination of Alcohols via Radical Relay Chaperones. *J. Am. Chem. Soc.* **2017**, *139*, 10204–10207.

(20) Sandoval, J. E.; Pesek, J. J. Hydrolytically Stable Bonded Chromatographic Phases Prepared through Hydrosilylation of Olefins on a Hydride-Modified Silica Intermediate. *Anal. Chem.* **1991**, *63*, 2634–2641.

(21) Sandoval, J. E.; Pesek, J. J. Synthesis and Characterization of a Hydride-Modified Porous Silica Material as an Intermediate in the Preparation of Chemically Bonded Chromatographic Stationary Phases. *Anal. Chem.* **1989**, *61*, 2067–2075.

(22) Copéret, C.; Comas-Vives, A.; Conley, M. P.; Estes, D. P.; Fedorov, A.; Mougel, V.; Nagae, H.; Núñez-Zarur, F.; Zhizhko, P. A. Surface Organometallic and Coordination Chemistry toward Single-Site Heterogeneous Catalysts: Strategies, Methods, Structures, and Activities. *Chem. Rev.* **2016**, *116*, 323–421.

(23) Marrone, M.; Montanari, T.; Busca, G.; Conzatti, L.; Costa, G.; Castellano, M.; Turturro, A. A Fourier Transform Infrared (FTIR) Study of the Reaction of Triethoxysilane (TES) and Bis[3-Triethoxysilylpropyl]Tetrasulfane (TESPT) with the Surface of Amorphous Silica. *J. Phys. Chem. B* **2004**, *108*, 3563–3572.

(24) Riccio, M.; Montanari, T.; Castellano, M.; Turturro, A.; Negroni, F. M.; Busca, G. An IR Study of the Chemistry of Triethoxysilane at the Surface of Metal Oxides. *Colloids and Surfaces A: Physicochemical and Engineering Aspects* **2007**, *294*, 181–190.